Structural Engineering Report No. 113

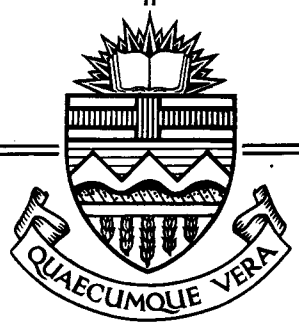

LATERAL COAL PRESSURES IN A MASS FLOW SILO

by

ANDREW B. B. SMITH

and

SIDNEY H. SIMMONDS

Department of Civil Engineering
The University of Alberta
Edmonton, Alberta, Canada

NOVEMBER, 1983

Lateral Coal Pressures in a Mass Flow Silo

by

Andrew B. B. Smith

and

Sidney H. Simmonds

Structural Engineering Report No. 113

Department of Civil Engineering

The University of Alberta

Edmonton, Alberta, Canada

November, 1983

Acknowledgements

The authors wish to acknowledge the contributions to this study of a number of persons and organizations. Special thanks are due to Dr. C.J. Montgomery who was instrumental in the planning and initiation of this study and for providing continuing encouragement and support. We are indebted to Fording Coal Ltd. for permission to instrument the Fording River silo and for providing the accommodations for our field personnel. Personal thanks are due Mr. J. Gardner, Plant Manager, and his on-site staff, for their cooperation and assistance during the procurement of field data. It is a pleasure to thank Mr. M. Morrison and Mr. M. Kinash, of Associated-Kellogg Ltd., consulting engineers for the project, for their interest, assistance, and enthusiastic support during the study. Thanks are also extended to the contractor, Barnett-McQueen Ltd., and to Mr. H. Knynsberg, site engineer for Associated-Kellogg Ltd., who assisted in placing instrumentation during construction. The technical assistance of Mr. L. Burden and Mr. R. Gitzel is appreciated as is the invaluable computing expertise of Mr. T. Casey. Thanks are due to Janet Smith for typing the manuscript. Much of the funding for this research was provided by the Natural Sciences and Engineering Research Council of Canada, Operating Grant A1691.

Abstract

This study attempts to provide a better understanding of the lateral pressures that stored materials may exert on their containment vessels. In this respect, particular emphasis is placed on pressures that ensue during an expanded or mass flow of granular coal from a full sized cylindrical silo. Included is an examination of the available literature as it pertains to this more general purpose and following this, field measurements taken from an operational silo are reported and discussed.

Field measurements obtained include outer and inner hoop steel strains recorded both dynamically and statically for six vertical locations along a single meridian. The results indicate a minimum dynamic overpressure factor (i.e. the maximum observed ratio of flow pressure to initial pressure) of 2.0 can be justified for coal pressures at certain heights along this meridian in silos of similar diameter and outlet geometry.

Various static pressure theories are elaborated on and a derivation is given to allow for compressibility effects in granular materials within a Janssen-like pressure field. An apparent relationship between the earth pressure ratio K and relative density, also within a static field, is discussed. Under conditions of flow, Jenike proposes a minimum strain energy field in defining an upper bound to design pressures and this theory has been expanded upon to include wall strain energies.

Table of Contents

List of Tables

List of Figures

List of Symbols

A = cross-sectional area

A = Jenike strain energy parameter

A_c = contact area

A_c = area of concrete

A_s = area of steel

B = Jenike strain energy parameter

C = circumference

C_c = compression index

C_d = ACI 313-77 overpressure factor

C_i = integration constant

C_m = dimensionless silo flexibility factor

C_r = recompression index

C_s = shell circumference

C_γ = Janssen-Compressibility unit weight constant

D = bin diameter

D = shell flexural rigidity

D_r = relative density

E = Young's modulus

E_c = modulus of elasticity for concrete

E_{dy} = dynamic modulus of elasticity

E_m = modulus of elasticity for contained material

E_s = modulus of elasticity for steel

E_s = equivalent modulus of elasticity for shell

E_{st} = static modulus of elasticity

Et = extensional stiffness per unit height

EYL = effective yield locus

e = eccentricity

e = void ratio

e_o = initial void ratio

Fu = design force per unit measure of height

fc = concrete stress

$f\acute{c}$ = concrete cylinder compressive strength

f_{ij} = frequency

fs = steel stress

f_v = shear strength

f_y = yield strength

G_s = specific gravity of solids

H = contained material height or silo height

h_1 = height of material cone

h = film coefficient

K = coefficient of earth pressure

K_o = at-rest coefficient

Ka = active coefficient

K_{dy} = dynamic coefficient

K_t = strain energy boundary condition at transition

K_j = Janssen's earth pressure coefficient

K_m = maximum coefficient within contained materials

Kp = passive coefficient

K_s = value of coefficient at switch

K_{st} = static coefficient

k = thermal conductivity

M = Jenike strain energy parameter or moment

M_2 = wall strain energy parameter

m = Jenike bin geometry parameter (0 or 1)

m = relative density exponent

m_k = Lvin's ratio for K_p/K_a

m.c. = moisture content (w)

m_v = coefficient of volume compressibility

N = normal force

N = Jenike strain energy parameter

n = modular ratio; E_s/E_m or Es/Ec

o.p.f. = overpressure factor

P = pressure

P_d = dynamic lateral pressure

P_{des} = ACI 313-77 design pressure

P_h = horizontal pressure

$P_{h_{max}}$ = maximum horizontal pressure

P_s = static horizontal pressure

P_v = vertical pressure

$P_{v_{max}}$ = maximum vertical pressure

p = consolidating pressure

p = mean of the principal stresses

Q = weight of contained materials

Q_m = vertical load in a contained material

Q_{max} = maximum vertical load in a contained material

Q_o = surcharge due to cone of material

Q_T = total material weight

Qw = material weight supported by walls

R = hydraulic radius (A/C)

$\mathcal{R}$ = thermal resistance

r = radial distance

r_o = radius

S = nondimensionalized stress parameter

S' = above differentiated with respect to z

S_o = nondimensionalized stress parameter at the switch

T = tensile force

T = temperature

$T_{i,o}$ = inner, outer temperatures

T_{max} = fully mobilized shear force

t = wall thickness

t = time

t_s = equivalent thickness of shell

V_s = shell volume

W = strain energy

W_s = shell extensional strain energy

w = nondimensionalized strain energy

w = water content (m.c.)

w_s = nondimensionalized strain energy in shell

WYL = wall yield locus

X = Jenike strain energy parameter

x_1 = Jenike transformed coordinate

x = horizontal distance from centre-line

y = out-of-plane direction in two-dimensional bin

z = vertical distance from effective surface

z = Reimbert's vertical distance from base of cone

z_c = Lvin's depth of maximum static pressure

z_o = depth to switch location

α = thermal expansion coefficient

α = thermal diffusivity

β = compressibility coefficient (slope of $log\ \gamma$ - $log\ \sigma$ curve)

γ = unit weight

γ_d = dry unit weight

γ_{dmax} = maximum dry unit weight

γ_{dmin} = minimum dry unit weight

γ_o = initial unit weight

γ_T = total unit weight

γ_w = unit weight of water

ϵ = strain

ϵ_d = dynamic local strain

$\epsilon_{i,o}$ = inner, outer strains

ϵ_m = measured strain

ϵ_s = static local strain

ϵ_s = shell strain

$\epsilon_{x,y,z}$ = Cartesian strain components

λ = dimensionless frequency parameter

μ = coefficient of internal friction

μ' = coefficient of wall friction

μ'_k = kinetic coefficient of wall friction

μ'_s = static coefficient of wall friction

ν = Poisson's ratio

ξ = slope of $log\ \gamma$ - e curve

ρ = density

ρ = wall deflection, settlement

σ = normal stress

σ_1 = consolidating pressure

$\sigma_{1,2,3}$ = principal stresses

σ_h = horizontal stress

$\sigma_{i,o}$ = inner, outer stresses

σ_o = initial consolidating pressure

σ_r = radial stress

σ_s = shell stress

σ_V = vertical stress

$\sigma_{x,y,z}$ = Cartesian stresses

σ_θ = circumferential stress

τ = shear stress

τ_V = vertical shear stress at wall

ϕ = effective angle of internal friction of a bulk material

ϕ' = effective angle of wall friction

ψ = rotation of the principal planes

Δ = incremental change in

1. Introduction

1.1 Overview

The word 'silo' originated in the Greek language as 'siros' meaning a pit to store grain and over the centuries has managed to retain this particular emphasis. Today, the complete reference is more general, including below and above ground storage of a variety of materials and objects. In the context of this study, a silo is an elevator or free standing bin, and may store a variety of bulk products in addition to grain, such as coal or cement. It is ideally suited to these types of product; it acts as a storage device, provides protection to and from the environment, and allows for a relatively problem free loading system using a rather inexpensive motive force, gravity.

In western Canada today the long range prospects are encouraging for continued resource development, particularly for thermal and metallurgical coal. Consequently, the need for additional bulk materials handling facilities can be foreseen. Because large diameter silos fulfill the dual role of tertiary storage and loadout, they are now and will continue to be a common sight at most mine sites, particularly if unit trains continue to provide the primary means of transport. The need for efficient and safe silo designs is therefore firmly established.

A major concern of the structural designer is to know, within reasonable limits, the loads that these structures

will be required to withstand during their operational life. This has proven to be somewhat of a problem with silos; bulk materials do not always manifest predictable behaviour. The mechanics of granular materials, even for reasonably homogenous and noncohesive materials, are little understood when one imposes dynamic conditions as occur during flow. This lack of predictability is compounded when this flow channel develops within complex hopper geometries that are generally the norm in silo applications.

Designs for silos must satisfy two major requirements; flowability and strength. Flowability is determined through a set of criteria involving a range of bulk material properties, wall roughnesses, and most importantly, hopper geometries (i.e. hopper slopes and outlet dimensions). Strength requirements are related directly to material pressures. For a rectangular bin, bending is the primary resistive mode. For a cylindrical bin, extensional wall strength or membrane action is the primary resistive mode, although eccentric flow effects can cause large moments to develop.

Some indication of the many problems silo designers have historically encountered is contained in discussions of actual silo failures by Sadler (1980) and Theimer (1969). Although the former deals largely with coal storage and the latter deals exclusively with grain storage, both conclude that serious structural deficiencies have most often occurred due to inadequate consideration of material

pressures under flow and/or eccentric loading conditions. This lack of consideration is primarily a result of;

1. the complexity of solid material flow and subsequent obstacles to theoretical solutions
2. the observational difficulties in procuring pressure data for a wide variety of silo-hopper configurations

In the review to follow, the developments in this field of engineering are presented, from the historical perspective.

1.2 Historical Review

The experimental study of lateral pressures produced by stored materials on their containment structures originated in the works of Issac Roberts (1882, 1884). Roberts conducted experiments on bin models and on intermediate sized rectangular grain bins and found that upon filling, once a material height of between two and three times the smaller cross-sectional dimension was achieved, there occurred no further increase in the lateral or vertical material pressures. This was an important observation for up until this time and indeed for a considerable time thereafter, designers had assumed that bulk solids behave similarly to fluids. Applied literally, this assumption could result in a design that was both overly conservative and unsafe in terms of horizontal and vertical loads respectively. The design lateral pressure, according to Roberts (1884), was then;

" something less than the pressure of a similar

column of water, but how much less did not appear to be to be known either in England or America."

Roberts' early work therefore recognized the role of wall friction in reducing material pressures.

In 1895, H.A. Janssen (1895) published his now famous and still widely used theory on pressures in silos. This theory will be presented in detail in Sect. 2.1.3, but generally it involves vertical equilibration of normal, friction, and body forces acting on and within a differential slice of material. Janssen conducted a series of tests on small rectangular model bins using wheat and corn as bulk materials and found the results compared favourably with his analytical work. He recognized at this time that the ratio K', an important parameter in his material stress formulae, would probably require experimental evaluation and he endeavoured to establish K for each material he used.

Janssen's investigations dealt with predicting initial pressure curves. The first reference in the literature to what are now termed dynamic loads was made by another German, Prante (1896), who reported increases as much as four times the static loads on discharge from full size silos.

In that same year, Koenen (1896) suggested the application of Rankine's (1857) theory of active earth

---

[1] K = the ratio between intensities of horizontal and vertical pressures at a given point in a (soil) mass (Terzaghi and Peck 1967). It is commonly referred to in soil mechanics as the *coefficient of lateral (earth) pressure.*

pressures in evaulating K in Janssens' formula. This gives K as a function of the angle of internal friction, ϕ;

$$Ka = \frac{1 - sin\phi}{1 + sin\phi}$$

Although this is a reasonable assumption if one considers the material to be in a state of incipient active failure using the Mohr-Coulomb failure criterion, it is generally recognized that the use of Ka will lead to a lower bound to the lateral pressures. The use of Ka in Janssen's formulae, coupled with a general nonrecognition of substantial dynamic pressures, has probably contributed to many historical silo failures.

The science of lateral material pressures in silos regressed somewhat with the publication by Airy (1897) of his theories on sliding wedges of material in bins, a theory somewhat similar to Coulomb's (1776) method of wedges for retaining walls. Airy, due to an incorrect application of Coulomb's theory, predicted a decrease in vertical pressures after some particular height of material was achieved. This decrease was not supported by then concurrent tests, although an experimental aberation in earlier work by Roberts did provide corroborative results.

Full size tests began on the North American continent in 1897 in New York under Toltz. He used a 14 foot square, 65 foot high wooden bin containing wheat, however Toltz did not publish his results. The first mention of these findings

appeared in a latter discussion of Jamieson's (1903) experiments, in which Toltz expressed general agreement with Jamieson's results on discharge pressures.

J.A. Jamieson, a Canadian engineer, at the turn of the century initiated tests on a full size grain silo located in St.John, N.B. At that time, full size grain bins consisted of rectangular compartments 12 to 14 feet square and were constructed of 2" x 6" or 8" boards placed flat and nailed to heights of 60 to 70 feet. Jamieson utilized perhaps for the first time, the hydraulic diaphram in measuring bin pressures and found his static results compared favourably with Janssen's. While monitoring discharge pressures Jamieson found lateral pressure increases of only four percent and for this reason took a dim view of Prante's results. Jamieson continued his investigations, and in the winter of 1903-04 conducted a series of well documented tests on model bins in which he varied a number of the recognized parameters. Again his static results agreed with Janssen while his dynamic overpressures ranged from 5 to 9.3 percent, the latter occuring during a rapid discharge of material. He also observed the increased pressures caused by an eccentric draw off on an opposite face. His attempts to establish flow regimes within the bin using coloured grains seem to indicate that he was experiencing funnel flow, at least in the lower bin portions. Jamieson presented a condensed version of his results in 1904.

Later that year Bovey (1904) published a paper in which he described similar tests that he conducted on two full size grain bins in Montreal and Quebec City. These tests were commissioned by the City of Montreal in connection with several condemned grain bin designs produced by Jamieson. The condemnations came from advocates of the equivalent fluid pressure theory but Bovey's static results supported Jamieson and again there appeared to be no appreciable dynamic effects.

Eckhardt Lufft (1904) revealed his findings from tests conducted in Buenos Aires on reinforced concrete wheat bins of 23′-10″ and 11′-3″ inside diameters, both having a height of 54′-9″. Unfortunately there appeared no mention of wall thicknesses in the report although accompanying figures suggested walls of 12 to 18 inches. Once again, Janssen's theory approximated the static results while only slight dynamic increases occured.

Tests conducted by Pleissner (1906) also found agreement with Janssen's solution although Pleissner reported more substantial pressure increases on discharge.

Coincident to this period was the work of Ketchum, who conducted tests in 1902-03 and again in 1909. In 1920 Ketchum's third edition of "The Design of Walls, Bins, and Grain Elevators" summarized well the work up to that point in time. Ketchum's state-of-the-art survey for this earliest historical period can generally be summarized in 12 important points;

1. there is a law for semi-fluids that differs substantially from fluid pressure theory
2. P_h ranges from 30 to 60 % of P_V and increases little after a depth of 2 1/2 to 3 times the diameter
3. the ratio of P_h to P_V, K, is not constant and therefore must be determined experimentally for different materials and geometries
4. during withdrawal, P_h can increase up to 10%
5. discharge gates should be centrally located
6. eccentric discharge gates can result in lateral pressures on an opposite side as much as 2 to 4 times static
7. tie rods do not affect pressures
8. a maximum value for P_h is achieved immediately after filling and this value can be affected by the rate of filling
9. Janssen's or Airy's calculations agree with observed pressures
10. measured unit pressures on small surfaces agree with measured unit pressures on large sufaces
11. calculations on existing wooden bins revealed that fluid theory design is overly conservative for lateral considerations
12. buckled steel-walled bins were evidence that fluid theory design can be unsafe for vertical considerations

Sundaram and Cowin (1979) have described the period from 1920 to 1965 as a time of misconceptions and misinformation, particularly when compared to the relatively well documented tests of the pre-1920's. Support for this viewpoint can be found, starting with a paper by R. Fleming (1922) that appeared in the Engineering News Record in which tables predicting coal pressures in bins were presented. Ensuing issues contained a lively set of discussions that centered on the relative applicability of several different theories, including the equivalent fluid pressure theory. In retrospect, there existed, even at this early period, experimental and theoretical studies to support a variety of theories. These studies, combined with the complexity of granular media mechanics, particularly during discharge, give little reason to believe this divergence of opinion should not have occured. The advocates of Janssen's theory gradually prevailed over the equivalent fluid pressure theorists, probably due in part to the influence of Ketchum's text since it was frequently cited in the literature of that period.

Quite probably, strict adherence to a Janssen analysis of lateral pressures would have resulted in structural failures on a grand scale, especially as there was occuring at this time a shift to larger and more flexible containers. By 1924, reinforced concrete storage bins for coal were commonplace (Anonymous 1924), usually cylindrical, with heights varying from 30 to 60 feet, diameters varying from

12 to 20 feet, thicknesses 6" and greater, and generally side unloading. This structural evolution apparently spawned from increasing fire insurance costs.

Failures were not predominant, even though many designers had accepted the meager 10% dynamic increases over static pressures on discharge as reasonable (Long 1931). Safety factors may have provided the margin although Janssen's formula does allow room for discretion in that the material parameters can be chosen conservatively. For example, Ward (1925), described designs for a reinforced concrete cement silo in which an internal angle of friction of 6° was used. This is approaching ϕ for liquids, (0°), and results in a large value for Ka (i.e. 0.81).

Frenzel (1932), gave account of the shift in grain storage structural material from wood to reinforced concrete slip-formed circular bins, generally in rectangular rows, from 15 to 30 feet in diameter, and from 50 to 120 feet high. He quotes 7" as being the wall thickness for the commonly used 24 foot diameter bin and also tells of the widespread use of the Janssen formula.

Experimental study on bulk materials in bins is sporadic during this period when compared to the intensity of testing that occured along with Jamieson's valuable work in the early 1900's. Malcalmont and Ashby (1934), while testing ear corn in rectangular 24 ft high wooden cribs, rediscovered the effects of wall friction in limiting material pressures. Ten years later, Malcalmont and Besley

(1939) are the major reference in an American Concrete Institute recommendation for farm silos (1944) however the contained material is now silage. Grass and corn silage are by definition bulk materials but their behavior indicates the wide ranges bulk material pressures can span. The usual concave downwards (exponentially decreasing) curve for lateral pressures is not evident and in fact slightly reversed indicating the effects of compressibility.

Kramer (1944) experimented with rough rice, another fairly compressible bulk material, and also found a slight upward concavity in the lateral pressure curve immediately below the free surface. His unique tests indicated that K was not constant but increased to a steady value of approximately 0.48.

Admundson (1945) measured band stresses on the perimeter of a relatively shallow bin containing wheat. He found an overall K of 0.46 if Janssen's formula was employed and concluded that this formula was safe for design.

Theoretical work on the predictions of lateral pressures in silos had also been conspicuously absent for the half century following the work of Janssen and Airy until Jaky (1948) published his theories. Although his solution was extremely complex and therefore too cumbersome for design use, he did bring to light a number of important ideas; his major contribution was that he was the first to suggest that K should be understood as being the earth pressure at rest (i.e. K_o) and gave this to be;

$$K_o = 1 - \sin\phi$$

This has since been recognized as a major contribution to the science of soil mechanics.

Caughey *et al.* (1951) published their results on extensive static model experiments with wheat, corn, soy beans, cement, sand, and pea gravel. Generally they found agreement with Janssen's theory although several of their materials gave pressures far below a Janssen curve.

In 1954 there appeared the first documentation on tests of large sized silos that indicated that the flexibility of a containment structure may have some influence on lateral pressures. North (1954), while monitoring pressures in horizontally corrugated metal grain silos found radical departures from Janssen's curve and he attributed this to the vertical flexibilty of the walls.

The work of two brothers, Marcel and Andre Reimbert deserves special mention due to the fact that their involvement in the practical study of silo pressures and structures has been long and productive. M. Reimbert (1955) conducted tests an several full sized grain silos, of 13.5 foot square cross section, 10 meters high and made of thin sheet steel. His results indicated that large dynamic overpressures can exist, that they can achieve a value as high as 2.4, but that they are highly variable.

Reimbert made a further contribution to the field that has been incorporated into a present day recommended practice as an alternative method to Janssen's when

calculating static loads. Somewhat empirical in derivation, it is nevertheless an important practical result and so for this reason will be discussed further in Sect. 2.1.3.

The mid 1950's marks the beginning of a final stage in the development of both silo pressure theories and experimental methods to measure silo pressures. This most recent quarter century, to 1980, gave rise to a vast number of publications that deal in whole or in part with this problem. "A Bibliography on Silos (1857-1979)", prepared by Walli and Schwaighofer (1979), contains 409 references for this later period alone. For the period prior to the end of 1955, this bibliography contains only 215 references. Because Reimbert's work could be considered representative of prevailing thought at that time, and because to some extent it still is, this marks a suitable point to end this historical review of the literature. The literature review will in effect continue in Chap. 2 but in a topical rather than historical perspective.

1.3 Contemporary View

The historical evidence for large flow induced material pressures renders their existence no longer an issue at this point in time. Quantifying these highly variable dynamic pressures is now the focus of attention in the literature.

Established practice is to quantify these overpressures, be they experimentally or theoretically derived, in terms of static pressure theories. Hence the

term 'overpressure' is somewhat self-explanatory. The reasons for this practice are straightforward enough. Static pressures provide predictable and generally reproducible reference points when compared to the highly transitory and and generally inconsistent dynamic pressures. The connection between these static and dynamic pressure levels has never really been justified except in very broad terms.

Part of the problem stems from what are a wide variety of dynamic and/or eccentric pressure fields. Broadly speaking, material pressures are classified as 'static', 'flow', and 'switch', the latter being a transitional and usually short-lived phenomenon occuring at the onset of flow. The term 'static' is more aptly described as 'initial' because dynamic pressures will, on stoppage of flow, be 'locked-in' to a static stress field. Throughout this study, these 'locked-in' pressures are termed 'quasi-static' and the terms 'static' and 'initial' are used interchangeably. These definitions are in keeping with current literature.

This broad categorization is further complicated by reference to two limiting flow types; mass flow and funnel flow. True mass flow requires the flow channel to impinge on the containment structure while funnel flow includes those situations in which the flow channel boundary forms within the material. This distinction will be treated in more detail in Sect. 2.2.

Current design methods are embodied in a number of codes and standards. The North American standard,

'Recommended Practice for Design and Construction of Concrete Bins, Silos, and Bunkers for Storing Granular Materials (ACI 313-77 1975)', is the most recent of these to date. The underlying philosophy of this standard is examined in the following text in order that we may introduce at this time several principles fundamental to bin design. Although rectangular bins are treated just as thoroughly in ACI 313-77 as are cylindrical bins, the essential features are presented with respect to the latter.

The well known formula for stress in a thin-walled cylinder is

$$\sigma = \frac{P\,r}{t} \qquad \text{or} \qquad \sigma\,t = P\,D\,/\,2 \tag{1.1}$$

where σ = wall stress

t = wall thickness

D = inside diameter of cylinder

r = cylinder radius

P = internal pressure

The design force per unit measure of height, Fu, as given in ACI 313-77, is simply a restatement of Eq.[1.1].

$$Fu = 1.7\,P_{des}\,D\,/\,2 \tag{1.2}$$

where P_{des} = lateral design pressure

The required area of hoop steel (principal reinforcement) per unit measure of height is

$$A_s = Fu\,/\,\phi\,f_y \tag{1.3}$$

Here ϕ is a performance factor. The load factor of 1.7 in Eq.[1.2] reveals that, at this time, the unpredictability of material pressures renders them necessary to be treated as a live load. The lateral design pressure, P_{des}, is calculated from static pressure theories (i.e. initial loading conditions obtained upon filling) using either a Janssen or Reimbert pressure distribution. These static solutions will be discussed in detail in the following chapter. Depending on the expected nature of material flow during discharge, this design pressure may be adjusted upwards with an overpressure factor, C_d, given in a table provided by ACI for various height/diameter ratios and vertical ranges over the silo's height. It should be noted that this table is footnoted with:

> "C_d values given in this table are inadequate for the higher loads associated with mass flow."

Thus the most recent standard leaves the designer with little information to proceed if a mass flow system is under consideration. Other codes, such as the German code DIN 1055 (1964), do not even mention mass flow as an alternative (although the stated terms of reference are sufficient to include mass flow), perhaps because this method of silo discharge has been defined only recently. Therefore, there is at this time a need for further experimentation and research in this area.

1.4 Scope

This study attempts to do two things. The primary objective is to provide badly needed experimental data that quantifies material overpressures within full size mass flow silos. The secondary objective, borne of requirements to satisfy the primary objective, has evolved into a semi-critical examination and a state-of-the-art discussion of static and mass flow pressure theories.

The theoretical works are presented first, beginning with static pressure theories. The need for explicit treatment of these initial static pressure theories is two-fold. Firstly, many of the material properties in the static case are of some consequence in the dynamic case. Secondly, the nature of the data acquired during this study requires some interpretation in reference to extensional wall stiffnesses and it is these generally accepted static pressure theories that are relied upon. Dynamic pressure theories are discussed with a particular emphasis on mass flow theories. Comparisons are made to codes of practice currently in use as well as to results from recent experimental investigations in this area.

The experimental portion of this thesis was conducted on an operational coal silo, owned by Fording Coal Limited, located in the coal rich south-eastern corner of British Columbia. Experimental studies on silo pressures can be of several types. Most frequently, direct lateral pressure measurements are sought and here the pressure cell is

instrumental. In some cases, vertical pressures (on silo floors and on remote in-situ devices) and wall strains (vertical or lateral) have provided indirect information; the latter method was utilized in this study. There is some advantage to be had in measuring directly the response of that part of a structure which specifically is designed to resist a particular loading condition. Pressure measurements, although generally reliable on local scales, are characterized by their erratic behaviour and overall a certain lack of reproducibility; some of the reasons for this are discussed in detail.

Bin or silo tests are most often conducted on model bins for obvious reasons and theoretically this practice should pose no inherent problems for larger scale application, as concluded convincingly by Pieper (1969). Practically, with particular reference to material densities and their resultant effects on earth pressure ratios, difficulties can occur, and often the experimenter indiscriminately will suggest extrapolation to larger systems. This can often result in erroneous conclusions. Additionally, recent work (and to some extent this study) support contentions that wall flexibility may play an important role in dynamic lateral pressure levels. Model tests on the other hand most often incorporate relatively stiff containers. This brings to light an important but historically ignored concept of material-structure interaction. These ideas are further developed.

2. Material Pressures in Silos

2.1 Static Pressure Theories

2.1.1 Introduction

Static, or more appropriately, initial pressure theories, can be categorized into three distinct methods. These are, in order of historical development (and decreasing size of elemental free body):

1. the method of sliding wedges of material, developed by Coulomb (1776) for retaining walls, but applied to silos by Airy (1897).
2. the method of differential slices as proposed by Janssen (1895) and used to some degree by Reimbert (1955).
3. characteristic or numerical methods in the solution of the equilibrium equations obtained from differential volumes, used initially by Sokolovskii (1954) but applied to two-dimensional bins by Horne and Nedderman (1976).

Examples of each category are presented. The Janssen and Reimbert methods are treated individually because they are the basis for all current design codes and are used here to familiarize the reader to the various material-property/ stress-relationships fundamental to static pressure theories. Following presentation of the various methods, the different assumptions employed by each are examined. Finally, the more important parameters involved in

predicting static pressures are discussed in light of these assumptions.

2.1.2 The Method of Sliding Wedges

Coulomb (1776) developed a method for analysing forces on retaining walls using sliding wedges of material and his technique will be mentioned here only in the interest of completeness. This wedge method appears to have appealed only to Airy (1897), and his analysis resulted in the dubious prediction that horizontal pressures will reach a maximum at some intermediate level and then begin to decrease. This occurred because Airy had neglected the contribution of one of the walls in his force balance. Hancock and Nedderman (1974) corrected Airy's method and have shown it to be a viable technique, although the relative complexity of the solution renders it unsuitable for design purposes. The wedge method is still best suited for analyzing shallow bins and retaining walls.

2.1.3 The Method of Differential Slices

2.1.3.1 Janssen's Method

Janssen investigated the equilibrium of a thin lamina of granular material, extending over the full cross-section, under the following assumptions: (1) vertical pressures are uniform at a horizontal cross-section, (2) horizontal pressures are uniform over the perimeter of a cross-section, (3) the ratio of these pressures, K, is a constant

throughout the material height, and (4) the shear stress at the wall is a linear function of the horizontal pressure.

The free body diagram for a material slice at depth z is shown in Fig. 2.1. Vertical equilibrium of the stress resultants and the material body force (weight) gives

$$\gamma dz A + \sigma_z A = A(\sigma_z + d\sigma_z) + \mu' K \sigma_z dz C$$

$$\frac{d\sigma_z}{dz} = \gamma - \frac{\mu' K \sigma_z}{R} \tag{2.1}$$

Introducing a nondimensionalizing stress parameter, $S = \sigma_z / R\gamma$,

$$\frac{dS}{dz} R = 1 - \mu' K S \tag{2.2}$$

$$\int \frac{dS}{1 - \mu' K S} = \int \frac{dz}{R}$$

Integrating,

$$\ln[1 - \mu' K S]\left[\frac{-1}{\mu' K}\right] = \frac{z}{R} + C_i$$

$$1 - \mu' K S = e^{-\mu' K (z/R + C_i)}$$

A boundary condition requires that $S = 0$ when $z = 0$ and this forces the constant of integration to vanish.

$$S = \frac{1}{\mu' K}\left[1 - e^{-\mu' K z / R}\right] \tag{2.3}$$

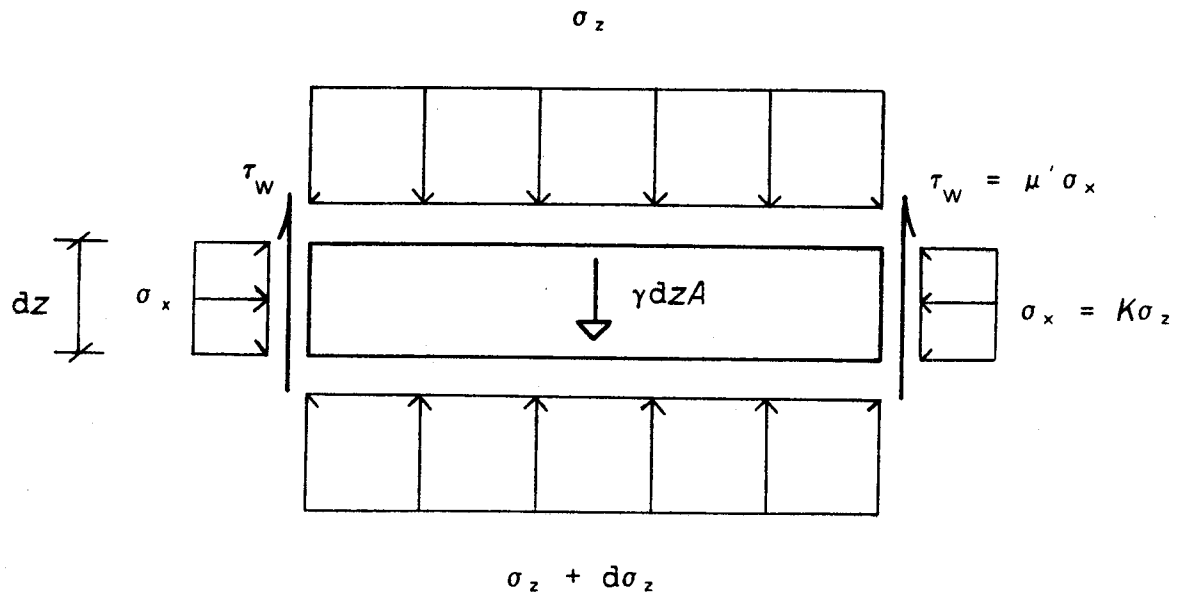

σ_z, σ_x	vertical and horizontal material pressures
τ_w	wall frictional (shear) stress
μ'	coefficient of wall friction
γ	material unit weight
A	container cross-sectional area
C	container circumference
R	hydraulic radius (A/C)

Figure 2.1 Janssen's Differential Slice

Therefore

$$\sigma_z = \frac{\gamma R}{\mu' K}\left[1 - e^{-\mu' K z/R}\right] \qquad (2.4)$$

and Janssen's formula for the lateral pressure becomes

$$\sigma_x = \frac{\gamma R}{\mu'}\left[1 - e^{-\mu' K z/R}\right] \qquad (2.5)$$

The solution is applicable to axisymmetric and two-dimensional (plane strain) conditions because symmetry requires that no shear stresses occur on a plane orthogonal to the x direction (which for the axisymmetric case is the radial direction). Polygonally shaped bins (generally rectangular or hexagonal silos) will have these shear stresses along lines of nonsymmetry that will put in question the assumption of uniformity of horizontal pressures over the perimeter. If Janssen's assumptions are strictly adhered to, the substitution of an appropriate value for the hydraulic radius, R, will provide a solution, although with unconventional cross-sections, some loss in accuracy might be expected. Fig. 2.2 includes two examples of the Janssen lateral pressure curve, calculated using the particular silo geometry and material properties deemed appropriate for the silo used in this study.

From Eq.[2.5] it is apparent that as z increases to infinity the maximum attainable lateral pressure becomes

$$P_{h_{max}} = \frac{\gamma R}{\mu'} \qquad (2.6)$$

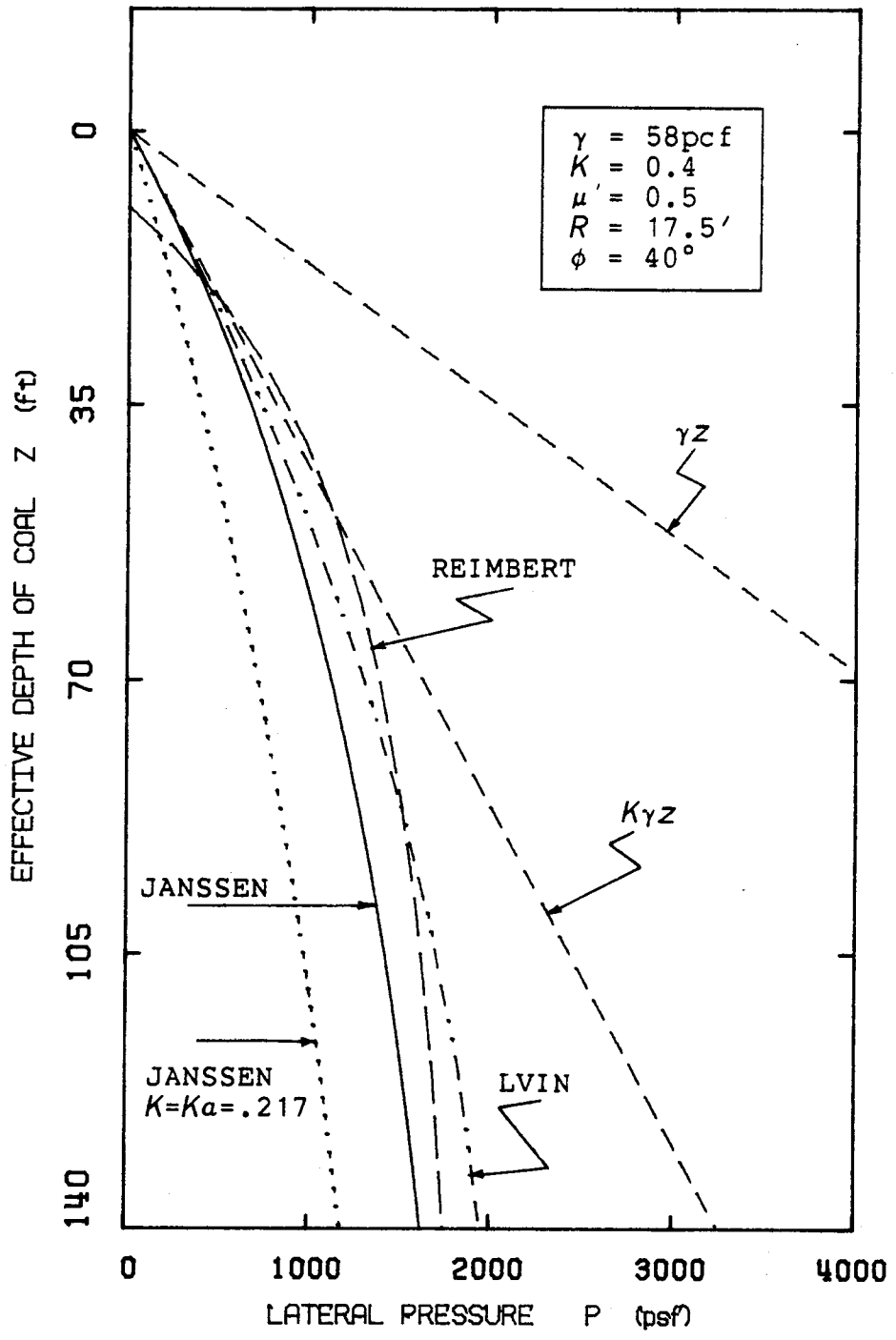

Figure 2.2 Static Lateral Pressures for the Fording Silo

This is a direct result of a maximum vertical pressure in which wall friction exactly balances the added weight of material at an infinite depth and this limit is common to all initial pressure theories.

Various authors, such as Walker (1966) and Sundaram and Cowin (1979), have sought to improve upon Janssen's original formula. Their solutions are essentially Janssen's solution with only minor modifications and these are a result of their taking issue with several of Janssen's assumptions. For this reason, they will be presented in the discussion of Sect. 2.1.5.

2.1.3.2 Reimbert's Method

Labiosa (1970) has given a fairly concise yet complete discussion of Reimbert's (1955) theory for initial silo loadings. Of primary importance to this theory's derivation is it's empirical basis. Fig. 2.3 reveals graphically the various asymptotes Reimbert employed in his derivation.

Reimbert defined the total vertical weight of material above any depth z as the force Q_T. This is shown in Fig. 2.3 as Curve I with the weight of a conical surcharge indicated as Q_o. He further defined Q_w as that component of the vertical wall force transferred to the silo wall by friction. This force increases from zero at the free surface to an asymptote parallel to Curve I because, again, at great depths, the added weight of material is exactly balanced by wall friction. This is shown by Curve II. Based on experimental results, he concluded that Q_w could be

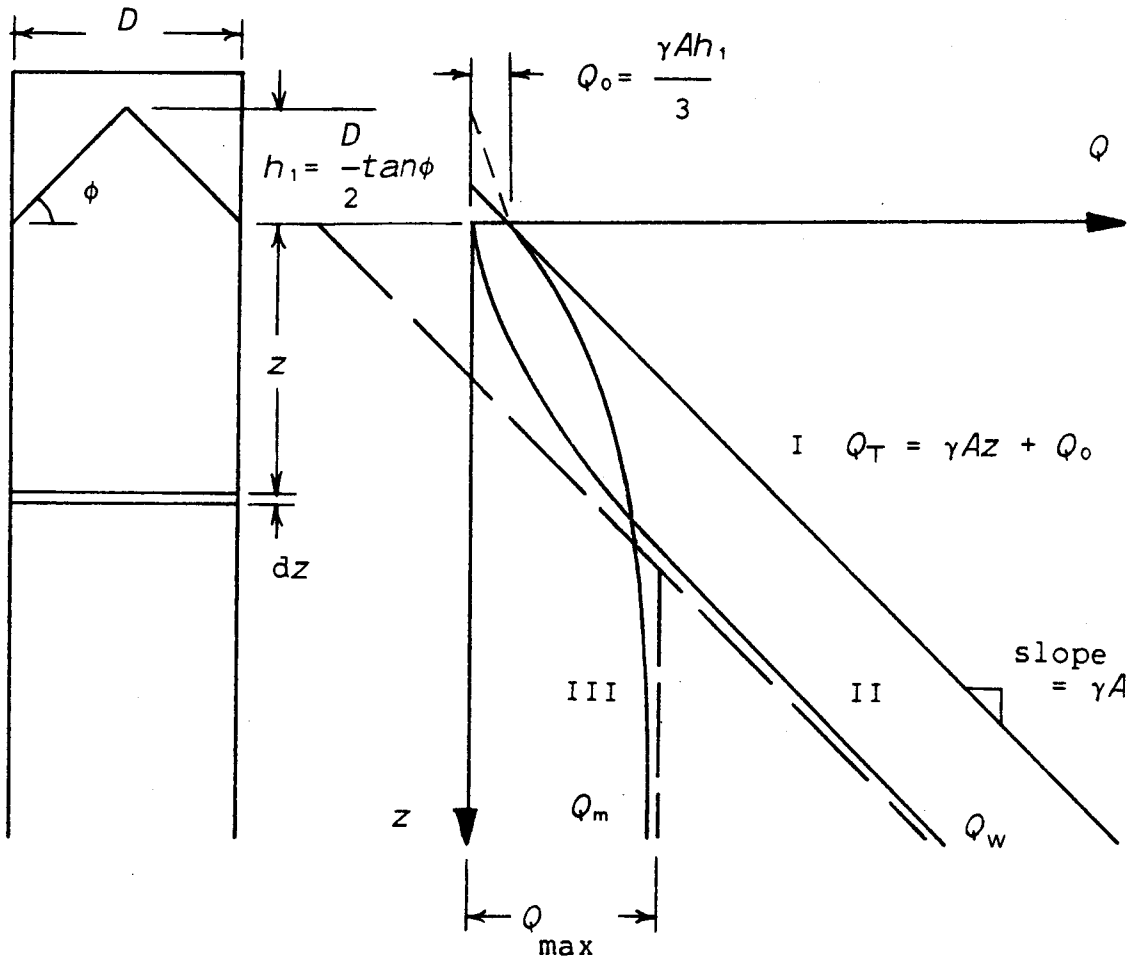

Curve I = II + III

$$Q_{max} = AP_{Vmax} = \frac{A\gamma D}{4\mu' K}$$

Figure 2.3 Distribution of Material Weight in a Silo

expressed as a hyperbolic funtion. Therefore, in general,

$$Qw = \frac{a(z)^2 + bz + c}{ez + f}$$

Four conditions are necessary for determining the above coefficients:

1. at $z = 0$, $Qw = 0$, and $\therefore c = 0$

2. at $z = 0$, $\frac{dQw}{dz} = 0$, $\frac{b}{f} = 0$, and $\therefore b = 0$

3. as $z \to \infty$, $\frac{dQw}{dz} \to \gamma A$, and $\therefore a = e\gamma A$

The above three constraints give

$$Qw = \frac{e\gamma Az^2}{ez+f}$$

Subtracting γAz from both sides,

$$Qw - \gamma Az = -\frac{f\gamma Az}{ez+f}$$

The final boundary condition is a consequence of vertical equilibrium ($Qw = Q_T - Q_m$) and the asymptote to which Qw tends. This asymptote is a function of Q_{max}, the maximum attainable vertical force in the material.

4. as $z \to \infty$, $Qw \to Q_T - Q_{max} = \gamma Az - (Q_{max} - Q_o)$

and $\therefore Qw - \gamma Az \to Q_o - Q_{max} = -\frac{f\gamma A}{e}$

Rearranging, $f = \frac{e(Q_{max}-Q_o)}{\gamma A}$

Substituting for f in the expression for Qw,

$$Qw = \frac{\gamma A(z)^2}{z+B} \qquad \text{where} \quad B = \frac{D}{4\mu' K} - \frac{h_1}{3} = \frac{Q_{max}-Q_o}{\gamma A}$$

Differentiating,

$$dQw = \frac{\gamma A[(z)^2+2Bz)dz}{(z+B)^2}$$

At depth z, the wall load varies as the product of circumferential area, $C(dz)$, and friction. Therefore

$$dQw = P_h C\mu' dz$$

from which

$$P_h = \frac{\gamma A}{\mu' C}\left[1 - \frac{1}{\left[\frac{z}{B} + 1\right]^2}\right] \qquad (2.7)$$

Both Janssen's and Reimbert's formulae have similar asymptotes as $z \to \infty$. Whereas Janssen's solution approaches this asymptote exponentially, Reimbert's solution takes a hyperbolic form. Therein lies the major difference between the two theories. A numerical comparison can be made with Janssen's method in Fig. 2.2.

Reimbert has made some provision in his theory for including as a surcharge the material cone commonly found at the top of siloed materials with centrally located charging chutes. For pressures at greater depths it is quite acceptable to treat the cone of material as a level surface originating at the centroid of the cone.

2.1.4 Characteristic or Numerical Methods

This approach encompasses a number of methods that formulate the equilibrium equations using a differential volume rather than a cross-sectional slice and therefore the solutions are labelled as "exact". This is a very subjective description because often the initial assumptions, such as the adoption of a particular failure criteria, are more important than the method of solution.

The standard elemental volume for plane strain conditions is depicted in Fig. 2.4 and the resulting equilibrium equations are

$$\frac{\partial \sigma_z}{\partial z} + \frac{\partial \tau_{xz}}{\partial x} = \gamma \qquad \frac{\partial \sigma_x}{\partial x} + \frac{\partial \tau_{zx}}{\partial z} = 0 \qquad (2.8)$$

Sokolovskii (1954) solved Eqs.[2.8] numerically for a retained soil mass using the method of characteristics.[1] The problem was statically indeterminate so he adopted the Mohr-Coulomb failure criterion;

$$\sigma_z = p(1 + \sin\phi \cos 2\psi) \qquad (2.9a)$$

$$\sigma_x = p(1 - \sin\phi \cos 2\psi) \qquad (2.9b)$$

$$\tau_{zx} = -\tau_{xz} = p \sin\phi \cos 2\psi \qquad (2.9c)$$

where p is the average of the principal stresses

ψ is the angle of rotation of the principal plane

---

[1] The solution for initial or boundary value problems can be considered as a surface over which the initial data propagates. It is these well-defined paths that are generally labelled as characteristics.

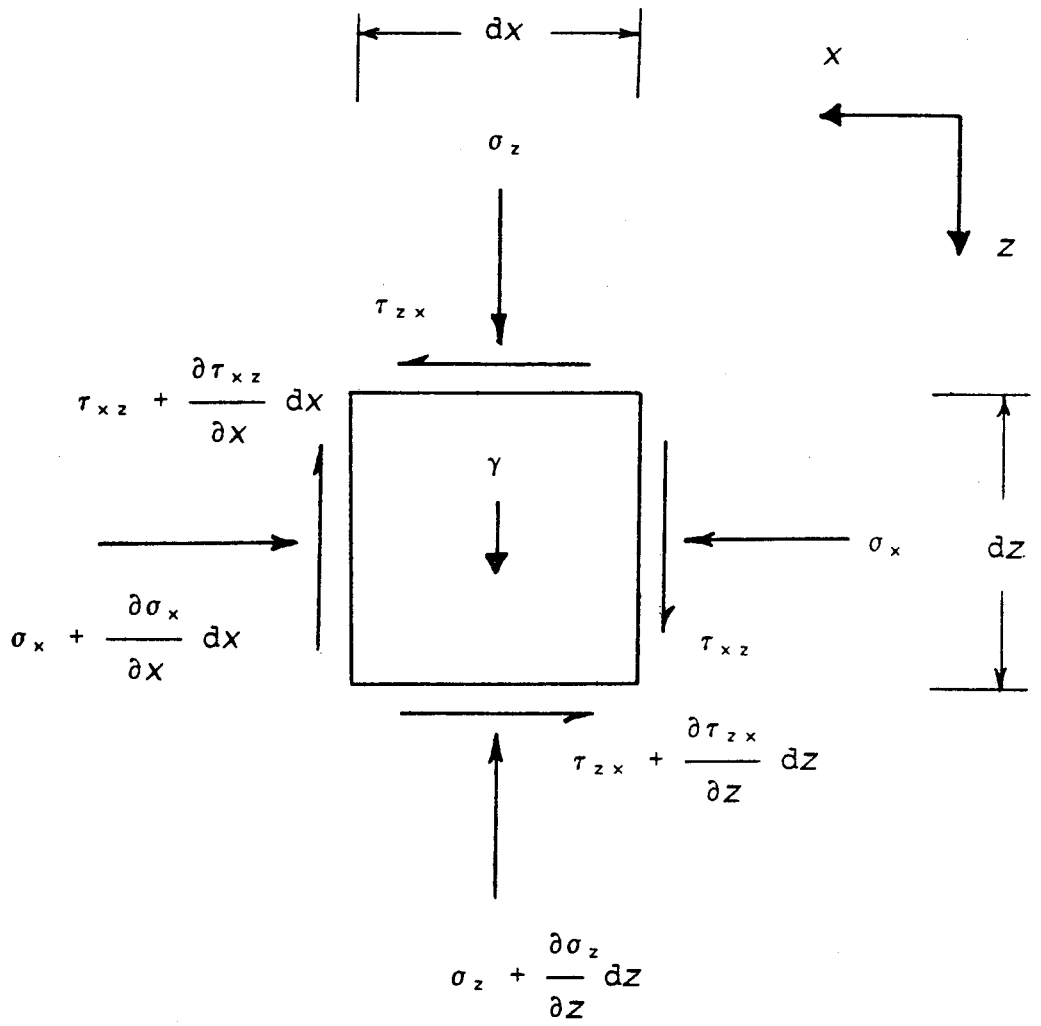

Figure 2.4 Average Values of Stress on a Material Element (Plane Strain)

Development of this criterion is described in Appendix A and its adoption assumes that throughout the mass, the material is in a state of incipient active failure. Given appropriate boundary conditions such as the surcharge at the material's surface and the frictional relationships at the bin walls (or a line of symmetry at the bin centre line), a numerical solution can proceed along a mesh of characteristics that intersect one another at the angle $\pi/2 - \phi$.

Savage and Yong (1970), Hancock and Nedderman (1974), and Horne and Nedderman (1976) have applied this technique to two-dimensional bins. Horne and Nedderman found that the solution followed a Modified-Janssen solution (Walker 1966) that tended to similar values with increasing depth. At shallow depths however, and depending on the amount of surcharge, this "exact" solution yielded distinct variations in the rate of change of material pressures that forced the pressure curve to oscillate about the Modified-Janssen solution. A characteristic, propagated from an upper corner (where the boundary conditions are discontinuous), will cause a discontinuity in the stress derivatives where it intersects the far wall.

Lvin (1970) suggested that vertical pressures are not uniform over a horizontal cross-section and he sought to remedy this by equilibrating vertical forces on a differential ring element (as opposed to Janssen's disc shaped element). He therefore formulated his equilibrium equations on what essentially is the free body in Fig. 2.5.

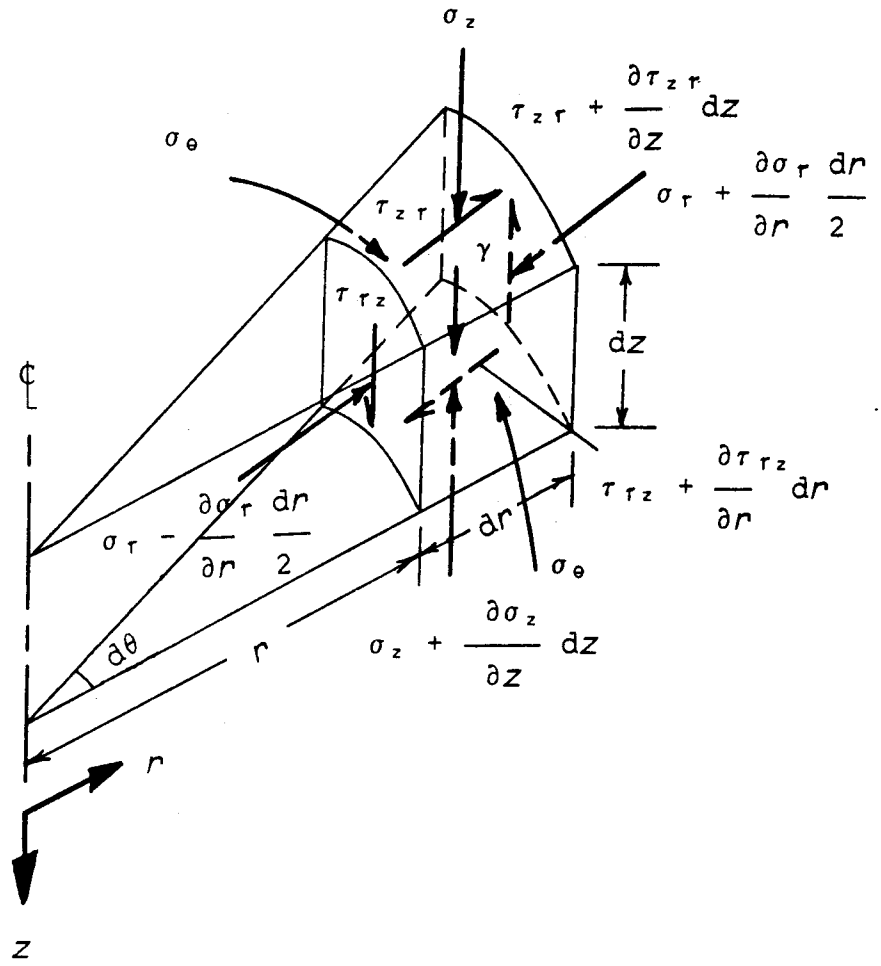

Figure 2.5 Average Values of Stress on a Material Element (Axisymmetry)

The equilibrium equations are;

$$\frac{\partial \sigma_z}{\partial z} + \frac{\partial \tau_{rz}}{\partial r} + \frac{\tau_{rz}}{r} = \gamma \qquad (2.10a)$$

$$\frac{\partial \sigma_r}{\partial r} + \frac{\partial \tau_{zr}}{\partial z} + \frac{\sigma_r - \sigma_\theta}{r} = 0 \qquad (2.10b)$$

The complete solution, not given here, describes a family of curves, of which Janssen's solution is the one in which P_h is made independent of horizontal coordinates. Lvin's suggested solution, the upper bound to this family, provides for a variation in lateral pressure over a cross-section, and in this sense has the potential to more accurately describe these pressures. He made one questionable assumption, however, to arrive at a solution for this upper bound curve. For vertical equilibrium in Eq.[2.10a] he used

$$\tau_{rz} = \mu' K \sigma_z \qquad (2.11)$$

This gave

$$\frac{\partial \sigma_z}{\partial z} + \mu' K \left[\frac{\partial \sigma_z}{\partial r} + \frac{\sigma_z}{r} \right] = \gamma$$

In fact, Eq.[2.11] only holds true at the wall. At the centre line of a bin, vertical shear becomes zero as required by symmetry. Lvin did go on to describe the true variation in τ as being linearly dependent on the distance from the centre however he held to his upper bound result because of its conservative position in the family.

His solution is unique in that it consists of two regions; the upper region of a cylinder exhibits a parabolic increase in pressure that becomes a tangent to the usual maximum lateral pressure common to the lower region, where it remains constant. The parabolic increase is described by

$$P_h(z) = \gamma K z \left[1 - \frac{\mu' K z}{4R} \right] \qquad (2.12)$$

The region of constant pressure begins at

$$z_c = \frac{D}{2\mu' K}$$

Substituting z_c for z in the lateral pressure formula,

$$P_h(z_c) = \frac{\gamma K D}{2 \mu' K} \left(\frac{1}{2}\right) = \frac{\gamma R}{\mu'}$$

which again is the maximum expected value for horizontal pressures.

This curve is also plotted in Fig. 2.2 for comparison with previously mentioned theories. Its concise formulation renders the method useful for design purposes, however, in light of the above remarks it would appear that it tends to overestimate lateral pressures.

2.1.5 Discussion

In Chap. 4, an extensional stiffness evaluation will be made using Janssen's formula but with the slight modifications described in Sect. 2.1.6.3 with respect to compressibility effects. The arguments in support of this decision are now presented.

Janssen's method was the first to emerge that dealt specifically and rationally with container pressures, and as such has received the most criticism in regard to the assumptions he used. Sundaram and Cowin (1979) questioned the assumption that the full frictional force at the walls is mobilized for if not, the Janssen solution would be a lower bound to the actual material pressures. They suggest that Janssen's formula be modified to an inequality, but of course this is not suitable for design purposes. On the other hand, Walker (1966) describes how the compression of loaded material below charging material will cause subsidation and subsequent full mobilization of wall friction. Walker's point of view has the obvious advantage in that it assumes the existence of some homogeneity throughout a granular mass, an assumption that is necessary at the outset if actual expected pressures are desired and not just a series of lower bound curves.

Criticism of Janssen's assumption that vertical and horizontal pressures are uniform throughout a cross-section have been raised by a number of authors. The solution provided by Lvin (1970) has been discussed in detail. The

Modified-Janssen solution given by Walker (1966) dealt specifically with this assumed cross-sectional nonuniformity by describing a variation in K over the cross-section. This was the end result of the assumption that the contained mass behaved as a Mohr-Coulomb material and not surprisingly Walker's solution can be thought of as a 'smoothed' approximation to the "exact" analysis presented earlier. Cowin (1977) rederived Janssen's formula in terms of 'average' vertical and horizontal pressures over the cross-section and perimeter respectively, related again by a constant K. This approach effectively circumvents the stated problem by restating it, however the question persists as to what effect cross-sectional nonuniformities have on K and the distribution of pressures overall.

The excellent study by Hancock and Nedderman (1974) revealed that the assumption of uniformity results in Janssen's solution as being only marginally different from a so-called "exact" method, and this discrepancy is of consequence only in the upper section of a silo. As the depth increases to the region in which vertical and lateral pressures are becoming constant with height, Janssen's assumption of uniform horizontal pressures is borne out.

This is easily demonstratable for the two dimensional case although the arguments are similar for the axisymmetric case. Shown in Fig. 2.6 is a layer of material at a depth where practically speaking there is no further increase in lateral wall pressure with depth. This will occur at depths

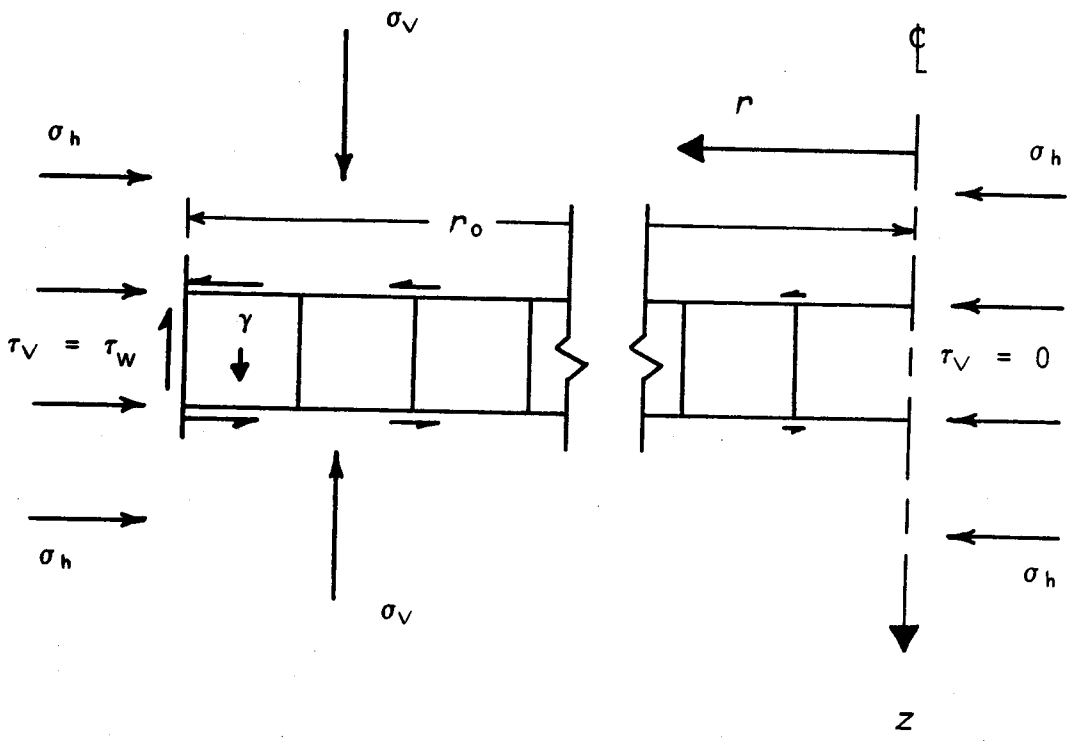

$$\sigma_h = P_{h\,max} = \frac{\gamma r_o}{2\mu'}$$

$$\tau_w = \mu' \sigma_h = \frac{\gamma r_o}{2}$$

$$\tau_v = \frac{\gamma r}{2}$$

$$\sigma_v = \sigma_h \; / \; K$$

Figure 2.6 Material Stresses at $z = \infty$

approximately 2 1/2 to 3 times the lateral dimension of the container but theoretically speaking when z reaches infinity. As the elements above and below are exerting equal but opposite horizontal shear on the upper and lower faces, horizontal equilibrium requires the lateral pressure to be everywhere equal. This condition is approximated everywhere within a contained mass (except near a nonlevel surface) because the horizontal shear on a cross-section is small when compared to the horizontal normal stress. This is in fact why Horne and Nedderman were able to show that Janssen's method is comparable to an "exact" solution, given the same value for K is used (Ka). The slight discrepancy is due to Janssen's implied use of a constant K across the section whereas the "exact" solution provides for a marginal variation in K across the section. Further examination of Fig. 2.6 suggests that vertical pressures are unknown unless a value for K is assumed because wall friction balances the weight of material at any cross-section, regardless of what levels vertical pressures attain. Assuming a constant value for K as did Janssen would result in the state of stress within the contained mass as being represented by a series of concentric Mohr's circles (the loci for horizontal and vertical pressures are parallel to the τ axis). This situation is graphically illustrated by the smaller Mohr's circles in Fig. 2.7.

This view of the state of stress within a contained bulk material is different from previous descriptions that

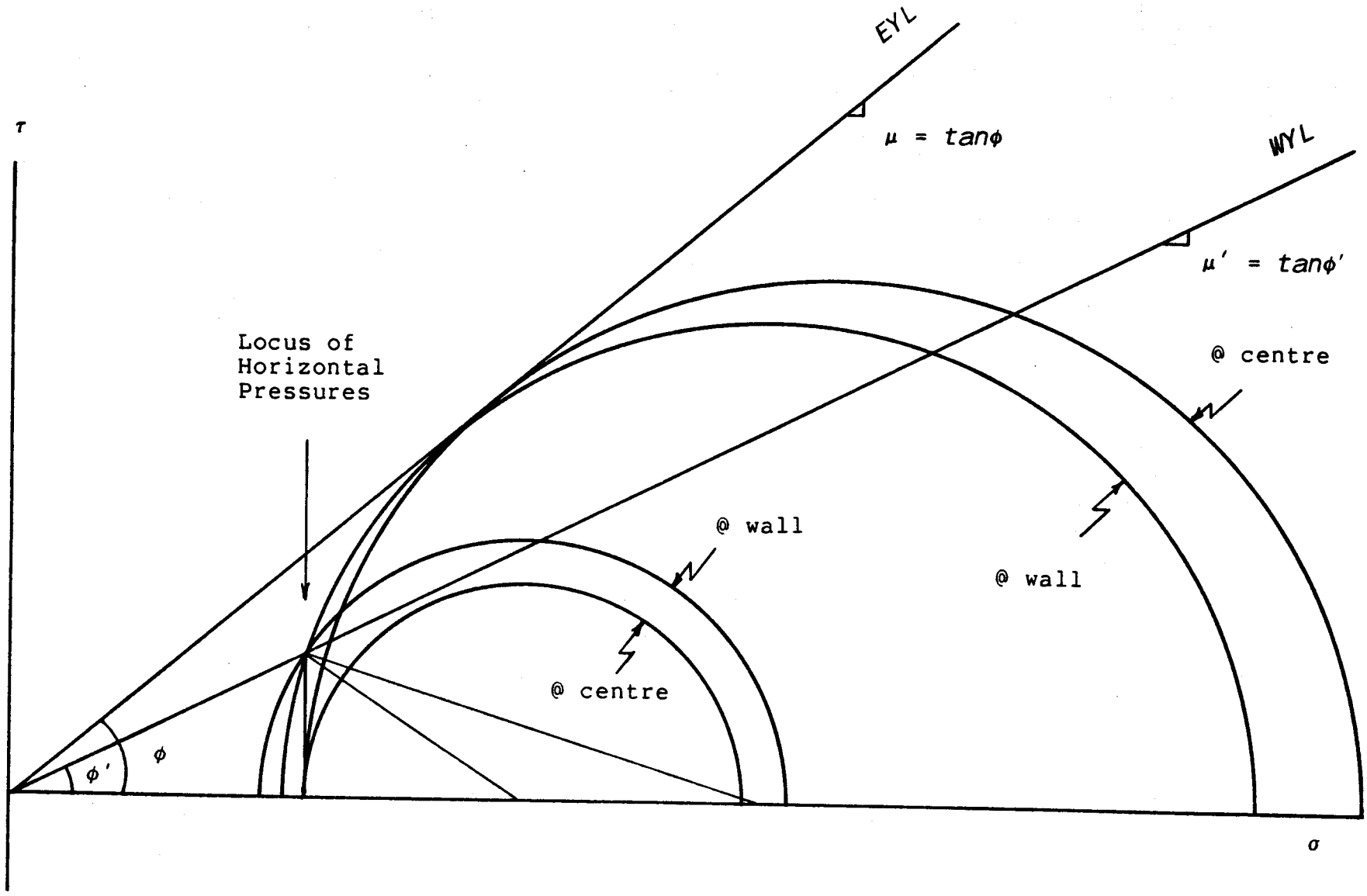

Figure 2.7 Mohrs Circle Representation of Stress States at $z = \infty$

tend to place the complete mass in a state of plastic equilibrium (incipient failure). Fig. 2.7 suggests that the mass can be considered to be in an elastic state while it is only at the walls (and only along a vertical plane) that incipient failure exists. The "exact" analysis, or similar approximations, are conducted using the Mohr-Coulomb failure criteron within an active pressure field, therefore assuming that an earth pressure coefficient relating *principal* stresses is in effect and at a minimum (= K_a) everywhere throughout the mass. At great depths, this "exact" solution also provides for uniform horizontal pressures through a cross-section however vertical pressures do not remain uniform. This is because K is forced to vary slightly as the centre line is approached in order that incipient failure is maintained. The larger Mohr's circles in Fig. 2.7 describe this condition.

Hence the argument switches from its original concern with the relative merits of each solution technique to a discussion of what value for K is most correct and whether or not a cross-sectional variation is justified. The plastic (limiting) solution assumes σ_1/σ_3 is a constant (= K_a) and therefore the bias is towards the effect principal stress orientation has on K. The elastic solution, if it assumes a constant K as did Janssen (and = σ_z/σ_x), has a vertical-horizontal bias. The discussion therefore must include such topics as deposition effects, consolidation effects, and shear effects on K, which together greatly

complicate matters. Certainly, within silos, consolidation strains are almost entirely vertical. It is important to state that assuming an elastic state of stress does not require K to be predefined as an active coefficient and perhaps an "exact" solution will surface that uses K as a variable parameter.

In reference to the distribution of vertical pressures on a cross-section, the two most comprehensive studies to date, one experimental (Lenczner 1963) and the other analytical (Chandrangsu and Bishara 1978), indicate that Janssen's assumption of uniform vertical pressures is for the most part correct. This is true providing the cross-section is reasonably distant from the boundary effects of a free surface or flat bottom. Because horizontal pressures must be uniform over a cross-section at greater depths, this would suggest that Janssen's use of a constant K (at a cross-section) is supportable. Janssen's use of a constant K over the complete silo height bares further examination.

The historical treatment earlier made reference to the fact that experimental studies found agreement with Janssen's predictions, however this was with the use of experimentally determined values for K. Therefore K will be examined as a separate and distinct parameter in the section to follow in order that we may better understand its range and variability.

2.1.6 Material Property Effects on Static Pressure Theories

2.1.6.1 The Coefficient of Lateral Earth Pressure, *K*

The coefficient of lateral earth pressure, defined as the ratio of lateral to vertical pressure, has been discussed briefly in preceding sections. In the discussion that follows the enormous variability and importance of this coefficient to lateral static pressures in silos will be examined.

Plastic theory for granular non-cohesive materials establishes two limits on *K*, known as the active and passive coefficients, *Ka* and *Kp* respectively. These coefficients, developed in Appendix A, are related numerically as inverses. To be strictly correct, the development of these two bounds should allow for wall friction effects however the theory is based on the assumption that there is no shear stress on a vertical surface. The vertical shear imposed by the wall on the contained mass in effect changes the direction in which the principal stresses act. Elementary texts on soil mechanics reveal this effect to be negligible on *Ka* but of some influence on *Kp*. In either case, theoretical soil mechanics describes the need for sufficient wall movement to take place before either limit is attained (i.e. incipient failure in the soil mass). These limits are depicted qualitatively in Fig. 2.8 for loose and dense sand.

Analytical evaluations of *K* for granular masses within a silo are numerous. Frequently they involve the manipulation of yield lines or failure envelopes on a Mohr's

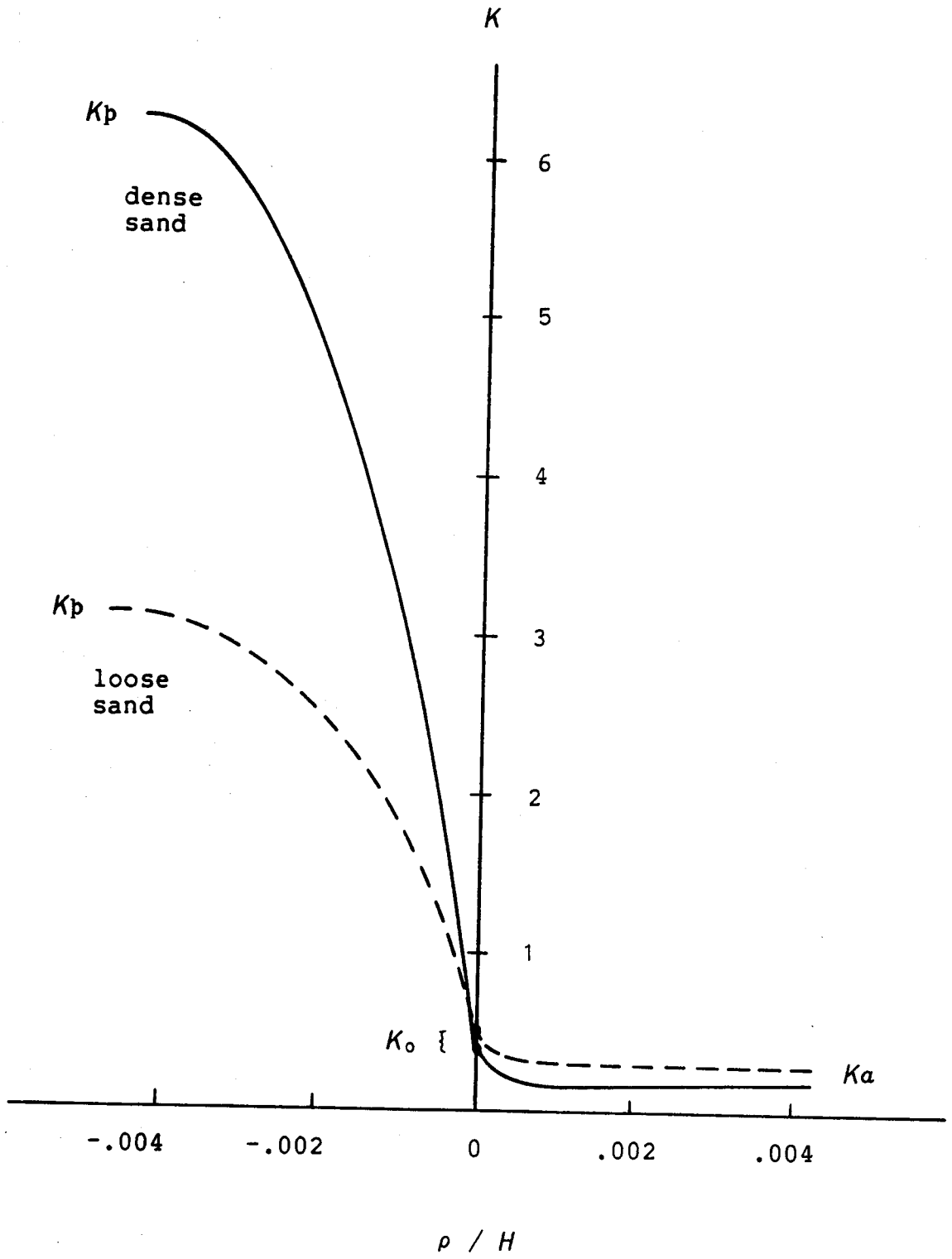

Figure 2.8 Relationship Between K and Wall Deflection

circle representation of the state of stress within the mass. The active and passive coefficients just mentioned are prime examples of this. Bagster (1971) suggests K should vary between the two limiting values;

$$Ka = \frac{1 - \sin\phi}{1 + \sin\phi} \qquad K = \frac{1 - \sin^2\phi}{1 + \sin^2\phi}$$

The latter ratio results from assuming that the bin wall is fully rough. This was earlier suggested by Dabrowski (1965) and Walker (1966), the former basing his recommendation on experimental work. Walker recognized that the principal stresses at the bin center are not equal to the principal stresses at the wall as apparently assumed by Bagster. Walker, working with the larger Mohr's circles in Fig. 2.7, derived a BD factor (generally a function of ϕ, ϕ', and z), that replaces $\mu' K$ in Janssen's formula but he concludes that these products are nearly equal for all but the very rough walled pipes. Because Walker has assumed incipient failure throughout the mass, (both curves touch the effective or powder yield locus, EYL) he must have a variation in K at a cross-section although the effective K is again similar to Ka. For any theory that assumes incipient failure throughout the mass, Eqs.[2.9a] and [2.9b] give K to be a function of principal stress orientation (in addition to being a function of the internal friction angle);

$$K = \frac{1 - \sin\phi \cos 2\psi}{1 + \sin\phi \cos 2\psi}$$

This would be true for cohesionless Mohr-Coulomb materials.

As material is charged into a silo and lateral pressures begin to build, a number of things may occur. The walls begin to extend and bend, the material itself will compress under the added weight, and some slippage may occur at the wall. These conditions may or may not lead to an active stress field at a particular location but there is good evidence in the literature that an active field will not occur simultaneously throughout the contained mass. (Stewart 1972, Mahmoud and Abdel-Sayed 1980)

That an active stress field will not likely occur in a full sized coal silo can be demonstrated as follows. Table 2.1 contains estimated vertical wall deflections required to develop limiting stress states in sand. For a cylindrical silo, radial wall movement is proportional to circumferential strain (the radius is proportional to the circumference). Because Table 2.1 was developed for semi-infinite masses against walls we will consider the situation at a depth equal to the radius so as to eliminate the effects of the far wall. For a seventy foot diameter silo, the circumferential strain required to achieve an active state of stress at a depth of 35 feet is

$$\epsilon = \frac{\Delta C}{C} = \frac{\Delta r}{r} = \frac{0.001 \times 35 \text{ ft}}{35 \text{ ft}} = 0.001$$

Table 2.1 Wall Displacements Required to Develop Active Pressures in Sand

State of Stress	Type of Movement	Displacement Necessary
Active	Parallel to wall	0.001 *H*
Active	Rotation about base	0.001 *H*
Active	Rotation about top	0.02 *H*
Passive	Parallel to wall	0.05 *H*
Passive	Rotation about base	>0.1 *H*
Passive	Rotation about top	0.05 *H*

Wu (1976)

As an example, the silo in this study exhibited initial static circumferential strains at depths of 35 feet approximately 1/5 to 1/7 of that calculated above. In addition, the stiffness evaluations in Chap. 4 will show that these strain measurements were made at locations of greater than average flexibility. It may be argued that within a cylindrically shaped mass of material, a radial wall movement would require less material to strain than for the two-dimensional case. Lambe and Whitman (1979) tested triaxial specimens and found that horizontal strains of 0.005 are required to take sand from the at-rest to the active condition, a level 5 times that calculated above and 25 to 35 times that measured.

It is therefore reasonable to ask whether K approaches or possibly exceeds a value equal to K_o , the at-rest coefficient of lateral earth pressure. Fig. 2.8 indicates that an inward wall movement is normally required for K to exceed K_o in the wall movement experiment however, if the material is being compressed by the weight of charging material, the conditions are no longer the same. Terzaghi (1934) obtained a value for K_o of about 0.40, based on his wall movement experiments with sand. Jaky (1948) predicted that K_o could be approximated by $1-sin\phi$ and this was later supported experimentally by Bishop (1958) for normally consolidated soils. Applying this approximation to a cleaned angular coal with ϕ of 38 to 40 degrees, produces a K_o of 0.384 to 0.357, well above an associated Ka of 0.23. Blight

and Midgley (1980) have followed Bishop's procedures in determining K_o for such a material and found a value of 0.48. This value occurred with increasing vertical pressures in the 2000 to 8000 psf range. With decreasing vertical pressures, K_o jumped up to a value near unity.

The values for K cited above are for experimental evaluations of K_o. More appropriate are experimental evaluations for K as it pertains to ensiloed materials. Sundaram and Cowin (1979), in a 'reassessment of static bin pressure experiments', discuss the work of Jamieson (1903), Caughey *et al.* (1951), and Huang and Savage (1970) in this area. Their technique is to take the lowest reported set of vertical and/or horizontal stress data and, using least squares, curve-fit to Janssen's formula to find $\mu' K$ and/or K. They suggest that lower bound data occurs when mobilized wall friction is a maximum, even though there are a number of other possible reasons for inconsistent results in tests of this nature. In a table of recommended values for K, they suggest a K for wheat of 0.57-0.64, a K for cement of 0.38-0.40, and a K for sand of 0.50-0.55. Jenike *et al.* (1973 Part 3) reported that a value of 0.40 reasonably predicted static lateral pressures of sand in a model cylinder, using Janssen's formula.

At this point, it becomes expedient to develop a physical understanding for K. Sundaram and Cowin (1979) suggest that K is a material property through which vertical

pressures translate into lesser horizontal pressures, or vice-versa for the passive case. It is a mechanism whereby interstitial penetration imparts some component of thrust at 90 degrees to this penetration.

The mechanism itself is complex, however recent developments in stochastic modeling of particulate media have produced some interesting insights. Harr (1977) outlines the theoretical considerations necessary for a probabilistic determination of K in two and three dimensional particulate systems, assuming the material behaves elastically. The results for the two dimensional system are particularly note-worthy in that this situation models a long-sided rectangular bin (a plane strain condition) or a large diameter cylindrical bin (which in the limit approaches a two dimensional wall and that effectively experiences no circumferential material strain). The similarity between the experimental evaluations for K_o discussed above and the value predicted of $\pi/8$ (0.39) is encouraging, at least to elasticians.

The above discussion of the lateral earth pressure coefficient does not mean to suggest that K is not extremely variable, but rather to place emphasis on possibly better representations for an initial K than those currently employed by codes. As Fig. 2.8 clearly indicates, relatively slight wall movements will considerably alter K, and there are at present no theories that can adequately predict this relationship for a wide range of materials and properties.

To complicate this discussion on the lateral earth pressure cofficient would be to suggest that K may vary in the vertical direction within a storage vessel. Until recently, K has usually been considered a constant in experimental evaluations as well as in the design process. At much greater depths, Lambe and Whitman (1979) describe how increased vertical pressures within a laterally confined mass will bring about a stiffening of the material (increasing ϕ) with an ensuing reduction in K_o.

A study by Kramer (1944) on rough rice indicates that, for small depths, K may have a variation with depth opposite to that just described for confined materials. Using a bin one foot square by two feet deep, he found that K increased rapidly from 0.30 as a superposed vertical load was applied and soon leveled off at a value of 0.48. Although the plot of K versus load appeared to extend from the origin, the curve could not be extrapolated to this point because with zero vertical and lateral pressures, K is of course undefined.

Well documented tests by Lenczner (1963) on sand contained within a 10 inch diameter model silo do shed some light on the initial portions of this curve. Lenczner plotted K as a function of the depth to diameter ratio. He calculated a required K such that Janssen's equation could be made to satisfy measured wall and bottom loads. Again K could be observed to increase to a constant value, this time leveling off at 0.21. This is well below the active

coefficient for a material with ϕ = 32° (Ka = 0.31) and less than half of the at-rest value (K_o = 0.47). Important here was the decrease in K to zero at zero depth.

Neither Kramer nor Lenczner offered an explanation for results that are at first glance inconsistent with established concepts of K for ensiloed materials. The results can be explained however if K is considered to be some function of relative density[1], Dr. In its loosest state, a material has a relative density of 0%; in its densest state, 100%. This coincides with the above observed variation in K and ties in somewhat with the discussions by Harr (1977) on the influence porosity might have on K. A functional relationship such as this is really an endpoint definition that in fact may be difficult to observe. At the first layer of particles K is of course zero however at subsequent layers a jump in K will occur. Glastonbury and Bratel (1966) used inelastic spheres to model this effect for many layers and found K increasing from 0.138 to 0.167. They also reported that packing densities had considerable influence. Results such as these might be expected for zones of very low pressure where a vertical deposition process has taken place.

The three studies mentioned thus far indicate a limiting value for K. In Lenczner's experiment, this limiting value was not a maximum K (i.e. K_o) nor even Ka but

---

[1] Relative density is given by;

$$Dr = \frac{\gamma_{dmax}}{\gamma_d} \times \frac{\gamma_d - \gamma_{dmin}}{\gamma_{dmax} - \gamma_{dmin}} \times 100\%$$

an unknown value apparently determined by the actual degree of consolidation. The maximum vertical pressure in Lenczner's "silo" was well below what might be achieved in larger diameter silos. Using the reported wall friction angle ϕ' of 25° (μ' = tan 25° = 0.466) and the reported average density of 100 pcf, the maximum attainable vertical pressure in a 10 inch diameter silo is, from Eq.[2.4]

$$P_{V_{max}} = \frac{\gamma R}{\mu' K} = \frac{(100\text{pcf})(10/12)\text{ft}/4}{(0.466)(0.21)} = 213 \text{ psf}$$

and

$$P_{h_{max}} = 45 \text{ psf}$$

The curve describing K leveled off at a ratio z/D of approximately 10 (100 inches down) so that in a large diameter silo P_V at this same depth would be expected to be about 4 times the maximum vertical pressure calculated above. This would occur however at a level only 8 feet into the larger silo, a relatively shallow depth for most bins. The foregoing suggests that K might require interpretation, at least in small model studies, in relation to the bin diameter.

Both Lenczner and Kramer did not supply enough information to calculate actual relative densities and therefore it is only possible to speculate on what type of relationship may exist between K and Dr. The literature examined thus far tends to support the following relationship;

$$K = Dr^{m}K_{m} \qquad (2.13)$$

where m is at this time an undetermined quantity and K_m is a maximum value for K, similar to K_o but not necessarily limited by.

A generalized plot of this relationship is shown in Fig. 2.9 but with material height z as the abcissa instead of relative density. The particular curve that a material exhibits is dependent on the value chosen for m, the material's compressibility, and the rate of attenuation of larger vertical pressures (i.e. geometry effects). Excepting the works of Kramer and Lenczner, material pressure observations are normally made at depths sufficient to miss this initial zone where K may be increasing. The later reduction in K_o at greater pressures is also illustrated conceptually in Fig. 2.9.

To summarize this discussion of the lateral pressure coefficient and its influence on initial static pressures within contained materials, we can say without exaggeration that it is the least understood but the most important of the various material parameters. It is clear that K is more related to K_o than to Ka however the relationship is not well defined. Revisions to DIN 1055 (Martens 1980) will incorporate this viewpoint with the adoption of Jaky's expression for K_o, $(1-sin\phi)$, however this will be in lieu of tabulated values for a static K. For a perfectly elastic, homogeneous, and incompressible particulate material, K

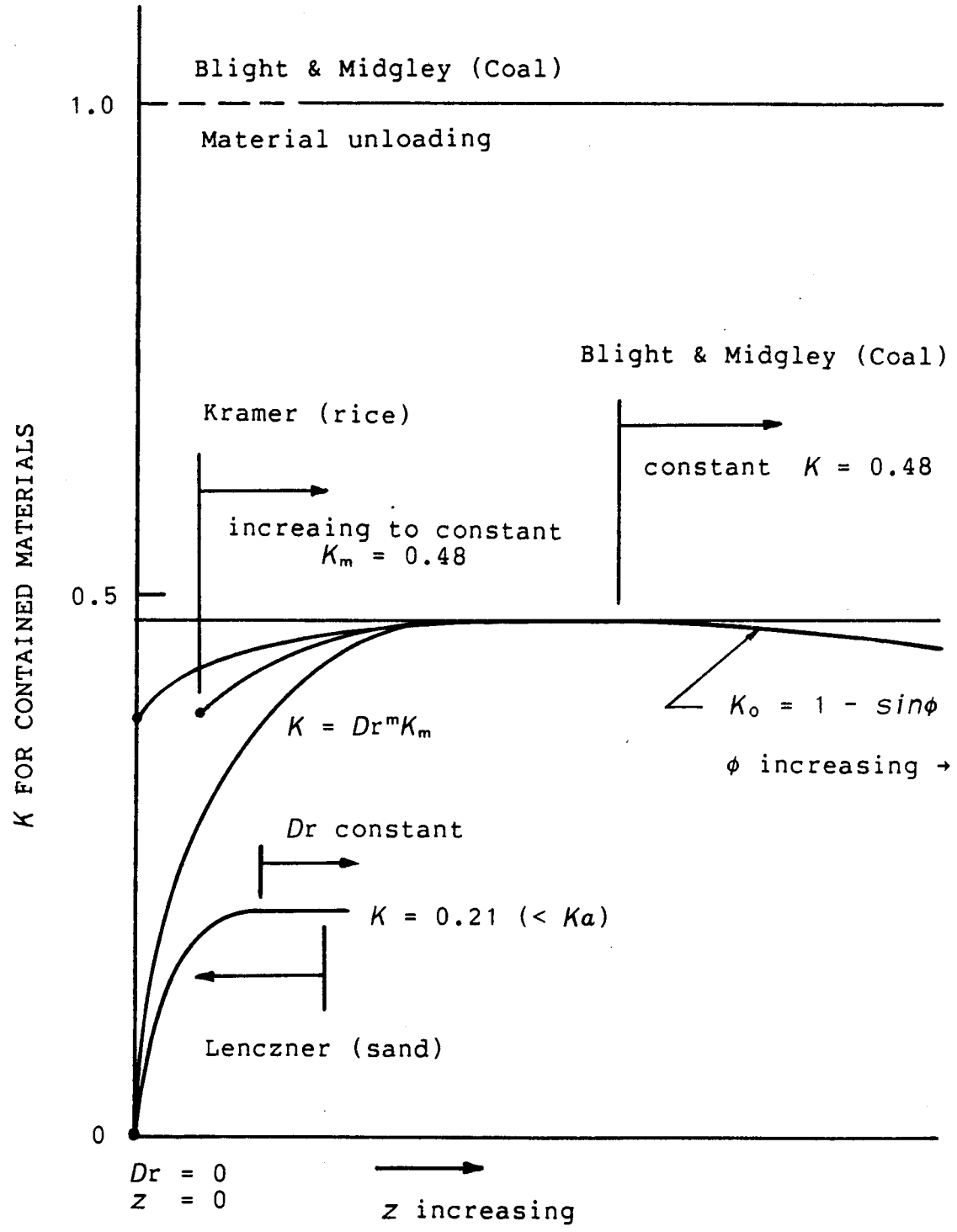

Figure 2.9 Observed Variations in K

should be close to 0.39 in the two dimensional case and close to 0.33 in the three dimensional case (Harr 1977). In general, compressibile materials exhibit a larger K (e.g. grains) while lower consolidating pressures may result in a reduced K, possibly below an active coefficient. There is some evidence that K may vary significantly within a contained mass at small depths.

When using a constant K in Janssen's formula, the actual value chosen has its greatest effect on lateral pressures at the free surface, where lateral pressures are smallest. Here they change in a manner that is directly proportional to changes in K. This influence reduces to zero as the depth becomes large and hence Eq.[2.6] does not contain this parameter.

2.1.6.2 Wall Friction

Wall friction is the one parameter responsible for the exponential, hyperbolic, or parabolic shape of the lateral pressure curve for silos. The friction coefficient, μ', is equal to $\tan \phi'$, where ϕ' is the wall friction angle. Although its macroscopic contribution to the reduction of lateral pressures in silos is well understood, the microscopic mechanisms involved are still under discussion (Lambe and Whitman 1979).

Students of soil mechanics generally subscribe to the adhesion theory which implies that friction is independent of surface roughness. For two surfaces in contact, the weaker material will plastically deform until the contact

area Ac is equal to the normal force N divided by the material's compressive strength, f_y. The maximum attainable shear force T_{max} is then the product of the contact area and the material's shear strength, f_V;

$$Ac = \frac{N}{f_y} \qquad T_{max} = f_V Ac = N \frac{f_V}{f_y} = N\mu_s'$$

Hence the maximum shear force to impending motion is directly proportional to the normal force and a material parameter μ_s'. The subscript s denotes that this is a static coefficient. The kinetic coefficient is normally less than its static counterpart and will be discussed in the second part of this chapter.

As the surface roughness increases, microscopic protuberances, (asperities), begin to interlock with greater frequency and thereby increase the friction coefficient. If a wall is fully rough or corrugated in some horizontal manner, the angle of wall friction becomes the angle of internal friction of the material. In this case larger shearing forces are required to overcome rolling, sliding, and lifting resistances. If graded materials are being deposited in a central cone, larger particles will collect at the walls. As the average particle size increases, μ' should decrease; with the centre of gravity farther from the plane of shear, rolling becomes easier (Rowe 1962). This has important ramifications for predicting silo pressures using shear box results for μ'.

More generally, wall friction is a property of a granular material and the type of surface it impinges on and it is determined experimentally. A shear box or shear cell apparatus is often used in this endevour and because ACI 313-77 only provides ranges of values for certain materials, this test is normally specified as a design parameter. DIN 1055 gave the wall friction angle as 75% of ϕ for the filling case and 60% for the emptying case. Current revisions to this code (Martens 1980) will give μ' for various materials and for three degrees of wall texture (fully rough, semi-smooth, and smooth). This change may primarily be due to a study by Pieper (1969) that suggests wall friction will tend to a certain value for many different surfaces as continued use causes material to rub off at the rougher locations.

The quantitative effects of varying μ' or the errors introduced by assuming μ' different from a truly effective friction coefficient, become constant as depth becomes large. The lateral pressure asymptote, $\gamma R/\mu'$, indicates this constant amount is approximately the inverse of the change in μ'. A 10% increase and decrease in μ' gives respectively (-)9.1 and (+)11.1 percent changes in pressure and these are maximum errors. As z increases from zero in Eqs.[2.5], [2.7], and [2.12], the errors increase from zero; at 50 feet, with K = 0.4, R = 17.5′, and μ' = 0.50±10%, Janssen would predict a ±2.5% change in lateral pressure, Reimbert a ±5% change, and Lvin a ±1.7% change. Therefore, for lesser

material depths, reasonable errors in the assumed value for μ' have a negligible effect on lateral pressures.

2.1.6.3 Bulk Density and Compressibility

For granular materials, bulk density depends on particulate properties such as size and shape, the manner of assembly of these particles, and the specific gravity of the constitutive solids. Examining the three initial pressure theories presented thus far, Eqs.[2.5], [2.7], and [2.12], it is immediately apparent that in all three, horizontal material pressure is a direct function of unit material weight. Many granular materials exhibit a variable unit material weight and for bulk solids such as grains, cement, and granular coal, this variation can be sizeable. For example, the cleaned coal delivered to the silo in this study could be placed with a unit weight from 40 to 60 pcf, depending on the consolidating pressure. This 50% increase in γ obviously must have some influence on vertical and therefore horizontal initial pressures.

General practice in most design situations has been to use a maximum expected density for γ. This is only slightly conservative for most materials in most silo applications however for a small head of material (or for a very compressible material) this can lead to inaccuracies. The lower coal heads that are used in the analysis in Chap. 4 suggest this may be a consideration. Hence a critical examination of possible variations in the material density is required.

Granular materials undergo volumetric changes in a variety of mechanisms but for the vertical stress ranges that ensiloed materials experience (i.e. 0 to $\gamma R/\mu' K$ during initial charging), the primary mechanism is 'locking' (Lambe and Witman 1979). In this range, structural deformations result in a progressive stiffening of the particulate system, hence a nonlinear stress-strain relationship exists. In soil mechanics terminology, this material property is called compressibility and the associated parameter, Cc (the compression index) is used to relate void ratio e with the logarithm of pressure p on the well known e - $log\ p$ curve:

$$Cc = -\frac{\Delta e}{\Delta log\ p} \quad \text{or} \quad e = c_1 + Cc\, log\ p \qquad (2.14)$$

Density and void ratio are related from first principles by the following expression for total unit weight;

$$\gamma_T = \frac{1 + w}{1 + e} G_s \gamma_w \qquad (2.15)$$

where w = water content by weight

G_s = specific gravity of solids

γ_w = unit weight of water

Jenike has found that, over a certain range of γ, material unit weight is well represented by this formula;

$$\gamma = \gamma_0 \left[\frac{\sigma_1}{\sigma_0}\right]^{\beta} \quad \text{or} \quad log\ \gamma = log\ C_\beta + \beta log\ \sigma_1 \qquad (2.16)$$

Here σ_1 = vertical or consolidating pressure

σ_0 = initial or contact pressure, usually 13.0 psf

γ_0 = initial unit weight

β = Jenike's compressibility coefficient

C_β = a constant $(= \gamma_0/[\sigma_0]^{\beta})$

This relationship appears reasonable if a plot of $log\ \gamma_T$ versus e from Eq.[2.15] is examined (Fig. 2.10). The near linear relationship between $log\ \gamma$ and e and the well established linearity between e and $log\ p$ (within certain ranges), together indicate that Jenike's equation can be tied in with conventional soil mechanics parameters.

These relationships have enabled the writer to develop a formula for describing initial stress fields, while at the same time allowing for a variable density utilizing Janssen's simplifying but reasonable assumptions. The advantage of Eq.[2.16] over the more familiar Eq.[2.15] is that it can readily be inserted into Janssen's equilibrium equation, (Eq.[2.1]), developed from Fig. 2.1, because γ occurs as a function of σ_z (or σ_1) rather than void ratio. Jenike's expression for γ is substituted into Eq.[2.1];

$$\frac{d\sigma_1}{dz} = \gamma_0\left[\frac{\sigma_1}{\sigma_0}\right]^{\beta} - \frac{\mu' K \sigma_1}{R} \qquad (2.17)$$

$$= C_\beta \sigma_1^{\beta} - c_2\sigma_1$$

$$\int \frac{d\sigma_1}{C_\beta \sigma_1^{\beta} - c_2\sigma_1} = \int dz \quad \text{or} \quad z = \int \sigma_1^{-1}(C_\beta \sigma_1^{\beta-1} - c_2)^{-1} d\sigma_1$$

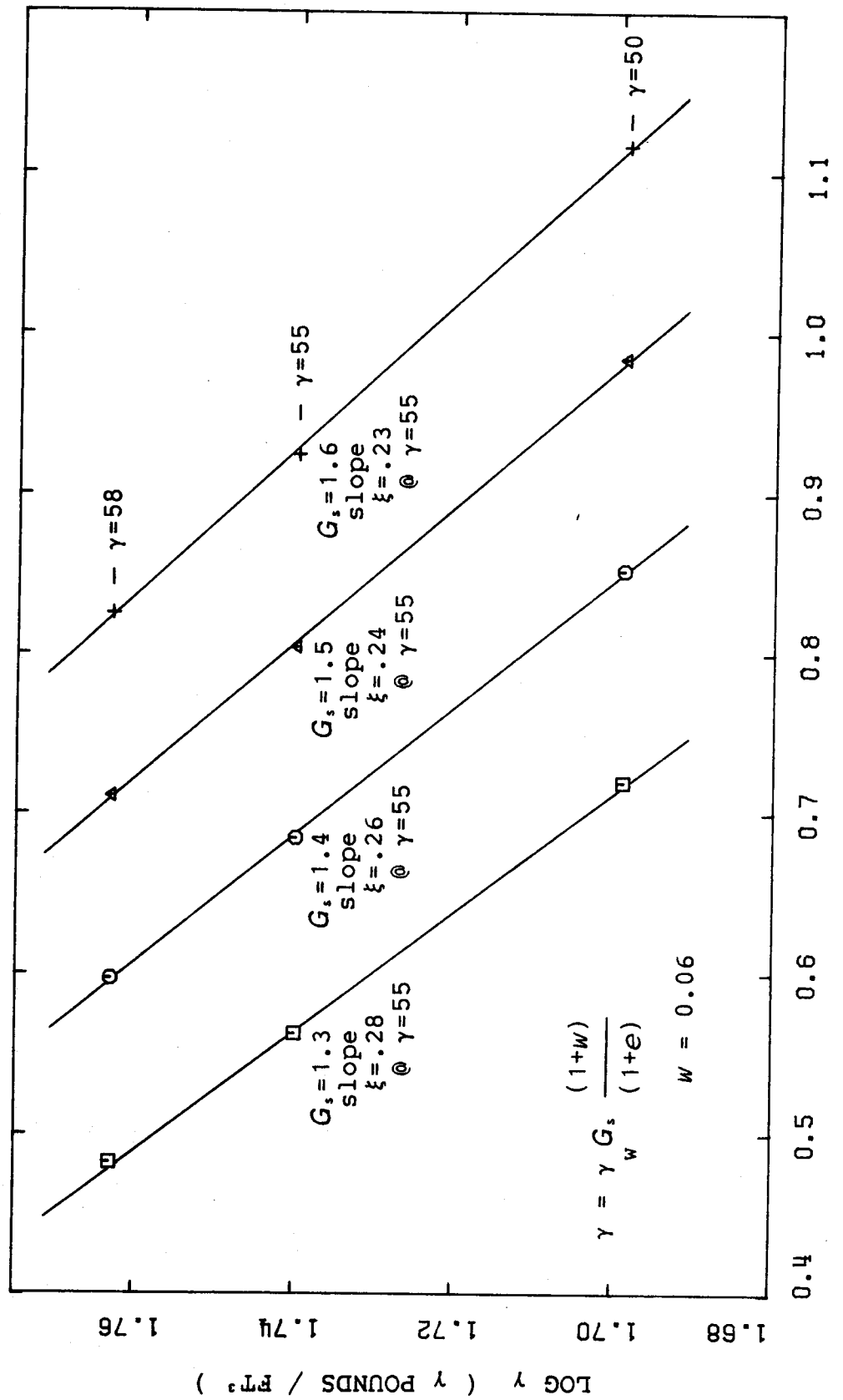

Figure 2.10 Relationship Between Void Ratio and Unit Weight

The following substitution is useful at this time:

$$\sigma_1 = \left[\frac{u + C_2}{C_\beta} \right]^{\frac{1}{\beta-1}}$$

Performing the above integration with respect to u yields the expression for z (the constant of integration vanishes because $\sigma_1 = 0$ at $z = 0$),

$$z = \frac{\ln \left| 1 - \frac{C_2}{C_\beta} \sigma_1^{1-\beta} \right|}{C_2(\beta-1)} \qquad (2.18)$$

Rearranging,

$$1 - \frac{C_2}{C_\beta} \sigma_1^{1-\beta} = e^{zC_2(\beta-1)}$$

Substituting for C_2 $(\mu' K/R)$;

$$\sigma_1^{1-\beta} = \frac{C_\beta R}{\mu' K} \left[1 - e^{-\mu' K z(1-\beta)/R} \right] \qquad (2.19)$$

and

$$\sigma_2 = K\sigma_1 = P_h$$

Eq.[2.19] is very similar to Janssen's equation and in fact becomes so when β is taken as zero (the material is assumed incompressible).

In Reference [39], a series of material tests are reported on for various samples of cleaned coal products expected to occupy the Fording silo. Most of these results

are discussed in Chap. 3, however, to underscore the contribution of compressiblity effects on intial pressure fields, some quantitative input is required at this time. Plots of unit weight against effective material head for coal at various moisture contents were given and from the 6% moisture content curve, a number of points were taken. The respective logarithims of these values are shown plotted in Fig. 2.11 and the resulting near linear relationship lends support to Eq.[2.16]. The slope of this line is β and is calculated as 0.0786. Reference [39] also gave the initial contact pressure, σ_o, to be 13.0 psf and the range of γ over which Eq.[2.16] is applicable as 38 - 58 pcf. If β is known then the initial material density, γ_o (or more directly, C_β), can be calculated. Horizontal (or vertical) pressures calculated using Janssen's formula can be compared to results using Eq.[2.19], and the effects of material compressibility become readily apparent. Table 2.2 summarizes this comparison and indicates clearly the loss in accuracy that occurs when Janssen's formula is applied to a compressible material. The two solutions do however merge at greater depths.

Table 2.2 Errors Induced by Ignoring Material Compressibility

z Coal Ht. (ft)	Janssen		Janssen-Compressibility		% Deviation
	γ (pcf)	P_h * (psf)	$\gamma(z)$ (pcf)	P_h ** (psf)	
10	58.0	219.2	49.4	172.7	27
20	58.0	414.8	52.1	346.5	20
30	58.0	589.2	53.7	509.4	16
40	58.0	744.8	54.8	659.8	13
50	58.0	883.6	55.7	797.5	11
60	58.0	1007.4	56.3	923.1	9
70	58.0	1117.9	56.8	1037.3	8
80	58.0	1216.4	57.3	1140.9	7
90	58.0	1304.2	57.6	1234.8	6
100	58.0	1382.6	57.9	1319.8	5

$K = 0.40$ $\quad \beta = 0.0786$

$\mu' = 0.50$ $\quad \sigma_o = 13.0$ psf $\quad \gamma(z) = \gamma_o \left[\frac{P_V}{\sigma_o} \right]^{\beta}$

$R = 17.5$ ft $\quad \gamma_o = 37.48$ pcf

$\gamma = 58.0$ pcf $\quad C_\beta = \gamma_o / [\sigma_o]^{\beta}$

$$* \; P_h = \frac{\gamma R}{\mu'} \left[1 - e^{-\mu' K z / R} \right] = K P_V$$

$$** \; P_h = K \left[\frac{C_\beta R}{\mu' K} \left[1 - e^{-\mu' K z (1-\beta)/R} \right] \right]^{\frac{1}{1-\beta}} = K P_V$$

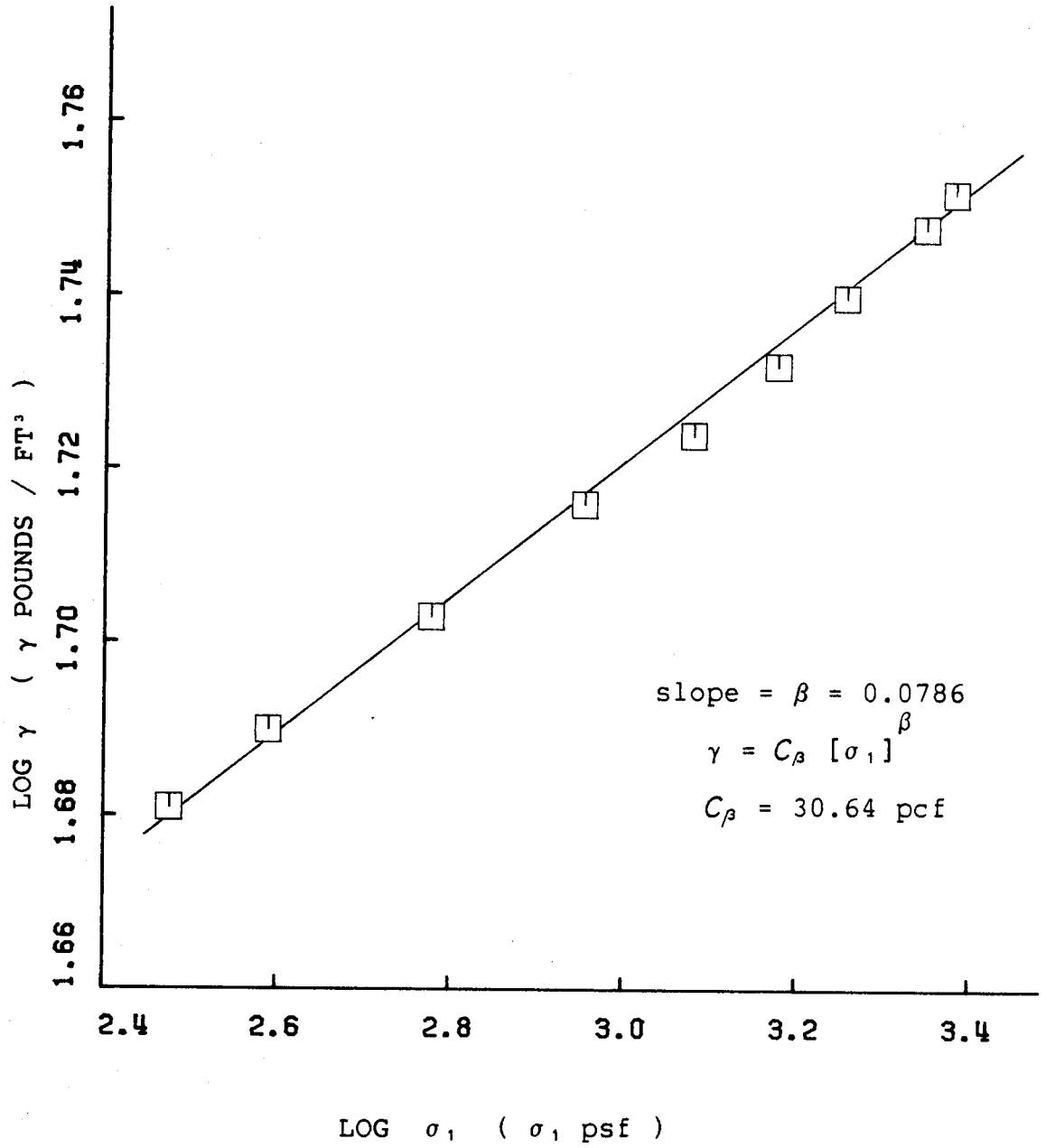

Figure 2.11 Relationship Between Unit Weight and Consolidating Pressure

2.2 Flow Pressure Theories - Mass Flow

2.2.1 Introduction

Flow within silos manifests itself in two distinct and limiting patterns; mass and funnel flow. Mass flow is said to occur when the flow channel boundary coincides with the storage vessel's walls. Funnel flow occurs when the flow channel boundary is within the contained material. Recognition of this physical distinction can be attributed to Turitzan (1963) however Jenike (1964) has developed the analytical techniques required to define the limit between the two flow patterns.

The pattern of flow is influenced by the outlet geometry and it follows that a material flow may incorporate elements of both flow types simultaneously. An expanded flow bin utilizes mass flow outlet hoppers in order to expand the flow channel into the bin, thereby restricting the formation of large stable ratholes. Alternatively, a funnel flow hopper may have its flow channel expand independently until it meets the bin wall, and above this point mass flow can be said to occur. Obviously, it can be argued that within any funnel of flowing material, a mass flow exists.

Qualitatively, two conditions must be satisfied for true mass flow. For a given bulk material, the outlet hopper must not exceed a limiting combination of inclination from the vertical and material-hopper wall friction. This requires that mass flow systems provide greater hopper

heights and consequently greater silo heights. The second condition requires that sufficient vertical pressures must act on the material in the hopper to exceed the radial material pressures (Jenike and Johanson 1968). Although less critical, this condition provides for situations wherein a mass flow bin-hopper may revert to a funnel flow bin-hopper after a certain amount of material has been withdrawn. Of course actual flow is always predicated on the requirement that the outlet itself is large enough to prevent a stable arch from forming.

Funnel flow results in lower dynamic wall pressures than those due to mass flow and this can be attributed to the muffling effect of non-flowing material against the walls. Mass flow is however desirous in many applications; the essential advantage is that it creates a relatively rapid and problem free material withdrawal. In a bin of this type, there are no dead zones and therefore storage capacity is one hundred percent of the contained volume. First in - first out is a term that refers to an important mass flow storage feature. Certain bulk material properties may change and/or the material itself may deteriorate with time and therefore might require sequential handling. In addition, this feature allows, to some extent, the layering of different grades of materials however this would be practical only with a centrally located discharge chute. Finally, it is extremely difficult to eliminate particle segregation completely using any charging method. The radial

flow inherent to mass flow hoppers allows for the continuous remixing of particle sizes even in continuous flow operations.

Within a multitude of flow pressure theories that have surfaced within the recent quarter century, few have attempted to differentiate between mass and funnel flow other than in descriptive terms only. All of the discussions to follow deal generally with the prediction of mass flow material pressures. To date, the strain energy method proposed by Jenike, Johanson, and Carson (1973) is the only presently available analytical technique that rationally attempts to predict levels of overpressure in a mass flow situation and that also has some experimental support. For this reason, the Jenike method will be discussed in detail in the following section and only brief mention will be made of alternate dynamic theories.

2.2.2 Jenike's Energy Method

Jenike *et al.* (1973 Parts 3 & 4) have developed analytical methods for dealing with both mass and funnel flow in bins, relying on an energy approach with the former. In short, Jenike's method places an upper bound on wall pressures through minimizing the elastic (recoverable) strain energy in a mass of bulk solid.

Jenike *et al.* (1973 Part 2) observed wall pressures in models of flowing bulk materials. They found that a diverging channel of 0.5 degrees resulted in flow pressures

being similar to a Janssen distribution while with the introduction of ledges or by using a 0.5 degree converging channel, local pressures often exceeded a Janssen distribution by a factor of two or three. Apparently, thin boundary layers form at the walls that try to reshape a cylinder into a slightly converging shape. According to the authors of this theory, it is with this shape that a minimum energy field can fully develop. Geometric and material inhomogeneities continually cause the formation and breakdown of these boundary layers, thereby resulting in intermittent and/or oscillatory wall pressures, as the field 'switches' from a Janssen to a minimum strain energy distribution. This so-called 'switch' can conceivably locate at various vertical positions in a bin and it is there that large overpressures (discontinuities in the lateral pressure curve) are predicted. An envelope enclosing these maximum expected pressures is therefore an upper-bound solution.

To develop this upper-bound for a given bin geometry and material, a number of simplifying assumptions must be made.

1. The switch is assumed to locate at some level z. Above this level, a Janssen field is assumed to prevail while below this level elastic strain energy is minimized.
2. Symmetry is assumed to exist, either two dimensional (plain strain) or axial symmetry and here Janssen's assumption of constant pressure throughout a slice is employed.

3. Kinetic energy is neglected and both the modulus of elasticity E and Poisson's ratio ν are considered constants.

Using coal properties and geometries pertinent to the Fording silo, the Jenike solution provides the curves given in Fig. 2.12. Curve I represents the instantaneous lateral pressures; the pressure discontinuity reveals the switch location used here. By arbitrarily assuming the switch to locate at various positions, the envelope of maximum material pressures is defined (Curve II in Fig. 2.12). Jenike *et al.* discussed their findings when they include in the solution the minimization of strain energy from the material contained in the hopper. They suggest that the curve be modified, as has been done in Fig. 2.12 to include for this effect, by assuming no reduction in the maximum lateral pressure once attained. They further suggest that the strain energy contained in the vessel's walls should also be included in the minimization. The writer has carried this aspect of the strain energy theory a step further by including for this effect in the original formulation. This slight addition to the work of Jenike, Johanson, and Carson is presented at the end of this section.

It will now be evident that calculating Jenike's maximum predicted lateral pressure for a given silo requires knowledge of that location of the switch that produces this maximum. Jenike *et al.* left their solution in a form not readily conducive to this task and therefore a condensed

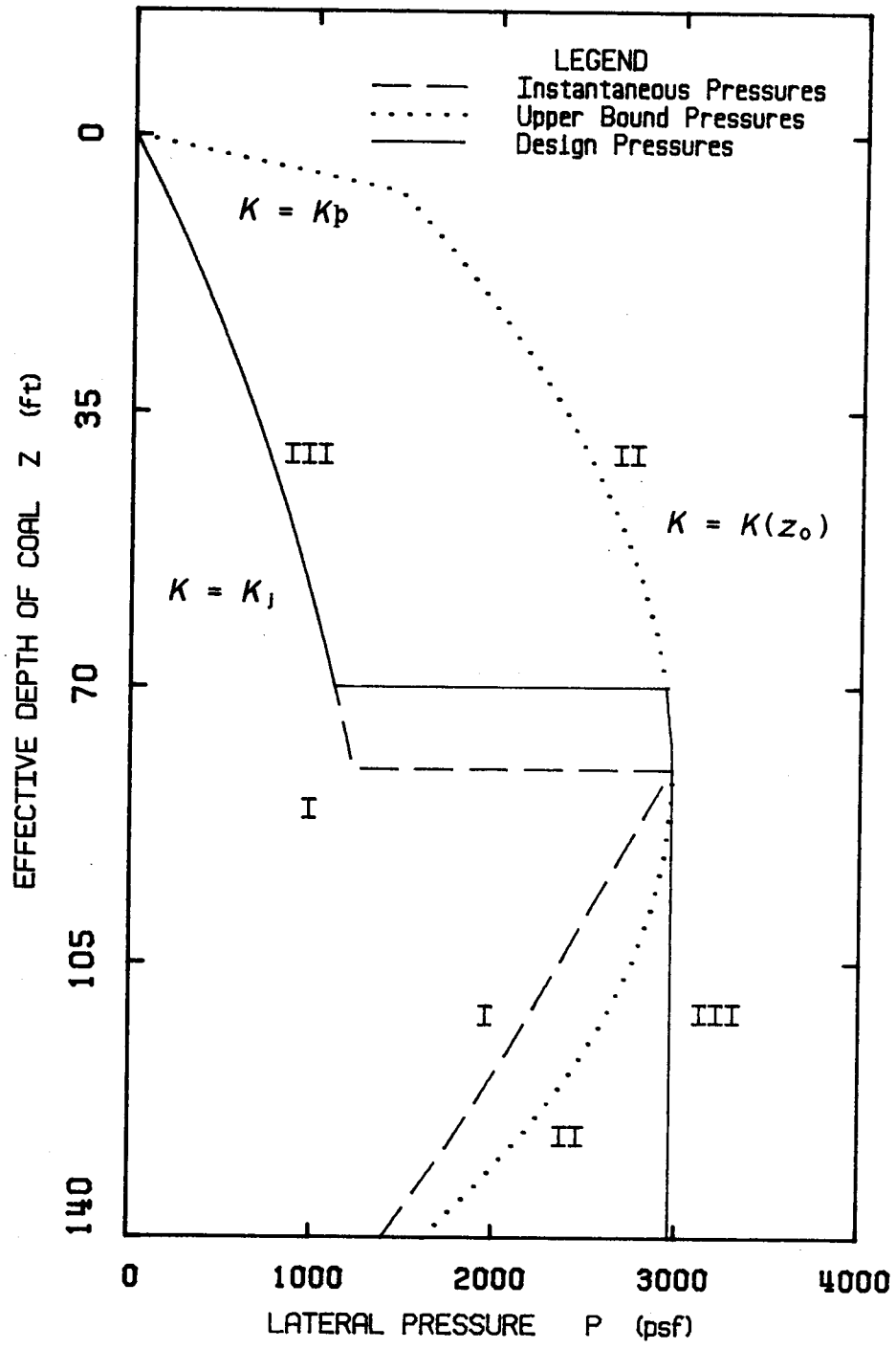

Figure 2.12 Theoretical Instantaneous and Upper Bound Pressures

procedure is given here. The equation numbers given below correspond to equation numbers located in Appendix B, where the formulation is treated in detail.

To construct the instantaneous pressure curve for an arbitrary switch location, z_o, the following three constant parameters are required.

$$M = \sqrt{2(1 - \nu)} \qquad \text{(B.16)}$$

$$N = \frac{2\nu}{\mu' M^{2(1-m)}} \qquad \text{(B.28)}$$

$$K_t = \frac{\nu}{1-\nu} \qquad \text{at } z = H \qquad \text{(B.23)}$$

where m is a geometric parameter (introduced in the development of Eq.[B.15])

A further parameter is defined conditional on z_o.

$$X = \frac{\mu'(H - z_o)}{M^m R} \qquad \text{(B.33)}$$

At the level of the switch and above, the nondimensionalized stress parameter, S (= $\sigma_z/R\gamma$), takes on values described by a Janssen (static) distribution. Therefore, at the switch,

$$S_o = \frac{1}{\mu_s' K_j}\left[1 - e^{-\mu_s' K_j z_o/R}\right] \qquad \text{(B.31)}$$

where K_j is the Janssen (static) value for the material, assumed constant above the switch.

At the level of the switch and below, S and K vary in such a way so as to minimize strain energy within the region $z_0 \leq z \leq H$. Two coefficients, A and B, are computed using the parameters introduced thus far.

To calculate coefficient A,

$$A = \frac{S_o - N + a_1 e^x}{1 + a_2 e^{2x}} \qquad \text{(B.38)}$$

with

$$a_1 = \frac{M^m[\mu_k'^{-1} - K_t N]}{1 - K_t M^m}$$

and

$$a_2 = \frac{1 + K_t M^m}{1 - K_t M^m}$$

Coefficient $B = S_o - N - A$ (B.32)

Computation of S and K can now procede for any point z ($\geq z_0$) on Curve I (Fig. 2.12). In this region, we define

$$x_1 = \frac{\mu'(z - z_0)}{M^m R} \qquad \text{(B.30)}$$

$$S = Ae^{x_1} + Be^{-x_1} + N \qquad \text{(B.29)}$$

A restatement of Janssen's equilibrium equation (Eq.[2.1]) gives K as

$$K = \frac{1 - RS'}{\mu_k' S} \qquad \text{(B.25)}$$

where

$$S' = \frac{\mu_k'}{M^m R}(Ae^{x_1} - Be^{-x_1}) \qquad \text{(B.35)}$$

and horizontal pressure, σ_x (or σ_2), at z, is then

$$\sigma_x' = KR\gamma S \qquad \text{(B.5b)}$$

This instantaneous pressure curve is generally of academic interest only at this stage because in a design situation we are concerned with the bound of maximum pressures that occur at each of those curve's discontinuities. In the foregoing, μ' has taken on both its static and kinetic values although in their original formulation, Jenike *et al.* use only one coefficient for wall friction.

For the upper bound pressures only (pressures at each switch location), $z = z_o$ always and the procedure is to calculate S_o, X, (K_t and N are constant), A, and B for $0 \leq z_o \leq H$. With $z = z_o$, $x_1 = 0$, and σ_x(at $z = z_o$) = $K_s R\gamma S_o$. The lateral pressure ratio is discontinuous at z_o, going from K_j to K_s.

$$K_s = \frac{1 - RS_o'}{\mu_k' S_o} \qquad \text{(B.25)}$$

where

$$S_o' = \frac{\mu_k'}{M^m R}(A - B) \qquad \text{(B.35)}$$

Differentiation of this upper bound curve with respect to z_o would provide the maximum design pressures as well as the switch location that produces this maximum. As yet, this has not been done, although McLean and Arnold (1976) have provided an approximate method, discussed below.

Because of the complexity of each set of calculations per switch location, any detailed study of Jenike's method should be undertaken with the aid of a few simple computer programs. Appendix C contains two such programs that have been used throughout this study; first in attempting to predict experimental results and second in studying the method itself. One program produces the instantaneous pressure curve for any assumed switch location (Curve I on Fig. 2.12), while the other produces the complete upper bound solution (Curve II).

McLean and Arnold (1976) have attempted to simplify the design process associated with Jenike's method. They have shown that a switch location from the top of $0.5H$ to $0.7H$ will produce this maximum pressure and suggest construction of a single bound to estimate this location. By evaluating the equations at the quarter points of a silo's height, the position of maxima on this plotted curve will produce this estimate within reasonable error. They also propose simply evaluating the equations at $0.6H$ (for a cylinder) and for their example, produced sufficient accuracy. In a parameter study of Jenike's method this was found to be the case for a wide variety of material properties and geometries.

Comparisons made between Jenike's method and other flow pressure analyses reveal immediately one unique feature of this theory and that is that within the mass of material beneath a switch, K varies. A natural boundary condition at the transition (required for an absolute minimum of strain energy) sets K there as;

$$K_t = \frac{\nu}{1-\nu} \tag{2.20}$$

This can also be shown to be a result of two important conditions:

1. Janssen's assumption of horizontal strains being independent of horizontal coordinates

   for plane strain; $\sigma_x = \sigma_h$

   for axisymmetry; $\sigma_x = \sigma_y = \sigma_h$

2. Jenike's theory predicts that transition strains due to cylinder pressures are small (similar to initial pressures) when the maximum pressure is achieved in the cylinder. When this maximum occurs, the switch is located near $0.6H$ and therefore flow pressures (generally lower pressures) will exist above the transition, which also happens to be a location of much greater stiffness in most silos. Although large strains and/or pressures are frequently observed at the transition, these are probably due to the large pressures acting just below this position (i.e. the enormous upper hopper pressures).

Using Hooke's law

$$\epsilon_y = \frac{1}{E} [\sigma_y - \nu(\sigma_x + \sigma_z)]$$

$$\epsilon_x = \frac{1}{E} [\sigma_x - \nu(\sigma_y + \sigma_z)]$$

and that $\epsilon_y = \epsilon_x = 0$ at the transition for both plane strain and axisymmetry (i.e. condition 2);

$$\sigma_y = \nu(\sigma_x + \sigma_z)$$

$$\sigma_x = \nu(\sigma_y + \sigma_z)$$

Combined, these give

$$\sigma_x = \left[\frac{\nu}{1-\nu} \right] \sigma_z$$

or

$$\sigma_x = K_t \, \sigma_z$$

Above the transition, K increases gradually with height to values near or slightly over unity, depending on the location of the switch. As the switch approaches the contained material's free surface, the increase in K becomes rather pronounced while for a switch located at the free surface, K becomes infinite. Jenike *et al.* suggest halting the analysis at a distance of 1/2 to one diameter from the top, citing experimental observations and explaining that increased energy dissipation will halt the upward progression of the switch.

Material Property and Geometry Effects

The variables in Jenike's solution include four material parameters (γ, μ', K_j, and ν) and two geometric parameters (H and D). The complete formulation is made assuming E for the material is constant and it drops out when strain energy is nondimensionalized. In the following analysis, these parameters are varied from those values used in Fig. 2.12. Horizontal pressure is directly proportional to unit weight γ because it is assumed constant and this is similar to most static theories. Young's modulus, E, is discussed in Sect. 2.2.3 where representative values are given.

In the preceding description of Jenike's solution, wall friction was treated as two parameters. It is generally recognized that the kinetic coefficient is less than the static coefficient given the same material and surface conditions. DIN 1055 (1964) recognizes this by setting μ' on filling (μ_s') equal to $tan\ 0.75\phi$ and μ' on emptying (μ_k') equal to $tan\ 0.60\phi$. For ϕ ranging from 20° to 40°, the ratio μ_k'/μ_s' ranges from 0.77 to 0.79 and therefore a ratio of 0.8 is used hereafter. Allowing μ' to vary causes only minor adjustments to the maximum pressure; a 20% reduction results in a 5% increase. This increase is due to the variation in μ_s' (above the switch) because varing μ_k' has an opposite but lesser effect on the maximum horizontal pressure.

Poisson's ratio is a difficult property to evaluate for granular materials. Lambe and Whitman (1979) describe ν in

the early stages of loading as having a value in the 0.1 to 0.2 range while under cyclic and/or increased loading, becoming constant at 0.3 to 0.4. As with most other engineering applications, the influence of ν on Jenike's maximum pressure is minimal although it does have considerable influence on the vertical location of this maximum. The two requirments at the transition for minimum strain energy mentioned above allow a determination of ν in terms of K_t, a parameter similar to K_o (zero wall movement and therefore zero lateral strain).

The vertical pressure at the switch acts as a surcharge that must be carried below the switch and therefore an increase in K_j should decrease the maximum pressure. A 20% increase or decrease typically nets a 7% to 8% change in this maximum. This parameter has been discussed at length in Sect. 2.1.6.

A study of the effects the two geometric parameters, H and D, have on maximum pressures (as predicted by Jenike *et al.*) reveals several important points. Variations in D have only a slight influence; a 10% increase in D yields only a 2.1% increase in maximum pressure. This is very different from static solutions which predict D and P_h to approach asymptotically a linear relationship (Eq.[2.6]). Variations in H have a greater influence; a 10% increase in H causes a 7.2% increase in maximum pressure. Although this effect reduces with increasing height, a peculiarity of Jenike's solution emerges that is very different from static

solutions and other dynamic solutions (discussed shortly). The method predicts that increasing the amount of stored material below a certain point increases the maximum pressure that will occur at that point. This is of course a result of minimizing strain energy over what amounts to the lower 40% of the contained volume. As this volume increases, so too does the maximum pressure at the upper extremity of this volume (at $\simeq 0.6H$).

Jenike's mass flow solution is compared to ACI 313-77 C_d factors for non-mass flow in Table 2.3. Providing K_j is kept constant in Janssen's formula, these C_d factors can be shown to be dependent on the H/D ratio only and are relatively insensitive to the remaining material properties. This is a result of several factors. Unit weight γ has been shown to be related linearly to dynamic pressures however this is precisely the relation γ has to static pressures. Poisson's ratio ν, though difficult to predict (it can be evaluated in terms of K_0), is of little influence anyway. Wall friction μ' has a greater effect on maximum dynamic pressures but can also be said to have a similar effect on static pressures. Therefore, the overall effect of changes to the above parameters on equivalent C_d ratios should be minimal. Table 2.3 reveals that the assumed value for K is important and this is primarily because of its influence on static pressures. The largest C_d factors given by ACI 313-77 occur in the lower regions at $H-2(H-H_1)/4 = (H+H_1)/2$ which, as a fraction of H, is

Table 2.3 Equivalent C_d Factors using a Strain Energy Approach (Mass Flow)

		Overpressure Factor			
K_j	z	$\frac{H}{D} \leq 2$	$\frac{H}{D} = 3$	$\frac{H}{D} = 4$	$\frac{H}{D} \geq 5$
0.4	0.6H	2.43	2.59	2.66	2.69
	H	1.83	2.16	2.37	2.51
0.5	0.6H	1.98	2.13	2.19	2.22
	H	1.59	1.85	2.02	2.12
0.6	0.6H	1.67	1.79	1.85	1.87
	H	1.41	1.62	1.75	1.82
Ka *	$\frac{H+H_1}{2}$	1.65	1.75	1.85	1.85

* ACI 313-77 recommendations (non-mass flow)

$$Ka = \frac{1 - \sin\phi}{1 + \sin\phi} \qquad H_1 = D \tan\phi$$

$$\left[\frac{H + D \tan\phi}{2} \right] / H = \left[1 + \frac{\tan\phi}{H/D} \right] / 2$$

This is very nearly $0.6H$ for most combinations of ϕ and H/D so that the point of maximum pressure generally corresponds to this location. The lower values for each whole H/D ratio represent C_d values at the bottom if the maximum pressure is held constant as suggested by Jenike. The discussion at the end of this chapter indicates why, for design purposes, it may be prudent to parallel the dynamic pressure curve with the static pressure curve over the region $0.6H$ to H.

2.2.3 A Re-examination of Jenike's Method with Allowance for Wall Strain Energy

Jenike *et al.* (1973 Part 2) discuss conceptually the requirements for a rational development of a stain energy method for bin loads. In their discussion, reference is made to the strain energies contained in the vessel's walls, specifically, that these energies should be included in the analysis. In the following text the writer will attempt to provide some insight into this aspect of bin loads as it pertains to a strain energy method.

In this treatment of wall strain energies only extensional strains along a circumference will be considered. Extensional stiffness is the primary resistive element in a thin-walled cylinder so long as lateral pressures are described by a continuous curve.

For shell material strained in the elastic range and obeying Hooke's Law, the strain energy density is given by the area under the stress-strain curve and is equal to

$$\frac{1}{2}\sigma_s \epsilon_s \tag{2.21}$$

The total extensional strain energy of the shell is given by

$$W_s = \int_{V_s} \frac{1}{2}\sigma_s \epsilon_s dV_s \tag{2.22}$$

where dV_s indicates an elemental volume

With a constant horizontal cross-section of circumference C_s and shell thickness t_s, Eq.[2.22] can be restated in nondimensional form.

$$w_s = \frac{W_s}{\frac{A\,R}{2E_m}(R\gamma)^2} = \frac{1}{R}\int_0^z \frac{2E_m}{A(R\gamma)^2}\left[\frac{1}{2}\frac{\sigma_s^2}{E_s} C_s t_s\right]dz \tag{2.23}$$

For the sake of comparison, the nondimensionalizing term contains variables directly related to those found in Jenike's nondimensionalizing term (Eq.[B.8]of Appendix B). If the pressure field is assumed to be increasing or decreasing gradually, then the shell stress can be approximated by the thin-walled pressure vessel formula;

$$\sigma_s = \frac{P_h r}{t} = \frac{\sigma_2 D}{t_s 2} \tag{2.24}$$

A modular ratio, n, can be introduced comparing the elastic moduli for the contained material (E_m) with that of the silo shell material;

$$E_m = \frac{E_s}{n} \tag{2.25}$$

With the above substitutions and letting $C_s = \pi D$, we have

$$w_s = \frac{1}{R} \int_0^z \frac{\sigma_2^2 D dz}{n t_s (R\gamma)^2} \tag{2.26}$$

In order to compare directly with the expressions as they occur in Jenike's formulation, the following substitution should be made at this time;

$$\sigma_2 = KR\gamma S \tag{2.27}$$

where S the nondimensional material stress parameter first employed in Sect. 2.1.3 (Eq.[2.2]). On substitution, this gives

$$w_s = \frac{1}{R} \int_0^z \frac{K^2 S^2 D}{n t_s} dz \tag{2.28}$$

We have only to evaluate the dimensionless factor D/nt_s (henceforth designated C_m) in order to make a direct comparison with Jenike's parameter M (Eq.[B.16]), in the final term of Eq.[B.15] in Appendix B. For a reinforced concrete container, wall thickness t_s can be equated with a transformed area of steel per vertical unit length of wall

(i.e. a measure of the effective tensile stiffness) while D is simply the silo's diameter. A reasonable value for $n = E_s/E_m$ must now be found.

Young's modulus for granular materials is a property generally used in settlement calculations. It is conceptually related to the inverse of the coefficient of volume compressibility, m_v and in fact, for a laterally confined mass, such as in a consolidation apparatus or a storage bin, E and m_v can be considered as inverses. This is readily demonstratable with reference to Fig. 2.13. Vertical strain is given by

$$\epsilon_z = \frac{\rho}{H} = \frac{\Delta\epsilon}{1 + e_o} \qquad \text{or} \qquad d\epsilon = \frac{d\epsilon}{1 + e_o} \tag{2.29}$$

This description of incremental strain is for a uniaxial state of stress (no lateral strain) and therefore Poisson's effect is not applicable.

Because Young's modulus (in this case the constrained modulus) is by definition the slope of a material's stress-strain curve we find

$$\frac{1}{E} = \frac{d\epsilon}{d\sigma} = \frac{1}{1 + e_o}\frac{de}{d\sigma} \tag{2.30}$$

This expression is also recognizable as the coefficient of volume compressibility, m_v as it appears in texts on soil mechanics. Using the compression index, Cc, discussed in Sect. 2.1.5, Eq.[2.30] becomes

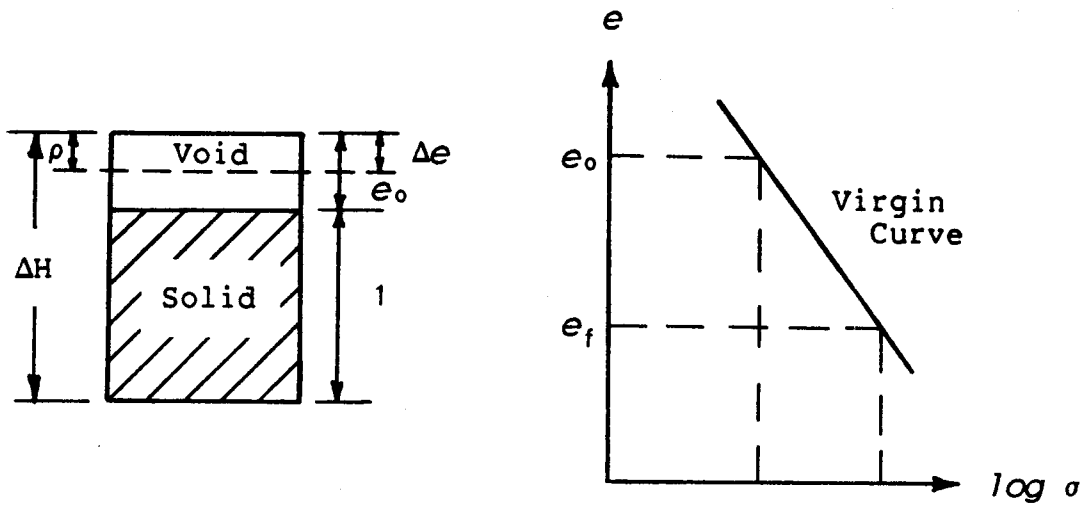

Figure 2.13 Relating Incremental Strain to Changes in Void Ratio

$$m_v = \frac{Cc}{2.3\sigma_v(1+e_o)} \qquad (2.31)$$

The above formulation for $1/E$ $(=m_v)$ immediately reveals the important material property necessary for an evaluation of a bulk material's constrained modulus. We find it dependent on the initial void ratio, e_o as well as being inversly related to Cc. However, given a linear *e-log p* curve (i.e. constant Cc), E can be seen to vary linearly with consolidating head, σ_v. This is in keeping with a generally accepted formula for calculating E for a loose sand where it is approximated by $100\sigma_v$ (Terzaghi and Peck 1967 p.94)

References to Jenike's coefficient of compressibility, β, and its counterpart in soil mechanics, Cc, were made earlier (pp.59-60) however this discussion no longer involves an initial field (the so-called virgin curve on an *e-log p* curve). Concern shifts to the situation during flow in which there is occurring within the mass a continual loading and unloading. This establishes the need for a second compressibility parameter, Cr, or recompression index that denotes the slope of the path followed by the *e-log p* trace on rebound, a property of all soils that also has been well documented in the literature.

There is little available literature relating quantitatively an initial E to its value on rebound or even Cr to Cc. Pariseau and Nicholson (1979), while examining

stress and displacement fields in hoppers using finite elements, briefly discussed their treatment of this aspect of bulk material behaviour. They incorporated an E on discharge that was approximately 20 times the E used on filling. Harr (1977), in a tabulation of various material properties, reveals a compression/recompression ratio of about 15 for a silty clay.

From Eqs.[2.14] and [2.16] and Fig. 2.10, an attempt at finding E_m can now be made.

The established relationships are;

$$\Delta e = Cc\ \Delta log\ p$$

$$\Delta log\ \gamma = \beta\ \Delta log\ p$$

$$\Delta e = \xi\ \Delta log\ \gamma$$

where ξ was introduced in Fig. 2.10 as the slope of the $log\ \gamma$ - e curve.

This gives

$$Cc = \xi\ \beta$$

Because ξ is typically 0.2 to 0.3, and with β = 0.0786 from Fig. 2.11, Cc for this material is approximately 0.02. Using Eq.[2.31], e_o= 0.7 from Fig. 2.10, and an average consolidating pressure of 2500 psf, E on initial loading becomes 3.4 ksi. Assuming a token increase on rebound to give E_m = 10 ksi, the modular ratio comparing E_s to E_m becomes about 3000.

Finding an effective value for t_s is a difficult task if the wall is of reinforced concrete because extensive cracking will render the structure progressively less stiff with each load cycle. A 70 foot diameter silo will typically have about 3 in² of steel per foot of height in the lower regions. Assuming that uncracked concrete effectively quadruples this 'area of steel', t_s can be approximated by 1.0 in² of steel per inch of height. This gives

$$C_m = \frac{D}{nt_s} = \frac{70 \times 12\text{in}}{3000 \times 1\text{in}} = 0.28$$

In Eq.[B.15] of Appendix B, the dimensionless coefficient for K^2 becomes, from Eq.[2.28], M^2+C_m. Therefore, wherever M, M^2, or M^m appears in the solution, M must be substituted with

$$M_2 = \sqrt{(C_m + M^2)}$$

Jenike's solution has been run using the above substitution. The resulting effect on maximum attained pressures, as a function of C_m, is shown in Fig. 2.14. Depending on the various assumptions made in the foregoing discussion, it is apparent that including wall strain energies in the solution may reduce lateral dynamic pressures. Not shown is the effect this inclusion has on the location of these maximum pressures. The analysis indicates that this location moves up the wall as C_m increases, revealing that the loads are being redistributed rather than

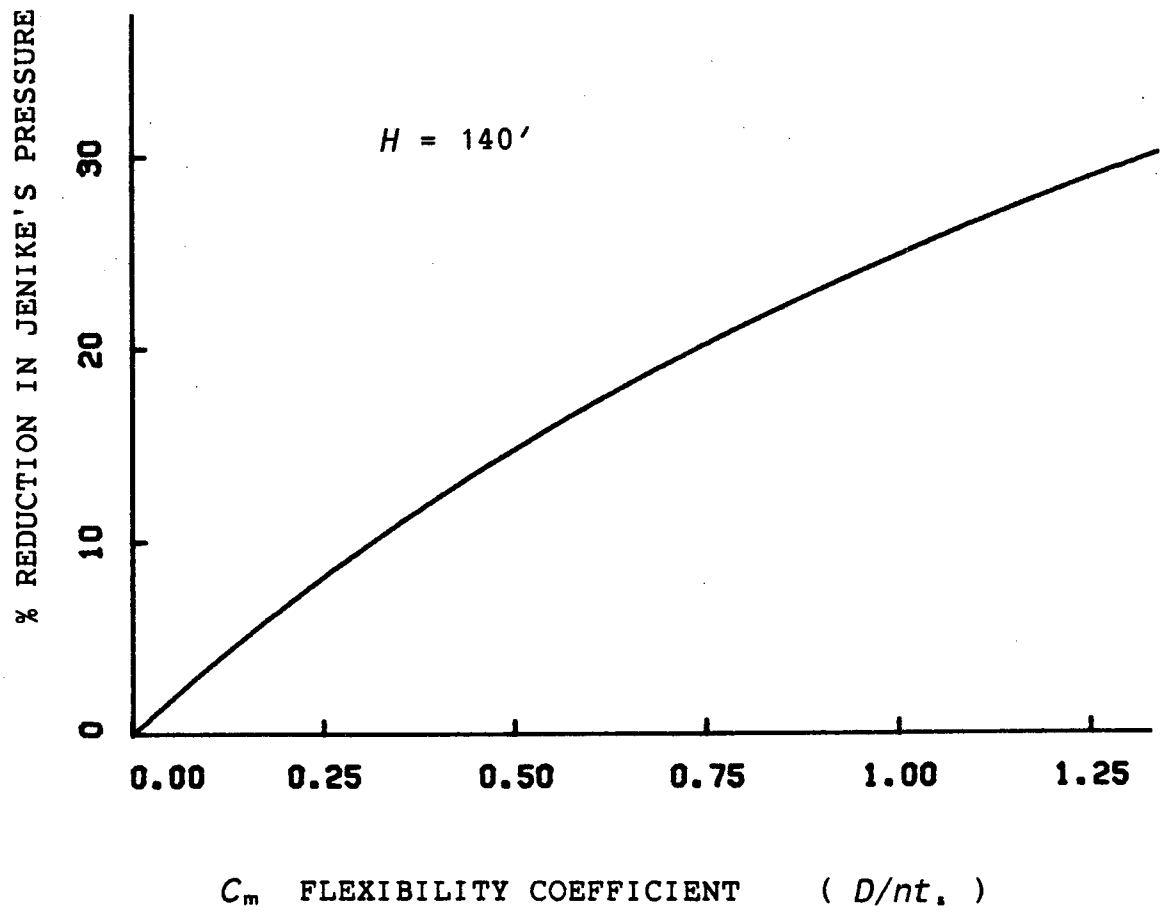

Figure 2.14 Dynamic Pressure Reductions Due to Wall Flexibility

reduced, a not unexpected result from a structural standpoint.

A more involved analysis would require better indications of the values that E_m and E_s might take on. With ensiloed materials that are stiffer and/or as the wall becomes less stiff, this analysis predicts that C_m will increase and lateral pressures will decrease.

2.2.4 Alternate Theories

A good many theorists have concentrated their efforts in mass flow pressure predictions to primarily within the hopper. What has resulted is a number, and a diversity, of solutions that overall reveal some quantitative similarities (see for example Horn and Nedderman 1976). It appears that converging-side configurations common to all hoppers are conducive to theoretical analysis through much the same reasons that Jenike *et al.* (1973) found slight values of divergence and convergence will define active and minimum strain energy stress fields respectively.

Wall convergence within a hopper forces lateral contraction within the flowing material and as the major principal stress generally aligns with the direction of contraction an 'arched' or passive field is set up. Conversly, the near vertical sides of most bins set the contained material flowing within an undefined flow channel, apparently leaving open the choice of which stress bound to analyse with (i.e. active or passive). The Jenike method

skirts this apparent stumbling block by uniquely employing an energy technique. Most other theories tend to rely on the passive bound.

Of these theories, Lvin's treatment of dynamic pressures most closely parallels Jenike's approach. Lvin describes a 'rupture level' which in fact is synonymous with a 'switch' position. Above this level occurs a zone of transition and above this zone the mass is stabilized, with pressures being described by a static analysis. We have already discussed Lvin's contribution in this area. In the zone of transition , the coefficient of earth pressure is assumed to vary linearly from a stabilized K to a multiple, m_k, of this value. Here the range of K, according to Lvin, is bounded by active and passive, or upper and lower limits.

This multiplier m_k plays an important role in the solution because not only does it predict the depth of this transition zone but it also appears as the only parameter in a formula describing, in effect, an overpressure factor.

$$o.p.f. = 2\left[\frac{1}{2} + \frac{1}{7}(m_k + 1)\right]$$

For example, values for m_k of 4.5 and 8.0 give respectively overpressures of 2.0 and 3.0. Ratios of Kp/Ka can often exceed these levels, depending on the material properties. A discussion by Moysey (1979) of Lvin's results applied to the Fording coal silo (with $\phi = 35°$ and $\phi' = 26.5°$) suggests that an overpressure factor less than 2 might be expected.

Lvin does not predict actual pressures but instead leaves it to the reader to choose appropriate values for K in an analysis. He correctly recognizes the problem of evaluating K to be one of some difficulty as the various states of stress within a bulk mass are more tied in with the stress-strain history of the material than so much as with the material's properties. This conclusion will be shown to be justified by the experimental results.

Again, Lvin's derivation is based on a constant vertical-shear/lateral-pressure relation existing between adjacent differential rings and this fact somewhat lessens the methods validity, although the consequences may be more acceptable for a constantly shearing (flowing) mass than they were for the static case.

Horne and Nedderman (1976) applied Sokolovskii's solution technique to the passive case and found the results to follow a discontinuous curve. Because they assumed incipient passive failure throughout the mass, much of the discussion concerning the active case will apply here also. It is extremely difficult to conceive of a chain of events that could in fact produce this type of stress field, except perhaps within the converging hopper, and therefore the solution is of academic interest only. The solution would be similar to one using Janssen's formula with K_p and in fact it oscillates about while asymptotically approaching a modified Janssen solution incorporating K_p.

Van Zanten and Mooij (1977) discuss local overpressures occuring at irregularities in the wall and describe the condition as "Local Passive Bracing". Above this position on the wall, the stress field is active and at the irregularity, the major active principal stress becomes the minor passive principal stress (K changes from Ka to Kp discontinuously). This would therefore be equivalent to an overpressure factor of Kp/Ka (or Kp^2).

Walters (1973) has extended Walker's (1966) modified Janssen approach for predicting static pressures to one that can predict dynamic and switch pressures. The approach is similar to one employed by Jenike and Johanson (1968) when they first discussed the possibility of enormous 'switch' forces acting on a bin wall. The method is an overall equilibrium technique; greatly reduced dynamic (flow) pressures well below a switch require, for overall equilibrium, greatly increased pressures to act immediately below the switch. Walters gives a chart showing localized overpressure factors of 50 or more, depending on values chosen for ϕ and ϕ'. Although pressures of this magnitude have never been recorded, Walters gives several possible reasons why, including their short lived nature and small area of application.

Jenkyn (1978) uses a different approach than previous theories. He evaluates a 'flow value' for K based on the variation in μ' from μ'_s to μ'_k (in his notation, $\mu'_s = \tan\mu$ and

$\mu_k' = \tan\mu_2$ although Jenkyn appears to interchange ϕ with ϕ' in his comparisons). His solution falls between DIN 1055 and ACI 313-77 in the upper regions of a silo but approximates ACI values near the bottom, where DIN 1055 (1964) exhibits a reduction in effective overpressures. Jenkyn's results are therefore not suitable as mass flow pressures in so far as ACI 313-77 suggests that their design values are inadequate.

2.2.5 Recent Research on Mass Flow Pressures

Literature relating experimental results to a strain energy solution is still rather sparse at this point in time, evidently a result of that theory's relatively recent evolution (1973). Jenike *et al.* (1973) discuss briefly tests with sand in a 0.95 foot cylinder and report good agreement with their theory. They indicate that results from pressure measurements near the transition tend to exceed their 'adjusted' curve but suggest this could be due to their not including hopper strain energies in the analysis.

These findings tend to be supported by a number of tests conducted in Amsterdam on a larger mass flow bunker of 1.5 m diameter (12 m^3 capacity). Richards (1977) and Van Zanten and Mooij (1977) reported in detail pressure measurements on three materials (two PVC powders and a sand with $\phi = 37.5°$). Maximum flow pressures were considerably in excess of a strain energy prediction while mean flow pressures generaly fell within these bounds. These mean flow pressures presumably were derived from sets of four

transducers, equally spaced circumferentially, and therefore more realistically approximates values to be used in determining hoop tensions. This does not mean to suggest that maximum observed pressures should be ignored but instead they should be treated as local perturbations only. This idea will be discussed more fully in a Chap. 6. The above authors also emphasized the observed wide variability (and as well the importance of local effects) in wall pressure magnitudes.

3. Description of Field Measurements

3.1 Description of the Silo

The silo used in this study to obtain field measurements can be considered representative of size and construction practice for contemporary coal industry application. It is a slip-formed reinforced concrete cylinder of 70 feet inside diameter, 12 inch wall thickness, and with a total height of 250 feet. The cylindrical portion of the silo which resists coal pressures directly, rises 155.7 feet from the transition hopper to the upper side of the bin's roof slab. Two silo cross-sections are depicted in Figs. 3.1 and 3.2.

Principal (hoop) reinforcement is provided in two concentric rings and consists of 30M bars at 8 inch spacing below elevation 269'-0", 25M bars at 9 inch spacing to elevation 205'-0" and 20M bars at 9 inch spacing for the top 43'-8 1/2". Vertical reinforcement consists of two layers of 15M bars at 12 inch spacing placed just inside each ring of hoop reinforcement.

The hopper portion of this bin actually consists of a transition hopper and two pyramidal outlet hoppers (with rounded edges) , all of steel plate construction. Both outlet hoppers are lined in a 304 stainless steel with a 2B finish. The transition hopper is affixed to the cylinder at elevation 193'-0" through welding to a 12"X 3/4" continuous steel plate. This detail is important for a general

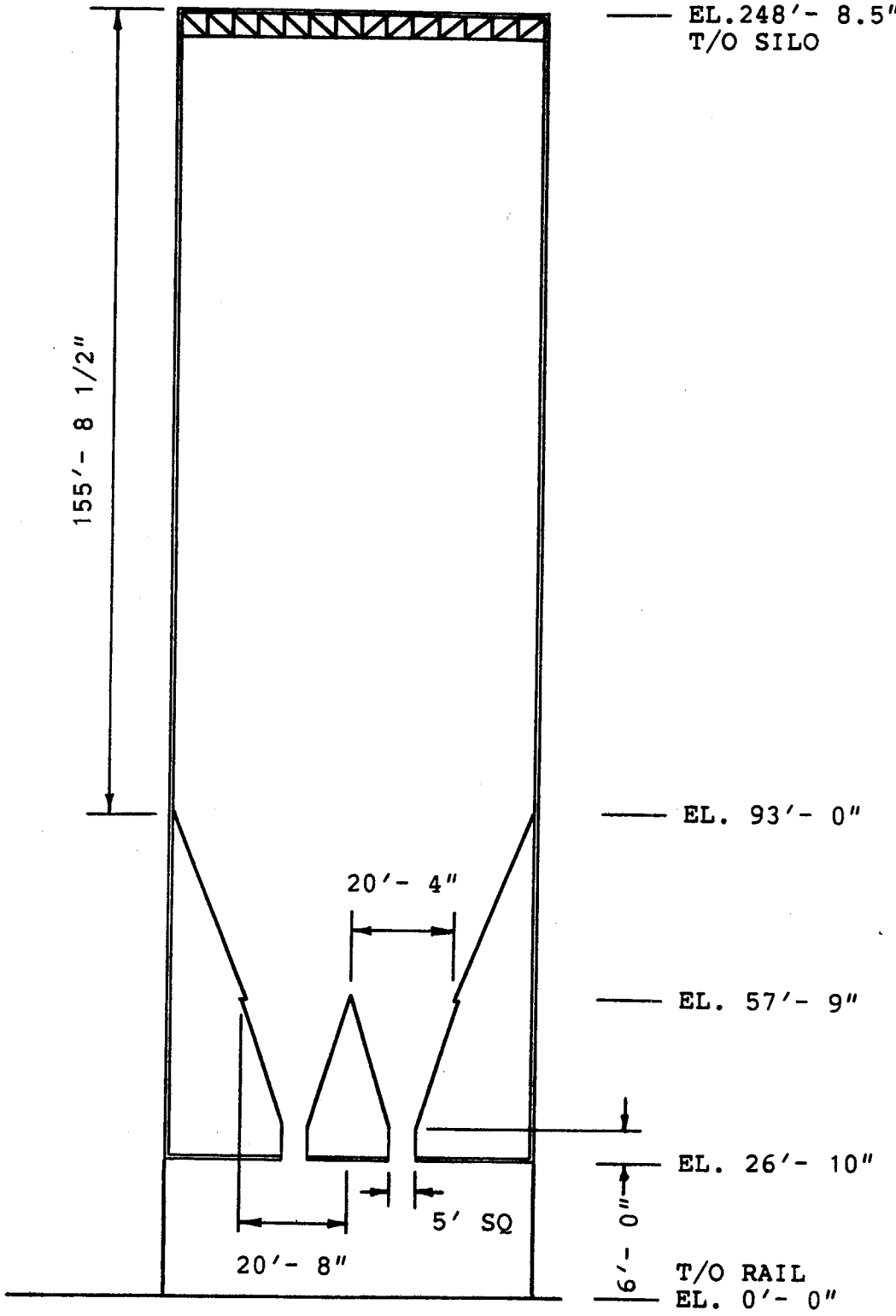

Figure 3.1 Section Through Silo Looking East

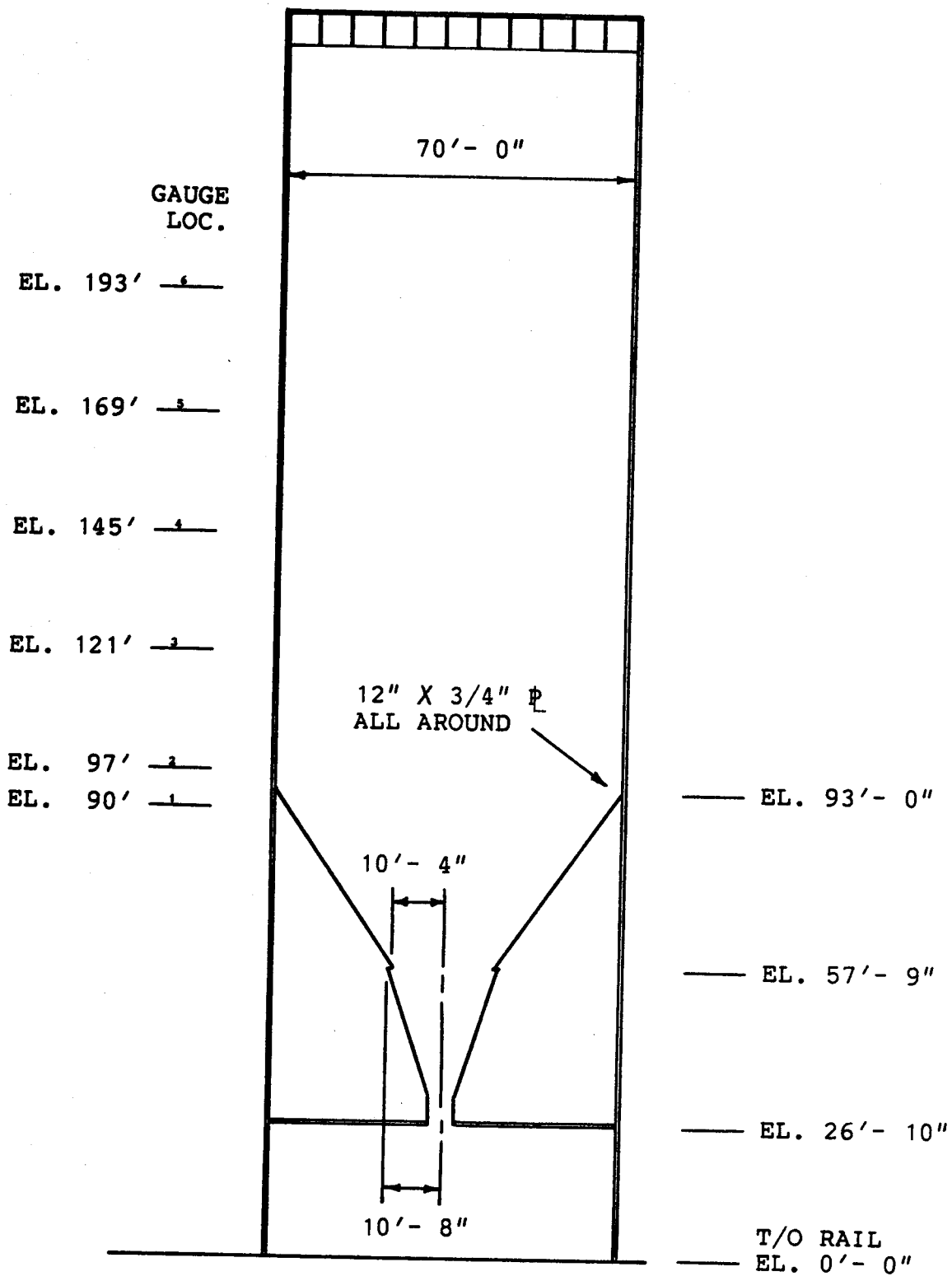

Figure 3.2 Section Through Silo Looking North

interpretation of transition strains and therefore is shown in Fig. 3.3.

The bin's roof slab, monolithic with the bin walls, is a 6 inch steel-concrete composite, supported on steel trusses, that in turn supports the silo's top house. This top house encloses the upper end of the 10 foot diameter conveyor tube and a charging chute that effectively divides the incoming flow of material into two separate charging flows, displaced lateraly approximately twenty feet. This flow separation results in additional material storage at the top as now two adjacent cones of material will form instead of one. This complicates to some extent the calculation of an equivalent coal height.

3.2 Properties of Stored Material

A complete series of tests was considered to be unjustified for this study however information contained in a number of material reports (Reference [39]) already in existence was drawn upon. The silo is designed for containment of a two inch minus well-graded cleaned coal that possesses an average bulk density of 60 pcf. Compressibilty effects and moisture content variations can act to cause a large difference between measured minimum and maximum densities (from 34 to 64 pcf) (Reference [39]) and, along with various internal, external, and effective frictional properties, can radically alter material flowability. It is however, only those effects necessary in

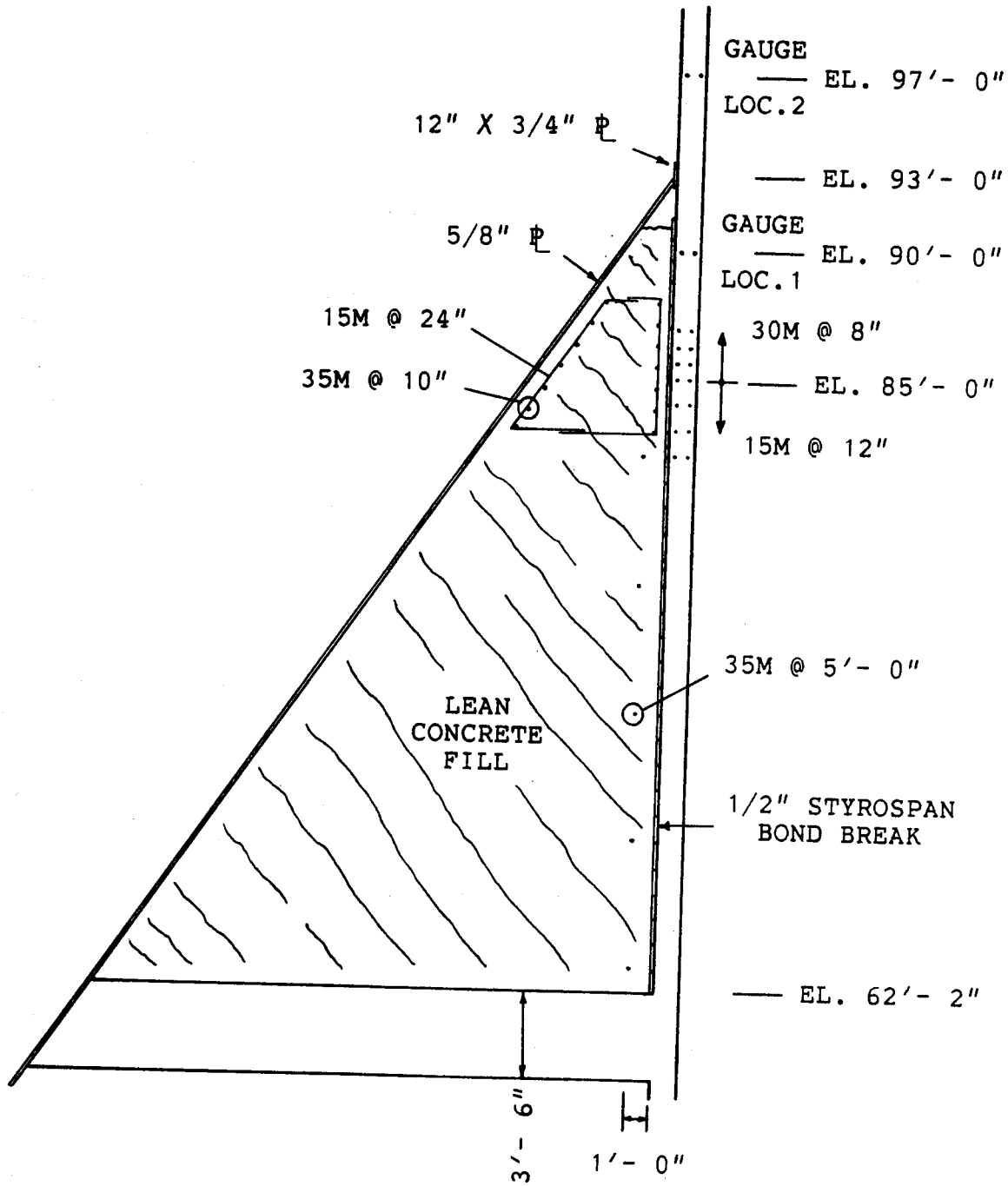

Figure 3.3 Cylinder - Hopper Transition

pressure calculations that will be considered here.

Compressibilty effects have been discussed at length in the previous chapter. Sufficient accuracy for design purposes can be achieved most simply be utilizing an average maximum expected material density in the design equations. In the following chapter however, compressibility is included in the analysis as to do so requires no great effort and should in fact increase accuracy for the lower coal heights employed.

The moisture content of cleaned and dried coal charging into the bin is related to the temperature of the material as it exits the dryer. At 120°F (49°C) moisture content is about 6% while at 95°F (35°C) and 65°F (18°C) moisture content is respectively 10% and 14% (Reference [39]). A temperature of 117°F (47°C) was recorded for material entering the silo on one occasion, suggesting a moisture content nearer to 6%. This is in keeping with tests done on samples taken in January 1981 where moisture contents of around 7.5% were measured using the ASTM Standard.

For the material reports of Reference [39], tests were conducted on the material passing a number 8 mesh (60 to 80% of the material as revealed by the sieve analyses conducted by the writer and contained in Appendix D). For the coal at a moisture content of 6%, the angle of internal friction (ϕ) ranged from 38° to 40° while the angle of wall friction on concrete was recorded at 26° to 31°. The afformentioned sieve analyses describe a very well graded material.

3.3 Loading and Unloading Considerations

Coal heights within the bin were determined using a variety of methods. Originally it was hoped that a reasonable estimate could be obtained from the silo's six coal level indicators. These occured at 24′ intervals starting at 4′ above the transition and if feed rates and discharge rates are known, a good estimate could be had of coal height, at least at the western meridian. Runs #1 through #3 had heights established in this way but it was soon discovered that these indicators were susceptible to jamming and therefore an alternate method was used. Prior to the start of all remaining runs a weight on the end of a graduated line was lowered into the bin at one or both of two openings and this gave a more accurate knowledge of coal height. During discharge, a running tally of loaded-out weights was provided by the computer for most later runs and this allowed a calculation of the remaining material's height. The results are summarized in Table 3.1.

Unloading of the silo into a variety of coal car types that comprise a unit train is accomplished automatically with the aid of electric eye and mechanical limit controls, a continuous weight monitoring device, a software package developed specifically for this system, and the onsite loadout computer. At the time of final strain measurements, full computer operation had not been achieved and loadout was undertaken either fully manually or with one chute on automatic control.

Table 3.1 Measured and Effective Coal Heights Above the Transition

Fig# App. J	Remarks	Coal Levels		
		at wall	at W chute	eff.
C1	coal in hopper only	-	-	-
C2-C8	silo empty	0	0	0
C9	Start of Run#6A, (1 measurement 77′ down at wall), assumed cone ht. of 18′	78.7	96.7	84.7
C13	Prior to Run#6B, (back - calc. from Fig. J.C15 level as shown	88.5	107.7	94.9
C14	in Chap. 4, p.153)	95.6	116.6	102.6
C15	Start of Run#6B, (first estimate from back - calc. on full silo),	103	125	110.3
C15	Final estimate from calc. in Chap. 4, p.141	102	124	109.3
C16	Prior to Run#7, (3 measurements) Silo full - 35′ down at wall	120.7	153.2	131.5
C17	- 5′ down at W chute - 0′ down at E chute	120.7	153.2	131.5
C18	Average cone ht. = 32.5′	120.7	153.2	131.5
C19	Start of Run#7, Silo full	120.7	153.2	131.5
C20	End of Run#7, (2 measurements) - 100′ down at wall - 95′ down at W chute Assumed conal surface	55.7	60.7	57.4
C21	Filling for 4 hours	-	-	-
C22	Start of Run#8, (1 measurement) - 63′ down at wall Assumed cone ht. of 20′	92.7	112.7	99.4
C23	Robot Diesels Run#8, (calc. Δht. from scale output) Assumed cone ht. of 10′ (for plotting only)	65.5	75.5	68.9
C24	End of Run#8, (calc. Δht. from scale output) Assumed cone ht. of 5′ (for plotting only)	23.6	28.6	25.3
C25	Prior to Run#9, (2 measurements) - 52′ down at wall	103.7	125.7	111.0
C26	- 30′ down at W chute	103.7	125.7	111.0
C27	Start of Run#9, (see above)	103.7	125.7	111.0
C28	Robot Diesels Run#9, (calc. Δht. from scale output) Assumed cone ht. of 10′ (for plotting only)	79.8	89.8	83.1
C29	End of Run#9, (calc. Δht. from scale output) Assumed cone ht. of 5′ (for plotting only)	39.8	44.8	41.5

As revealed in Fig. 3.1, the two outlet hoppers have centers approximately twenty feet apart and therefore the operable chutes used in controlling the coal level within each car would similarily be displaced. This system results in only one gate being open at a time, unless manual override is employed and the south gate is left open beyond its normal shut-off. When in use, the computer program negates this possibility.

The preceding description of the loadout operation has important consequences on material flow within the silo. With only one gate in operation at a time, the attainment of mass flow within the complete bin cylinder is unlikely as an expanded type flow within either the north or south hemicylinder would be expected. The location at which this expanded flow channel first touches the wall is difficult to predict at this time and consequently discussions in this area should follow presentation of the results.

3.4 Description of Instrumentation and Field Measurements

Strains in the cylindrical concrete wall are measured with strain gauges mounted on the hoop reinforcement at various locations along a single meridinal line as shown in Fig. 3.1. At each of these six locations, two AILTECH SG129 weldable strain gauges are attached; one each on the outer and inner bars. Prior to concreting, gauges and bars were thoroughly greased along a three foot length, hopefully to act as a bond breaker. Actual bar strain measurements were

recorded as either static or continuous.

Continuous readings were deemed necessary at the outset due to the expected transitory nature of the coal flow pressures and they were accomplished with the aid of a portable signal demodulator. In this capacity, a ten channel Validyne (model MC1) Multi-Channel Transducer Control and Signal Conditioning System was employed, with each gauge acting as the active arm in a quarter bridge configuration. Each of the ten modules in the demodulator generates an independent signal of 5V a.c. (rms) at 3 kHz that varies with the strain. This signal is then amplified and converted to d.c. output to facilitate recording; in this case recording was generally done on magnetic tape however in some cases actual strip chart records were produced as the run progressed. Discharge events, recorded in the continuous mode, are labelled as Runs #1-10.

Static readings were undertaken initially as a means of checking whether or not gauges were functioning adequately and later as a means of discerning long term gauge response to shrinkage stresses, silo usage, etc. It was soon discovered that static readings also gave very accurate indications of short term effects, (as opposed to instantaneous dynamic effects) such as temperature, lateral charging pressures, and quasi-static lateral pressures brought about through discharge. Each full set of static readings would take approximately five minutes as they were recorded manually and therefore restricted the use of this

means of measurement to periods of slack in the discharge sequence, for instance just before or after loadout procedures or during passage of the intermediate (robot) diesel engines. This latter event occured approximately 40 to 45 cars into a loadout operation that generally comprised 105 to 110 coal cars in total. Static readings were generally numbered sequentially in a three series grouping. Series A included readings taken at each gauge location (#1-#3a) and those taken through the 100+ ft cables but without ground straps. All of these readings were used for long term observations. Series B and Series C readings utilized ground straps; Series B were taken in January 1981 and Series C in June 1981.

Temperature stresses are directly observable provided the strain measuring devices are reasonably temperature compensating over the range of expected temperatures. The gauges used in this study carry a 6S designation that describes their suitability for attachment to steel and an overall coefficient of thermal expansion of 6 $\mu\epsilon$ per F (10.8 $\mu\epsilon$ per C). For a steel-concrete composite, this value is an oft quoted average for this coefficient. Fig. 3.4 is an apparent strain vs. temperature curve for these particular gauges and therefore indicates the amount of strain that must be subtracted from the measured strain if an actual strain is desired.

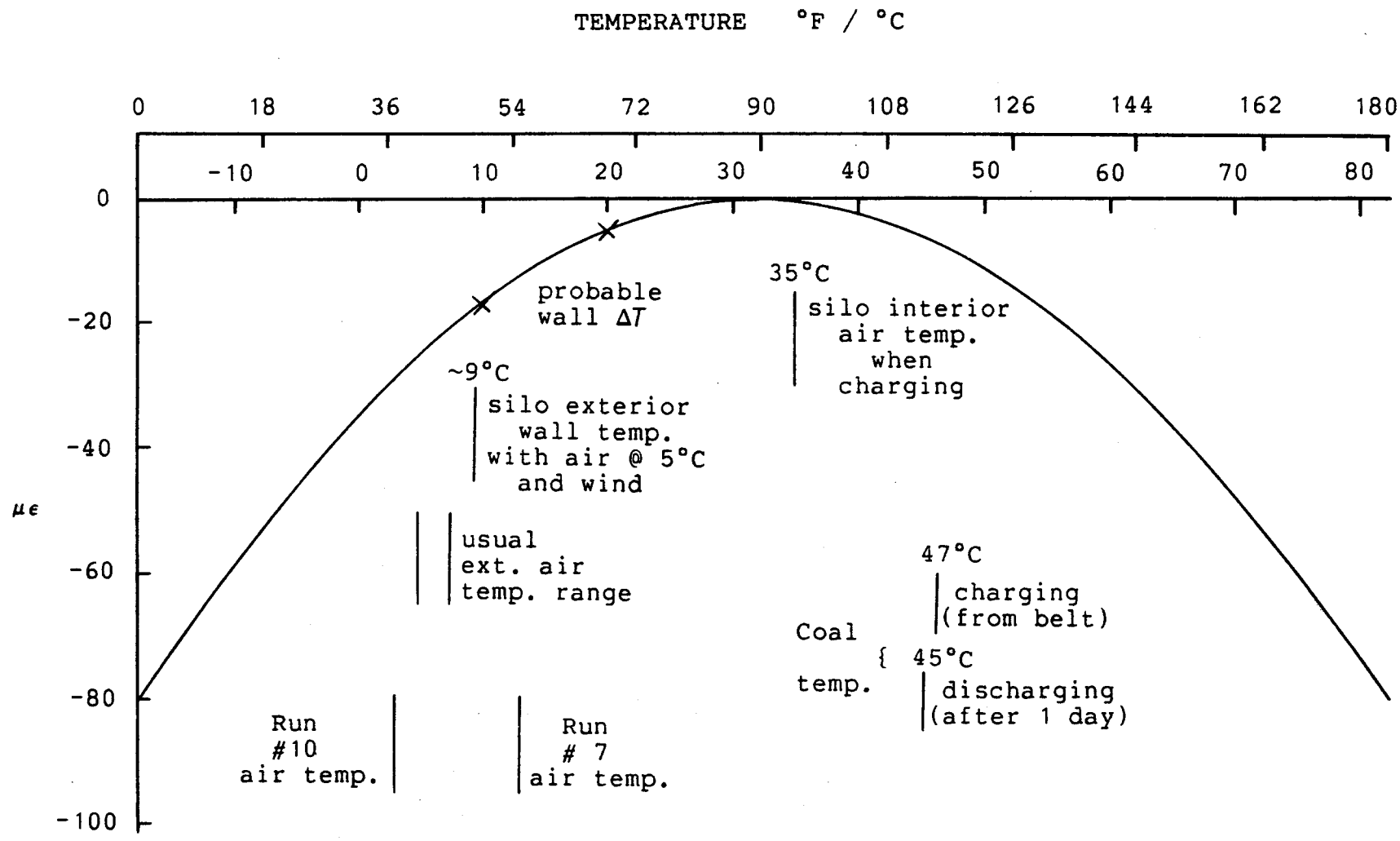

Figure 3.4 Apparent Strain vs Temperature Curve of AILTECH SG 129 - 6S Gauges

3.5 Chronology of Field Measurements

September, 1979

- Silo slip-formed

February 26, 1980

- Initial static Reading #1, Series A. This was a one day field trip to provide an initial gauge check 5 months subsequent to installation. At this time hoppers were not yet installed.

October 6-8, 1980

- This field trip involved cable installations, initial equipment checks, and monitoring of virgin loading of silo. Static Readings #2 and #3a were taken at individual gauge locations while #3b through #10 were undertaken by way of newly installed cables. Continuous readings were conducted (Run #1) with the bin portion of the silo approximately 50% filled (according to indicator lights).

January 8-12, 1981

- This was intended to be the start of full data acquisition however a series of site events rendered the silo dormant for this period. Static Readings #11 through #16 were used in attempts to correlate static and continuous readings. Electronic drift problems were first noticed at this time.

January 19-27, 1981

- This field trip resulted in data collected for four runs (#2 throught #5) and Static Readings #17 through #120 Series A, and #1 through #10 Series B. At this time it became apparent that the coal level indicator lights were unreliable and an alternate method was employed as discussed earlier.

June 15-25, 1981

- This was the final field trip. The silo had been in continuous operation for 1/2 year and the readings taken at this time are considered to be representative of the behavior of an operating silo. A preliminary evaluation of data from the previous field trip had pointed out the need for more reliable static measurements while at the same time equipment limitations were fully understood. Therefore, a fairly comprehensive set of readings extending over ten days were obtained. Runs #6 through #10, complete with a number of invaluable reference readings (Series C; #1 through #35), were recorded. The detailed analyses of Chap. 4 and 5 deal almost exclusively with this final set of test data.

4. Static Test Results and Analysis

4.1 Introduction

In this chapter, the static results are presented and analysed in an effort to evaluate the extensional wall stiffness at various gauge locations. As such, the evaluation of initial static material pressures for a range of effective coal heights and known or assumed material properties, represents a calibration technique.

The development of a suitable stress-strain relationship that will consistently predict the gauge response for a particular location necessitates an understanding of any and all phenomena that may affect these strains. Therefore the discussions to follow include such topics as thermal effects and the effects of cracking on local strains. The second unknown in the stiffness equation is of course stress (i.e. load) and in this regard material pressures are needed. This requires an appropriate assumption for the value of or the range of variation of K, and, to a lesser extent, the static pressure theory to be employed. For the latter, a Janssen-Compressibility formulation will be used because of the smaller depths of coal involved in the analysis. Both a constant and a variable K will be examined.

The static and quasi-static results for January 1981 and June 1981 are given in (Appendix J) Figs. J.B1 to J.B10 and J.C1 to J.C35 respectively. Data from these plots are

drawn upon at various times throughout Chap.4.

4.2 Shrinkage and Hopper Installation Strains

Because the silo is a reinforced concrete structure, one would expect shrinkage to occur. For unrestrained concrete, shrinkage strains can be expected to range from about 200 to 600 microstrain but may go as high as 1000 microstrain (Park and Pauley 1975).

Fig. 4.1 reveals that in the seven month period from February 26, 1980 to October 7, 1980 (this period begins five months after completion of the slip-form), an approximate compressive strain occurred circumferentially of 300 to 400 microstrain at the upper four gauge locations. It should be noted that during this period the transition hopper and ring plate were installed and this would account for the erratic gauge behaviour at Locations 1 and 2. If all or most of this compressive strain is attributable to shrinkage, it is a simple task to calculate the resultant concrete tensile stress due to the restraint provided by the hoop steel. Steel stresses of 10 ksi would result from an average 350 microstrain compression and to maintain equilibrium;

$$f_s A_s = f_c A_c$$

$$f_c = \frac{f_s A_s}{A_c} \quad \frac{10 \text{ ksi} \times 3.27 \text{ in}^2}{(144-3.27)\text{in}^2} = 0.232 \text{ ksi (Tension)}$$

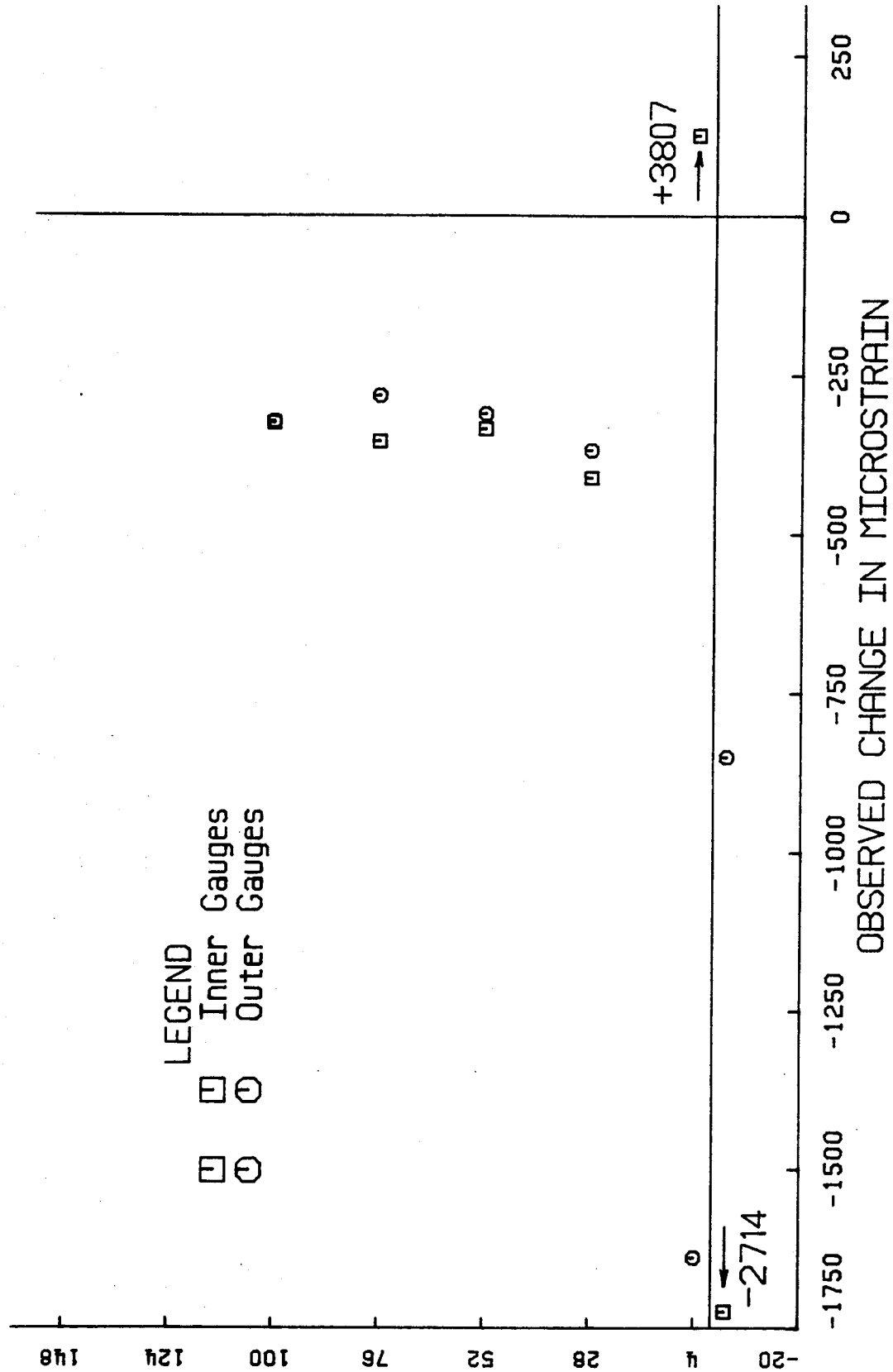

Figure 4.1 Shrinkage and Hopper Installation Strains - Feb. 26 to Oct. 7, 1980

This shrinkage stress results from only the measured portion of shrinkage strains because there probably occurred at least an equivalent amount of shrinkage between September 1979 and February 1980.

Tests at the University of Alberta (Chitnuyanondh *et al.* 1979) on wall segments of similar thickness to this silo have shown that initial cracking occurs at stresses of approximately $3.65\sqrt{f'c}$, in this case at about 230 psi for 4000 psi concrete. Preliminary observations at the silo, before any material loadings occurred, revealed an extensive lattice of hair line cracks, generally undirectional, and what were therefore primarily surface cracks only. However, this surface cracking would tend to reduce the effective area of concrete in the equilibrium equations given above. In the vertical direction, the self weight of the structure would prevent the formation of horizontal cracks extending into the wall's core however this force is absent circumferentially. One may surmise at this point in the discussion that prior to actual usage of the silo, a state of stress existed in the circumferential direction that approached or even exceeded the concrete's cracking strength.

4.3 Strains due to Operational Loads for the Period October 1980 to June 1981

The silo became operational in October 1980 but received only sporadic use until January 1981. All of the

static and dynamic analyses done for the silo use the June 1981 observations and therefore it is important to establish that a settling-in period had transpired prior to June. If it can be shown that through-the-wall cracking had occured during this period, the assumptions of constancy of extensional stiffnesses and linearity of the stress-strain curves for the June readings become easier to accept.

Long term observations of hoop strains after October 1980, for an empty silo, reveal a general increase in tensile strains however this behavior is fairly erratic. Tensile strains of less than 50 microstrain and approaching 400 microstrain occurred in the upper four locations without any particular vertical nor inner-outer correlations emerging. In contrast, the two gauge locations at the transition have experienced similar October 1980 to June 1981 strains and of large proportion. Here, the outer gauges strained +624 and +690 microstrain at Locations 1 and 2 respectively while the inner gauges strained +205 and +238 microstrain. This obvious difference in inner-outer gauge response can readily be explained when it is realized that, at the transition proper, 73% of the hoop steel occurs as a 12" x 3/4" plate, affixed to the inner side of the wall. This has the effect of moving the neutral axis closer to the inner gauges.

Examining hoop strains at the transition for the emptied silo (Figs. J.C1 to J.C8 and J.C33 to J.C35) shows the relative stability that occurs there and this fact,

coupled with the rather large strains that have occurred at this location in June, (i.e. Fig. J.C28) leads to the conclusion that extensive through-the-wall cracking has occurred at this level. This statement is supported by the observed cracking behaviour of the silo. In January, vertical continuous cracks were noticed near the transition but their appearance was little more than hairline. Prior to one of the later runs in June, crack sizes approaching 1/2 mm in width, and continuous for several feet, were observed at the transition level. Smaller but still continuous cracks were observed as high as Location 5 (i.e. 1/2 way up the cylindrical bin portion of the silo).

4.4 Initial Static Material Pressures and Extensional Wall Stiffness Evaluations

4.4.1 Methods of Analyses

In Chap. 1, Eq.[1.1] was given as the starting point for computing a circumferential design force and required area of hoop steel. It is repeated here to illustrate the relationship between horizontal pressures, circumferential strains, and the circumferential extensional stiffness of the wall at a particular location.

Average thin-walled stress in a cylinder is given by;

$$\sigma = \frac{P_h r}{t} \qquad (4.1)$$

This formula is correct for a horizontal pressure constant with height as well as a horizontal pressure exhibiting a linear variation with height. It is also correct for a nonlinearly varying horizontal pressure so long as the variation is gradual and continuous. This is true of the Janssen exponential static pressure curve but not of the instantaneous switch pressures which, according to theory, are discontinuous at the switch.

Using Hooke's Law, extensional stiffness, Et, is then given by;

$$Et = \frac{P_h r}{\epsilon} \tag{4.2}$$

This relationship describes the basis for all calculations dealing with a range of probable horizontal pressures and measured circumferential strains. Inherent in its application is an assumed linear stress-strain response for a particular wall location. At service load levels this is reasonable, providing there is no bond slip nor further crack propagation. Implicit with these requirements then is the need for a constant extensional stiffness over the complete sequence of runs used in the analyses. This will be shown to be justified in Sec. 4.5.2.

If average circumferential wall strains due to observed heights of coal are known, techniques contained in the literature, and summarized in Chap. 2, can be used to find an associated horizontal pressure. The following section

discusses the treatment of measured circumferential strains.

4.4.2 Localized Circumferential Wall Strains

4.4.2.1 General Comments

Comments on measured circumferential strains should be preceded by a discussion of strain reproducibility and expected accuracy. When dealing with relatively small strain measurements such as were obtained during this study, confidence in applying certain types of analyses to the results can only stem from a good knowledge of the instrumental and procedural limitations. During the fourth field trip it became apparent that the equipment used for continuous strain measurements was susceptible to drift over periods longer than several hours. Therefore, in order to compare one set of strains with another that occurred some time previous, accurate static (or quasi-static) readings would be required.

To determine the accuracy and reliability of the static readings, successive readings were made on one gauge. Between readings the leads were disconnected and any strain indicator settings altered. This procedure indicated that the Budd Strain Indicator can be read fairly consistently to within one or two microstrain provided care is taken in making the connections and balancing the meter. Much of the discussion to follow will involve the average strain computed for a gauge location and clearly if small variations of more than two microstrain are discernable with

one gauge, an averaging procedure involving two gauges should give changes in strain that are even more reliable.

This reliability is best illustrated by reference to the chronological record of static strains contained in Figs. J.C1 to J.C35. Of particular note are short term strain variations for the periods June 16 to 17, (Figs. J.C4 to J.C8) when the silo was empty (and cooling), June 19 to June 20 (Figs. J.C16 to J.C19) with a full silo over a twelve hour period, and June 22 to June 23 (Figs. J.C25 to J.C27) when the silo contained a constant amount of coal for a nine hour period.

Although the measured strain differences between two readings are reliable to a few microstrain, the absolute strains, as given by the Budd Indicator, are accurate to within 3% over the range of operation of these gauges. This accuracy was verified using a very accurate ohmmeter and the resistance to strain proportionality by comparing changes in resistance of a dummy gauge to changes in strain.

Short term circumferential strain variations are brought about through local changes in both temperature and pressure on interior and exterior faces. Wind pressures will be ignored due to the low velocities observed over the test period. The effects of varying vertical wall loads (i.e. vertical material loads transfered to the walls through friction) will be commented on later. Circumferential strain variations occur across a section as a rotation (or apparent rotation) and overall at a section as an extension.

Differentiating between temperature and pressure induced strains is necessary for any analyses that follow and to do so requires knowledge of temperature induced stresses in structures of this nature.

4.4.2.2 Thermal Effects

Thermal Moments in Shells

Inner and outer strains at each gauge location were observed to vary at different rates under the apparent effects of varying thermal gradients in the wall. These thermal gradients were due to exterior heating by the sun and interior heating by charging the silo with heated coal.

Cylindrical shells of revolution can, in an overall sense, be considered as unrestrained with respect to temperature effects. Therefore, an overall increase in wall temperature of ΔTavg will produce strains of $\alpha\Delta T$avg without associated stresses.

Shells experience differential strains across their thickness when subjected to a temperature gradient. The expression for the moment at a section subjected to a linear temperature gradient is derived in Appendix F and is

$$M_T = \frac{\alpha\ \Delta T\ D(1+\nu)}{t} \qquad (4.3)$$

where α = coefficient of thermal expansion

ΔT = temperature drop across wall $(T_i - T_o)$

t = wall thickness

$D = Et^3 \ / \ 12(1-\nu^2)$

If the assumption is made that the wall section at which the two gauges are located is symmetric, then the neutral axis for this apparent thermal bending is at the middle surface. Equal and opposite measured strains will therefore occur at the bar locations; strains due to an average increase in the wall temperature will go unobserved because the gauges are temperature compensating. In theory, this then is justification for averaging inner gauge and outer gauge strains to arrive at strains due to circumferential thrust only.

In reality, the above justification for the averaging procedure depends on several important assumptions, summarized here:

1. temperature gradients through the wall are linear
2. wall sections at gauge locations are symmetric
3. changes in average wall temperature do not effect average measured strains

The first assumption will be dealt with in the discussion to follow. The second assumption is important for treatment of strains due to circumferential normal forces as well as those due to thermal moments and will be dealt with in the section on stiffnesses. With respect to the third assumption, strains were observed to depart somewhat from theory as an apparent thermal shift in average strains occured, and shall be discussed more fully at the end of this section.

Wall Temperature Gradients

Heat flow through a wall under normal operating conditions such as occur within this silo will very seldom reach a steady state. With heated coal filled to beyond a certain level, a transient flow exists as the material, at an initial 116°F (47°C), seeks to equilibrate heat content with the surroundings. It is required that a linear or near linear gradient be established in order for the averaging of inner and outer bar strains to be an acceptably accurate method for computing total wall strain.

In Fig. J.C21, at gauge Locations 5 and 6, inner and outer strains exhibit the widest recorded split, in both cases about 174 microstrain, and this occurred after four hours of continual filling. Heat storage for materials is proportional to the product of density and specific heat. Because the heat storage capacity for granular coal is approximately 1000 times greater than that for air, very little energy must be given up by the charging coal to heat the air in the silo's interior to a high ambient temperature.

This was determined directly through observations of temperature levels of in-going and out-going material. A temperature of 117°F (47°C) was recorded from the conveyor belt material on the evening of June 23 prior to Run #9, and because of its deposition at a higher level, this material did not exit from the silo until Run #10. At the time of exit for Run #10 material, a temperature of 113°F (45°C) was

noted for coal discharging into rail cars.

A thermometer was lowered into the silo approximately 10′ below the roof slab and registered a temperature of 95°F (35°C). Although it is difficult to predict air temperature levels within the silo along its unfilled height, it would seem reasonable to base any calculations on the observed level of 95°F (35°C) as free convection and turbulence would provide for efficient mixing. Using the approximate average outside air temperature for the analysed runs as 41°F (5°C), there would exist a 54 F (30 C)[1] total air temperature difference.

The thin-walled *steady state* temperature gradient has been shown to be linear. The task now is to quantify both this gradient and the time required to reach this steady state. Hutchinson (1952) has suggested air film coefficients h of 2.0, 4.0, and 6.0 Btu/hr ft²F for outside air moving at 0, 5, and 10 mph which allow for both convective and radiative losses. For inside air, h was given as 1.65 however within a partially filled silo, air motion corresponds more with outside free convection (i.e. 0 mph wind) and therefore h_i and h_o shall be given as 2.0 and 4.0 respectively. ACI 318-77 utilizes a unit air film thermal resistance ($1/h_o$) of 0.17 which corresponds to an h_o of 5.9.

The coefficient of thermal conductivity, k for concrete is quoted by numerous articles and is very dependent on unit

---

[1]Temperature differences are given in Fahrenheit (F) [or Centigrade (C)] units whereas temperatures are given in °F (or °C).

weight. ACI 318-77 utilizes a k for concrete of about 1.0 Btu/hr ft F however Chapman (1967) and Jakob (1957) would suggest k of 0.8 as more appropriate for normal weight reinforced concrete.

Using the above thermal coefficients, we may calculate the steady state temperature drop in the wall for a total air temperature difference of 54 F (30 C);

$$\mathcal{R}_T = \mathcal{R}_W + \mathcal{R}_i + \mathcal{R}_o = \frac{\Delta x}{k} + \frac{1}{h_i} + \frac{1}{h_o}$$

$$\mathcal{R}_T = \frac{1 \text{ ft}}{0.8 \text{ Btu/hr ft F}} + \frac{1}{2.0 \text{ Btu/hr ft}^2\text{F}} + \frac{1}{4.0 \text{ Btu/hr ft}^2\text{F}}$$

$$\mathcal{R}_T = 1.25 + 0.50 + 0.25$$

$$\Delta T_W = \frac{\mathcal{R}_W \Delta T_T}{\mathcal{R}_T} = \frac{1.25(54 \text{ F})}{2.0} = 33.75 \text{ F}$$

This result is shown as the upper gradient in Fig. 4.2.

A transient analysis is required if sufficient time is not available for this steady state condition to occur and this involves the application of a few simple finite difference equations, given by Dusinberre (1961), (Appendix G). Fig. 4.2 summarizes the above conditions for various lengths of time from zero gradient and reveals that approximately 12 hours is required to get a near linear distribution in the wall. This time would be considerably reduced had a non-zero initial gradient been employed, as would occur during continuous silo usage. This final gradient shall be used therefore as an initial condition in

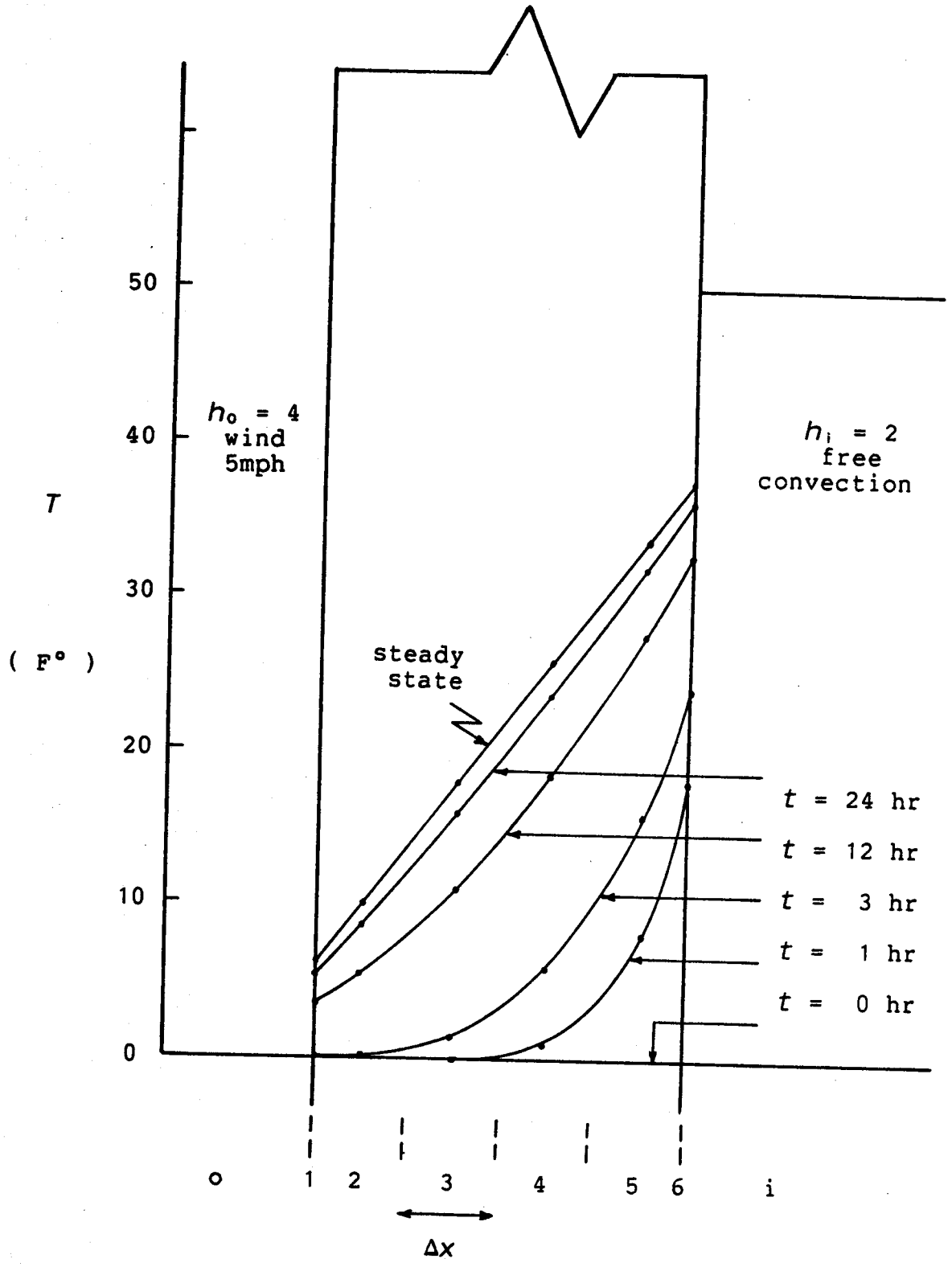

Figure 4.2 Transient Wall Temperatures Due to Heated Air

a transient analysis of temperature gradients in the wall that arise due to contact with heated granular coal.

Particulate well-graded coal with its many and small voids acts as a semi-insulator. Chapman (1967) reports properties of powdered coal with a density of 46 lbm/ft^3 (737 kg/m^3) at 86°F (30°C). The specific heat and thermal conductivity are respectively 0.31 Btu/lbm F and 0.067 Btu/hr ft F although no mention is made of moisture content (m.c.) which can dramatically alter thermal conductivity. Krupiczka (1967) studied air-coal systems analytically and compared results to experimental values reported in the literature that averaged 0.074 Btu/hr ft F (0.11 kcal/m hr C). With a 6% m.c. this value would be closer to 0.08 (0.12 S.I.) assuming the same relative increase of k with m.c. as would occur with a very dense wood. This results from an extrapolation on a chart given by Jakob (1957) of density versus conductivity of wood at various m.c.

The transient analysis of this system is slightly more complex than the previously dealt with situation however Appendix G highlights the process. Fig. 4.3 shows the transient response of this system for the above stated properties.

Placing a heated material against the inner wall face should initially raise the concrete surface temperature. As indicated by the two hour gradient however, this rise is short-lived as the insulating properties of the coal comes into play. Thereafter, the rate of heat flux into the wall

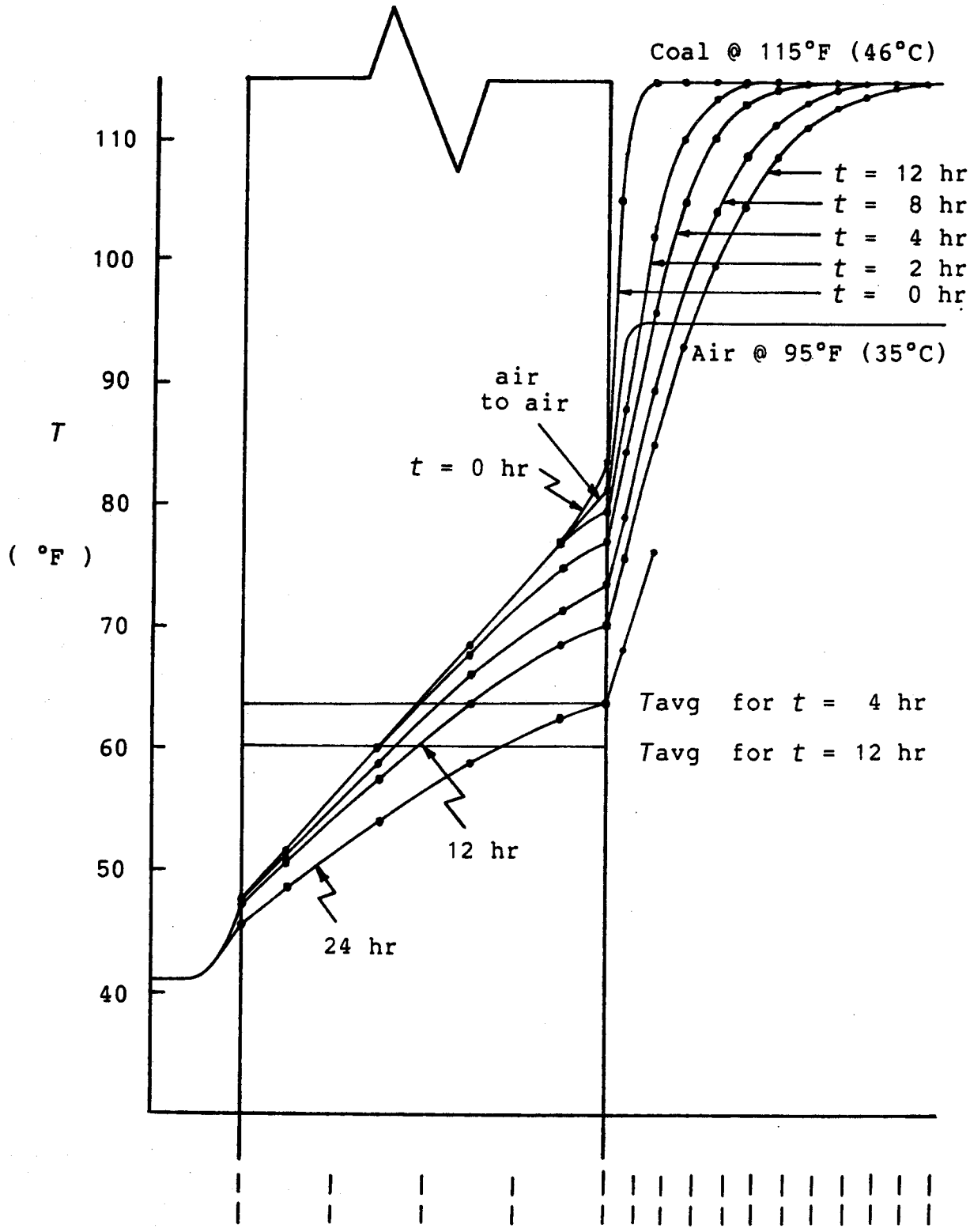

Figure 4.3 Transient Wall Temperatures Due to Heated Coal

is decreasing and will continue to do so as long as conditions remain static. The nature of each plotted gradient in Fig. 4.3 indicates that no appreciable heat content 'bulge' occurs in the wall at any time. Consequently, the assumption of linearity appears justified when one considers that strains, like temperatures, will only deviate from a linear gradient in a singularly curved form. Because the average strain (temperature) crosses this increasingly curved gradient (increasing to the right) slightly to the left of the wall center line (i.e. total wall section temperature stresses, therefore strains, must equilibrate), locations approximately 2 inches from each face (bar locations) will strain similarly and opposite. This occurs even though extreme fibre strains/stresses will show much greater absolute value departures from one another when occurring due to a curved temperature gradient.

This section on wall temperature gradients has established:

1. air-to-air wall temperature gradients during charging of heated coal will normally be greater than 30 F (17 C)
2. air-to-coal wall temperature gradients are approximately 20 F to 30 F (11 C to 17 C), depending on the initial gradient, and are decreasing (at a decreasing rate) with time
3. assumptions of linear temperature gradients are justified within a 1 F latitude
4. average wall temperature is greatest when charging coal

height is below point of interest

5. average wall temperatures will decrease due to insulating nature of cleaned coal
   -approximately 0.8 F (0.4 C) in first four hours from contact
   -approximately 1.8 F (1.0 C) in next four hours and thereafter (with a decreasing rate of decease after twelve hours)

Apparent Thermal Shift in Strain

As discussed earlier, a thin-walled cylinder is free to expand radially when subjected to an increasing average wall temperature and stresses will not occur due to this change in average wall strain. In addition, changes in temperature on an unrestrained member are local in nature. Therefore, at a gauge location that is assumed to be cross-sectionally symmetric, and in light of the previous discussions on temperature gradients, the average of inner and outer bar strains at any location due to temperature only would be expected to equal zero. Refering to Figs. J.C5, J.C6, J.C7, and J.C8 shows this did not generally hold true.

Readings for Fig. J.C5 were chosen as reference for all June 1981 static readings. At the time readings were taken for Fig. J.C5 (12:00 midnight June 16) the silo had been empty for more than fourteen hours and therefore, if some amount of air mixture within the empty structure is assumed,

the inside wall temperature at all locations would be fairly uniform. Average wall temperature would be decreasing slightly and a linear temperature gradient could be expected. In fact, Reading #5 was chosen here as the reference because this was the first empty reading that was followed by readings exhibiting fairly consistent change. Reading #6 (Fig. J.C6), taken 1.25 hours later shows little change in gradient although all locations have shifted approximately 12 microstrain in tension. This shift increases to approximately 15 and 20 microstrain for Readings #7 and #8 (Figs. J.C7 and J.C8) respectively (14.75 and 17.75 hours later) while the gradient is reduced by 20 and 30 microstrain respectively. This degree of consistancy in recorded strains for all six locations has been remarked on earlier. The response being emphasized here is the apparent increase in wall tension at these gauge locations due only to an overall temperature decrease. This phenomenon of thermal shift can be observed throughout the remaining static plots, particularly at the upper gauge locations where, in environments of higher air temperatures that occurred during filling with hot coal, average shifts into compression are indicated. The largest observable thermal shift occured for Reading #21 (Fig. J.C21) when an average compression of -57 microstrain was measured along with a gradient of 174 microstrain at Location 6, which was well above the coal level (i.e. see Fig. J.C20). Location 5 registered a similar gradient however the shift is not as

pronounced, possibly indicating the effects of a 'bulge' in the lower bin region.

The apparent thermal shift cannot be explained in terms of gauges responding to unequal cracking at a section since this approach would require more inner wall than outer wall cracking. This is opposite to what would be expected considering the size of positive moments observed during Runs #8 and #9 (Figs. J.C23 and J.C25 to J.C28). In addition, readings taken on the empty silo, Figs. J.C1 to J.C8, and Figs. J.C9, J.C13, J.C20, and J.C22 to J.C24 indicate that both gauges will strain into compression for greater wall temperatures. This eliminates the possibility that the shift can be calculated as a disproportionate combination of both strain readings.

If these thermal shifts were random, they could be explained as originating in the actual strain indicator but their consistency discounts this possibility. Consistent instrument errors can often explain consistent departures from predicted strains. One such error is possible when using temperature self-compensating gauges and this is the effect of temperature on lead resistance. In this test, however, leads of several feet would be required for this to occur and these gauges had leads of negligible length. The apparent strain versus temperature curve for these gauges (Fig. 3.4 p.108) reveals that these temperature effects are of an opposite nature than that observed (and too small) and therefore we must look elsewhere for an explanation.

One explanation involving bond slip and a variable stiffness at low circumferential stresses does suggest a possible mechanism for this behavior. In the section on stiffness evaluations to follow, it will be shown that this apparent shift in strains is not confined to thermal effects only. Even larger shifts can be shown to occur under circumferential strains due to coal pressures, and this seems to support a bond slip mechanism as being a reasonable description of an apparent strain shift.

4.4.3 Localized Extensional Stiffnesses

4.4.3.1 General Comments

The theoretical stiffness bounds are derived initially and following this, the local extensional stiffness is evaluated for Location 4 and Location 3. The dynamic results indicated that for this series of field measurements, appreciable dynamic pressures occured only at Location 3. The Location 4 stiffness is derived as an additional check on the methods used and as a confirmation of the results for Location 3. To this end, a useful technique is presented for determining the local stiffness at one gauge location by utilizing the known stiffness at a second location. Evaluating stiffnesses for Locations 1 and 2 is difficult at this time given their proximity to the transition. Locations 5 and 6 in most cases are fairly close to the inclined coal surface and this casts doubt on the effective coal heights.

4.4.3.2 Stiffness Bounds

An initial discussion on local circumferential stiffnesses should include the expected upper and lower bounds to these values. At a crack, extensional stiffness is provided by steel area alone. For 30M bars at 8 inches inside and outside, the minimum Et per foot of wall height is;

$$Et = Es(As/ft)$$

$$Et = 29000 \text{ ksi } (3 \times 1.09 \text{in}^2/\text{ft}) = 0.095 \text{ kip/ft/}\epsilon x10^{-6}$$

Gauges at Locations 5 and 6 are mounted on 25M bars:

$$Et = 29000 \text{ ksi } (3 \times 0.78 \text{in}^2/\text{ft}) = 0.068 \text{ kip/ft/}\epsilon x10^{-6}$$

With the modular ratio $n = 8$, a fully effective section would be about 6 times as stiff. For example, at 30M bar locations;

$$Et = \frac{29000}{8} \text{ Ksi } (144-3.27)\text{in}^2/\text{ft} + 0.095 \text{ kip/ft/}\epsilon x10^{-6}$$

$$= 0.60 \text{ kip/ft/}\epsilon x10^{-6}$$

For 25M bar locations;

$$Et = 0.58 \text{ kip/ft/}\epsilon x10^{-6}$$

4.4.3.3 Extensional Stiffness Calibration for Location 4

Location 4 was chosen for the initial stiffness evaluation because it provided the most and widest range of usuable static loadings and associated strains. The second column in Table 4.1 shows the set of four readings used and they in turn correspond to four initial loadings (i.e. previous runs had left the coal height below the elevation of Location 4). The stiffness evaluation can therefore

Table 4.1 Initial Stiffness Evaluation for Location 4

Run#	Fig.# App.J Ser.C	z Effective Coal Height (ft)	P_h * Computed Static Pressure (psf)	Measured Bar Strains ($\mu\epsilon$)				Extensional Stiffness Et ** (kip/ft/$\mu\epsilon$)		
				Outer	Inner	Δ	Avg.	K=0.40	K=0.20	K=0.60
6A	9(M1)	32.7	551.3	95	6	89	50.5	.382	.209	.526
6B	15(Est)	58.3	902.6	170	80	90	125	.253	.147	.328
8	22(M1)	47.4	762.9	123	69	54	96	.278	.158	.370
9	27(M2)	59.0	911.1	254	5	249	129.5	.246	.144	.319

$$P_V^{(1-\beta)} = \frac{C_\beta R}{\mu' K}\left[1 - e^{-\mu' K\, z(1-\beta)/R}\right]$$

where $C_\beta = \gamma_o / [\sigma_o]^\beta$

γ_o = 37.48 pcf

σ_o = 13.0 psf

β = 0.0786

K = 0.40

μ' = 0.50

$R = D/4$ = 17.5

r = 35 ft

* $P_h = K\, P_V$

** $Et = \dfrac{P_h r}{\epsilon}$

note: P_h for K = 0.20 or 0.60 has not been tabulated.

proceed using techniques that predict initial pressures as outlined in the second chapter and described below. Intermediate and final results are also tabulated in Table 4.1. The run number indicates, in each case, the run to follow, but the figure number indicates the set of data used. These figure numbers have included with them, in brackets, an indication of the relative confidence that is placed is their associated coal heights. From these material heights, using a Janssen-Compressibility formulation, reported material properties, and an assumed constant K, one can calculate an associated lateral pressure. The equations and properties used in the calculation are noted beneath Table 4.1. The calculated lateral pressure corresponds to an average thin-walled stress that should in most part be responsible for the measured strains that are reported in the next two columns. Their differences and their averages are also computed, the difference giving some indication of the size of the moment at this section. For example, Run #6A theoretically should have no material pressure induced moment at a reasonable distance from the transition because the coal is deposited in a near axi-symmetric cone. Therefore what appears should be primarily a temperature effect. Similarly Run #6B indicates a comparable temperature effect with no apparent residual moment from the previous run. Runs #8 and #9 however exhibit these residual moments (and of opposite sign) therefore suggesting previous runs established a sizeable 'bulge' at some lower level in the

silo that is still measurable at Location 4.

Extensional stiffness is derived using Eq.[4.2] and so entered in Table 4.1. Expressing the difference in calculated stiffnesses between Run #6A and Run #9 as a percent of the larger Run #6A value, indicates that for all three values of K, a difference of 33% or greater occurs. This is a sizeable gap that must be narrowed or eliminated if any confidence in these Et values is desired. For now it is assumed that K is constant. If this assumption held true, we would expect Et not to vary at all with coal depth or at least exhibit a random variation. For K taken as 0.2, 0.4, and 0.6 (where a minimum K is actually Ka = 0.23), the obvious correspondence of Et with depth of coal z is shown by the results in Table 4.1.

As an initial interpretation however a few useful observations can be made. For Runs #6B and #9, the effective coal heights are approximately the same and an examination of derived stiffnesses for these cases indicate similar values. This fact suggests that Et at Location 4 is constant over the June 1981 test period as previously assumed. It is also important to note that these two readings exhibit radically different inner and outer bar strains for essentially the same coal height. The average bar strains are however within 3% of each other, indicating symmetry of wall section at gauge Location 4. For a widely ranging K, all stiffness results are well within the stiffness bounds for this location (i.e. 0.095 and 0.60) however within each

column the variations are too large, and, as noted above, exhibit a correlation with height. Obviously, the stiffness at any section will be a property of that section and not a function of the height of coal.

If the average measured strain values in Table 4.1 are increased by a constant amount, this will counter the height correspondence to some extent, depending on the overall increase, and the justification for this is the so-called apparent strain shift alluded to earlier. A second technique would be to vary K with depth of coal. Again, to counter the Et-to-z correspondence would require a more rapidly increasing P_h therefore an increasing K with depth. This aspect of initial pressure predictions has seen prior discussion in Chap. 2, and generally involves some speculation so for now we shall concentrate on the apparent strain shift.

To eliminate the unknown effects of this apparent shift and at the same time find an actual K that may be different from what was used in the initial evaluation (0.4), a certain amount of data manipulation is required. If the shift is constant for a location and not a function of load level, it should be possible to compare two sets of strains and two sets of associated pressures directly, effectively eliminating any constant shifts. In essence then, this method uses Eq.[4.2] in the following form:

$$Et = \frac{\Delta P_h r}{\Delta e} \qquad (4.4)$$

Fig. 4.4 reveals graphically why this procedure is better than a procedure using absolute values of P_h and ϵ. The derivation of Et in this way, and its subsequent use, depends only on it being constant over the range of measured strains and the following analysis will show this to be so.

Again, the results taken for Location 4 prior to Runs #6A, #6B, #8, and #9 will be used however instead of treating each individual run, an examination of their respective strain and pressure differences from each of the three remaining sets will be tabulated. This is shown in Table 4.2. The first columns of this table are self-explanatory however the derived Et values in column 6 require some additional comment. The upper three values are based on measured coal heights and show close agreement (2.5% COV) and no apparent correlation with height. The lower three values all involve Run #6B which relied on at best a rough estimate for coal height (i.e. assumed charging rates of dubious constancy) and again exhibit a height correlation. At this point the opportunity now exists to adjust this estimated height to one that more readily 'fits' the known strains while at the same time observing the effects of errors in coal height measurements on calculated stiffnesses.

By assuming for the moment that 0.159 kip/ft/ϵx10^{-6} is the actual extensional wall stiffness at gauge Location 4 over this period of time (i.e. average of upper three values), one can back-calculate the required coal height

Table 4.2 Stiffness Evaluation for Location 4: Comparison Method

Compared Runs		z Coal Heights (ft)		Δz (ft)	ΔP_h from column 4 Table 4.1 (psf)	$\Delta\mu\epsilon$ Avg. column 8 Table 4.1	Et $\frac{\Delta P_h r}{\Delta\mu\epsilon}$ (k/ft/$\mu\epsilon$)
6A	8	32.7	47.4	14.7	211.6	45.5	.163
6A	9	32.7	59.0	26.3	359.8	79	.159
8	9	47.4	59.0	11.6	148.1	33.5	.155
6A	6B	32.7	58.3 (57.3)	25.6 (24.6)	351.3 (339.1)*	74.5	.165 (.159)
8	6B	47.4	58.3 (57.3)	10.9 (9.9)	139.7 (127.5)*	29	.169 (.154)
6B	9	58.3 (57.3)	59.0	0.7 (1.7)	8.5 (20.7)*	4.5	.066 (.161)

* with K = 0.4 and z = 57.3 feet, P_h = 890.4 psf

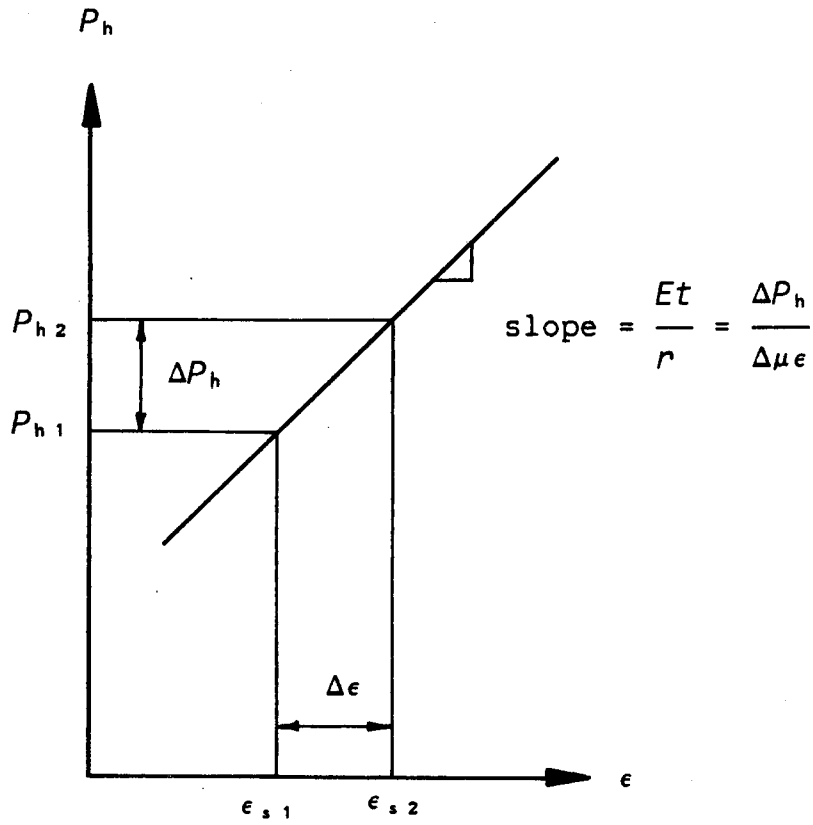

Figure 4.4 Local Stiffness Evaluation

necessary to produce material pressures that will result in the observed strains at this section for Run #6B. This involves solving for z in Eq.[2.18], restated here with the appropriate substitutions.

$$z = \frac{\ln \left| 1 - \sigma_v^{(1-\beta)} \frac{\mu' K}{C_\beta R} \right|}{-\mu' K (1-\beta)/R} \qquad (4.5)$$

Here $\sigma_v = (P_h)_{15} / K$

$(P_h)_{15} = (P_h)_9$[Run #6A] + $(\Delta P_h)_{9-15}$[Run #6A to #6B]

$$(\Delta P_h)_{9-15} = \frac{Et(\Delta\epsilon)_{9-15}[\text{Run \#6A to \#6B}]}{r}$$

This yields a coal height of 57.3′ rather than 58.3′. A change in z such as this is possible as it is well within range of the approximately determined value. In fact, the calculated value is only relative to the coal height used for Run #6A and as such can only be as accurate as this measured height. Run #6A was chosen for the comparison in this back-calculation because its use results in the biggest difference in $\Delta\epsilon$ of the possible runs, thereby minimizing any errors in this technique. If now the adjusted height is used in a re-analysis of Et for Location 4, the result will be the adjusted values shown in brackets. The #6A-#6B comparison will of course yield a stiffness of 0.159 but the remaining two comparisons are reassuring. In addition, choosing any stiffness values (or choosing any possible K that results in these values) in the 0.10 to 0.18 range will

result in 57.3′ as being the optimum adjusted height. The #6B-#9 comparison is a result of dividing a small number by a small number and therefore should not be expected to yield an *Et* value this close to that assumed.

Results are shown in Table 4.3 for *K* ranging from 0.2 to 0.7 in 0.1 increments and indicate that for the present analysis only a good knowledge of this coefficient of lateral earth pressure can ultimately define an accurate extensional stiffness for this location. This becomes apparent when one considers that for the assumed values for *K* the COV is less than 7% if all readings are used in the analysis. The minimum COV occurs when *K* is set at 0.40 however additional data points would be needed to confirm that statistically this is indeed the best *K* for an analysis such as this.

Although we can now say with confidence (but keeping in mind previous assumptions) that the extensional stiffness for Location 4 is in the 0.10 to 0.19 range, (i.e. close to fully cracked at the lower limit and 30% of fully effective at the upper limit) we must rely on judgement and/or information contained in the literature to further refine this value.

Initially, the computed value for *Et* using a *K* of 0.3 or less can be disregarded as this would require an active or close to active pressure field to exist. It is not as clear however whether or not values for *K* of 0.6 or 0.7 are as inappropriate, given that recorded values for *K* with

Table 4.3 Stiffness at Location 4 as a Function of K

Compared Runs	Δz (ft)	Extensional Stiffness Et (kip/ft/$\mu\epsilon$)						
		K=.2	K=.3	K=.4	K=.5	K=.6	K=.7	K=.48
6A 8	14.7	.101	.136	.163	.182	.196	.205	.179
6A 9	26.3	.102	.135	.159	.176	.187	.193	.173
8 9	11.6	.104	.134	.155	.167	.174	.175	.165
6A 6B	24.6	.102	.135	.159	.176	.187	.194	.173
8 6B	9.9	.102	.133	.154	.167	.173	.175	.165
6B 9	1.7	.111	.142	.161	.172	.176	.175	.170
Mean of 6 Rdgs.		.104	.136	.1585	.173	.182	.186	.171
Mean (Top 3)		.102	.135	.159	.175	.186	.191	.172
Stnd.Dev. (6)		.0037	.0032	.0034	.0058	.0092	.0129	.0054
Stnd.Dev. (3)		.0015	.0010	.0040	.0075	.0111	.0151	.0070
COV (6)		3.6%	2.3%	2.2%	3.4%	5.1%	6.9%	3.2%
COV (3)		1.5%	0.7%	2.5%	4.3%	6.0%	7.9%	4.1%

* with K = 0.4 and z = 57.3 feet, P_h = 890.4 psf

grains have been in this range. A judgement based on all reported data for K thus far observed in the literature would suggest K for granular coal as being less than that for the lower density materials such as grains and greater than that for higher density materials such as sand or cement.

Therefore, for lack of any consolidation or compression tests on the material contained within the Fording silo, use will be made of data obtained for a similar material as reported by Blight and Midgely (1980). For a minus 2.4 inch (60mm) cleaned coal that exhibited a gradation line very similar to that given by the sieve analysis done on the Fording sample, they found that a K of 0.48 would accurately represent the ratio of horizontal to vertical pressure in a normally consolidating, laterally confined sample under vertical pressures of approximately 2000 psf and greater. This value is greater than the best fit value between 0.3 and 0.4 suggested by Table 4.3 but is still statistically acceptable and therefore any further analysis shall be undertaken with $K = 0.48$.

Table 4.4 reveals the apparent shifts that are necessary to 'bring in line' the expected (calculated) strains due to material pressures with the observed strains as referenced to an empty silo. The total apparent shift at gauge Location 4 is about 80 microstrain in compression when referenced to Fig. J.C5 data. This increases to approximately 100 microstrain when Fig. J.C8 data is used.

Table 4.4 Apparent Strain Shift at Location 4: K = 0.48

Run#	z Effective Coal Height (ft)	P_h * Computed Static Pressure (psf)	Average Computed Strain ** ($\mu\epsilon$)	Average Observed Strain ($\mu\epsilon$)	Apparent Strain Shift *** ($\mu\epsilon$)
6A	32.7	638.8	131.5	50.5	-81.0
6B	57.3	1007.9	207.5	125	-82.5
8	47.4	871.5	179.4	96	-83.4
9	59.0	1029.8	212.0	129.5	-82.5

* K = 0.48 (refer also to * - Table 4.1)

** $\frac{P_h r}{Et}$ Et = 0.17 kip/ft/$\mu\epsilon$

*** This shift is for Reading 5 data. If Reading 8 data is used, these shifts would change by approximately -20$\mu\epsilon$.

If this Table contained similar calculations using instead a K of 0.20 (and the associated Et of 0.10 from Table 4.3), the required shift would still be approximately 55 microstrain. This fact indicates that the data cannot be meaningfully interpreted without allowing for this shift in strain, whatever its origin, and perhaps the best evidence for this apparent shift can be seen in Fig. 4.5. This graph is a plot of coal heights above Location 4 versus measured strains at Location 4 for the majority of recorded static (and quasi-static) strains. The curve joining the initial static points should resemble the familiar Janssen curve and in this case parallels it (as it has been shown to do so numerically). However, an extrapolation of this curve does not intersect the origin and this fact alone suggests the need for an overall 'shift' of all measured strains (taken at a reasonable depth of coal) to the right by the amount given in Table 4.4.

The need for a shift of this magnitude and the fact that a different set of reference readings will give a different shift immediately raises the question as to what effects exterior air temperature differences might have on the measured strain differences used. For the four sets of data used, exterior weather conditions were reasonably constant; continuous cloud cover, light winds, and temperatures between 5° and 8°C were recorded.

The good correlation in Table 4.4 for these strain shifts stems from the earlier correlation found in Table 4.3

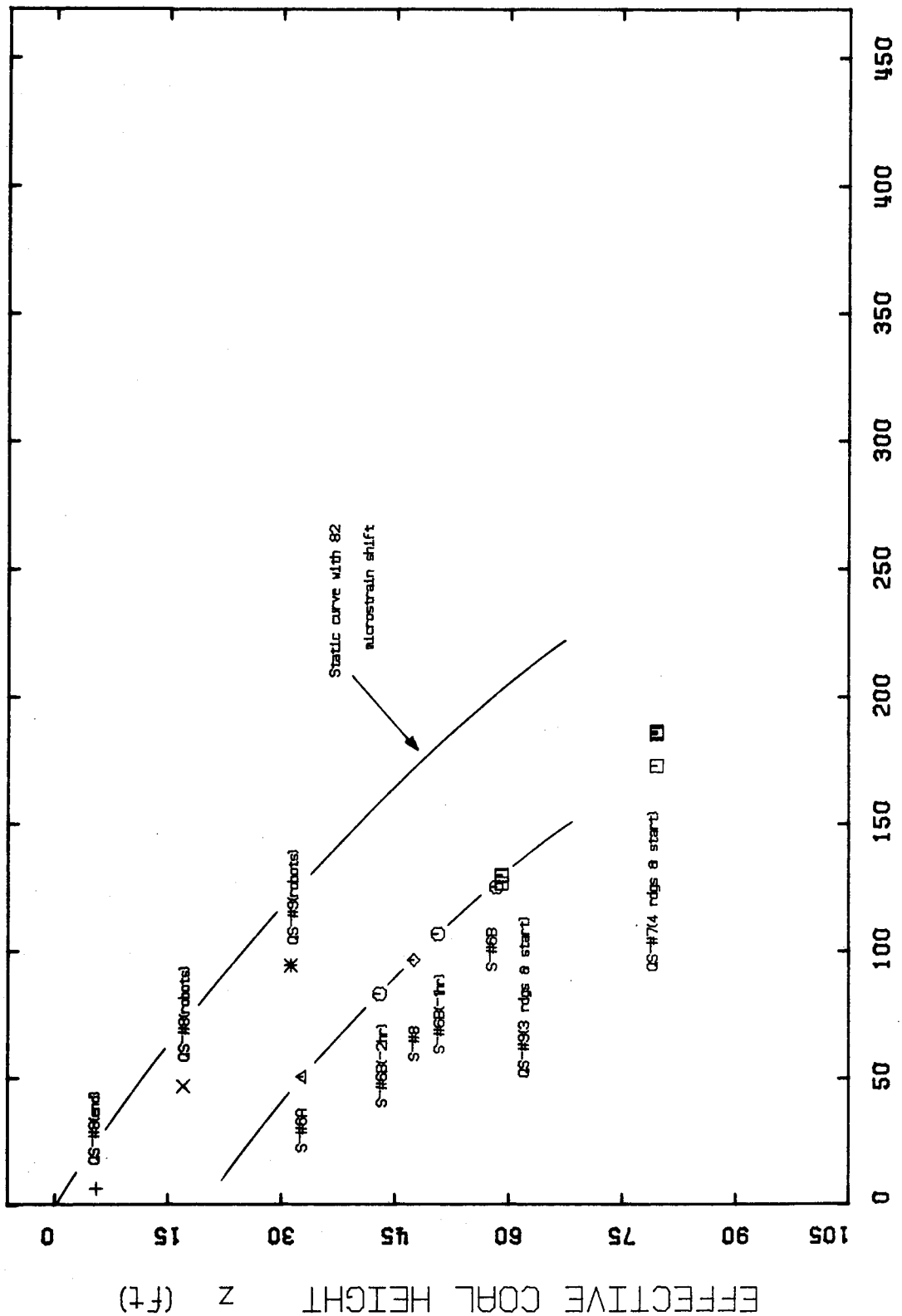

Figure 4.5 Average Static and Quasi-static Readings for Location 4

for Et values using K = 0.48. This correlation is partly a result of adjusting the effective coal height for Run #6B although the COV for the top three readings is certainly reasonable at 4.1%. The low values for the COV for a widely ranging K may also be a reflection of the analytical method; comparing pressures, strains etc.

For example, a 2′ error in the measured coal height seems entirely possible considering the apparatus used and the fact that a circumferentially nonsymmetric material surcharge will form at the surface (i.e. twin peaked). For Run #9, with z = 59.0′, this translates into a 2.5% error in horizontal pressure however if this error is applied to the differences in pressure between Run #6A and Run #9, the result is a 7% deviation in the calculated stiffness. This error increases substantially as the difference in coal heights decreases. In reality, a 2′ error in an effective coal height, as opposed to a measured coal height, is unlikely when it is considered that all measured levels are adjusted for either a measured or assumed material cone in a similar manner. This results in a 2′ measured error reducing to a 2/3′ effective error if two measurements were taken and only one was in error by 2′. In addition, the coal height errors are most likely consistent, and therefore the comparison method eliminates for the most part these types of deviation from fact.

4.4.3.4 Extensional Stiffness Calibration for Location 3

Thus far, the effective extensional stiffness for Location 4 has been established as approximately 0.17 kip/ft/ϵx10^{-6} if the ratio of horizontal to vertical material pressure is assumed to be a constant of 0.48. This result can also be used to derive an extensional stiffness for Location 3. As a first attempt however, *Et* for Location 3 will be determined independently of Location 4. Only data for readings prior to Runs #6A, #6B, and #8 can be used for this purpose. The coal level may not have fallen below Location 3 at the end of Run #6A (see Fig. J.C10) however the Location 3 gradients are similar for Fig. J.C9 (Run #6A) and Fig. J.C15 (Run #6B) and therefore an initial comparison can be made using these three sets of data.

The method is identical to that followed previously and Tables 4.5 and 4.6 summarize the results. The final column in Table 4.6 reveals that *Et* for this location has a mean of 0.094 kip/ft/ϵx10^{-6}. The COV of 12% for this evaluation is relatively large when compared to the values entered in Table 4.3 for Location 4. An additional check on this mean value of 0.094 is therefore needed. Because a fully cracked section should exhibit an *Et* near to 0.095, it is immediately apparent that Location 3 gauges may be situated at or near a complete through-the-wall crack.

A second evaluation of the extensional stiffness at Location 3 can be made if the stiffness at some other point is known. The procedure followed here assumes a reference at

Table 4.5 Stiffness Evaluation for Location 3: Comparison Method

Run#	Fig.# App.J Ser.C	z Effective Coal Height (ft)	P_h * Computed Static Pressure (psf)	Measured Bar Strains ($\mu\epsilon$)			
				Outer	Inner	Δ	Avg.
6A	9(M1)	56.7	1000.1	134	110	24	122
6B	15(Est)	81.3	1279.8	242	218	24	230
8	22(M1)	71.4	1177.1	227	165	62	196

* K = 0.48 (see Table 4.1 for additional information)

Table 4.6 Stiffness for Location 3: K = 0.48

Compared Runs		z Coal Heights (ft)		Δz (ft)	ΔP_h from column 4 Table 4.5 (psf)	$\Delta\mu\epsilon$ Avg. column 8 Table 4.5	Et * $\frac{\Delta P_h r}{\Delta\mu\epsilon}$ (k/ft/$\mu\epsilon$)
6A	6B	56.7	81.3	24.6	279.7	108	.091
6A	8	56.7	71.4	14.7	177.0	74	.084
8	6B	71.4	81.3	9.9	102.7	34	.106

* Mean = .094, COV = 12.0%

Location 4 which includes a stiffness value and a corresponding K along with an effective coal height and the corresponding strains. Using a second set of initial static strain measurements for both locations and knowing that the vertical distance between locations is 24', a corresponding stiffness at Location 3 can be calculated.

The calculations can be made using any two sets of data so long as the material height is known for one set. The data sets that will be evaluated here are the three static records taken prior to Run #6B (Figs. J.C13, J.C14, and J.C15). Only one hour separates each of these readings and therefore temperature effects and the effects of changes in K will be minimized (see conclusions at end of section on wall temperature gradients, p.128). During this period coal was being charged at a rate of approximately 450 Tons/hr. Tables 4.7 and 4.8 summarize the results for the following calculations.

The horizontal pressure at Location 4 for Fig. J.C15 (Run #6B) was given earlier but is repeated here.

$$(P_{h_4})_{15} = 1007.9 \text{ psf [from column 3, Table 4.4]}$$

This assumes an Et of 0.17 kip/ft/$\mu\epsilon$ and K = 0.48. The changes in average strain at Location 4 between Figs. J.C14 and J.C15 and Figs. J.C13 and J.C14 are

$$(\Delta\mu\epsilon_4)_{14-15} = 18.5\ \mu\epsilon$$

$$(\Delta\mu\epsilon_4)_{13-14} = 23.5\ \mu\epsilon$$

Table 4.7 Horizontal Pressures and Strains for Location 3 from ΔP_h Location 4

Fig. # **	P_h Loc. 4 see text (psf)	z Loc.4 (ft)	z Loc.3 (col.3 +24ft) (ft)	P_h Loc. 3 * (psf)	Measured Bar Strains Loc. 3 ($\mu\epsilon$)			
					Outer	Inner	Δ	Avg.
13	803.9	42.87	66.87	1126.2	195	164	31	179.5
14	918.0	50.64	74.64	1211.7	224	193	31	208.5
15	1007.9	57.3	81.3	1279.8	242	218	24	230

* K = 0.48 (see Table 4.1 for additional parameters)

** Appendix J, Series C

Table 4.8 Stiffnesses for Location 3 from Location 4 Results

Compared Rdgs. Series C		Δz (ft)	ΔP_h from column 5 Table 4.7 (psf)	$\Delta\mu\epsilon$ Avg. column 9 Table 4.7	Et * $\frac{\Delta P_h r}{\Delta\mu\epsilon}$ (k/ft/$\mu\epsilon$)
13	14	7.7	85.5	29	.101
14	15	6.7	68.1	21.5	.111
13	15	14.4	153.6	50.5	.107

* Mean = .107, COV = 3.8%

The following relationship gives corresponding changes in lateral pressure at Location 4.

$$\Delta P_{h4} = \frac{Et_4 \Delta\mu\epsilon_4}{r}$$

from which

$$(\Delta P_{h4})_{14-15} = 89.9 \text{ psf}$$

$$(\Delta P_{h4})_{13-14} = 114.1 \text{ psf}$$

Therefore

$$(P_{h4})_{14} = 1007.9 - 89.9 = 918.0 \text{ psf}$$

$$(P_{h4})_{13} = 918.0 - 114.1 = 803.9 \text{ psf}$$

The required coal heights to achieve these pressures are then computed from Eq.[4.5] and recorded in column 3, Table 4.7. Coal heights at Location 3 are simply 24′ below these levels and their associated pressures are tabulated in column 5. These pressures, along with average strains reported in the last column, are used in calculating the differences in pressures and strains that appear in columns 3 and 4, Table 4.8. The resultant extensional stiffnesses are computed for Location 3 and so entered.

The coal heights calculated in this way are relatively insensitive to the stiffness value (and corresponding K) assumed for Location 4. The above operations were repeated using $(Et)_4 = 0.159$ (with $K = 0.40$) and $(Et)_4 = 0.175$ (with $K = 0.50$) and the resulting coal heights at Location 3 (for Fig. J.C14) were, respectively, 74.7′ and 74.5′. However, the final stiffness value computed for Location 3 is again a

function of K, just as it was for Location 4.

The results in Table 4.8 tend to support the previously derived stiffness value of 0.094, although with some discrepancy (14%), and again indicate that extensive or near complete bond loss has occured at the Location 3 gauges.

Apparent shifts are tabulated in Table 4.9 and reveal a much larger compressive strain shift occured at this location than that observed at Location 4. Fig. 4.6 is a plot for Location 3 similar to that done for Location 4 and again indicates graphically the apparent strain shift.

4.4.3.5 Stiffness Evaluations using Variable K

The discussion in Sect. 2.1.6 suggests that K is probably a variable parameter. This possibility will be investigated here only briefly because the rate of variation and the maximum value of K are as yet unknown.

It was postulated that K may be a function of a material's relative density in an initial pressure field (Eq.[2.13], repeated here).

$$K = Dr^m K_m \qquad (4.6)$$

A closed form solution to an equivalent Janssen type formulation of the problem with both γ and K as functions of consolidating pressure[1] is nonintegrable and therefore a numerical technique is employed to examine this theory. This program is contained in Appendix G, complete with portions

---

[1]Relative density is a function of γ and therefore consolidating pressure.

Table 4.9 Apparent Strain Shift at Location 3: K = 0.48

Run#	Fig.# App.J	z Effective Coal Height (ft)	P_h * Computed Static Pressure (psf)	Average Computed Strain ** ($\mu\epsilon$)	Average Observed Strain ($\mu\epsilon$)	Apparent Strain Shift ($\mu\epsilon$)
6A	C9	56.7	1000.1	333.4	122	-211
6B	C13	66.9	1126.2	375.4	179.5	-196
6B	C14	74.6	1211.7	403.9	208.5	-195
6B	C15	81.3	1279.8	426.6	230	-197
8	C22	71.4	1177.1	392.4	196	-196

* K = 0.48 (refer also to * - Table 4.1)

** $\frac{P_h r}{Et}$ Et = 0.105 kip/ft/$\mu\epsilon$

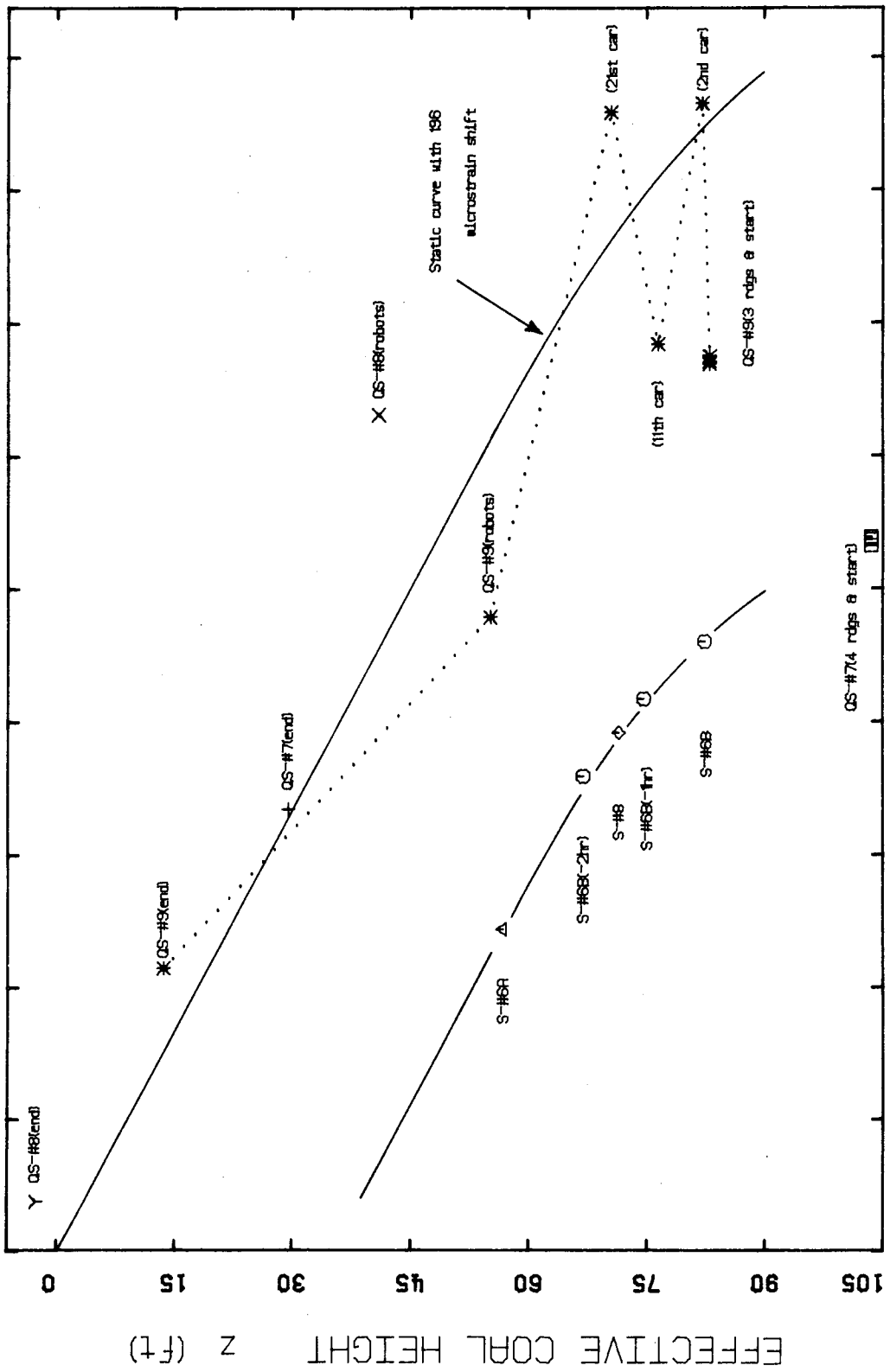

Figure 4.6 Average Static and Quasi-static Readings for Location 3

of the input and output used in this examination.

In short, the program formulates equilibrium on a number of Janssen elements, (i.e. disc shaped for a cylinder) and in doing so numerically integrates the various disc pressures. The accuracy of the program has been compared to an actual Janssen solution and to a Janssen-Compressibility solution and was found to give results within 1% error if the disc element's height is kept small.

An analysis similar to that done previous to this section for the data from Locations 3 and 4 is summarized in Table 4.10. The procedures for dealing with changes in strains and pressures are identical and the pressure data used has been obtained directly from linear interpolations of output from the Appendix G program for 0.2′ increments. The maximum value for K was set at 0.50 (to correspond with the value reported by Blight and Midgely of 0.48) and up to that point K varies directly with relative density (m = 1). Compressibility effects were also included. The results for Location 4 exhibit an acceptable COV (2.7%) however they are inconclusive when compared to the previous stiffness results utilizing a K that is constant. The Location 3 results that are based on the Location 4 stiffness not surprisingly exhibit a similar COV (3.3%) however the Location 4 stiffness derived from a comparison of static readings for Runs #6A, #6B, and #8 reveal a more sizeable discrepancy with a COV of 11.6% and this compares well with the results

Table 4.10 Stiffness Evaluation with K Variable

	Compared Runs or Rdgs.	z (K) Coal Heights (with corresponding K) (ft)	(ft)	P_h K variable to 0.50 (psf)		ΔP_h (psf)	$\Delta\mu\epsilon$ Avg.	Et (kip/ ft/$\mu\epsilon$)	
LOC 4	6A 8	32.7(.432)	47.4(.456)	581.2	843.6	262.4	45.5	.202	
	6A 9	32.7(.432)	59.0(.469)	581.2	1024.2	443.0	79	.196	mean .194
	8 9	47.4(.456)	59.0(.469)	843.6	1024.2	180.6	33.5	.189	
	6A 6B	32.7(.432)	57.3(.467)	581.2	999.2	418.0	74.5	.196	COV 2.7%
	8 6B	47.4(.456)	57.3(.467)	843.6	999.2	155.6	29	.188	
	6B 9	57.3(.467)	59.0(.469)	999.2	1024.2	25.0	4.5	.194	
LOC 3	C13 C14	66.9(.475)	74.6(.480)	1133.8	1230.7	96.9	29	.117	mean .12
	C14 C15	74.6(.480)	81.3(.484)	1230.7	1307.5	76.8	21.5	.125	
	C13 C15	66.9(.475)	81.3(.484)	1133.8	1307.5	173.7	50.5	.120	COV 3.3%
	6A 6B	56.7(.466)	81.3(.484)	990.3	1307.5	317.2	108	.106	mean .106
	6A 8	56.7(.466)	71.4(.478)	990.3	1191.6	201.3	74	.095	
	8 6B	71.4(.478)	81.3(.484)	1191.6	1307.5	115.9	34	.119	COV 11.6%

in Table 4.6 using a constant K.

The program used in this analysis to calculate these lateral pressures allows for a variation in both K_m and m in Eq.[4.6]. It was found that for m of 0.5, 1.0, 2.0, and 4.0, the change in pressure did not reduce the COV and with K_m ranging from 0.45 to 0.60 only a slight reduction in the COV was noted. In addition, changes in K_m had very little effect on the mean value for Et, however an increase in m from 1.0 to 4.0 caused Et to increase from 0.106 to 0.138.

4.4.4 Summary

The stiffness bounds for Location 3 have been narrowed to values ranging from 0.095 kip/ft/$\mu\epsilon$ to approximately 0.12 kip/ft/$\mu\epsilon$ (fully cracked to a section with about 5% of the concrete effective). From this initial static strain record and the associated effective coal heights, it is difficult to say with any certainty which value for Et is most appropriate. Although the data presented here is conducive to plotting smooth curves (Figs. 4.5 and 4.6), a best-fit analysis would be presumptuous, given the meager number of data points. Therefore , a constant value for K of 0.48 will be employed in that this assumption has some support in the literature. The analysis does not show however that K is constant, only that for present purposes this assumption of constancy gives reasonable error.

The larger COV for the Location 3 stiffness cannot be reduced by manipulating the variation of K (i.e. m) nor the

upper limit to K (i.e. K_m). Two possibilities remain. Firstly, the assumptions made in this chapter could be sufficiently inaccurate and could combine in such a way so as to produce uninterpretable smooth curves. Secondly, and in the author's opinion more likely, the calculated lateral pressures are, in all cases, proportionally greater than those that actually occurred within the silo and this error is of a nature that increases with depth. This would mean that the Location 4 evaluations, which generally have smaller COV's, would be less affected than those for Location 3, which were done using 70 and 80 foot depths. It was found that reducing (relatively) lateral pressures, at a rate that increased with height, brought Location 3 stiffnesses more in line. A conceivable mechanism for this increasing rate of reduction is an increasing mobilization of wall friction with depth. This idea has been discussed in Chap. 2 and will receive further discussion in Chap. 6.

For the dynamic analysis to follow, the extensional stiffness for Location 3 will be taken as 0.105 kip/ft/$\mu\epsilon$. This value is an approximation that should be within 10% of the true Et and that also coincides with the means in Table 4.8 and the bottom of Table 4.10.

5. Dynamic Test Results and Overpressure Factors

5.1 Introductory Remarks

In this chapter, the overpressure factors (o.p.f.'s) observed during the final three runs will be given. Although the o.p.f.'s derived in this study are similar to the ACI C_d factor, they are not directly comparable. Because ACI 313-77 uses Ka to calculate initial static pressures, the o.p.f.'s given in the following analyses would necessarily be much larger if applied to these unrealistically low static pressures. In some cases, comparisons will be made between the overpressure factors derived in this study and equivalent C_d factors.

Fig. 5.1 describes graphically the methodology used to calculate an o.p.f. in this chapter. The abscissa represents average measured strains (referenced to an empty silo) for one gauge location. The ordinate represents calculated coal pressures; P_s is given by a Janssen curve or some similar distribution while P_d falls on an assumed straight line extrapolation of the stiffness relation corresponding to a particular measured strain on the abscissa.

The value selected for Et is important in that it assumes a particular K (or variation in K) to be the more plausible of many. In terms of its effect on o.p.f.'s however, K appears to be of relatively minor influence. This becomes evident on closer examination of Fig. 5.1. If a second stiffness value, $(Et)_2$, is used in the analysis in

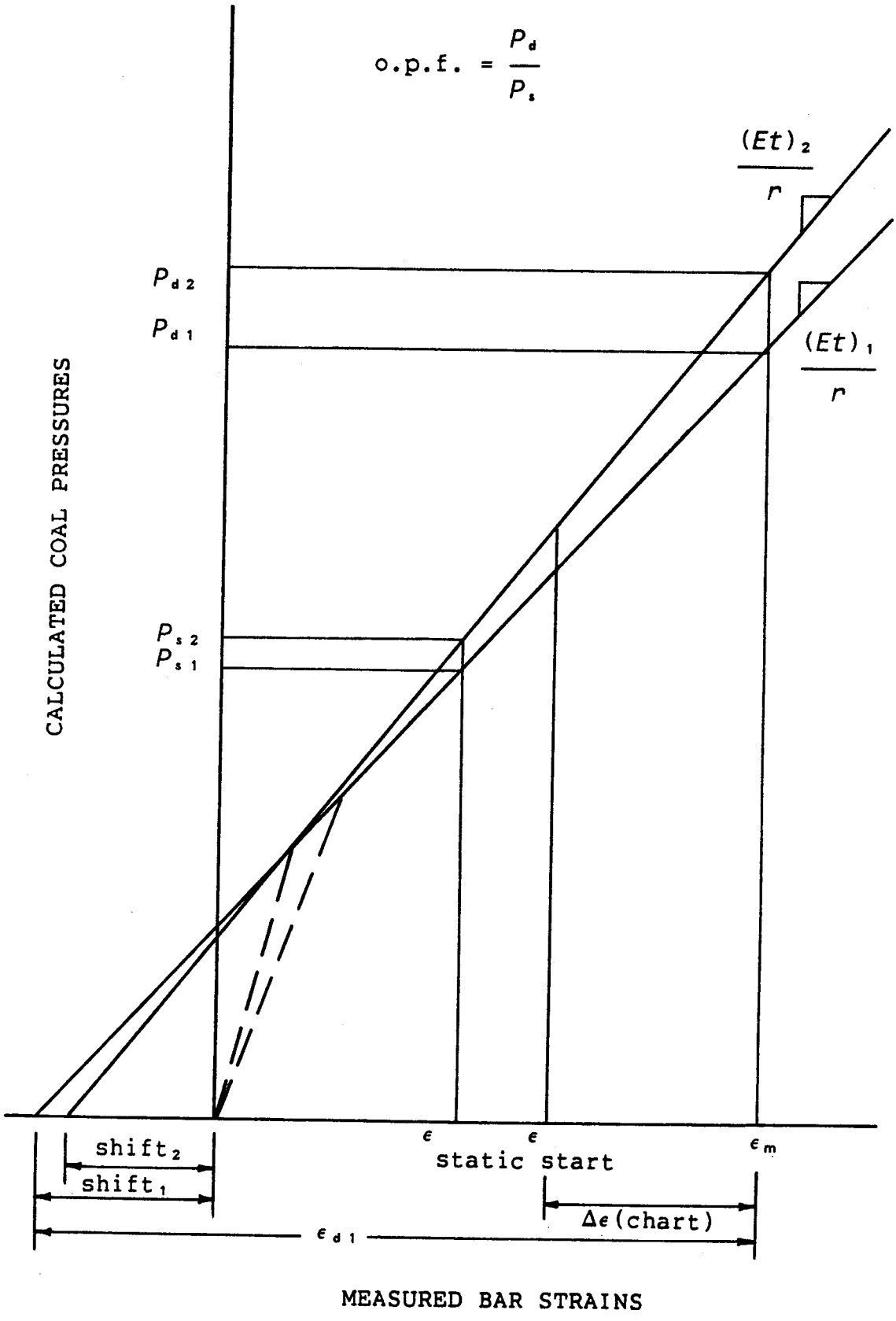

Figure 5.1 Overpressure Factors

place of $(Et)_1$, the o.p.f. calculated varies only marginally as P_s and P_d will increase at Location 3 in a manner nearly proportional to their magnitudes. A value of 0.105 kips/ft/$\mu\epsilon$ for Location 3 is assumed in the calculations to follow.

Because overpressures for this silo are normally accompanied by larger moments, eccentricities will also be computed and this will require knowledge of the local flexural stiffness. The following evaluation of the flexural stiffness at a particular location assumes that EI is symmetric about the wall's midsurface. This assumption was implicit in Chap. 4 when Et, the unit extensional stiffness, was assumed symmetric because this allowed the average of inner and outer bar strains to represent the average wall strain. Locating the effective concrete area requires an additional assumption, however this area of concrete is small for Location 3.

With Et = 0.105 kips/ft/$\mu\epsilon$ = EA/ft ;

$EA = Es\ As + Ec\ Ac$

$0.105x10^6 \text{kips} = 29000\text{ksi}(3.27\text{in}^2) + Ec\ Ac$

$Ec\ Ac = 0.0102x10^6 \text{kips}$ (i.e. 10% of EA)

Using a modular ratio, n = 8,

$$\frac{29000\text{ksi}}{8} Ac = 0.0102x10^6 \text{kips}$$

Therefore Ac = 2.81 in^2. Assuming 1/2 of this

concrete area to act at the location of each bar,

$$EI/\text{ft} = 2\left[\frac{3.27\text{in}^2}{2}(4\text{in})^2 29000\text{ksi} + \frac{2.8\text{in}^2}{2}(4\text{in})^2\frac{29000\text{ksi}}{8}\right]$$

$$EI/\text{ft} = \left(3.27 + \frac{2.8}{8}\right)\text{in}^2(4\text{in})^2(29000\text{ksi}) = 1.68x10^6\,\text{k}\cdot\text{in}^2$$

Therefore 90% of the flexural stiffness at Location 3 is provided by the hoop steel. The stress in each bar is related to the moment by the *elastic flexure formula.*

For a section subjected to a unit positive moment, M/ft:

$$\frac{\sigma_o - \sigma_i}{2} = \frac{(M/\text{ft})y}{I/\text{ft}}$$

where $y \simeq 4$ inches and σ_o, σ_i are actual bar stresses. Using the stress - strain relationship,

$$M/\text{ft} = \frac{(EI/\text{ft})\epsilon}{4\text{in}} \qquad \epsilon = \frac{\epsilon_o - \epsilon_i}{2}$$

The unit tensile force, T/ft, in the wall is given by

$$T/\text{ft} = P_h r$$

Eccentricity, e is therefore

$$e = \frac{M/\text{ft}}{T/\text{ft}} = \frac{(EI/\text{ft})(\epsilon_o - \epsilon_i)}{(4\text{in})(2)P_h r}$$

$$e = \frac{1.68x10^6\,\text{k}\cdot\text{in}^2/\text{ft}\ (\epsilon_o - \epsilon_i)}{(4\text{in})(2)P_h(35x12\text{in})}$$

With $(\epsilon_o - \epsilon_i)$ in $\epsilon x10^{-6}$ and P_h in psf, e in inches is

$$e = \frac{(\epsilon_o - \epsilon_i)6.0}{P_h}$$

Fig. 5.2 represents an example of dynamic output for Run #9. It includes two load-out events (i.e. the loading of two cars) and the associated strains for Locations 2, 3, and 4, as recorded for the start of Run #9. The noticeably larger peaks are typical of the wall response to individual gate openings. Just prior to the first gate at the first car the strain output appears as a straight line and this is in fact the strain levels given by Budd readings prior to this run (Fig. J.C27). A slight amount of electronic noise is superposed on these initial static (or quasi-static) strain levels; this noise was absent on chart records taken on site and is therefore associated with the recording equipment. Deflections were taken directly from these charts, calibration factors applied to these deflections, and associated changes in strain computed. This information will be presented in tabular form for each of the individual runs studied in detail.

5.2 Runs #1 - #5 : General Observations

As indicated at the end of Chap. 3, Run #1 (Oct. 1980) was the first attempt at collecting dynamic strain readings for this silo. This was also the virgin loading-unloading sequence for the upper bin portion of this structure and as

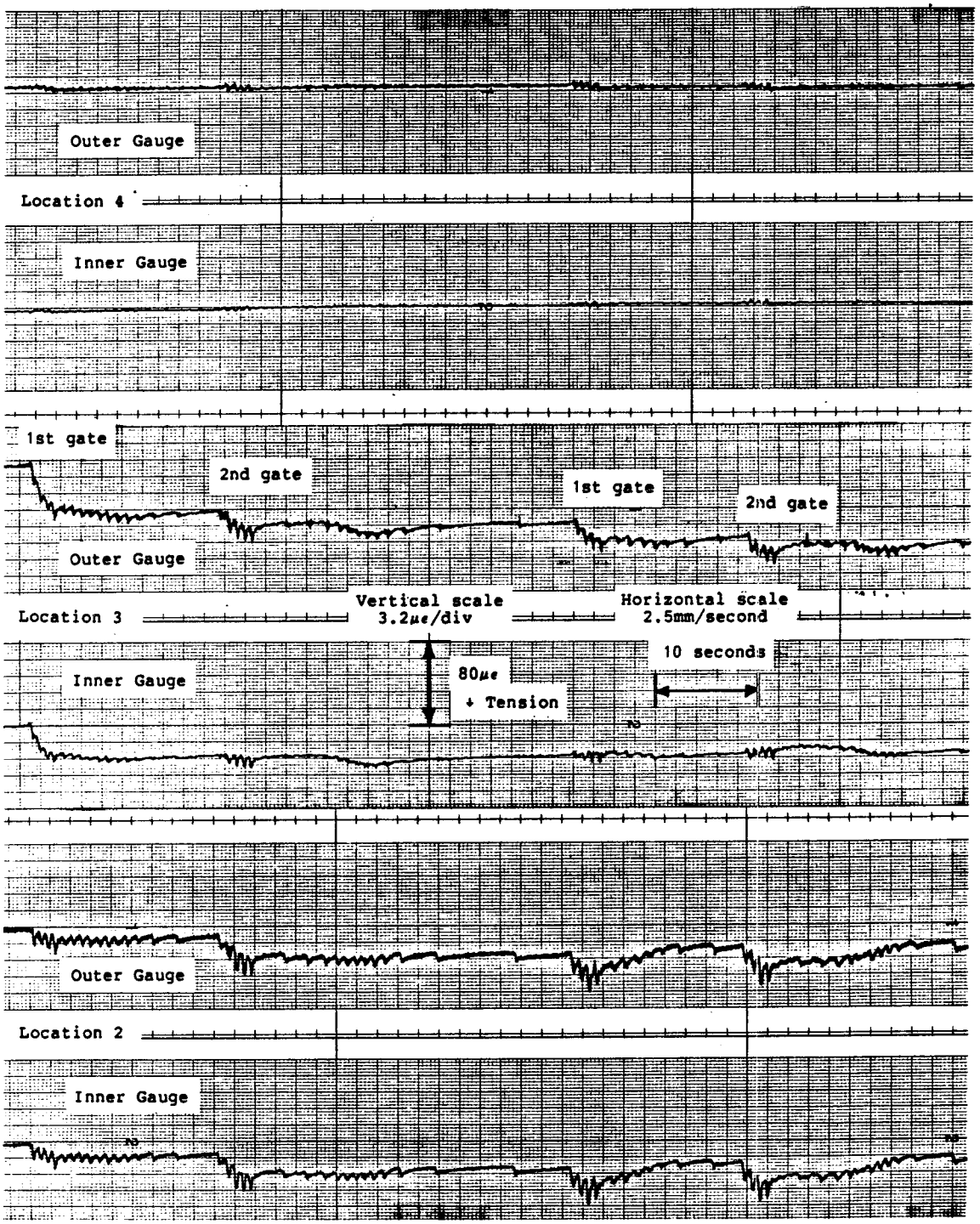

Figure 5.2 Continuous Strain Output

for Locations 2, 3, and 4 at the Start of Run #9

such the silo was approximately 2/3 full, with coal at about 80′ from the transition (50% into the cylinder). Although dynamic strains were observed to occur at the lower gauges when monitored by the Budd Indicator (i.e. slight galvanometer deflections), recorded strain levels were virtually unaffected as equipment sensitivity was set too low. This was unfortunate because it negated the possibility of deriving o.p.f. for the structure in its stiffest state.

For Runs #2 through #5 (Jan. 1981), the output from the signal conditioner was increased by a factor of 2.4 (to full gain) and every effort was made to observe even minor fluctuations. During Runs #2 and #3 the cylinder contained coal to about 60% of its height and for Runs #4 and #5 the silo was full at the start of unloading. For these runs, initial train speeds of 0.2 mph were used and therefore drawoff was much slower than for later runs. The dynamic results indicated in all cases except for Run #3 that maximum tensile strains occured at the first car and for Run #3 these occured at the third car.

The silo received very little use between the virgin loading of Oct. 1980 and Jan. 1981 and quite possibly had not cracked sufficiently at the gauge locations to warrant application of June 1981 derived stiffnesses. As discussed earlier, the more extensive vertical cracks did not become evident until the June field trip. A stiffness evaluation could not be done for any gauge location in the January runs because coal levels were either unknown or coal pressures

were not of an initial static distribution.

In Chap. 3, mention was made of balance and drift problems that hindered direct strain level comparisons of dynamic readings more than a few hours old; often more than a few minutes old. Therefore, much of the effort expended in data collection for Runs #2 through #5 was directed at solving these types of problems. A preliminary analysis of these results, not reported here, indicated the need for more static and/or quasi-static readings (i.e. reference readings) as well as better knowledge of effective coal heights and these areas were concentrated on during the final field trip.

5.3 Runs #6A - #10 : Dynamic Overpressures

5.3.1 General Comments

Runs 6A through 10 warrant individual treatment because at this point in the collection of data, equipment settings had been finalized and equipment limitations were fairly well understood. During these last runs, the chart recorder proved invaluable as it provided simultaneous monitoring of events. It also provided generally distortion free output and therefore gave the largest possible gain. A chronological presentation of the remaining runs will be used here. It was observed that quasi-static strains evident at the start of one run often originated in the previous run. This was expected, and was first observed during the

January field trip. Strain readings for a full silo prior to Run #4 (Fig. J.B6) differed noticeably from those for Run #5 (Fig. J.B8), again a full silo.

5.3.2 Run #6A

This run could not be used for a direct determination of an o.p.f. because only the outer gauges were monitored by reliable channels on the Validyne. Several observations can be made however.

Fig. J.C9 shows static strains observed just prior to this run and as such reveals the only set of static strains in which all six locations are strained under an initial static field (i.e. including the hopper and transition). The inner-outer strain reversal evident at the two transition gauge locations suggests that a negative moment has developed in this side of the silo (probably with the silo bulging at the transition in a north - south direction). Jenike *et al.* (Part 3, 1973) predict hopper transition loads under initial conditions that for this silo would result in hopper transition wedge pressures (east - west pressures) of $1.2\sigma_v$. This is 1.7 times the hopper transition cone pressures ($0.7\sigma_v$) in the north - south direction) forcing an ovalization opposite to what Fig. J.C9 strains would suggest. The explanation may be that transition stiffness is more important in strain development than initial pressures are. It is also apparent from Fig. J.C9 that this transition moment is large enough to negate the thermal moment at

Location 2.

For Run #6A, the train speed began at 0.5 mph but was increased at the 14th car to 0.7 mph. The wall strains were observed to bottom out (in tension) at the 15th car and then move rapidly in the compressive direction in a series of wildly fluctuating loading events. This then was the first evidence for wall strains being influenced by the rate of material withdrawal. This behavior was most evident at Location 3 however Location 4 did behave in a similar but more subdued fashion. Location 5 showed no response at all except at the first gate opening but this was negligible. The frequency of the large oscillations that normally occur upon gate opening were also seen to be independent of flow rate.

5.3.3 Run #6B

Run #6B occured with little warning time of the approaching train and therefore only one channel was monitored during loadout. In this run, an 11 car train was being loaded and therefore maximum strains probably did not have time to develop. This did however provide an opportunity to more accurately determine the oscillatory period of the strain fluctuations during flow, and this was done by increasing chart speed to an abnormal level. These oscillations were found to have a frequency of 1.5 to 1.6 Hz and although composed of a variety of smaller fluctuations, they appear to approximate a sinusoidal shape.

At the end of the 11th car, the chart revealed that the outer gauge at Location 3 was still moving slowly into tension. Because gauges at Locations 3 and 4 probably did not have the opportunity to strain into the normally expected higher dynamic ranges during this run, quasi-static readings prior to Run #7 at these locations are near to initial static. This is shown in Figs. 4.5 (p.147) and 4.6 (p.156). The stiffness calibrations in Sect. 4.4.3.3 and Sect. 4.4.3.4 did not include these points specifically because it was felt that some locked-in dynamic pressures would be present at the end of Run #6B that might cause the static readings taken prior to Run #7 to not accurately reflect strains caused by an initial pressure field.

5.3.4 Run #7

Of the June runs, Run #7 was the only run in which the silo was unloaded from a completely filled state. This fact by itself would suggest that this run might therefore result in the largest measured static and dynamic pressures (although not necessarily the largest o.p.f.'s). Although this was true for static pressures, this was not the case for dynamic pressures.

Figs. J.C16 to J.C19 reveal the quasi-static strains observed prior to Run #7, and, as discussed in the previous section, were largely set up by Run #6B overpressures and superposed by an initial field above. At the first gate, the train speed was 0.5 mph and Location 2 strains were observed

to decrease by approximately 90 microstrain. The strain on the outer gauge at Location 3 increased approximately 40 microstrain on the first gate and reached a maximum of approximately 120 microstrain at the 20th car. As will be seen shortly (Runs #8 to #10), this is a relatively modest increase and probably has much to do with the 0.5 mph speed that the train was kept at for the duration of Run #7.

Coal height measurements taken before and after Run #7 afforded the opportunity to check on the assumed in-situ density of coal for these runs. With the silo filled completely at the start, an accurate initial coal level is known. Two depth readings were taken at the end of this run, one beneath the west charging chute and one at the wall. These two readings differed by approximately 5′ and the effective coal level could be expected to fall within these two bounds. Using levels reported in Table 3.1, the change in effective coal height can be calculated at 74′. Out-loaded gross weight data indicated that, for Run #7, a total of 108 cars weighing 22791 kips registered at the scales. With average tare weights of 56 kips per car, the resulting net weight of coal removed was 16700 kips. The cylindrical volume for 74′ of coal with a 35′ radius is 285170 ft^3 and these two values yield an in-situ density of 58.7 pcf, not far off the assumed maximum of 58 pcf.

The amount of coal taken from the silo during this run equaled just under 1/2 the silo's capacity and therefore the withdrawn volume included only material that in-situ was

under at least 90′ of head. This withdrawn material can then be said to have experienced close to its maximum densification and therefore similar but more detailed calculations in the runs to follow should yield reasonably accurate changes in coal height.

5.3.5 Run #8

Run #8 is the first of the remaining runs in which enough dynamic strain data was available for a detailed study of overpressures and this is presented in Table 5.1 for Location 3. Location 4 strains were also closely monitored at this time but subsequent examination of chart output indicated negligible strain response at that height.

The final two columns in Table 5.1 are of primary importance; descriptions of eccentricity and overpressure calculations have been given in Sect. 5.1. The second column contains information provided by the on site load-out system and previous use has been made of these weights to calculate an in-situ material density. These weights are used here to keep a running tally of approximate loaded-out weights to give approximate changes in coal height. The remaining columns are self-explanatory.

The o.p.f. starts at 1.00 (i.e. Fig. 4.6 indicates pressures are close to intial static) but with some initial moment, part of which is thermal in origin. During loading of the first car, only one gate was in use. Both inner and outer gauges strained to a similar 4% over static shortly

Table 5.1 O.P.F.'s Observed During Run #8

n car no.	Gross Vehicle Weights (lbs)	Cumulative Vehicle Weights (Tons)	Δz from z=71.4' (ft)	z Coal Height (ft)	P_s Static Pressure (psf)	$\epsilon_o - \epsilon_i$ Δ from Ref.Rdg. ($x10^{-6}$)	ϵ_m Measured Strain ($x10^{-6}$)	ϵ_d Dynamic Strain ($x10^{-6}$)	P_d Dynamic Pressure (psf)	e $\frac{M}{P_d}$ (in)	o.p.f. $\frac{P_d}{P_s}$	Remarks
-	-	0	0	71.4	1177	62	196	392	1176	0.32	1.00	Start of run
1	-	-	~0.2	71.2	1175	62	210	406	1218	0.31	1.04	35% of car 1
1	-	-	~0.4	71.0	1173	76	210	406	1218	0.37	1.04	70% of car 1
1	-	-	~0.5	70.9	1171	86	210	406	1218	0.42	1.04	90% of car 1
1	180440	90.2	0.56	70.8	1170	86	201	397	1191	0.43	1.00	End of car 1
2	-	-	~1.2	70.2	1164	114	215	411	1233	0.55	1.06	After 2nd gate
2	216490	198.5	1.28	70.1	-	-	-	-	-	-	-	End of car 2
3	-	-	~1.5	69.9	1160	117	216	412	1236	0.57	1.07	After 1st gate
3	222370	309.7	2.02	69.4	-	-	-	-	-	-	-	End of car 3
4-5	435490	527.4	3.47	67.9	-	-	-	-	-	-	-	End of car 5
6	-	-	~4.0	67.4	1132	126	164	360	1080	0.70	0.95	After 2nd gate
6	217360	636.1	4.19	67.2	-	-	-	-	-	-	-	End of car 6
7	-	-	~4.4	67.0	1127	138	165	361	1083	0.76	0.96	After 1st gate
7	217130	744.6	4.92	66.5	-	-	-	-	-	-	-	End of car 7
8	215020	852.2	5.63	65.8	-	-	-	-	-	-	-	End of car 8
9	-	-	~5.9	65.5	1110	169	249	445	1335	0.76	1.20	After 1st gate
9	223920	964.1	6.38	65.0	-	-	-	-	-	-	-	End of car 9
10	-	-	~6.6	64.8	1101	176	263	445	1377	0.77	1.25	After 1st gate
10	230440	1079.3	7.16	64.2	-	-	-	-	-	-	-	End of car 10
11	-	-	~7.4	64.0	1092	205	282	478	1434	0.86	1.31	After 1st gate
11	187010	1172.8	7.75	63.7	-	-	-	-	-	-	-	End of car 11
12	215580	1280.6	8.46	62.9	-	-	-	-	-	-	-	End of car 12
13	-	-	~8.7	62.7	1076	219	291	487	1461	0.90	1.36	After 1st gate
13	227270	1394.3	9.23	62.2	-	-	-	-	-	-	-	End of car 13
14-15	459830	1624.2	10.79	60.6	-	-	-	-	-	-	-	End of car 15
16	-	-	~11.0	60.4	1047	264	295	491	1473	1.08	1.41	After 1st gate
16	222590	1735.5	11.54	59.9	-	-	-	-	-	-	-	End of car 16
17	-	-	~12.1	59.3	1034	281	310	506	1518	1.11	1.47	After 2nd gate
17	203670	1837.3	12.20	59.2	-	-	-	-	-	-	-	End of car 17
18	-	-	~12.4	59.0	1030	283	325	521	1563	1.09	1.52	After 1st gate
18	195600	1935.1	12.82	58.6	-	-	-	-	-	-	-	End of car 18
19	-	-	~13.1	58.3	1021	304	334	530	1590	1.15	1.56	After 1st gate
19	191870	2031.0	13.43	58.0	-	-	-	-	-	-	-	End of car 19
20	-	-	~13.7	57.7	1013	326	335	531	1593	1.23	1.57	After 1st gate
20	-	-	~13.9	57.5	1010	338	339	353	1605	1.26	1.59	After 2nd gate
20	202370	2132.2	14.09	57.3	-	-	-	-	-	-	-	End of car 20
21	-	-	~14.3	57.1	1005	357	346	542	1626	1.32	1.62	After 1st gate
21	-	-	~14.6	56.8	1001	361	346	542	1626	1.33	1.62	After 2nd gate
21	204860	2234.7	14.75	56.7	-	-	-	-	-	-	-	End of car 21
22	-	-	~15.0	56.4	996	354	349	545	1635	1.30	1.64	After 1st gate
22	-	-	~15.3	56.1	992	366	346	542	1626	1.35	1.64	After 2nd gate
22	203730	2336.5	15.42	56.0	-	-	-	-	-	-	-	End of car 22
23-34	2429830	3551.4	23.29	48.1	-	-	-	-	-	-	-	End of car 34
35	-	-	~23.8	47.6	874	452	305	501	1503	1.80	1.72	After 2nd gate
35	197960	3650.4	23.93	47.5	-	-	-	-	-	-	-	End of car 35
36-44	1801640	4551.2	29.74	41.7	-	-	-	-	-	-	-	End of car 44
45	234620	4668.5	30.54	40.9	773	496	316	512	1536	1.94	1.99	Budd Rdg(robots)

after the gate was opened and the eccentricity therefore remained at what it started out at. During the continued (but reduced) flow that followed, the outer gauge continued into tension while the inner gauge reversed its initial movement and by the end of the car, had actually moved slightly into compression (relative to the initial value). The overall wall strain at the end of car 1 is therefore only slightly into tension but with an increase in eccentricity of about 0.1" (approximately 40% of the starting moment).

The increase in pressure is minimal up to the 7th car, where P_d actual drops below P_s. A large moment appears to build in this initial phase as eccentricity rises rapidly to 3/4". At this time, and for no immediately apparent reason, strains begin to increase and at the 9th car, a major deflection occurs right after the first gate. The train speed had remained constant at about 0.65 mph and correspondingly, the flow rates remained unchanged. Following this, the o.p.f. and eccentricity continued to increase. At the 17th car, the speed was increased to 0.8 mph, and a noticeably greater trend in tensile strain increases occured. The maximum observed pressure (strain) came at the 22nd car, immediately after the first gate and the corresponding o.p.f. was calculated at 1.64. Thereafter, the dynamic pressure dropped, but not as fast as the coal height (i.e. and associated static pressures). The result was an o.p.f. of 1.72 occuring at the 35th car, which was

the last dynamic event recorded for this run. At the 45th car, during passage of the robot diesels, a Budd reading was taken. The o.p.f. here was calculated as 1.99 with a coal height of ~ 40.9′ and occured along with the largest observed moment (i.e. difference in inner-outer strains). No observations were made after the robots so it is possible that even greater o.p.f.'s and moments developed. It should be pointed out at this time that the o.p.f. of 2.0 observed during this run corresponds to an ACI C_d factor of approximately 3.2.

The moment reversal at the transition discussed in Sect. 5.3.2 has, in Run #8, disappeared and as evidenced by Fig. J.C28, follows the predictions of Jenike *et al.* in a qualitative manner. They predict large transition pressures during flow that come to approximately $4\sigma_v$ in the east - west direction and only $2\sigma_v$ in the north - south direction. This argument assumes however that transition pressures are more influencial in causing ovalization than the heretofore unknown effects of eccentric flow channels within the cylinder itself. For example, this large moment is very evident at Location 3, 24′ away from the transition.

5.3.6 Run #9

Both gauges at each of Locations 2,3,4, and 5 were monitored during Run #9. At the start of this run, the train speed was 0.7 mph and this had a marked effect on initial dynamic strains. Just prior to the first gate, a large

moment and 25% overpressures were evident at Location 3, locked in by the previous run, and this can be seen by referring to Fig. J.C27 and Table 5.2. At the first gate, there occured what was probably the largest immediate deflection over the June runs and this is indicated graphically in Fig. 5.2. The deflection on the first gate (what may almost be termed a discontinuity in the pressure trace), gives approximately 70% of the total 1st car deflection and is perhaps the most vivid evidence for what Jenike described as the 'switch', a transition from the peaked (near active) to the arched (near passive) pressure field. After this initial switch, during flow, the pressure continues to increase. Immediately following the opening of the second gate, a second switch seems to occur. In fact, coal above the second gate is in the north hemicylinder and this material may be largely unaffected by the first gate activities. Aside from the initial surge during the second gate opening, sustained flow is generally constricted by the high level of coal in the car from the first gate. A plateau forms on the chart immediately following this four spiked switch, but as the rear of the car approaches, additional space becomes available. This occurs because the first gate is automatically shut early so as not to cause coal contained in the second chute to overflow the car's rim.

This five part strain response is typical of the loading event when both gates are in use and the train is moving at higher speeds (i.e. 0.5 mph or greater). Although

Table 5.3 O.P.F.'s Observed During Run #10

n car no.	Gross Vehicle Weights (lbs)	Cumulative Vehicle Weights (Tons)	Δz from z=57.0' (ft)	z Coal Height (ft)	P_s Static Pressure (psf)	$\epsilon_o - \epsilon_i$ Δ from Ref.Rdg. ($x10^{-6}$)	ϵ_m Measured Strain ($x10^{-6}$)	ϵ_d Dynamic Strain ($x10^{-6}$)	P_d Dynamic Pressure (psf)	e $\frac{M}{P_d}$ (in)	o.p.f. $\frac{P_d}{P_s}$	Remarks
-	-	0	0	57.0	1004	~25	135	331	993	0.15	0.99	Start of run
1	-	-	~0.2	56.8	1001	34	157	353	1059	0.19	1.06	After 1st gate
1	-	-	~0.5	56.5	997	52	172	368	1104	0.28	1.11	After 2nd gate
1	203370	101.7	0.66	56.3	-	-	-	-	-	-	-	End of car
2	-	-	~0.9	56.1	992	61	185	381	1143	0.32	1.15	After 1st gate
2	187980	195.7	1.25	55.8	-	-	-	-	-	-	-	End of car
3	-	-	~1.5	55.5	984	52	193	389	1167	0.27	1.19	After 1st gate
3	-	-	~1.8	55.2	980	102	224	420	1260	0.49	1.29	After 2nd gate
3	209160	300.3	1.94	55.1	-	-	-	-	-	-	-	End of car
4	-	-	~2.2	54.8	975	108	233	429	1287	0.50	1.32	After 1st gate
4	-	-	~2.4	54.6	972	108	236	432	1296	0.50	1.33	After 2nd gate
4	-	-	~2.6	54.4	970	132	230	326	1278	0.62	1.32	Near end of car
4	211000	405.8	2.63	54.4	-	-	-	-	-	-	-	End of car
5	-	-	~2.9	54.1	966	132	236	432	1296	0.61	1.34	After 1st gate
5	206070	508.8	3.30	53.7	-	-	-	-	-	-	-	End of car
6	-	-	~3.5	53.5	957	147	226	422	1266	0.70	1.32	After 1st gate
6	219100	618.3	4.03	53.0	-	-	-	-	-	-	-	End of car
7	-	-	~4.5	52.5	944	162	215	411	1233	0.70	1.31	After 2nd gate
7	-	-	~4.7	52.3	941	179	212	408	1224	0.88	1.30	Near end of car
7	223000	729.8	4.78	52.2	-	-	-	-	-	-	-	End of car
8	-	-	~5.2	51.8	934	188	226	422	1266	0.89	1.36	After 1st gate
8	-	-	~5.5	51.5	930	203	224	420	1260	0.97	1.35	Near end of car
8	217870	838.8	5.51	51.5	-	-	-	-	-	-	-	End of car
9	-	-	~5.7	51.3	927	212	237	433	1299	0.98	1.40	After 1st gate
9	-	-	~6.0	51.0	923	200	237	433	1299	0.92	1.41	After 2nd gate
9	-	-	~6.2	50.8	920	224	240	436	1308	1.03	1.42	Near end of car
9	226180	951.9	6.27	50.7	-	-	-	-	-	-	-	End of car
10	-	-	~6.5	50.5	916	230	240	436	1308	1.06	1.43	After 1st gate
10	-	-	~6.7	50.3	913	221	242	438	1314	1.01	1.44	Middle of car
10	-	-	~6.8	50.2	912	230	240	436	1308	1.06	1.43	After 2nd gate
10	-	-	~6.9	50.1	910	232	234	430	1290	1.08	1.42	Near end of car
10	211820	1057.8	6.97	50.0	-	-	-	-	-	-	-	End of car
11	-	-	~7.4	49.6	903	239	242	438	1314	1.09	1.46	Middle of car
11	-	-	~7.6	49.4	900	266	237	433	1299	1.23	1.44	Near end of car
11	220100	1167.8	7.70	49.3	-	-	-	-	-	-	-	End of car
12	-	-	~7.9	49.1	896	266	234	430	1290	1.24	1.44	After 1st gate
12	-	-	~8.0	49.0	895	262	236	432	1296	1.21	1.45	Middle of car
12	-	-	~8.2	48.8	892	266	234	430	1290	1.24	1.45	After 2nd gate
12	213860	1274.8	8.41	48.6	-	-	-	-	-	-	-	End of car
13	-	-	~8.8	48.2	883	271	223	419	1257	1.29	1.42	After 2nd gate
13	208890	1379.2	9.10	47.9	-	-	-	-	-	-	-	End of car

the switch-flow-switch-plateau-flow sequence is evident in most loading events, the peak event pressure is not always associated with the switch. When this most important overpressure occurs, is a function of train speed, previous event strain levels, gauge location, and whether or not a large moment is developing at the section.

For example, while Location 3 is straining more into tension, the cross-sectional moment is also increasing (even though the eccentricity drops off some). During this 1st car load-out event, just after the second gate response, the dynamic pressure can be seen to equal 1851 psf. This is not much lower than the maximum that will occur for this run during the 2nd car event. Here, a pressure of 1887 psf occurs and is the largest dynamic pressure observed for all runs, even though the o.p.f. is only 1.47. The quickness with which this large overpressure is achieved is important because it implies that an o.p.f. may indeed have to be applied to a fully loaded silo.

Deflections for cars 3 and 4 were similar to the first car deflections although not quite as dramatic. During loading of the 3rd car, the outer gauge deflected a maximum for the first 20 cars however as this was matched by a simultaneous compressive change in the inner gauge, the o.p.f. remained at 1.46. Over the following 7 cars (to car 11) some moderation in outer gauge strains occurs, as it moved in a gradual compressive fashion. The inner gauge moved little and consequently the o.p.f. reduced to a low of

1.31 before reversing this trend.

At the 17th car, the train speed was increased to 0.8 mph and it was not long after that an accumulating number of overpressures led to a Run #9 high o.p.f. of 1.61 during the loading of car 21. Again, for comparison, this would be an ACI factor of 2.52. The remaining cars loaded to the robots generally showed little response of note as overpressures fell off to 1.33 by the 44th car, the last loaded car before the robots. This variation in average strains for this portion of Run #9 can be traced on Fig. 4.6.

Because a Budd reading had been taken at the robots (Fig. J.C28), the opportunity existed to compare Validyne measured gauge deflections to Budd measured defections between Fig. J.C27 (start of run) and Fig. J.C28. This comparison is the last two entries in Table R#9 and the differences are minimal. The inner gauge was off approximately 5 microstrain on 90 total while the outer gauge was right on for the two methods of strain measurement. This is again testimony to the accuracy to which small strain measurements were made throughout these tests.

Aside from the initial response to gate openings evident in Fig. 5.2 for Location 4, there were no apparent overpressures at this location during Run #9. The only observation that can be made is the development of the moment that appears in Fig. J.C28.

5.3.7 Run #10

Like the two previous runs, both inner and outer strains at Locations 3 and 4 were monitored with the best available channels on full gain, hence the dynamic results are interpretable. During Budd readings prior to and just after Run #10, the ground strap was found to be disconnected. This meant that any stray static build up within the 100+ ft leads might adversely affect the true strain levels as was found to be the case during the January field trip. The result was that no initial strain levels were known for this run. Fig. J.C31 indicates strain levels for the silo prior to filling for Run #10 and reveals that the silo was near empty at this time. With this in mind, sufficient accuracy can be had by assuming an initial static pressure distribution such as that obtained for Run #6A or #6B, along with a similar starting inner-outer strain differential. This has been done for Run #10 and the initial strain reading for column 8 in Table 5.3 is therefore at an assumed value only.

The coal level for this run was not measured but during load-out the 2/3 level indicator was observed to have gone out while the first 10 cars were being loaded. This gave a wall height for the coal of approximately 79′ above the transition, and, with an assumed 18′ cone, the effective height of coal above gauge Location 3 becomes 57′ (i.e. 79 + 18/3 - 28).

Table 5.2 O.P.F.'s Observed During Run #9

n car no.	Gross Vehicle Weights (lbs)	Cumulative Vehicle Weights (Tons)	Δz from z=83.0′ (ft)	z Coal Height (ft)	P_s Static Pressure (psf)	$\epsilon_o - \epsilon_i$ Δ from Ref.Rdg. ($x10^{-6}$)	ϵ_m Measured Strain ($x10^{-6}$)	ϵ_d Dynamic Strain ($x10^{-6}$)	P_d Dynamic Pressure (psf)	e $\frac{M}{P_d}$ (in)	o.p.f. $\frac{P_d}{P_s}$	Remarks
-	-	0	0	83.0	1296	357	338	534	1602	1.34	1.24	Start of run
1	-	-	~0.2	82.8	1294	381	399	595	1785	1.28	1.38	After 1st gate
1	-	-	~0.3	82.7	1293	386	404	600	1800	1.29	1.39	Flow
1	-	-	~0.5	82.5	1291	405	421	617	1851	1.31	1.43	After 2nd gate
1	-	-	~0.6	82.4	1290	403	420	616	1848	1.31	1.43	Flow
1	201320	100.7	0.65	82.4	1290	395	402	598	1794	1.32	1.39	End of car
2	-	-	~0.9	82.1	1288	426	427	623	1869	1.37	1.45	After 1st gate
2	-	-	~1.1	81.9	1286	447	433	629	1887	1.42	1.47	After 2nd gate
2	194860	198.1	1.27	81.7	-	-	-	-	-	-	-	End of car
3	-	-	~1.5	81.5	1282	457	428	524	1872	1.46	1.46	After 1st gate
3	-	-	~1.7	81.3	1280	464	429	525	1875	1.48	1.46	After 2nd gate
3	187420	291.8	1.86	81.1	-	-	-	-	-	-	-	End of car
4	-	-	~2.3	80.7	1274	461	419	615	1845	1.50	1.45	After 2nd gate
4	198300	391.0	2.50	80.5	-	-	-	-	-	-	-	End of car
5-10	1199860	990.9	6.37	76.6	-	-	-	-	-	-	-	End of car
11	-	-	~6.6	76.4	1230	422	342	538	1614	1.57	1.31	After 1st gate
11	214340	1098.1	7.08	75.9	-	-	-	-	-	-	-	End of car
12-18	1326340	1761.2	11.27	71.7	-	-	-	-	-	-	-	End of car
19	-	-	~11.5	71.5	1178	429	388	584	1752	1.47	1.49	After 1st gate
19	-	-	~11.8	71.2	1175	461	414	610	1830	1.51	1.56	After 2nd gate
19	213010	1867.7	11.97	71.0	-	-	-	-	-	-	-	End of car
20	-	-	~12.2	70.8	1170	464	413	609	1827	1.52	1.56	After 1st gate
20	-	-	~12.4	70.6	1168	483	422	618	1854	1.56	1.59	After 2nd gate
20	192320	1963.9	12.58	70.4	-	-	-	-	-	-	-	End of car
21	-	-	~12.8	70.2	1164	497	429	625	1875	1.59	1.61	After 1st gate
21	179250	2053.5	13.13	69.9	-	-	-	-	-	-	-	End of car
22-43	4345560	4226.3	27.08	55.9	-	-	-	-	-	-	-	End of car
44	229920	4341.1	27.86	55.1	979	345	237	433	1299	1.59	1.33	@ robots
44	229920	4341.1	27.86	55.1	979	340	239	435	1305	1.56	1.33	Budd Rdg.(@ robots)

Because this run initiated within an initial static pressure field, the immediate trend in Location 3 strains is a slow but determined move towards a maximum o.p.f. of 1.46 at about the 11th car. The inner-outer strains develop for the most part as a rotation with the inner gauge having strained little compared to the outer. As a result, a large change in eccentricity is evident as the now expected positive moment seeks to locate at the western meridian. This was also observed to be the case at Location 4, an area that showed little response during the two previous runs. Even though the overall wall strain at Location 4 was negligible, an inner-outer strain differential of approximately 100$\mu\epsilon$ developed.

The train speed for the entire set of dynamic strains observed during Run #10 was kept at 0.5 mph and this may partly explain the dissimilarity between overpressures for all three of these latter runs even with similar coal heights. For example, the maximum o.p.f. for Run #10 (1.46) occured with about 50′ of coal. For Run #9, with a train speed at 0.8 mph, the overpressure had peaked at a 70′ height (1.61) but at the last recorded height of 55′ the o.p.f. had dropped off to 1.33. For Run #8 the train speed had been increased at the 17th car to 0.8 mph and an overpressure of 1.64 occured at 56′ that was still seen to be increasing at 41′ (1.99). All of these comparisons suggest flow pressure and/or switch pressure fields of an

apparently complex nature. A discussion of these dynamic overpressures and their causes follows in Chap. 6.

5.4 Summary of Test Results

Figure 5.3 summarizes the maximum dynamic coefficients (i.e. o.p.f.'s and their equivalent C_d values) contained in Tables 5.1, 5.2, and 5.3. The "silo" heights given show that the maximum H/D ratio for these three tests was 1.6 however the greatest o.p.f. (worst case) occurred for a "silo" with an H/D of 1.4 (Run #8). All three o.p.f.'s in this column are reasonably bounded by the interpolated upper bound of 2.07 from Table 2.3 for $H/D \leq 2.0$ and $K = 0.48$. The z/H ratios at which these maximums occur are also in the 0.6 to 0.7 range, and this coincides with the location predicted by the strain energy method.

The worst case C_d values do not compare well with the bottom row of C_d values in Table 2.3, indicating that problems may occur if design pressures are based on *active* static pressures. The final column is interesting because it reveals that the maximum observed dynamic pressure (during Run #9) exceeded the maximum funnel flow design ACI pressure by a factor of 1.9/1.65 and this was for a silo filled to 85% capacity under close observation for only three complete unloadings. The 1.7 live load factor would however have provided a reasonable safety margin.

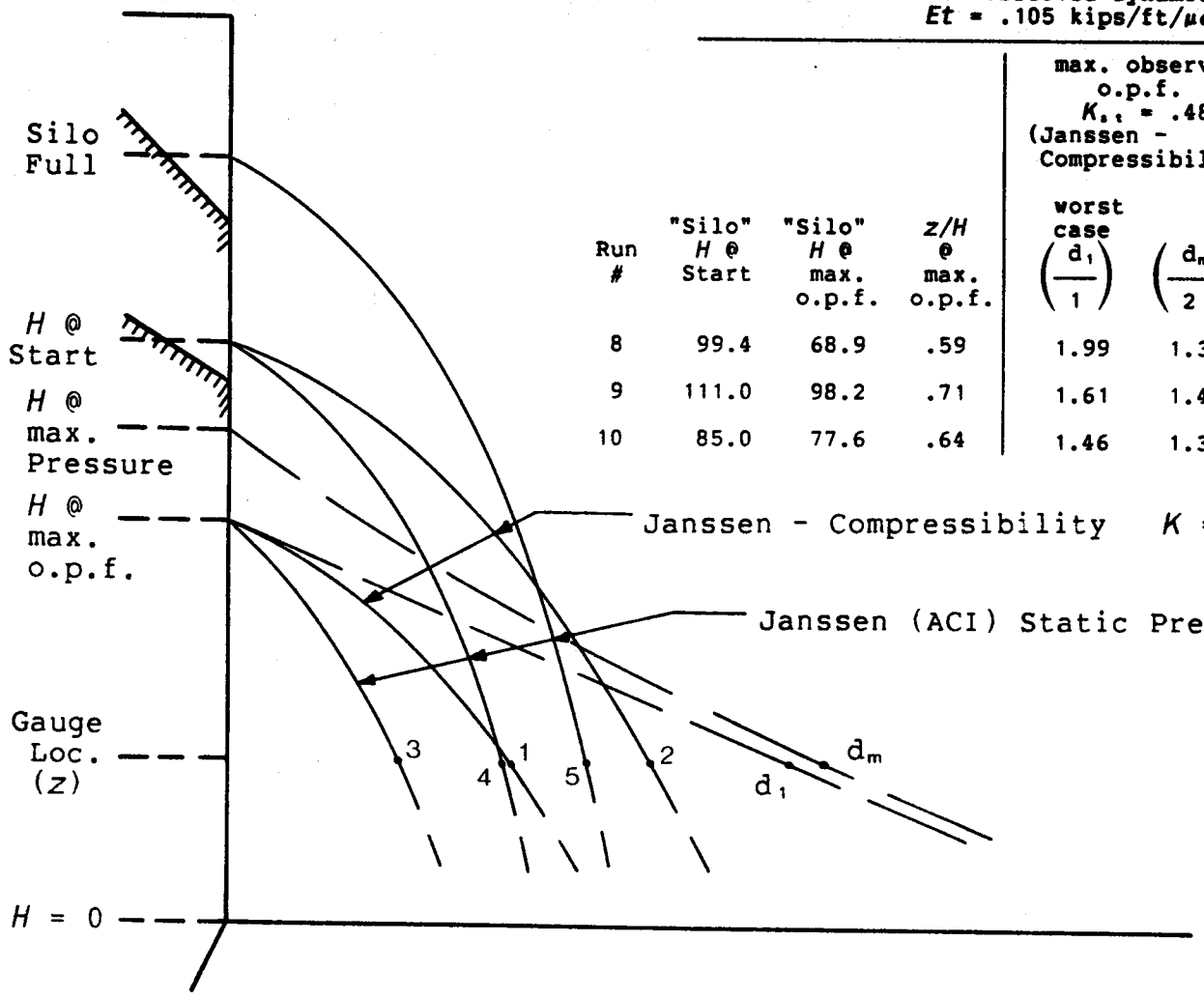

Maximum observed dynamic coefficients
Et = .105 kips/ft/*μe* (*K* = .48)

Run #	"Silo" *H* @ Start	"Silo" *H* @ max. o.p.f.	*z/H* @ max. o.p.f.	max. observed o.p.f. $K_{s,t}$ = .48 (Janssen - Compressibility) worst case $\left(\frac{d_1}{1}\right)$	max. observed o.p.f. $K_{s,t}$ = .48 (Janssen - Compressibility) $\left(\frac{d_m}{2}\right)$	max. observed C_d factors $K_{s,t}$ = Ka = .23 (Janssen) worst case $\left(\frac{d_1}{3}\right)$	max. observed C_d factors $K_{s,t}$ = Ka = .23 (Janssen) $\left(\frac{d_m}{4}\right)$	max. observed C_d factors $K_{s,t}$ = Ka = .23 (Janssen) absolute $\left(\frac{d_m}{5}\right)$
8	99.4	68.9	.59	1.99	1.39	3.24	2.17	1.64
9	111.0	98.2	.71	1.61	1.46	2.52	2.23	1.90
10	85.0	77.6	.64	1.46	1.31	2.35	2.09	1.31

Figure 5.3 Summary of Dynamic Coefficients

The large transition pressures were responsible for, on one occasion, a hoop steel tensile stress of 40% yield (Fig. J.C28). The complexity of the hopper-cylinder boundary conditions make it difficult to quantify these pressures. However, given these large transition strains and knowing that (1) *Et* at Location 2 cannot be much less than that calculated for Location 3 and (2) the stiffness at the transition is generally much greater than the average wall stiffness, there is at least tacit support for the relatively large upper hopper pressures predicted by Jenike *et al.* (1973) and Walters (1973). These observations therefore tend to corroborate to some extent the similar observations of Van Zanten and Mooij (1977), Jenike *et al.* (1973), and Perry and Jangda (1970) and it is suggested here that designs for transition reinforcement reflect these large forces.

6. Discussion of Analytical and Test Results

6.1 Introduction

In this chapter an attempt is made to consolidate, explain, and in some cases, expand upon, the various results of this study from both the theoretical and experimental investigations. Many of the questions concerned with mass flow in silos remain unanswered and certainly an investigation of this scope is bound to create additional questions. Therefore, the discussions to follow will contain conclusions that are both supportable and speculatory. It is the writer's belief that some informed speculation at this time may be helpful to any further research in this area.

Three general topics will be dealt with. Firstly, the assumptions used in the experimental analyses will be summarized and their effects on the results discussed briefly. Secondly, a number of conclusions can be made with respect to static pressures and these are presented along with their theoretical implications. Thirdly, the theoretical and experimental investigations into dynamic pressures are commented on.

6.2 Concluding Remarks: Experimental Assumptions

The analysis involved a number of assumptions, some of which have been dealt with in detail and others that have received only casual reference. The assumptions and conclusions regarding effective coal heights, temperature

gradients, and strain shifts were discussed at length in Chap. 4 and are therefore not included here.

The initial assumption in the data analysis was the decision to use the Janssen-Compressibility formulation derived in the text to account for the observed density variations of the material. This formulation employs Janssen's assumptions but permits a variable γ. For compressible materials, it has been shown that density variations can have a marked effect on a Janssen pressure field and are therefore incorporated into the analysis.

The thin-walled pressure vessel formula is employed throughout the dynamic analysis as the only rational means for relating lateral pressures with circumferential strains. This assumes that intense, very localized overpressures can be ignored. Nevertheless, if these structures are investigated using an assumption that is also employed in their design, the applicability of that assumption is maintained. Further justification for this assumption exists. A brief examination was made of the effects that a vertical discontinuity in the pressure distribution might have on the hoop tension. A direct stiffness computer analysis for use with shells of revolution (Shazly *et al.* 1978), revealed that the vertical stiffness of this silo structure would cause a normal tension, 97% of the direct thin-walled tension, to occur 4 feet below the level of a discontinuity. In all probability, the discontinuity modelled in the computer analysis was uncharacteristically

abrupt and symmetric.

The local strain behavior of twinned, concrete embedded, steel-mounted gauges, located within a cracked wall section, requires additional comment. The results of the static analyses indicate that a linear relationship between horizontal pressures and observed circumferential strains is justified. For this to occur, two conditions must be satisfied. The first condition is that the load - deformation response of each gauge must be linear and this requires that no further concrete tensile stiffening (or unstiffening) must take place as the load is changed. This might occur when bar deformations located between the gauge and crack come in contact (or break contact) with a concrete surface as the load varies. The second condition requires an equal distribution of the wall axial load to each gauge. At a crack, this is self-fulfilling, but at a location where concrete is providing some of the stiffness, this may be a concern. The stiffness of gauge Location 3 was calculated as being close to fully cracked so this effect was greatly reduced. Finally, the load-deformation response has also been shown to be constant over the final series of runs.

The instrumentation was able to provide very small changes in strain, of the order of a few microstrain. This was a result of measuring techniques that were always consistent. For example, the static strains occured within a completely balanced bridge, utilizing the same equipment, equipment settings, and personnel, within a constant

environment. In addition, all final gauge connections provided fully grounded and shielded cables.

If small circumferential wall strains are being measured, then it is advisable to examine what influence vertical wall strains will have due to Poisson's effect. Calculations reveal that this effect is about 3% of the $\Delta\epsilon$ values for varying coal heights using ν for concrete of 0.20. For cracked concrete, Poisson's effect is reduced.

6.3 Concluding Remarks: Initial Static Pressures

Most of the conclusions that can be made about this aspect of bin loads originate in the discussions of the first part of Chap. 2. The experimental portion of this investigation did provide additional material for comment however the conclusions that can be made are only general in nature.

The most important idea to emerge from Sect. 2.1 is that Janssen's original solution for initial static bin pressures is still very applicable today. This is not only because of the simple analytical form that it takes (as many authors suggest as a reason for its continued use), but also because Janssen's formula has the potential to most accurately describe the distribution of static pressures at the wall. This stems from the straightforward manner in which the equations are developed and the need for only a few basic assumptions that also appear sound from an engineering standpoint. A number of researchers describe

these assumptions as overly restrictive however will then go on to include less tenable restrictions, such as complete incipient failure, while others simply redefine these assumptions and end up saying what Janssen implies. The majority of codes still rely on Janssen's formula as a starting point for design lateral pressures and it would seem at this time that this position is fully justified (in so far as design lateral pressures are related to static pressures).

There are, however, certain situations in which Janssen's formula may not give sufficient accuracy. These arise when conditions are such that the three primary material properties (K, μ', and γ) are varying. The variability of K and γ seems to be associated with small scale tests and compressible materials respectively. With the former, K may be related to relative density and therefore the actual stress levels attained during the test; model studies very often achieve less than representative stress levels. On the other hand, very compressible materials in static model studies often exhibit a near constant K and γ yet if the variation in γ is allowed for in a full scale application, the results may be quite different from those assuming a constant γ. This is also why a Janssen-Compressibility formulation was developed for use in this study. Because it is conservative to ignore the lower density that a material may possess near the top of a silo, this influence can be ignored in design situations. When it

is considered that somewhat tentative and hopefully upper bound o.p.f.'s are going to be applied to these static loads, further refining of these base pressures is not warranted, providing K is known with reasonable accuracy.

The present reliance in North America on Rankine's Active Coefficient for K as a property of ensiloed materials has neither theoretical nor good experimental support. The value of 0.5 used in the German code is more likely closer to the true value but it is also rather arbitrary. For a purely initial static analysis, the literature contains some information on K_{s_t} for certain materials and applications (p.48). With untested materials, K_o, as given by Jaky's formula, $(1 - sin\phi)$, would appear a logical choice although material compressibility should increase this value. Curve-fitting to the observed lateral pressures may produce acceptable results if μ' is assumed constant with fully mobilized wall friction. Otherwise vertical pressure data will also be required to evaluate the product $\mu' K$ and then K from the lateral and vertical stress formuli. The analysis in this study found, for larger silo's at least, that K could be assumed to be constant in the vertical direction with no loss in accuracy. A definitive value for K was less certain.

The K_o test requires a triaxial cell and a sample of the material minus the larger particles (in this case, material passing the #8 mesh). A centrally deposited granular coal will segregate somewhat with a greater

proportion of the larger particles coming to rest at the wall. Therefore a more general test for K_{st} is in order. This should be along the lines of Kramer's investigation (1945) which in effect was a large scale consolidation test. With a suitably large fully instrumented cylinder, a fully representative sample of the material could be compressed to any desired consolidating pressure. The evaluation of vertical and lateral wall strain data, possibly augmented with pressure cell readings, would allow a complete evaluation of K_{st}, μ', and β. In addition, rebound properties such as K_{dy}, E_{dy}, etc. could be examined in a setting more representative of in-situ silo conditions.

Little has been said about the variability of the wall friction coefficient μ'. A discussion in this area brings to attention, more so than with any other parameter, considerations of material homogeneity. Earlier it was stated that if the the full frictional force is not mobilized within a bin, then Janssen's solution may be interpreted as a lower bound on the static lateral pressures. For a material being loaded gradually into a silo, and undergoing consolidation, this implies a lack of homogeneity. If failure initiates in a localized block of material because the wall frictional force can no longer counter any further increase in the consolidating force, the effective value for μ' becomes μ'_k along the region of sliding. Although its difficult to predict what the stress distribution is within the block of material when motion

ceases, it seems reasonable that the mobilized value for μ' will be between μ'_k and μ'_s. Depending on whether this failure causes an overall or local redistribution of stresses, the resulting inhomogeneities will vary respectively with time or position. A sudden and complete overall consolidation in which all of the material is in motion at once should end up with an effective coefficient of friction approaching μ'_k. A further consideration in this case would be whether failure initiated from the top, bottom, or some intermediate level.

Sudden changes in μ' to lower overall values would appear as equally sudden increases in circumferential tensile strain just as a gradual increase in μ' would appear as a gradual reduction in these strains. The dynamic record indicated that immediately following the closing of a gate, some stress redistribution was occuring and this appeared as a sharp jump in the strain trace. Most often these jumps appeared to occur simultaneously at all lower gauge locations and were always associated with a slight increase in tensile strains. This would indicate that a fairly general reduction to μ' was occuring due to an ensueing dynamic consolidation (i.e. with material flow). Following this, however, there occurred a gradual decrease in circumferential strains, to levels below those evident before the jump. This suggests a gradual and general consolidation in which μ' was again increasing (i.e. 'static' consolidation). These results indicate that this second type of consolidation is more prevalent in

influencing the state of stress in the lower bin regions. Material being deposited higher up in a silo does tend to consolidate more frequently and is therefore more susceptible to the 'dynamics' of consolidation. Hence the discussion at the end of Chap. 4 suggested that slightly divergent results could be explained under the assumption of an increasing mobilization of wall friction with depth.

For model tests incorporating 'bucket' filling methods (as opposed to a gradual feed), some amount of overconsolidation may occur due to the relatively large inertial forces involved. Not only can this practice lock-in a K that may be suspect, it can result in very little frictional force mobilization. In cases such as this, the apparent μ' may be less than μ_k'.

6.4 Concluding Remarks: Dynamic Mass Flow Pressures

The trend in design standards and codes of practice is towards relating static and design lateral loads via an o.p.f. and the obvious question is whether or not this is a realistic premise. Analytical techniques provide solutions that generally support this premise but this is a direct result of their incorporating the same equilibrium equations for both the static and dynamic cases. There is some difficulty in the initial acceptance of this incorporation when consideration is given to just how different the two stress distributions may be. Direct observation, stop-action photography, X-ray techniques, and analytical finite element

studies all indicate the very complex nature of flow and/or switch stress and velocity fields. The flowing mass very quickly develops a well distributed series of discontinuities, shear bands, and areas of reduced density, all in noticeably asymmetric patterns. This reduces the parameters common to both the static and dynamic calculations to geometry, unit weight, and the thin-walled pressure vessel formula, although even density variations cannot be ignored.

The experimental portion of this study indicates however that this is not an untenable premise. The dynamic record revealed that the larger instantaneous overpressures coincided with quasi-static overpressures of similar magnitude. It may be difficult to describe the equilibrium equations at a discontinuous switch moving upward through a granular mass as a shock wave, however, if these conditions bring about a quasi-static stress distribution that is similar in orientation and magnitude, than the generality of local and overall static equilibrium equations still apply, without the inclusion of dynamic forces. Jenike *et al.* (Part 2 1973) stated that inertial and kinetic forces are small enough to be neglected and the observations thus far support this. Therefore, mechanisms such as dilatancy, frictional mobilization, and energy minimization, the three principles of powder mechanics, are by themselves capable of developing these noninstantaneous or quasi-static overpressures.

If overpressures are directly observable as quasi-static pressures, than it should be possible to describe the vertical distribution of K as brought about by these dynamic conditions. For this particular silo study, this is difficult considering the meager number of usable gauge locations, however enough readings were taken to give an idea of this distribution. Overpressures were found to be almost nonexistent at Location 4 (although the development of a positive moment indicated that some pressure reductions may have occured in the north-south direction at that level). Locations 5 and 6 were virtually unaffected during discharge. The vertical distribution in lateral pressures was therefore close to static down to a level between Locations 3 and 4, even well into a particular run. This has the result that K_{dy} at Location 3 can be approximated by K_{st}x(o.p.f.), if it is assumed that μ' does not vary greatly. For this type of coal, K_{st} was probably close to 0.48, and with a maximum overpressure of 2.0, the largest measured value for K_{dy} was then near 1.0. This is supported by Blight and Midgely (1980). When unloading their triaxial sample of coal while at the same time keeping horizontal strains at zero, they found the ratio of confining pressure to vertical pressure to remain constant at 1.0. In addition, Jenike's strain energy method gives a value for K near to unity when the switch location is assumed to be greater than one diameter below the free surface. It is interesting to note that the German standard, DIN 1055, sets K on discharge

at 1.0 (for use in Janssen's formula) in order that observed overpressures will be enveloped by the resulting design curve. This standard will however, in the near future, be revised to an o.p.f. approach for use with experimentally or analytically determined values for K_o (Martens 1980).

Because a larger K can be locked-in to a nonflowing granular mass, depending on the particular history of that mass, it follows that a critical case scenario can be described for many silos. This condition could arise when a maximum overpressure had been achieved and had locked-in a certain maximum K value. Further charging of material on top of this mass will superpose a typical Janssen surcharge at the free surface and, even though some alteration to K might be expected by the additional consolidation, much of this vertical surcharge would appear as a lateral thrust. Load superpositions of this type occur quite commonly in operational silos and for this silo is best illustrated by Figs. J.B6, J.B7, and J.B8, although this set of events would not be classified as a critical case. For this silo, the worst case situation would probably happen with a full silo in which a series of rapid loading-unloading events occurred. This can be modelled as a continuous flow operation that in practice is difficult to achieve for a full sized structure yet may explain how silos that are apparently of sound design may achieve this limiting case and collapse even after years of service (see for example Sadler 1980).

The overpressures given by this study are related to the static load for an equivalent height of material at the instant the overpressure was measured. If a certain amount of material withdrawal is always required to develop these maximum overpressures, it may be argued that it is overly conservative to apply these overpressures to a full silo. For example, the o.p.f. of 2.0 was found to occur with an effective coal height of 41′ while the maximum measured o.p.f. for a 70′ depth was only 1.6. Although these values may not be the largest possible at each particular height, the extrapolation of an o.p.f. of 2.0 to the 70′ depth is not supportable from these tests. The proximity of Location 3 to the transition suggests a further influence that may not be a factor 41′ from the top in a full silo. Nevertheless, the few results given here indicate that for shallow large diameter silos with a similar outlet geometry (mass flow), ACI 313-77 C_d factors are certainly inadequate (as noted by ACI 313-77). If $K = Ka$ is used in place of $K = 0.48$ for the static calculations in Tables 5.1, 5.2, and 5.3, this inadequacy becomes unsafe even with a live load factor of 1.7.

Much of the experimental examination of bin pressures has taken place with the aid of models. This is a natural outcome of the enormous sizes to which the working silos now attain. The use of models in hydraulic applications requires dynamic similitude in relating measurments to the prototype,

however this requirment is often ignored in bin studies, perhaps because the dynamic mechanisms within granular materials are little understood when compared to fluids. Janssen's formula provides geometric similitude (a requirement for dynamic similitude) through the hydraulic radius, R. A further requirement is that there be kinematic similitude and although by definition this is not a concern with static pressures, there must indeed be a constant ratio of dynamic pressures at corresponding positions in model and prototype.

Because K may be considered a function of consolidating pressures, it is hard to ignore the possible differences that may exist between model and prototype even in the static case. The assumption of a constant K_{st} is sufficient for engineering accuracy in large structures but this is not necessarily so for models.

In the dynamic case, assuming kinematic similitude may be fundamentally incorrect in many cases. Of the three powder mechanics principles discussed earlier, two of these, dilatancy and energy minimization (strains), are certainly related to material compressibility. Frictional forces are generally considered unaffected by density changes (although friction mobilization may also have a more than tenuous relationship to compressiblity). As to what effect the differences in vertical pressure between model and silo have on the relative value that K attains in the dynamic case, requires some guesswork. Possibly a certain minimum ratio of

model to prototype should be sought if model studies are going to be the principal means for developing o.p.f.'s.

A further consideration for model studies is instrumentation sensitivity. Strains are directly proportional to both lateral pressures and container radius so if the model is small, the strains will be small unless a very flexible container is used. With small strains, experimental control becomes a priority as external influences such as temperature effects and zero drift will be present. Many of the model studies reported in the literature employed overly stiff containers because a certain lack of reproducibility is a common occurrence.

Previous experimental studies, several of which were discussed at the end of Chap. 2, have shown that dynamic pressures are extremely variable, circumferentially as well as vertically. Dynamic pressures appear to be a result of many local pertubations, therefore measuring these pressures directly can be a difficult task. Although pressure cells can provide an accurate indication of local overpressures, analyses that do not involve some type of statistical evaluation might seem inappropriate. If flow is expected to be asymmetric then the required circumferential distribution of pressure cells is compounded. A further problem associated with pressure cells is that diaphram deformation is required to register any changes in pressure. This is not a problem for gradually increasing material stresses, however, if the pressures are fluctuating or in fact

decreasing, the diaphram must be capable of inward movement. For this to occur, the passive resistance of the material at the wall may prevent such action unless the diaphram possesses sufficient stiffness to render this resistence negligible. Pressure sensitive diaphrams will therefore always measure the maximum pressure with their prescribed accuracy, however, because these dynamic pressures comprise local pertubations, any statistical evaluation of the results must recognize the possibility of hysteresis due to diaphram flexibility. In addition to these considerations, Paterson (1980) recommends that the diaphram diameter be greater than 1000 times its maximum deflection, at least 20 times the maximum particle size, and that the cell always fit flush with the silo wall.

The advantages of indirect pressure measuring techniques (strain gauges and transducers) are not only the above noted disadvantages of pressure cells. By measuring an actual wall stress, the local pertubations are smeared out and consequently the need for statistical evaluations reduced. Material and installation costs are greatly reduced as are the inherent problems associated with any field operation. All 12 gauges in this study worked flawlessly and are probably still operational for use in further studies. The disadvantages, such as not knowing the true extensional or flexural stiffnesses and the effects due to temperature and cracking, have been dealt with. A number of better methods and techniques are worth considering for future

large scale or model testing. A precracked gauge location would certainly have provided a reliable reference point and may have allowed more accurate determinations of K, μ' etc. Alternatively, if K and μ' are known to a reasonable degree of accuracy, the calibration efforts would be greatly simplified. Vertical gauges, although requiring very sensitive measuring techniques, would provide invaluable information on the wall loads. More direct information about the time and spatial variations of the wall temperature gradients would also have provided more confidence in the final results.

However, as discussed in Sect. 5.1, if the intent of the investigation is to find o.p.f.'s only, the methods employed in Chaps. 4 and 5 are satisfactory in that dynamic strains have been compared to static strains without the requirement that static pressures be known. A more complete study of lateral pressures in silos might utilize a combination of pressure cells and strain gauges, the former for investigating static pressure fields directly, perhaps providing an additional method of calibration in the study of dynamic pressures with the latter.

One final technique for investigating bin loads is the observation of actual wall deflections and/or the weight of material transferred to particular bin sections. It is a method that was employed primarily by early investigators, and most extensively in recent times by Lenczner (1963). In measuring overall deflections/loads, a real advantage exists

in that a further smearing of local strain irregularities is made possible. This in turn allows some correlation of circumferential deflections with an average (instead of localized) wall stiffness, while the quantifying of out-of-roundness is a further benefit. With respect to vertical strains, strains that can generally be expected to be small, the use of LVDT's or dial gauges will effectively integrate these strains.

No conclusions can be drawn in the area of material-structure interaction from these tests. The theoretical arguments presented in Sect. 2.2.3 indicate that energy considerations provide for a redistribution of lateral dynamic pressures within flexible containers. As the *H/D* ratio gets smaller, the material contained in the hopper has an increasing influence on lateral pressures while the wall flexibility has a decreasing role in load redistribution. This is because hopper walls are rigid when compared to the vertical bin walls. The experimental observations of Jenike *et al.* (1973), Van Zanten and Mooij (1977), and of this study typically do not show large overpressures extending into the upper cylinder regions. These analytical and experimental results will be reflected by the recommendations for mass flow design given in the final chapter. It would appear at this time that material-structure interaction is no impediment to increasing the size of storage structures. Quantitative

predictions await better knowledge of granular material properties under reloading conditions. In this case, an experimental investigation into this phenomenon should probably be undertaken with the aid of models.

The continuous strain records made during the later runs indicate that the rate of withdrawal may influence lateral pressures. Pieper (1969) reported that filling and emptying speeds had no effect in scaled down studies while Delaplaine (1956) found that, for a variety of tube-to-particle ratios, all stresses were independent of the solids velocity. The ability of overpressures to lock-in even as flow is halted suggest support for this view. It may be that under conditions of very slow withdrawal, such as occurred within the Fording silo, dynamic lateral pressures are much lower than normal. This would explain how early investigators often found overpressures of less than 10% while contemporaries were reporting o.p.f.'s of 2 or more. This aspect needs clarification.

6.4.1 Material Dilatancy/Pressure Oscillations

Within the literature, the role of dilatancy in the development of dynamic pressures appears to be gaining momentum as the primary mechanism. An in-depth study of the mechanisms involved in the deformation and flow of granular materials within bin/hopper geometries indicates a dominance of strongly dilatent behavior (Jian Lian Dong 1980). The investigation was analytical and included finite element

solutions using von Mises and extended von Mises (Drucker-Prager) plasticity models. By allowing for material inhomogeneities and inelasticities, the formation of rupture surfaces (shear bands) was an important result. These seemed to eminate from the transition as zones of intense dilation and distortion while their formation coincided with large material stresses.

These predictions are supported by a number of observations of large transition pressures, including this study, as well as time lapse X-ray photographs of material flow initiation (Blair-Fish and Bransby 1973) with two dimensional flow models. A rapid breakdown in symmetry is a consequence of shear bands forming alternately at each transition corner. This type of action may also explain the oscillatory nature of dynamic pressures that was reported by Wei and Johanson (1974), Connelly (1979), and Sadler (1980), and also observed during this investigation. Connelly found that the frequency of these oscillations was independent of material head and flow rate while Wei and Johanson found a slight dependence on material head. The strain fluctuations in the Fording silo also appeared independent of material head and flow rate.

The summary by Sadler is important in that it describes a number of silo incidents that required remedial action, several of which were a direct consequence of large vibrations. The measured strain oscillations from the Fording silo were not particularly large but were rather

evident to individuals using the exterior ladder. These oscillations coincided exactly with and were of the same frequency as the strain oscillations recorded during a gate opening event. The writer on one occasion felt the effects of these vibrations (transmitted by the conveyer tube) in the belt drive house, 500′ from the silo.

These oscillations are a result of material flow but their frequency corresponds with the lowest natural frequency of the silo structure, which happens to be the mode in which wall strain energy is minimized (see Appendix H). It cannot be concluded from this one result that a material-structure dynamic interaction is in fact occurring, however one may wonder what amplitude these oscillations might attain if the flow was allowed to achieve a steady state. While loading a rail car, usually only 4 oscillations could occur before the coal level in the car increased to the point where it slowed the discharge rate. It is still possible that these large amplitude initial oscillations are only a manifestation of initial switch conditions and therefore steady state flow may not necessarily induce the largest hoop stresses. Recommendations for further research in this and other areas follow in Chapter 7.

7. Summary and Recommendations

In the absence of any codified design criteria for mass flow silos, it is recommended here that a strain energy approach be employed. This is due in part to its inherently rational foundation, although experimental support may be found in several model studies on small and intermediate sized bins (Sect. 2.2.5). With respect to this particular study, the dynamic pressures were found to be satisfactorily bounded by the strain energy predictions contained in Table 2.3 (Sect. 5.4). Use of these overpressure factors, or linearly interpolated values, implies that design is based on the expectation of a worst case scenario. The design therefore may be very conservative for 99% of the structures lifespan. Because of the variety of operational variables and because silo wall failures are often catastrophic, this requirement is unavoidable.

The use of o.p.f.'s in mass flow design, in the same manner that funnel flow design is carried out, is also recommended here and for the following reasons; (1) the dynamic pressures have been found to be related to static pressures analytically, (2) it is by far the simplest design approach, and (3) the task of reporting observed overpressures from future investigations is put on common ground.

The first step therefore in obtaining a design pressure for use in Eq.[1.2] is the calculation of a suitable static pressure curve. With a judicious choice of values for the

lateral pressure coefficient K and the coefficient of wall friction μ', the static horizontal pressures exerted by most bulk materials for most applications will be adequately represented by Janessen's formula. Given the current lack of knowledge in the literature with regard to variations in these two parameters, alternate static theories that also depend on these parameters have no advantages whatsoever and in fact are at a disadvantage given their relative complexity and their use of untenable or arbitrary assumptions. The primarily vertical nature of the deposition/consolidation/load transfer processes within bins is probably responsible for the better applicability of Janssen's differential slice approach. For small scale tests or very compressible materials, variations in K, μ', and γ should be examined before any conclusions are drawn and with respect to unit weight γ, the Janssen-Compressibility formulation (Sect. 2.1.6.3), developed here for a cleaned coal, should be useful in dealing with many other materials.

With a suitable static pressure curve available, the suggested design procedure for mass flow silos is as follows:

For the first 1/2 diameter (or 1/2 bin width) down from the highest effective material level, the design pressure is based on the static pressure curve with no o.p.f. applied. [If potentially volatile materials such as grain or coal are involved, minimum requirements should provide for an estimated maximum blast pressure.]

For H/D ratios ≤ 2.0, it is recommended that the maximum o.p.f.'s be employed from 1/2 D to .6H and thereafter the design curve parallels the Janssen curve.

For *H/D* ratios ≥ 4.0, the maximum o.p.f. is used in conjunction with a wall strain energy reduction factor [1] however the equivalent o.p.f. should not be less than those currently tabulated by ACI 313-77. In the upper regions of tall narrow bins, design pressures are similar whether the bin is mass or funnel flow. From .6*H* to *H*, the Janssen pressure is again paralleled.

For *H/D* ratios between 2.0 and 4.0, both of the upper bounds just descibed should be examined; the first method will give higher loads in the lower bin region (i.e. no flexibility reduction) while the second method will generally give higher loads in the upper bin region.

Eccentricity effects should be treated as per ACI 313-77 given the current lack of information on mass flow applications.

Until further testing either denies or confirms the existence of predicted large transition hopper pressures, it is recommended that these loads be based on the methods proposed by Jenike *et al.* (1973) or Walters (1973). (see Sect. 5.4, p.186)

With reference to the C_d factors recommended by ACI 313-77, the arbitrary use of *Ka* for $K_{s,t}$ (K_j) should be discontinued. Either experimentally determined values should be used or, as per the revised German code, the at-rest coefficient K_o.

Recommendations for Further Study

1. Future full scale silo tests should seriously consider the application of wall strain measuring devices.
2. Analytical and experimental studies are required to indicate how model tests can be most effectively designed.
3. Both model and full scale studies are required to develop a better understanding of the effects of eccentric flow patterns.

---

[1] This will require additional input on the stored material's dynamic properties as outlined in Sect. 2.2.3. If this information is not available, it is conservative to ignore this effect.

4. Model tests specifically designed for an investigation into material-structure interactions; to study (1) container flexibility and (2) pressure oscillations.
5. Clarification is needed in reference to silo operational effects on design pressures; designing for an upper bound worst case may not be necessary.
6. More detailed observations of the instantaneous pressure/strain distribution are required for comparison with the instantaneous pressures predicted by the strain energy method.
7. A better understanding of the influence hopper material strain energies have on pressures in the cylinder.
8. The effects of vibration on dynamic pressures and whether these represent actual maximum dynamic pressures as suggested in Reference [82].
9. Laboratory large scale consolidation tests to provide consistant data on the variability of K and μ' from which standardized testing criteria for $K_{s,t}$ (particularly for compressible materials) can be developed.
10. The further application of increasingly sophisticated geomechanical finite element methods that are or will become available.

References

1. ANONYMOUS, *Concrete Coal Storage Bins*, The Canadian Engineer, V.47, Aug. 12, 1924, p. 245.

2. AMUNDSON, L.R., *Determination of Band Stresses and Lateral Wheat Pressure for a Cylindrical Bin*, Agricult. Engineering, V.26, 1945, pp. 321-324.

3. AIRY, W., *The Pressure of Grain*, Minutes of Proceedings, Institution of Civil Engineers, London, V. 131, 1897, pp. 347-358.

4. AMERICAN CONCRETE INSTITUTE, *Proposed Recommended Practice for the Construction of Concrete Farm Silos: ACI Committee 714*, Journ. Am. Concr. Inst., V.15, Jan., 1944, pp. 189-204, (Discussion) V.15, Supplement Nov., 1944, pp. 204'-204'.

5. AMERICAN CONCRETE INSTITUTE Committee 313, ACI-Report 72-37, *Recommended Practice for Design & Construction of Concrete Bins, Silos and Bunkers for Storing Granular Materials*, (pp. 529-548). ACI-Report 72-38, *Commentary on Recommended Practice for Design and Construction of Concrete Bins, Silos and Bunkers for Storing Granular Materials*, (pp. 549-565), ACI-Journ. Oct., 1975, No.10, V. 72.

6. BAGSTER, D.F., *A Note on the Pressure Ratio in the Janssen Equation*, Powder Technology, 4 (1971), p. 235.

7. BISHOP, A.W., *Test Requirements for Measuring the Coefficient of Earth Pressure at Rest*, Proc. Conf. on Earth Pressure Problems, Brussels, 1958, 1, p. 2.

8. BLAIR-FISH, P.M., and BRANSBY, P.L., *Flow Patterns and Wall Stresses in a Mass Flow Bunker*, Journ. Engineering for Industry, Transactions, ASME, V.95, Series B, No.1, February, 1973, pp. 17-26.

9. BLEVINS, R.D., Formulas for Natural Frequency and Mode Shape, Van Nostrand Reinhold Company, New York, N. Y., 1979, pp. 291-321.

10. BLIGHT, G.E., and MIDGLEY, D., *Pressure Measured in a 20M Diameter Coal Load-Out Bin*, International Conference on Design of Silos for Strength and Flow, Powder Advisory Centre, London, England, 1980.

11. BOVEY, H.T., *Experiments on Grain Pressures in Deep Bins and the Strength of Wooden Bins*, Engineering News, V.52, 1904, pp. 32-34.

12. CAUGHEY, R.A., TOOLES, C.W., and SCHEER, A.C., *Lateral and Vertical Pressure of Granular Material in Deep Bins*, Bulletin No. 172, Iowa State College of Agriculture and Mechanical Arts, Engineering Experimental Station, Nov. 14, 1951.

13. CHANDRANGSU, K. and BISHARA, A.G., *Nonlinear Finite Element Analysis of Farm Silos*, Proc. ASCE, Journ. Struct. Div., V.104, No. 7, July, 1978, pp. 1045-1059.

14. CHAPMAN, A.J., Heat Transfer, The Macmillan Company, New York, N. Y., 1967.

15. CHITNUYANONDH, L., RIZKALLA, S., MURRAY, D.W., and MACGREGOR, J.G., *An Effective Uniaxial Tensile Stress-Strain Relationship for Prestressed Concrete*, Structural Engineering Report No. 74, Department of Civil Engineering, University of Alberta, Edmonton, Canada, October, 1979.

16. CONNELLY, L.M., *Wall Pressure and Material Velocity Measurements for the Flow of Granular Materials under Plane Strain Conditions*, Mechanics Applied to the Transport of Bulk Materials, Edited by Cowin, S. C., The Applied Mechanics Division, ASME, New York, N. Y., 1979, pp. 35-39.

17. COULOMB, C.A., *Essais sur une application des regles des maximis et minimis à quelques problems de statique relatifs à l'architecture*, Mem. Acad. Roy. Pres. Divers, Sav. 5, 7, Paris, 1776.

18. COWIN, S.C., *Theory of Static Loads in Bins*, J. Appl. Mech. Trans. ASME, V.44, Ser. E, No. 3, Sept., 1977, pp. 409-412.

19. DABROWSKI, R., *Shell Analysis of Intermediate Silo Bin*, Journal of the American Concrete Institute, V. 62, No. 7, July, 1965, pp. 795-804.

20. DELAPLAINE, J.W., *Forces Acting in Flowing Beds of Solids*, AIChE Journal, V. 2, Mar., 1956, pp. 127-138.

21. DIN 1055, *Design Loads for Buildings; Loads in Silos*, German Standard, DIN 1055, Blatt 6, Berlin, Nov., 1964, pp. 1-6.

22. DONG, J. L., *Analysis of Deformation and Failure in Geological Materials*, M.S. Thesis, Massachusetts Institute of Technology, Jan., 1980.

23. DUSINBERRE, G. M., Heat-Transfer Calculations by Finite Differences, International Textbook Company, Scranton, Pennsylvania, 1961.

24. FLEMING, R., *Some Data on the Design of Steel Coal Bins*, Engineering News-Record, V.89, Aug. 31, 1922, pp. 346-350, (Discussion) Oct. 19, pp. 669-670; Nov. 9, p. 808; Dec. 28, pp. 1132-33.

25. FRENZEL, H.H., *Design Notes on Circular Concrete Bins for Grain*, Engineering News - Record, V.109, No. 10, Sept. 8, 1932, pp. 291-292, (discussion) No. 21, Nov. 24, 1932, p. 626.

26. GLASTONBURY, J.R., and BRATEL, P.G., *Pressures in Contained Particle Beds from a Two - Dimensional Model*, Trans., Institute of Chemical Engineers., 44, 1966, T128.

27. HANCOCK, A.W., and NEDDERMAN, R.M., *Prediction of Stresses on Vertical Bunker Walls*, Transactions of the Institute of Chemical Engineers, V. 52, April, 1974, pp. 170-179.

28. HARR, M.E., Mechanics of Particulate Media, McGraw-Hill, Inc, New York, N. Y., 1977.

29. HORNE, R.M., and NEDDERMAN, R.M., *Analysis of the Stress Distribution in Two - Dimensional Bins by the Method of Characteristics*, Powder Technology, Vol. 14, 1976, pp. 93-102.

30. HUANG, J.H.S., and SAVAGE, S.B., *Wall Stresses Developed by Granular Materials in Asymmetric Bins*, Dept. of Civil Engineering and Applied Mechanics, McGill Univeristy, FML-TR 70-1, 1970.

31. HUTCHINSON, F.W., Industrial Heat Transfer, The Industrial Press, New York, N. Y., 1952, p. 138.

32. JAKOB, M., and HAWKINS, G.A., Elements of Heat Transfer, John Wiley & Sons, Inc., New York, N. Y., 1957.

33. JAKY, J., *Pressure in Silos*, Proceedings, 2nd International Conference on Soil Mechanics and Foundation Engineering, Rotterdam, June 21-30, 1948, V. 1, pp.103-107.

34. JAMIESON, J.A., *Grain Pressures in Deep Bins*, Transactions, Canadian Society of Civil Engineers, V. 17, 1903, pp. 554-607, with discussion, pp. 608-654, condensed in Engineering News, V. 51, Mar. 10, 1904, pp. 236-243.

35. JANSSEN, H.A., *Versuche ueber Getreidedruck in Silozellen*, (Experiments about pressure of grain in silos), Zeitschrift, Verein Deutscher Ingenieure, V. 39, Aug. 31, 1885, pp. 1045-1049.

36. JENIKE, A.W., *Storage and Flow of Solids*, Bulletin No. 123, Utah Engineering Experiment Station, University of Utah, Nov., 1964.

37. JENIKE, A.W., and JOHANSON, J.R., *Bin Loads*, Journ. Struct. Div., Proceedings, ASCE, V.94, No. ST4, April, 1968, pp. 1011-1041.

38. JENIKE, A.W., JOHANSON, J.R., and CARSON, J.W., *Bin Loads - Part 2: Concepts*, pp. 1-5; *Bin Loads - Part 3: Mass - Flow Bins*, pp. 6-12; *Bin Loads - Part 4: Funnel - Flow Bins*, pp. 13-16, Journ. Engineering for Industry, Transactions, ASME, V. 95, Series B, No. 1, Feb., 1973.

39. JENIKE & JOHANSON LTD., *Flow Test Results for Fording Coal Limited (Standard and Loop Coal)*, Prepared for Associated Pullman Kellogg Ltd., Jenike & Johanson Ltd., Don Mills, Ontario, Project Report No. 8067-1, Mar. 27,1979.

40. JENKYN, R.T., *Calculations of Material Pressures for the Design of Silos*, Proc. Institute of Civil Engineering, Part 2 (GB), V. 65, Dec., 1978, pp. 821-838.

41. JOHNS, D.J., Thermal Stress Analysis, Pergamon Press, Oxford, England, 1965, pp. 80-83.

42. KETCHUM, M.S., The Design of Walls, Bins and Grain Elevators, McGraw-Hill Book Co., Inc., New York, N. Y., 3rd Edition, 1919.

43. KOENEN, M., *Berechnung des Seiten-und Bodendruckes von Silozellen*, (Calculation of side and floor pressure in silo walls), Zentralblatt der Bauverwaltung, 1896, p. 446.

44. KRAMER, H.A., *Factors Influencing Design of Bulk Storage Bins for Rough Rice*, Agricultural Engineering, V. 25, No. 12, Dec., 1944, pp. 463-466.

45. KRUPICZKA, R., *Analysis of Thermal Conductivity in Granular Materials*, International Chemical Engineering, Vol. 7, No. 1, January 1967, pp. 122-144.

46. LABIOSA, T.D., and KEMP, E.L., *Design Note on the Pressure Distribution in Silos used to Store Granular Materials*, ACI Journal, V. 67, May, 1970, pp. 418-420.

47. LAMBE, T.W., and WHITMAN, R.V., Soil Mechanics, SI Version, John Wiley & Sons, Inc., New York, N. Y., 1979.

48. LENCZNER, D., *An Investigation into the Behaviour of Sand in a Model Silo*, Structural Engineer, V. 41, Dec., 1963, pp. 389-398.

49. LONG, J.D., *Design of Grain Storage Structures*, Agricultural Engineering, V. 12, No. 7, July, 1931, pp. 274-275.

50. LUFFT, E., *Tests of Grain Pressure in Deep Bins at Buenos Aires, Argentina*, Engineering News, V. 52, 1904, pp. 531-532.

51. LVIN, J.B., *Analytical Evaluation of Pressures of Granular Materials on Silo Walls*, Powder Technology, Vol. 4, 1969-70, pp. 280-285.

52. MAHMOUD, A., and ABDEL-SAYED, *Loading on Shallow Cylindrical Flexible Grain Bins*, International Conference on Design of Silos for Strength and Flow, Powder Advisory Centre, London, England, 1980.

53. MARTENS, P., *DIN 1055 Part 6: The Performance of the Old Norm and a Progress Report on the Revised Edition*, International Conference on Design of Silos for Strength and Flow, Powder Advisory Centre, London, England, 1980.

54. McCALMONT, J.R., and ASHBY, W., *Pressures and Loads of Ear Corn in Cribs*, Agricultural Engineering, V. 15, No. 4, April, 1934, pp. 123-124, 128.

55. McCALMONT, J.R., and BESLEY, H.E., *Silo Pressures and Temperatures with Corn and Grass Silage*, Agricultural Engineering, V. 20, No. 6, June, 1939, pp. 227-230.

56. MCLEAN, A.G., and ARNOLD, P.C., *Predictions of Cylinder Pressures in Mass Flow Bins using Minimum Strain Energy*, Journ. Engineering for Industry, Nov., 1976, V. 98, pp. 1370-1374.

57. MOYSEY, E.B., *Active and Passive Pressures in Deep Grain Bins*, Transactions, Amer. Soc. Agr. Eng., Vol. 22, Part 2, 1979, pp. 1409-1413, Paper No. 77-4506.

58. NORTH, M., *Research into the Design of Horizontally Corrugated Grain Silos*, Journal, The Institution of Engineers, Australia, Jan.-Feb., 1954, EI/54, V. 26, No. 1-2, pp. 2-8.

59. PARISEAU, W.G., and NICHOLSON, D.E., *Elastic Plastic Finite Element Analysis of Hopper Filling and Flow Initiation*, Mechanics Applied to the Transport of Bulk Materials, Edited by Cowin, S. C., The Applied Mechanics Division, ASME, New York, N. Y., 1979, pp. 61-77.

60. PARK, R., and PAULAY, T., Reinforced Concrete Structures, John Wiley & Sons, Inc., New York, N. Y., 1975.

61. PATERSON, W.S., *Measurement of Pressures in Hoppers and Silos*, International Conference on Design of Silos for Strength and Flow, Powder Advisory Centre, London, England, 1980.

62. PERRY, M.C., and JANGDA, H.A.S., *Pressures in Flowing and Static Sand in Model Bunkers*, Powder Technology, V.4, No. 2, 1970, pp. 89-96.

63. PIEPER, K., *Investigation of Silo Loads in Measuring Models*, Journ. of Engineering for Industry, Transactions, ASME, May, 1969, pp. 365-372.

64. PLEISSNER, J., *Versuche zur Ermittlung der Boden und Seitenwanddrucke in Getreidesilos*, (Experiments to determine the floor and side pressures in grain silos), Zeitschrift, Verein Deutscher Ingenieure, V. 50, Part I, 1906, pp. 976-986.

65. PRANTE, V., *Messungen des Getreidedruckes gegen Silowandungen*, (Measurements of grain pressure against silo walls), Zeitschrift, Verein Deutscher Ingenieure, V. 40, 1896, pp. 1122-1125.

66. REIMBERT, M., *Design of Silos*, (Reimbert's Method), Concr. and Constr. Engineering, V.50, No. 9, Apr., 1955, pp. 170-172; also Acier-Stahl-Steel, V. 20, No. 9, Sept., 1955, pp. 359-365.

67. RICHARDS, P.C., *Bunker Design Part 1: Bunker Outlet Design and Initial Measurements of Wall Pressures*, J. Eng. Ind. Trans., ASME, V.99, Ser. B, No. 4, Nov., 1977, pp. 809-813.

68. ROBERTS, I., *Pressure of Stored Grain*, Engineering, V. 34, Oct. 27, 1882, p. 399.

69. ROBERTS, I., *Determination of the Vertical and Lateral Pressures of Granular Substances*, Proceedings, Royal Society, London, V. 36, 1884, pp. 225-240.

70. ROWE, P.W., *The Stress-dilatancy Relation for Static Equilibrium of an Assembly of Particles in Contact*, Proc. Roy. Soc. (London), Ser. A269, 1962, p. 500.

71. SADLER, J.S., *Silo Problems*, International Conference on Design of Silos for Strength and Flow, Powder Advisory Centre, London, England, 1980.

72. SAVAGE, S.B., and YONG, R.N., *Stresses Developed by Cohesionless Granular Materials in Bins*, Int. J. Mech. Sci., 12 (1970), 675.

73. SHAZLY, A.M., SIMMONDS, S.H., and MURRAY, D.W., *Numerical Analysis of General Shells of Revolution Subjected to Arbitrary Loading*, M.Sc. Thesis, University of Alberta, Edmonton, Canada, September, 1978.

74. SUNDARAM, V., and COWIN, S.C., *Reassessment of Static Bin Pressure Experiments*, Powder Technology, V. 22, No. 1, Jan.-Feb., 1979, pp. 23-32.

75. SOKOLOVSKII, V.V., *Statifca Sypuchei Sredy*, (Statics of Soil Media), Izdatelstvo Akademii Nauk SSSR, 1954, (in Russian); translated by D. H. Jones and A. N. Schofield, Butterworths, London, 1960.

76. STEWART, B.R., *Active and Passive Wall Pressures Induced by Sorghum Grain in a Shallow Bin*, Transactions, Amer. Soc. Agr. Eng., V. 15, No. 1, 1972, pp. 121-125.

77. TERZAGHI, K., *Large Retaining Wall Tests I. Pressure of Dry Sands*, Eng. News Record, 112, 1934, p. 136.

78. TERZAGHI, K., and PECK, R.B., Soil Mechanics in Engineering Pratice, 2nd Edition, John Wiley & Sons, Inc., New York, N. Y., 1967.

79. THEIMER, O.F., *Failures of Reinforced Concrete Grain Silos*, Journ. Engineering for Industry, Transactions, ASME, Series B, V. 91, No. 2, May 1969, pp. 460-477.

80. TOLTZ, M., *Discussion on Grain Pressures in Deep Bins*, Transactions, CSCE, Vol. 17, 1903, p. 641.

81. TURITZAN, A.M., *Dynamic Pressure of Granular Material in Deep Bins*, Journal of the Structural Division, Proceedings of the ASCE, V.89, No. ST2, 1963, pp. 49-73.

82. VAN ZANTEN, D.C., and MOOIJ, A., *Bunker Design Part 2: Wall Pressures in Mass Flow*, J. Eng. Ind. Trans., ASME, V. 99, Ser. B, No. 4, Nov., 1977, pp. 814-818.

83. WALLI, G., and SCHWAIGHOFER, J., *A Bibliography on Silos (1857 - 1979)*, Department of Civil Engineering, University of Toronto, Canada, August, 1979.

84. WALTERS, J.K., *Theoretical Analysis of Stresses in Silos with Vertical Walls*, Chemical Engineering Science, V. 28, No. 1, Jan., 1973, pp. 13-21.

85. WALTERS, J.K., *Theoretical Analysis of Stresses in Axially Symmetric Hoppers and Bunkers*, Chemical Engineering Science, V. 28, No. 3, Mar., 1973, pp. 779-789.

86. WARD, H.A., *Design of Reinforced Concrete Circular Bins for the Storage of Cement*, Am. Concr. Inst., Proceedings, V. 21, 1925, pp. 239-247, (Discussion) pp. 248-251.

87. WEI, M.L., and JOHANSON, J.R., *Elimination of Vibrations in an Ore Unloading Bin*, Journal of Engineerling for Industry, Series B, Transactions, ASME, Vol. 96, Auugst, 1974, pp. 761-765, Paper No. 73-MH-4.

88. WU, T.H., Soil Mechanics, Allyn and Bacon, Inc., Boston, Mass., 1976.

Appendix A

Rankine's Theory of Earth Pressure for Cohesionless Soils Against a Smooth Wall

Failure Criterion: $\tau = \sigma \tan\phi$ (A.1)

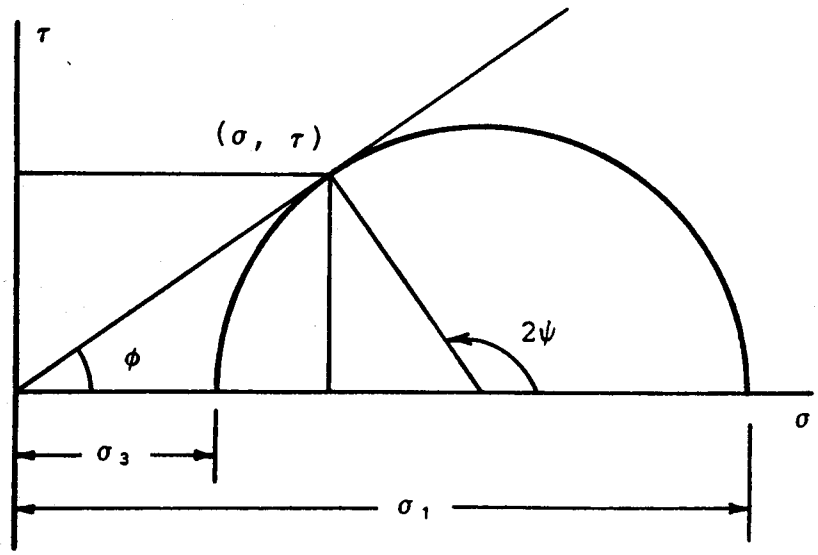

$$\sigma = \frac{\sigma_1 + \sigma_3}{2} \pm \frac{\sigma_1 - \sigma_3}{2} \cos 2\psi \quad = p \pm p \sin\phi \cos 2\psi \qquad \text{(A.2)}$$

$$\tau = \frac{\sigma_1 - \sigma_3}{2} \sin 2\psi \quad = p \sin\phi \sin 2\psi \qquad \text{(A.3)}$$

where p is the average of the principal stresses

Substituting (A.2) and (A.3) into (A.1) yields;

$$\sigma_1 = \sigma_3 + \frac{\sigma_3 \tan\phi}{\sin\psi \cos\psi - \cos^2\psi \tan\phi} \qquad \text{(A.4)}$$

σ_1 is a minimum if $\frac{d}{d\psi}(\sin\psi \cos\psi - \cos^2\psi \tan\phi) = 0$

for which

$$\psi = 45 + \phi/2 \qquad \text{(A.5)}$$

Substituting (A.5) into (A.4) yields;

$$\sigma_3 = \sigma_1 \tan^2(45 - \phi/2)$$

where σ_1 and σ_3 are respectively σ_z and σ_x if the mass is brought to incipient failure through a decrease of σ_x (i.e. outward wall movement active case), or vice versa if incipient failure is brought about through an increase of σ_x (i.e. inward wall movement - passive case).

Therefore

$$\tan^2(45 - \phi/2) = \frac{\sigma_3}{\sigma_1} = Ka = \frac{1}{Kp} = \frac{1 - \sin\phi}{1 + \sin\phi}$$

Appendix B

Instantaneous and Upper Bound Wall Pressures using a Minimum Strain Energy Approach[1]

For an elastic element of volume dV, the incremental increase in strain energy, W, is given by

$$dW = dV \int_0^{\epsilon} \sigma d\epsilon \qquad \text{(B.1)}$$

Neglecting extensional wall and material shear strains, the recoverable strain energy, in terms of principal strains is

$$dW = -A\, dz \left[\int_{\epsilon_1}^{0} \sigma_1 d\epsilon_1 + \int_{\epsilon_2}^{0} \sigma_2 d\epsilon_2 + \int_{\epsilon_3}^{0} \sigma_3 d\epsilon_3 \right] \qquad \text{(B.2)}$$

Jenike defines σ_1, σ_2, and σ_3 as the vertical, lateral, and hoop or third pressures respectively. In a three dimensional state of stress, the sum of any three orthogonal normal stresses is an invariant. Therefore, we may also say

$$dW = -A\, dz \left[\int_{\epsilon_V}^{0} \sigma_V d\epsilon_V + \int_{\epsilon_h}^{0} \sigma_h d\epsilon_h + \int_{\epsilon_3}^{0} \sigma_3 d\epsilon_3 \right] \qquad \text{(B.3)}$$

Hooke's Law gives the differential strain increment as

$$d\epsilon_V = \frac{d\sigma_V}{E} - \nu \frac{d(\sigma_h + \sigma_3)}{E} \qquad \text{(B.4)}$$

and similarly for $d\epsilon_h$ and $d\epsilon_3$.

---

[1]Adapted from Jenike *et al.*(1973 Part 3)

We may describe the three orthogonal stress components in terms of a nondimensional stress parameter, S and two lateral stress coefficients K and K_3 such that

$$\sigma_v = R\gamma S \tag{B.5a}$$

$$\sigma_h = KR\gamma S \tag{B.5b}$$

$$\sigma_3 = K_3 R\gamma S \tag{B.5c}$$

Substitution of Eqs.[B.5] and [B.4] into Eq.[B.3],

$$dW = \frac{-A\ dz}{E} R^2\gamma^2 \int_s^0 \Big[S[dS - \nu dS(K+K_3)] + KS[KdS - \nu dS(1+K_3)] + K_3S[K_3dS - \nu dS(1+K)] \Big] \tag{B.6}$$

Performing the above integration (note the reversed integration limits),

$$dW = \frac{-A\ dz\ R^2\gamma^2}{2E} \Big[-S^2(1+K^2+K_3^2) + S^2\nu(2K+2K_3+2KK_3) \Big] \tag{B.7}$$

Integrating again and expressing the strain energy as a nondimensional quantity,

$$w = \frac{W}{\frac{AR}{2E}(R\gamma)^2} = \frac{1}{R} \int_0^z \Big[1 + K^2 + K_3^2 - 2\nu(K+KK_3+K_3) \Big] S^2 dz \tag{B.8}$$

For conditions of plane strain (as exist within wedge shaped hoppers) $\epsilon_3 = 0$ and therefore

$$\epsilon_3 = \frac{\sigma_3}{E} - \frac{\nu}{E}(\sigma_V + \sigma_h) = 0$$

$$\sigma_3 = \nu(\sigma_V + \sigma_h) \qquad \text{(B.9)}$$

$$K_3 = \nu(1 + K) \qquad \text{(B.10)}$$

For conditions of axial symmetry (as exist within cone shaped hoppers), $\sigma_3 = \sigma_h$ at the bin centre line. The circumferential stress, σ_θ (σ_3 here) is always a principal stress under conditions of axial symmetry (i.e. there can be no shear stresses on a radial plane) but σ_h is a principal stress only at the bin's centre line. However, if we examine strains that occur as a result of outward wall movement, we find that circumferential material strains and radial material strains are identical (i.e. the radius and circumference are proportional). Thus it seems reasonable to extend this equality to radial and circumferential stresses, given a material that is reasonably isotropic in the horizontal direction. Because we define K as a horizontal-to-vertical ratio, we may conclude that, within cylinders,

$$K_3 = K \qquad \text{(B.11)}$$

Although these arguments cannot be presented rigorously, they do reinforce one of Janssen's initial assumptions; horizontal pressures are uniform throughout a slice.[1] This cannot be shown true analytically because we cannot analytically predict K or K_3 at this time, except as limiting values only.

This equality also allows us to predict ν within a contained mass as a function of K. From Eq.[B.10],

$$\nu = \frac{K}{1 + K} \qquad \text{(B.12)}$$

If significant wall movements are expected in the plane strain case (i.e. due to bending), we may continue the formulation with Eq.[B.10] substituted into Eq.[B.8]. Using the appropriate algebra,

$$w = \frac{1}{R} \int_0^z \left[K^2(1-\nu)(1+\nu) - 2K\nu(1+\nu) + (1-\nu)(1+\nu)\right] S^2 dz \qquad \text{(B.13)}$$

For the axisymmetric case, substitution of Eq.[B.11] into Eq.[B.8] yields

$$w = \frac{1}{R} \int_0^z \left[1 - 4K\nu + K^2 2(1-\nu)\right] S^2 dz \qquad \text{(B.14)}$$

At this point, Jenike *et al.* introduce a geometric parameter; m = 1 in axial symmetry and m = 0 in plane strain.

---

[1] This was also an essential conclusion from the discussions in Sect. 2.1.5

Nondimensional strain energy w can now be described by a combination of Eqs.[B.13] and [B.14].

$$w = \frac{1}{R}\left[\frac{1+\nu}{2}\right]^{1-m} \int_0^z \left[M^{2(1-m)} - 4\nu K + M^2K^2\right]S^2 dz \qquad \text{(B.15)}$$

where $$M = \sqrt{2(1-\nu)} \qquad \text{(B.16)}$$

Within any physically contained system, the total internal energy of this system will tend to a minimum as stated by the second law of thermodynamics. Jenike *et al.* apply this fundamental principle to the bulk mass over the region in which flow is occurring. Above this region, a Janssen field exists, and at the boundary between these two zones, a 'switch' is said to occur. Therefore, Eq.[B.15] is minimized from the level of the switch, z_0, to H. Within this region, S and K vary.

Minimizing this equation requires the application of variational calculus. The first variation of the functional w must vanish (i.e. w must have a stationary value to be minimized) and this requires that $\delta w = 0$.

$$\delta w = 0 = \frac{1}{R}\left[\frac{1+\nu}{2}\right]^{1-m} \int_{z_0}^{H} \left[2S(\delta S)M^{2(1-m)} - 2S(\delta S)4\nu K + 2S(\delta S)M^2K^2\right]dz \qquad \text{(B.17)}$$

Rearranging

$$0 = \frac{1}{R}\left[\frac{1+\nu}{2}\right]^{1-m} \int_{z_0}^{H} \left[2S(\delta S)M^{2(1-m)} - 4\nu[SK(\delta S) + S(\delta SK)] + 2M^2(SK)(\delta SK)\right]dz \qquad \text{(B.18)}$$

Janssen's equilibrium equation is employed throughout the silo (this is also given as Eq.[2.2] in text).

$$\frac{dS}{dz} R = 1 - \mu' KS \qquad \text{(B.19)}$$

Eq.[B.19] may be restated in the following form.

$$R \frac{dS}{dz} + \mu' SK = 1 = R \frac{d(S + \delta S)}{dz} + \mu' (SK + \delta SK)$$

because tentative solutions, $(S + \delta S)$ and $(SK + \delta SK)$, must also satisfy the equilibrium equation when substituted for S and SK respectively. Therefore

$$0 = R \frac{d(\delta S)}{dz} + \mu' \delta SK$$

or

$$\delta SK = - \frac{R}{\mu'} \frac{d(\delta S)}{dz} \qquad \text{(B.20)}$$

Substituting Eq.[B.20] into Eq.[B.18] and rearranging

$$0 = \frac{1}{R}\left[\frac{1+\nu}{2} \right]^{1-m} \int_{z_0}^{H} \left[\frac{R}{\mu'}(4\nu S - 2M^2 KS) \frac{d(\delta S)}{dz} \right.$$

$$\left. + \delta S[2S(M^{2(1-m)} - 2\nu K)] \right] dz \qquad \text{(B.21)}$$

Let

$$u = \frac{R}{\mu'}(4\nu S - 2M^2 KS)$$

$$dv = \frac{d(\delta S)}{dz}\, dz$$

and with $\int_1^2 u\,dv = uv\Big|_1^2 - \int_1^2 v\,du$

we may integrate the first term of Eq.[B.21] by parts.

$$\delta W = \frac{1}{R}\left[\frac{1+\nu}{2}\right]^{1-m}\left[\frac{R}{\mu'}(4\nu S - 2M^2 KS)\Big|_{z_0}^{H}\delta S\right.$$

$$\left. + \int_{z_0}^{H}\{-\delta S\frac{R}{\mu'}\frac{d}{dz}(4\nu S - 2M^2 KS) + \delta S 2S(M^{2(1-m)} - 2\nu K)\}dz\right] \qquad \text{(B.22)}$$

For an absolute minimum of the elastic strain energy, the first term in Eq.[B.22] must vanish at $z = H$.

$$4\nu S = 2M^2 KS = 4(1-\nu)KS$$

or

$$K = K_t = \frac{\nu}{1-\nu} \qquad \text{at } z = H \qquad \text{(B.23)}$$

This natural boundary condition is also derived in Sect. 2.2.2 as Eq.[2.20]. If satisfied, it becomes a free boundary condition.

The integrand of Eq.[B.22] must also vanish for any δS and hence

$$2S(M^{2(1-m)} - 2\nu K) = \frac{R}{\mu'}\frac{d}{dz}(4\nu S - 2M^2 KS) \qquad \text{(B.24)}$$

Solving Eq.[B.19] for K,

$$K = \frac{1 - RS'}{\mu' S} \tag{B.25}$$

Substituting this into Eq.[B.24] and expanding, yields

$$2SM^{2(1-m)} - \frac{4\nu}{\mu'} + \frac{4\nu RS'}{\mu'} = \frac{R}{\mu'}\left[4\nu S' - 2M^2 \frac{-RS''}{\mu'}\right]$$

$$SM^{2(1-m)} - \frac{2\nu}{\mu'} = \left[\frac{MR}{\mu'}\right]^2 S'' \tag{B.26}$$

Therefore

$$S - N = \left[\frac{RM^m}{\mu'}\right]^2 S'' \tag{B.27}$$

if we substitute with

$$N = \frac{2\nu}{\mu' M^{2(1-m)}} \tag{B.28}$$

The general solution to Eq.[B.27] is

$$S = Ae^{x_1} + Be^{-x_1} + N \tag{B.29}$$

where

$$x_1 = \frac{\mu'(z - z_0)}{M^m R} \tag{B.30}$$

and A and B are constants.

At the level of the switch, where $z = z_0$, the stress parameter S ($= S_0$) is determined from Eq.[2.3], Janssen's initial static distribution, which is repeated here.

$$S_0 = \frac{1}{\mu' K}\left[1 - e^{-\mu' K z_0 / R}\right] \qquad \text{(B.31)}$$

Eq.[B.29] is therefore reduced to an equation with two unknowns;

$$S_0 = A + B + N \qquad \text{(B.32)}$$

Although S is continuous across the switch, its first derivative with respect to z is not. The lateral pressure ratio K is also discontinuous at the switch, going from K_j, a Janssen value, to K_s, a value that may be determined from the complete solution if desired.

At the level of the transition, where $z = H$, we define three additional constants.

$$X = x_1(H) = \frac{\mu'(H - z_0)}{M^m R} \qquad \text{(B.33)}$$

$$S_t = S(H) = Ae^{X} + Be^{-X} + N \qquad \text{(B.34)}$$

$$S_t' = S'(H) = \frac{\mu'}{M^m R}(Ae^{X} - Be^{-X}) \qquad \text{(B.35)}$$

The equilibrium equation, Eq.[B.19], may be restated as

$$S_t = \frac{1 - RS_t'}{\mu' K_t} \qquad \text{(B.36)}$$

Substituting for both S_t and S_t' (Eqs.[B.34] and [B.35]) into Eq.[B.36],

$$Ae^{X} + Be^{-X} + N = \frac{1 - R\left[\frac{\mu'}{M^m R}(Ae^{X} - Be^{-X})\right]}{\mu' K_t}$$

Solving for B as a function of A,

$$B = \frac{\mu'^{-1}M^m - Ae^{X}(1+M^m K_t) - M^m K_t N}{(M^m K_t - 1)e^{-X}}$$

With Eq.[B.32], we may now solve for A in terms of predefined constants only.

$$A = S_0 - N - B \qquad \text{(B.37)}$$

$$A = \frac{-(S_0 - N)(M^m K_t - 1)e^{-X} + M^m(\mu'^{-1} - K_t N)}{(K_t M^m + 1)e^{X} - (K_t M^m - 1)e^{-X}} \qquad \text{(B.38)}$$

With A, B, and N known, Eqs.[B.29] and [B.30] can be used to solve for S for any location z below any assumed instantaneous switch location z_0. If knowledge of K is desired, its instantaneous value may be determined using Eq.[B.25].

Jenike *et al.* suggest that as the switch approaches to within 1/2 to one diameter of the effective material surface, energy dissipation will halt its upward progression. They terminate the upper bound pressure envelope once K achieves an arched value (i.e. K_p).

In this formulation, the kinetic energy of the solids is ignored. The authors suggest this contribution is small when compared to the elastic strain energy of the solids in sufficiently large bins. The reasonableness of this assumption can only be examined by a quantitative comparison of Eq.[B.15] (multiplied by the nondimensionalizing term in Eq.[B.8]), with the equation for kinetic energy. This is recalled here as

$$K.E. = \frac{1}{2} mv^2$$

where m is the mass (W/g) of material in motion at velocity v

For a silo unloading at a rate of 10000 tph,[1] the maximum material velocity is 0.025 ft/s. This assumes a 70′ diameter flow channel and a material unit weight of 58 pcf. If the total contained mass of 15000 Tons is in motion at once, this would be equivalent to 586 ft-lb of kinetic energy. The optimum switch location (for greatest lateral pressures) is near $0.6H$ from the free surface so that only 40% of the total mass should be assumed in motion. In addition, generally only one gate would be open at a time although this further reduced flow rate would be offset by a reduced flow channel diameter.

---

[1] For the Fording silo, the quoted design discharge rate of each outlet hopper is 5000 tph (i.e. 83 tpm during discharge) when loading cleaned coal at 8% m.c.

In order that we may compute elastic strain energy levels,average values of the differential in Eq.[B.15] may be calculated from the output in Appendix C for an optimum switch location z_o of 80 feet.

$$w = \frac{1}{R} \int_{z_o}^{H} (10.5)dz$$

This gives w = 36.0 for H = 140 ft and R = 17.5 ft. The nondimensionalizing term, with E = 3.4 ksi (from p.88) and R, γ, A as described above, gives

$$W = w\left[\frac{\pi 35^2 x 17.5 \text{ ft}^3}{2x3400x144 \text{ lb/ft}^2} (17.5 \text{ ft } x \text{ } 58 \text{ lb/ft}^3)^2\right] = 2.55x10^6 \text{ ft-lb}$$

Thus kinetic energy is small when compared to elastic strain energy.

```
C     This program calculates the instantaneous dynamic pressure
C     curve (Curve I in Fig. 2.12) for a particular switch location.
C     Strain energy is minimized in the region below the switch
C     location extending to the transition level.
C     The formulation follows the Jenike Strain Energy Method
C     but with allowance for a kinetic wall friction coefficient
C     and a wall strain energy flexibility parameter.
C
      REAL M,N,KJ,KH,KO,K(20)
      DIMENSION X(20),Z(20),S(20),SP(20),PGD(20),P(20),ZT(20),ZTP(20)
      READ(5,100) US,U,V,H,D,GAMMA,KJ,ZTO,HS,CM
  100 FORMAT(F7.3/F7.3/F7.4/F7.3/F7.3/F7.3/F7.3/F7.3/F7.3)
      WRITE(6,300)US,U,V,H,D,GAMMA,KJ,ZTO,HS,CM
  300 FORMAT('1',5X,'THE STATIC WALL FRICTION COEFF. IS = ',1X,F5 3
     I       /' ',5X,'THE KINETIC WALL FRICTION COEFF. IS = ',F5.3
     N       /' ',5X,'POISSON''S RATIO IS =',18X,F6.4
     P       /' ',5X,'THE COAL HEIGHT IS =',16X,F6.2
     U       /' ',5X,'THE DIAMETER IS =',20X,F5.2
     T       /' ',5X,'THE MATERIAL DENSITY IS =',11X,F6.2
     1       /' ',5X,'THE JANSSEN K VALUE IS =',12X,F6.2
     2       /' ',5X,'THE SWITCH LOCATION IS =',12X,F6.2
     3       /' ',5X,'THE SILO HEIGHT IS =',16X,F6.2
     4       /' ',5X,'THE WALL PARAMETER IS =',13X,F6.2)
      DO 200 I=1,20
      READ(5,110) ZT(I)
  110 FORMAT(F6.2)
      IF(ZT(I).EQ.0.0)GO TO 201
  200 CONTINUE
  201 NINPUT=I-1
      DOWN=HS-H
      ZO=ZTO-DOWN
      M=SQRT(2*(1-V))
      M=SQRT(CM+M**2)
      N=2*V/U
      KH=V/((1-V)+CM/2)
      R=D/4
      SO=(1-EXP(-US*KJ*ZO/R))/(US*KJ)
      XX=U*(H-ZO)/(M*R)
      AU=-(KH*M-1)*(SO-N)*EXP(-XX)+M*(1/U-KH*N)
      AL=(KH*M+1)*EXP(XX)-(KH*M-1)*EXP(-XX)
      A=AU/AL
      B=SO-N-A
      SOP=(A-B)*U/(M*R)
      KO=(1-R*SOP)/(U*SO)
  210 DIV=(H-ZO)/10
      Z(1)=ZO+DIV
      DO 220 I=1,9
  220 Z(I+1)=Z(I)+DIV
      DO 230 I=1,10
      X(I)=U*(Z(I)-ZO)/(M*R)
      S(I)=A*EXP(X(I))+B*EXP(-X(I))+N
      SP(I)=(A*EXP(X(I))-B*EXP(-X(I)))*U/(M*R)
      K(I)=(1-R*SP(I))/(U*S(I))
      PGD(I)=K(I)*S(I)/4
      ZTP(I)=Z(I)+DOWN
  230 P(I)=PGD(I)*GAMMA*D
      PGDSWT=KO*SO/4
      PSWT=PGDSWT*GAMMA*D
      WRITE(6,301)M,N,KH,A,B,XX,SO,SOP,KO
  301 FORMAT('-',5X,'PARAMETERS'/'O','M',6X,'N',6X,'KH',5X,'A',
     1    8X,'B',8X,'XX',7X,'SO',6X,'SOP',5X,'KO'
     2      /' ',3(F5.3,2X),3(F7.3,2X),2(F6.3,2X),F8.4)
      WRITE(6,302) PGDSWT,PSWT
  302 FORMAT('-',5X,'(P/GAMMA D)       = ',F5.3,10X'P-SWITCH = ',F8.3/
     1       ' ',15X,'SWITCH')
      WRITE(6,303)
  303 FORMAT('-',5X,'Z',8X,'S',8X,'SP',5X,'K',8X,'P/GAMMA D',4X,'ZT',
     1          12X,'P')
      DO 305 I=1,10
      WRITE(6,304)I,Z(I),S(I),SP(I),K(I),PGD(I),ZTP(I),P(I)
  304 FORMAT(' ',I2,3X,F6.2,2X,2(F6.3,2X),F6.3,4X,F5.3,8X,F6.2,3X,F9.3)
  305 CONTINUE
      WRITE(6,307)
  307 FORMAT('O','SPECIFIED LOCATIONS FOR PRESSURE')
      IF(NINPUT.EQ.0)GO TO 401
      DO 400 I=1,NINPUT
      Z(I)=ZT(I)-DOWN
      X(I)=U*(Z(I)-ZO)/(M*R)
      S(I)=A*EXP(X(I))+B*EXP(-X(I))+N
      SP(I)=(A*EXP(X(I))-B*EXP(-X(I)))*U/(M*R)
      K(I)=(1-R*SP(I))/(U*S(I))
      PGD(I)=K(I)*S(I)/4
      P(I)=PGD(I)*GAMMA*D
  400 WRITE(6,306)Z(I),S(I),SP(I),K(I),PGD(I),ZT(I),P(I)
  306 FORMAT(' ',5X,F6.2,2X,2(F6.3,2X),F6.3,4X,F5.3,8X,F6.2,3X,F9.3)
  401 STOP
      END
```

```
 THE STATIC WALL FRICTION COEFF. IS =  0.500
 THE KINETIC WALL FRICTION COEFF. IS = 0.400
 POISSON'S RATIO IS =                  0.2857
 THE COAL HEIGHT IS =                140.00
 THE DIAMETER IS =                    70.00
 THE MATERIAL DENSITY IS =            58.00
 THE JANSSEN K VALUE IS =              0.40
 THE SWITCH LOCATION IS =             80.44
 THE SILO HEIGHT IS =                140.00
 THE WALL PARAMETER IS =               0.0


 PARAMETERS

M       N       KH      A       B       XX      SO      SOP     KO
1.195   1.429   0.400   0.537   1.041   1.139   3.006   -0.010  0.9718


 (P/GAMMA D)       = 0.730          P-SWITCH = 2965.182
        SWITCH

    Z       S       SP      K       P/GAMMA D       ZT          P
 1   86.40   2.959  -0.006  0.937   0.693           86.40       2815.045
 2   92.35   2.931  -0.003  0.897   0.657           92.35       2668.512
 3   98.31   2.924   0.000  0.850   0.622           98.31       2523.683
 4  104.26   2.935   0.004  0.798   0.586          104.26       2378.670
 5  110.22   2.966   0.007  0.741   0.550          110.22       2231.597
 6  116.18   3.017   0.010  0.679   0.512          116.18       2080.551
 7  122.13   3.089   0.014  0.613   0.474          122.13       1923.569
 8  128.09   3.182   0.018  0.544   0.433          128.09       1758.614
 9  134.04   3.299   0.021  0.473   0.390          134.04       1583.544
10  140.00   3.439   0.026  0.400   0.344          140.00       1396.088

SPECIFIED LOCATIONS FOR PRESSURE
     80.44   3.006  -0.010  0.972   0.730           80.44       2965.183
```

```
C     This program calculates the theoretical maximum dynamic pressure
C     curve (Curve II in Fig. 2.12) using all possible switch locations.
C     Strain energy is minimized in the region below each switch
C     location extending to the transition level.
C     The formulation follows the Jenike Strain Energy Method
C     but with allowance for a kinetic wall friction coefficient
C     and a wall strain energy flexibility parameter.
C
      REAL M,N,KJ,KH,KO
      READ(5,100) US,U,V,H,D,GAMMA,KJ,CM
  100 FORMAT(F7.3/F7.3/F7.4/F7.3/F7.3/F7.3/F7.3/F7.3)
      WRITE(6,300)US,U,V,H,D,GAMMA,KJ,CM
  300 FORMAT('1',5X,'THE STATIC WALL FRICTION COEFF. IS = ',1X,F5.3
     I       /' ',5X,'THE KINETIC WALL FRICTION COEFF. IS = ',F5.3
     N       /' ',5X,'POISSON''S RATIO IS =',18X,F6.4
     P       /' ',5X,'THE HEIGHT IS =',21X,F6.2
     U       /' ',5X,'THE DIAMETER IS =',19X,F6.2
     T       /' ',5X,'THE MATERIAL DENSITY IS =',11X,F6.2
     1       /' ',5X,'THE JANSSEN K VALUE IS =',12X,F6.2
     2       /' ',5X,'THE WALL PARAMETER IS =',13X,F6.2)
      M=SQRT(2*(1-V))
      M=SQRT(CM+M**2)
      N=2*V/U
      KH=V/((1-V)+CM/2)
      R=D/4
      PGDMAX=0.0
      WRITE(6,301)M,N,KH
  301 FORMAT('-',5X,'PARAMETERS'/'0','M',6X,'N',6X,'KH'
     1       /' ',3(F5.3,2X)/'-',3X,'Z0',7X,'K0',4X,'P/GDSWITCH',
     2       2X,'PRESSURE')
      DO 215 I=1,20
      Z0=I*H/20
      S0=(1-EXP(-US*KJ*Z0/R))/(US*KJ)
      XX=U*(H-Z0)/(M*R)
      AU=-(KH*M-1)*(S0-N)*EXP(-XX)+M*(1/U-KH*N)
      AL=(KH*M+1)*EXP(XX)-(KH*M-1)*EXP(-XX)
      A=AU/AL
      B=S0-N-A
      SOP=(A-B)*U/(M*R)
      K0=(1-R*SOP)/(U*S0)
      PGDSWT=K0*S0/4
      P=PGDSWT*GAMMA*D
      WRITE(6,302)Z0,K0,PGDSWT,P
  302 FORMAT(' ',F8.3,2X,F8.4,2X,F6.4,4X,F8.3)
      IF(PGDSWT.GT.PGDMAX)GO TO 10
      GO TO 215
   10 PGDMAX=PGDSWT
      PLOC=Z0
  215 CONTINUE
      Z=PLOC-H/20+H/10000
      DO 220 I=1,999
      S0=(1-EXP(-US*KJ*Z/R))/(US*KJ)
      XX=U*(H-Z)/(M*R)
      AU=-(KH*M-1)*(S0-N)*EXP(-XX)+M*(1/U-KH*N)
      AL=(KH*M+1)*EXP(XX)-(KH*M-1)*EXP(-XX)
      A=AU/AL
      B=S0-N-A
      SOP=(A-B)*U/(M*R)
      K0=(1-R*SOP)/(U*S0)
      PGDSWT=K0*S0/4
      IF(PGDSWT.LE.PGDMAX)GO TO 220
      PGDMAX=PGDSWT
      ZATMAX=Z
  220 Z=Z+H/10000
      PMAX=PGDMAX*GAMMA*D
      WRITE(6,303)PGDMAX,PMAX,ZATMAX
  303 FORMAT('-',5X,'(P/GAMMA D)     = ',F7.4,10X,'P = ',F8.3/
     1       ' ',15X,'MAX'/' ',36X,'AT Z = ',F8.3)
      STOP
      END
```

```
 THE STATIC WALL FRICTION COEFF. IS =  0.500
 THE KINETIC WALL FRICTION COEFF. IS =  0.400
 POISSON'S RATIO IS =                   0.2857
 THE HEIGHT IS =                      140.00
 THE DIAMETER IS =                     70.00
 THE MATERIAL DENSITY IS =             58.00
 THE JANSSEN K VALUE IS =               0.40
 THE WALL PARAMETER IS =                0.0

 PARAMETERS

M       N       KH
1.195   1.429   0.400

   Z0        K0      P/GDSWITCH   PRESSURE
    7.000    3.7085   0.3564       1446.986
   14.000    2.2898   0.4232       1718.205
   21.000    1.8115   0.4831       1961.582
   28.000    1.5672   0.5365       2178.103
   35.000    1.4156   0.5834       2368.488
   42.000    1.3093   0.6239       2533.147
   49.000    1.2280   0.6582       2672.178
   56.000    1.1610   0.6860       2785.333
   63.000    1.1026   0.7074       2872.000
   70.000    1.0488   0.7220       2931.171
   77.000    0.9971   0.7294       2961.437
   84.000    0.9455   0.7293       2960.995
   91.000    0.8923   0.7211       2927.692
   98.000    0.8362   0.7042       2859.123
  105.000    0.7762   0.6780       2752.852
  112.000    0.7114   0.6420       2606.708
  119.000    0.6413   0.5959       2419.267
  126.000    0.5656   0.5395       2190.493
  133.000    0.4849   0.4735       1922.455
  140.000    0.4000   0.3990       1620.036

 (P/GAMMA D)     =  0.7303          P =  2965.186
        MAX
                                  AT Z =   80.438
```

Appendix D

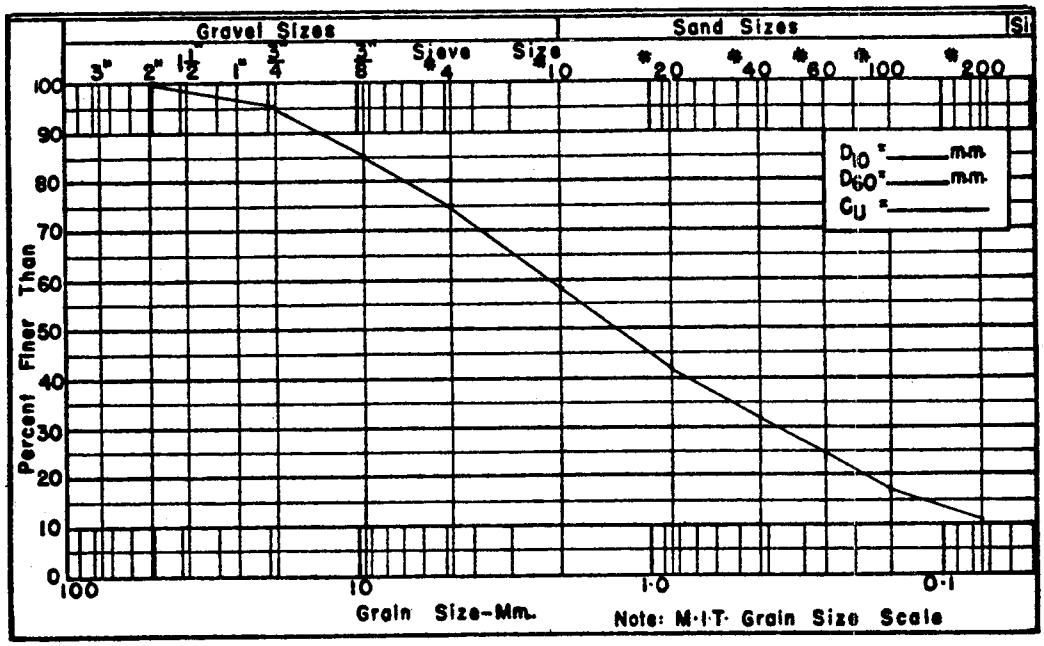
Gravel Sizes
Sand Sizes
Sieve Size
3" 2" 1½ 1" ¾ ⅜ #4 #10 #20 #40 #60 #100 #200
Percent Finer Than
100 90 80 70 60 50 40 30 20 10 0
100 10 1·0 0·1
Grain Size-Mm.
Note: M·I·T· Grain Size Scale
D_{10} = ____ mm
D_{60} = ____ mm
C_U = ____

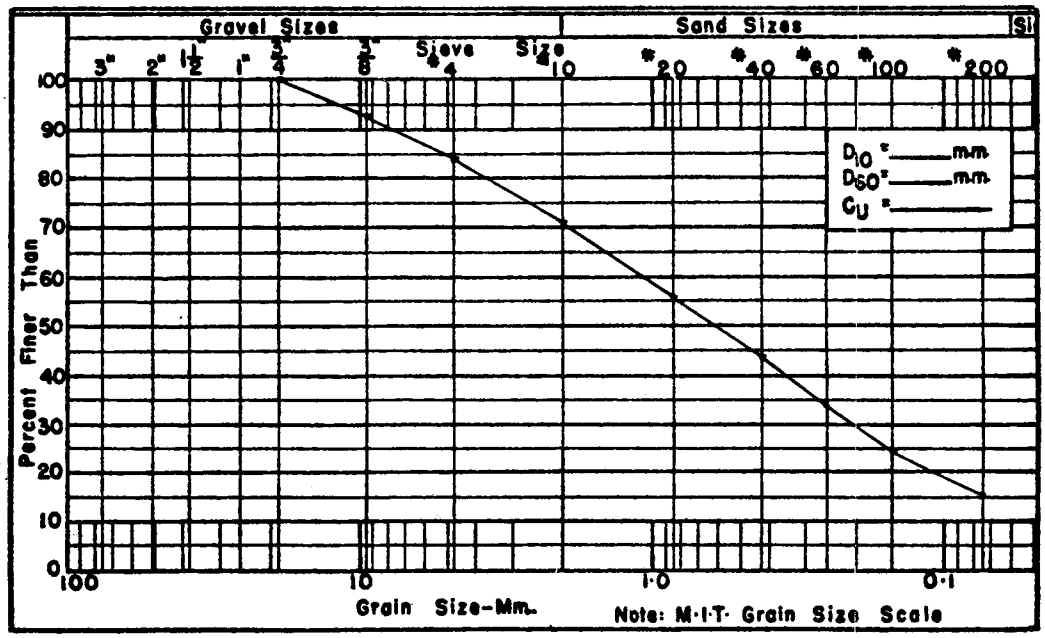
Gravel Sizes
Sand Sizes
Sieve Size
3" 2" 1½ 1" ¾ ⅜ #4 #10 #20 #40 #60 #100 #200
Percent Finer Than
100 90 80 70 60 50 40 30 20 10 0
100 10 1·0 0·1
Grain Size-Mm.
Note: M·I·T· Grain Size Scale
D_{10} = ____ mm
D_{60} = ____ mm
C_U = ____

Appendix E

One-Dimensional Transient Analysis of Temperature Gradients in a Silo Wall[1]

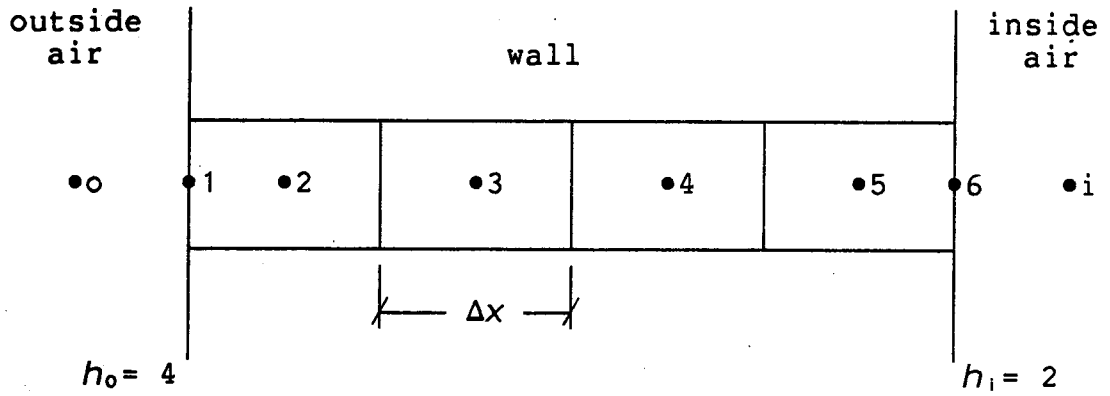

$$T_1 = F'_{01}T_0 + F'_{21}T_2$$

$$T_6 = F'_{i6}T_i + F'_{56}T_5$$

$$T'_2 = F_{12}T_1 + F_{22}T_2 + F_{32}T_3$$

$$T'_3 = F_{23}T_2 + F_{33}T_3 + F_{43}T_4$$

$$T'_4 = F_{34}T_3 + F_{44}T_4 + F_{54}T_5$$

$$T'_5 = F_{45}T_4 + F_{55}T_5 + F_{65}T_6$$

$$F'_{01} = \frac{N\beta_i}{N\beta_i + 2}$$

$$F'_{21} = 1 - F'_{01}$$

$$N\beta_i = \frac{h\,\Delta x}{k}$$

(Similarly for F'_{i6} and F'_{56})

$$F_{12} = F_{65} = 2/M$$

$$F_{22} = F_{55} = (M-3)/M$$

$$F_{33} = F_{44} = 1 - 2/M$$

$$F_{23} = F_{34} = F_{45} = F_{32} = F_{43} = F_{54} = 1/M$$

Here

$$M = \frac{\Delta x^2}{\alpha \Delta t} \qquad \alpha = \frac{k}{\rho C} \qquad M \geq 3$$

---

[1]Adapted from Dussinberre (1961)

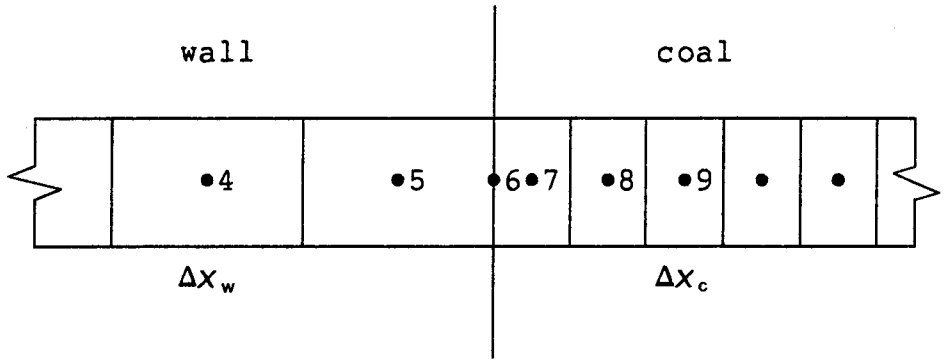

$$T_6 = F'_{56}T_5 + F'_{76}T_7$$

$$T'_7 = F_{67}T_6 + F_{77}T_7 + F_{87}T_8$$

$$T'_8 = F_{78}T_7 + F_{88}T_8 + F_{98}T_9$$

$$\vdots$$

$$T'_n = F_{(n-1)n}T_{n-1} + F_{nn}T_n + F_{(n+1)n}T_{n+1}$$

$$F'_{56} = \frac{K_{56}}{K_{56} + K_{76}} \qquad K_{56} = \frac{k_w A}{\Delta x_w / 2}$$

$$F'_{76} = 1 - F'_{56} \qquad K_{76} = \frac{k_c A}{\Delta x_c / 2}$$

$$F_{67} = 2/Mc$$

$$F_{77} = (Mc - 3)/Mc$$

$$F_{87} = 1/Mc$$

$$F_{88} = F_{99} = F_{nn} = 1 - 2/Mc$$

$$F_{78} = F_{98} = F_{89} = F_{(n-1)n} = F_{(n+1)n} = 1/Mc$$

Here

$$Mc = \frac{\Delta x_c^2}{\alpha_c \Delta t} \qquad \alpha_c = \frac{k_c}{\rho_c C_c} \qquad Mc \geq 3$$

where

A = cross-sectional area perpendicular to flow (ft^2)

c = specific heat (Btu/lbm/F)

h = film coefficient (Btu/hr ft^2F)

k = conductivity (Btu/hr ft F)

K = thermal conductance (Btu/hr F)

M = dimensionless modulus

$N\beta_i$ = dimensionless Biot number

Δt = time increment (hr)

Δx = length of lumped mass (ft)

α = thermal diffusivity (ft^2/hr)

ρ = density (lbm/ft^3)

Appendix F

Moments due to Thermal Effects in Isotropic Homogeneous Hollow Cylinders[1]

In general, the steady state temperature distribution for a hollow circular cylinder is curvilinear. With respective inner and outer surface temperatures of T_i and T_o, this distribution is given by;

$$T(r) = T_o + (T_i - T_o)\frac{\ln(r_o/r)}{\ln(r_o/r_i)}$$

where

r_i = inner radius of cylinder wall

r_o = outer radius of cylinder wall

r = radius at particular point in wall

The corresponding circumferential stress σ_θ becomes;

$$\sigma_\theta(r) = E\alpha(T_i - T_o)\left[1 - \ln\left(\frac{r_o}{r}\right) - \frac{r_i^2}{r_o^2 - r_i^2}\left(1 + \frac{r_o^2}{r^2}\right)\ln\left(\frac{r_o}{r_i}\right)\right] \Big/ 2(1 - \nu)\ln(r_o/r_i)$$

Using a three term expansion for $\ln(r_o/r_i)$ and that t $(= r_o - r_i) << 3r_i$, (i.e. a thin-walled cylinder), the stresses at the inner and outer faces reduce to

$$\sigma_\theta(r_i) = -E\alpha(T_i - T_o)/2(1-\nu)$$

$$\sigma_\theta(r_o) = E\alpha(T_i - T_o)/2(1-\nu)$$

with a linear stress distribution between these points.

---

[1]Adapted from Johns (1965)

These temperature induced stresses would tend to bow an unrestrained wall section and therefore the restraint due to wall continuity sets up a circumferential (and vertical) moment, M_T;

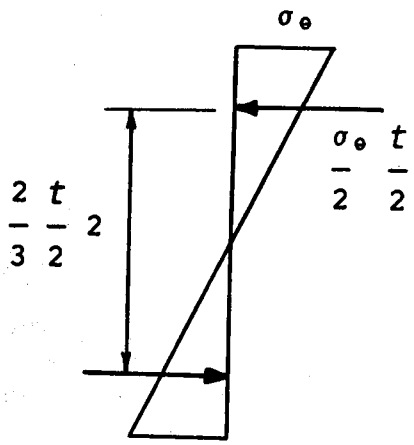

$$M_T = \frac{\sigma_\theta}{2} \frac{t}{2} \times \frac{t}{2} \frac{2}{3} \times 2 = \sigma_\theta \frac{t^2}{6}$$

with $$D = \frac{E\,t}{12(1-\nu^2)}$$

$$M_T = \frac{\alpha(T_i - T_o)\, D(1+\nu)}{t}$$

```
C     This program calculates static coal pressures using a
C     Janssen's differential slice element. It has the
C     cabability to provide for variations in both unit
C     weight and K.
C
      REAL KO,K(600),MEXP
      DIMENSION ZEFF(600),ZTOP(600),SIGMAV(600),SIGMAH(600),
     1 TAUW(600),GAMMA(600),RELDEN(600)
      READ(5,100) U,HTCOAL,DIA,GAMMAF,KO,HTSILO,BETA,SIGMAO,
     1            GAMMAO,MEXP,HTCONE,DELTAZ
  100 FORMAT(12(F7.3/))
      WRITE(6,300)U,HTCOAL,DIA,GAMMAF,KO,HTSILO,BETA,SIGMAO,
     1            GAMMAO,MEXP,HTCONE,DELTAZ
  300 FORMAT('1',5X,'THE COEFFICIENT OF WALL FRICTION IS = ',
     I  F4.2/' ',5X,'THE EFFECTIVE COAL HEIGHT IS =',6X,F6.2
     N       /' ',5X,'THE SILO DIAMETER IS =',15X,F5.2
     P       /' ',5X,'THE FINAL MATERIAL DENSITY IS =',5X,F6.2
     U       /' ',5X,'THE AT-REST K VALUE IS =',12X,F6.2
     T       /' ',5X,'THE SILO HEIGHT IS =',16X,F6.2
     1       /' ',5X,'THE COMPRESSIBILITY EXPONENT IS =',6X,F6.5
     2       /' ',5X,'THE INITIAL CONTACT PRESSURE IS =',4X,F6.3
     3       /' ',5X,'THE INITIAL MATERIAL DENSITY IS =',3X,F6.2
     4       /' ',5X,'THE RELATIVE DENSITY EXPONENT IS =',4X,F6.4
     5       /' ',5X,'THE CONE HEIGHT IS =',16X,F6.2
     6       /' ',5X,'THE SLICE HEIGHT IS =',16X,F5.2)
      R=DIA/4
      SIGMAV(1)=HTCONE*GAMMAO/3
      GAMMA(1)=GAMMAO
      K(1)=0.0
      SIGMAH(1)=0.0
      RELDEN(1)=0.0
      TAUW(1)=0.0
      REALNN=(HTCOAL-HTCONE/3)/DELTAZ
      NN=HFIX(REALNN)
      ZLAST=REALNN-NN*DELTAZ
      NNN=NN+1
      WRITE(6,301)
  301 FORMAT('-',1X,'Z(TOP)',2X,'Z(EFF)',3X,'GAMMA',4X,'Dr',8X,
     1   'K',8X,'P w',8X,'P v',8X,'P h')
      DO 10 I=2,NNN
      TOP=SIGMAV(I-1)+GAMMA(I-1)*DELTAZ-SIGMAV(I-1)*U*K(I-1)/R*
     1 DELTAZ/2
      BOT=1+U/R*K(I-1)*DELTAZ/2
      SIGMAV(I)=TOP/BOT
      GAMMA(I)=GAMMAO*(SIGMAV(I)/SIGMAO)**BETA
      IF(GAMMAF.EQ.GAMMAO) GO TO 6
    5 RELDEN(I)=((GAMMA(I)-GAMMAO)/(GAMMAF-GAMMAO))*GAMMAF/GAMMA(I)
      GO TO 7
    6 RELDEN(I)=1.0
    7 IF(RELDEN(I).GE.1.0) RELDEN(I)=1.0
      K(I)=RELDEN(I)**MEXP*KO
      SIGMAH(I)=K(I)*SIGMAV(I)
      TAUW(I)=SIGMAH(I)*U
      ZEFF(I-1)=HTCONE/3+DELTAZ*(I-2)
      ZTOP(I-1)=HTSILO-HTCOAL+ZEFF(I-1)
      IF(I.EQ.NN) DELTAZ=ZLAST
   10 CONTINUE
      ZEFF(NNN)=HTCOAL
      ZTOP(NNN)=HTSILO
      DO 20 I=1,NNN
      WRITE(6,302) ZTOP(I),ZEFF(I),GAMMA(I),RELDEN(I),
     1           K(I),TAUW(I),SIGMAV(I),SIGMAH(I)
  302 FORMAT(' ',1X,3(F6.2,2X),F6.4,2X,F6.4,2X,3(F9.3,2X))
   20 CONTINUE
      STOP
      END
```

```
 THE COEFFICIENT OF WALL FRICTION IS = 0.50
 THE EFFECTIVE COAL HEIGHT IS =      110.00
 THE SILO DIAMETER IS =               70.00
 THE FINAL MATERIAL DENSITY IS =      58.00
 THE AT-REST K VALUE IS =              0.50
 THE SILO HEIGHT IS =                155.70
 THE COMPRESSIBILITY EXPONENT IS =      .07860
 THE INITIAL CONTACT PRESSURE IS =    13.000
 THE INITIAL MATERIAL DENSITY IS =    37.48
 THE RELATIVE DENSITY EXPONENT IS =    1.0000
 THE CONE HEIGHT IS =                21.00
 THE SLICE HEIGHT IS =                0.20
```

Z(TOP)	Z(EFF)	GAMMA	Dr	K	P w	P v	P h
52.70	7.00	37.48	0.0	0.0	0.0	262.360	0.0
52.90	7.20	47.57	0.5995	0.2998	40.445	269.856	80.891
53.10	7.40	47.69	0.6053	0.3026	42.203	278.899	84.405
53.30	7.60	47.81	0.6108	0.3054	43.973	287.948	87.945
53.50	7.80	47.93	0.6162	0.3081	45.755	297.000	91.509
53.70	8.00	48.04	0.6214	0.3107	47.548	306.054	95.097
53.90	8.20	48.15	0.6265	0.3132	49.353	315.111	98.706
54.10	8.40	48.26	0.6314	0.3157	51.169	324.169	102.337
54.30	8.60	48.36	0.6361	0.3181	52.994	333.228	105.989
54.50	8.80	48.47	0.6407	0.3204	54.830	342.287	109.659
54.70	9.00	48.57	0.6452	0.3226	56.674	351.346	113.349
54.90	9.20	48.66	0.6496	0.3248	58.528	360.403	117.056
55.10	9.40	48.76	0.6538	0.3269	60.391	369.458	120.781
55.30	9.60	48.85	0.6580	0.3290	62.261	378.511	124.522
55.50	9.80	48.94	0.6620	0.3310	64.140	387.561	128.279
55.70	10.00	49.03	0.6659	0.3330	66.026	396.608	132.051
55.90	10.20	49.12	0.6697	0.3349	67.919	405.651	135.838
56.10	10.40	49.20	0.6735	0.3367	69.819	414.689	139.639
56.30	10.60	49.29	0.6771	0.3386	71.726	423.723	143.453
56.50	10.80	49.37	0.6807	0.3403	73.640	432.752	147.279
56.70	11.00	49.45	0.6841	0.3421	75.559	441.775	151.119
56.90	11.20	49.53	0.6875	0.3438	77.485	450.792	154.969
57.10	11.40	49.60	0.6909	0.3454	79.416	459.803	158.832
57.30	11.60	49.68	0.6941	0.3471	81.352	468.808	162.705
57.50	11.80	49.75	0.6973	0.3487	83.294	477.805	166.588
57.70	12.00	49.83	0.7004	0.3502	85.240	486.795	170.481
57.90	12.20	49.90	0.7035	0.3517	87.192	495.777	174.383
58.10	12.40	49.97	0.7065	0.3532	89.148	504.751	178.295
58.30	12.60	50.04	0.7094	0.3547	91.108	513.717	182.215
58.50	12.80	50.11	0.7123	0.3561	93.072	522.674	186.143
58.70	13.00	50.17	0.7151	0.3575	95.040	531.623	190.080
58.90	13.20	50.24	0.7179	0.3589	97.012	540.562	194.023
59.10	13.40	50.30	0.7206	0.3603	98.987	549.492	197.974
59.30	13.60	50.37	0.7232	0.3616	100.966	558.413	201.932
59.50	13.80	50.43	0.7259	0.3629	102.948	567.323	205.896
59.70	14.00	50.49	0.7284	0.3642	104.933	576.223	209.866

Appendix H

Natural Frequencies of Cylindrical Shells without Axial Constraint [1]

The natural frequency, f, in Hertz is given by

$$f_{ij} = \frac{\lambda_{ij}}{2\pi R}\left[\frac{E}{\rho(1-\nu^2)}\right]^{\frac{1}{2}}$$

where

λ_{ij} = dimentionless parameter

R = midsurface radius (35.5 x 12in)

E = modulus of elasticity (29 x 10^6psi/8)

ρ = density of shell (145 lb/386.1 in/s^2)(1/12in)^3

ν = Poisson's ratio (.19)

Therefore

$$\lambda_{ij} = f_{ij}/\ 50s$$

Using the observed frequency of ~ 1.5 Hertz,

$$\lambda_{ij} = 0.03$$

From Fig. H.1, and using the lowest axial length parameter (j = 1, L = 155, R = 35.5), the corresponding circumferential pattern is the i = 7 or i = 8 mode. The boundary conditions at the ends are considered as shear diaphrams and this is analagous to a simply beam. At higher circumferential modes, actual boundary condition effects are relatively insignificant. (Table 8.1, Reference [9])

---

[1] Adapted from Blevins (1979)

Figure H.2 indicates that total strain energy is minimized if the number of circumferential nodes, $2i$, is between 14 and 16.

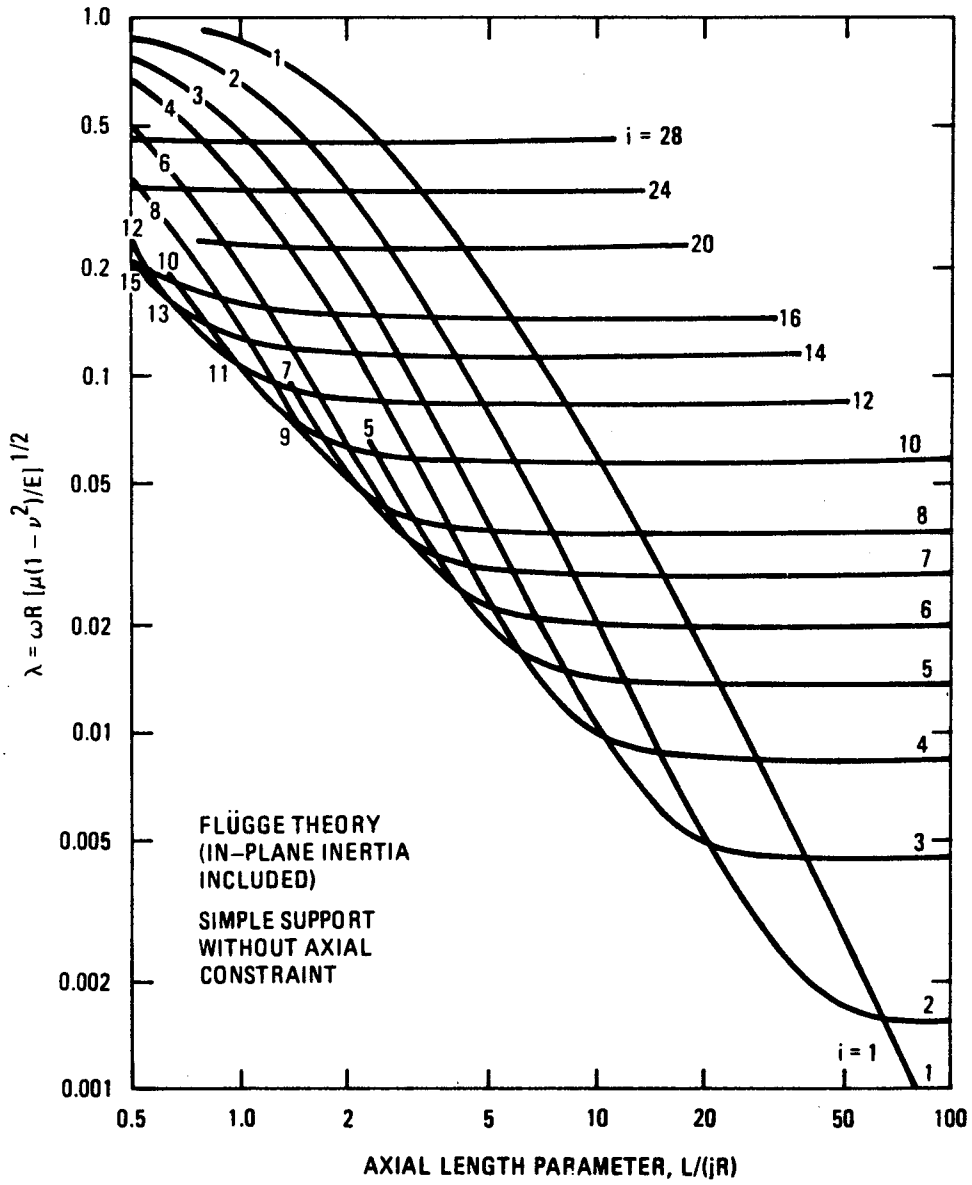

Figure H.1 Frequency Spectrum for a Cylindrical Shell From Reference [9]

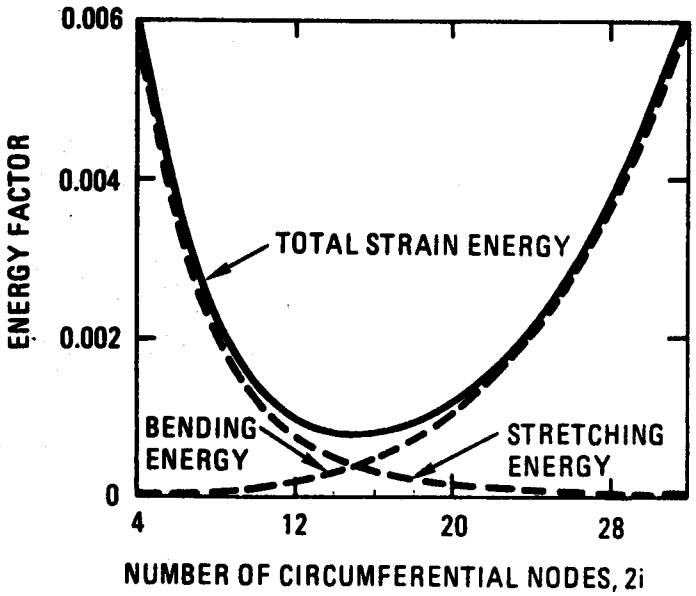

Figure H.2 Strain Energy in a Cylindrical Shell From Reference [9]

Appendix J

Static and Quasi-static Readings

Series B January 1981

Series C June 1981

- Coal levels, where shown, are from Table 3.1 and are either measured, calculated, or estimated as explained in Table 3.1.

- Exterior air temperatures were recorded on the more important occasions and, unless noted otherwise, correspond to cloudy conditions with little or no wind.

- Raw data (strain readings) used for plotting all of the following figures are given at the end of this appendix (p.293).

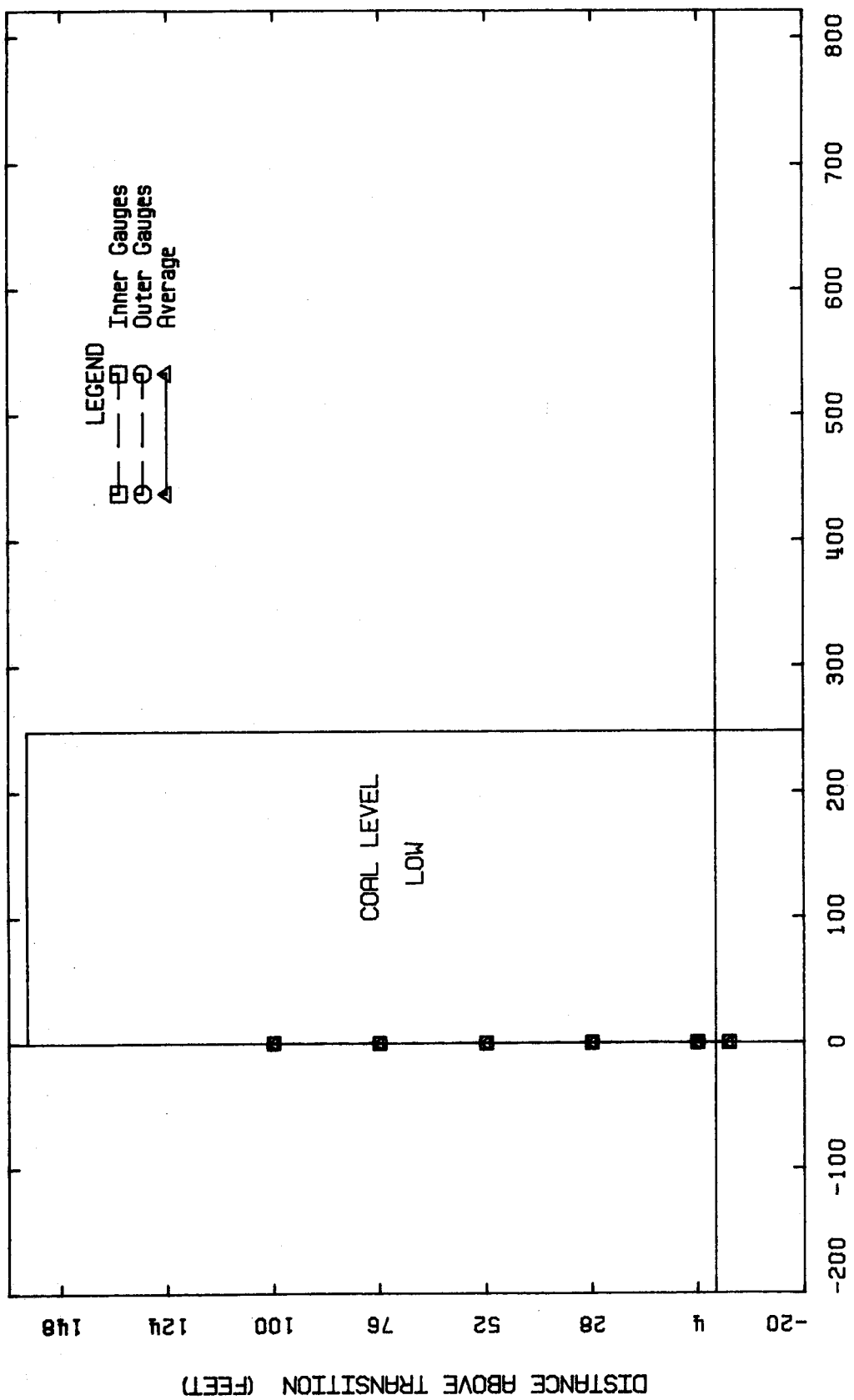

Figure J.B1 Vertical Variation in Hoop Strain - Reference Reading (zero strains) 8:30 PM Jan. 24

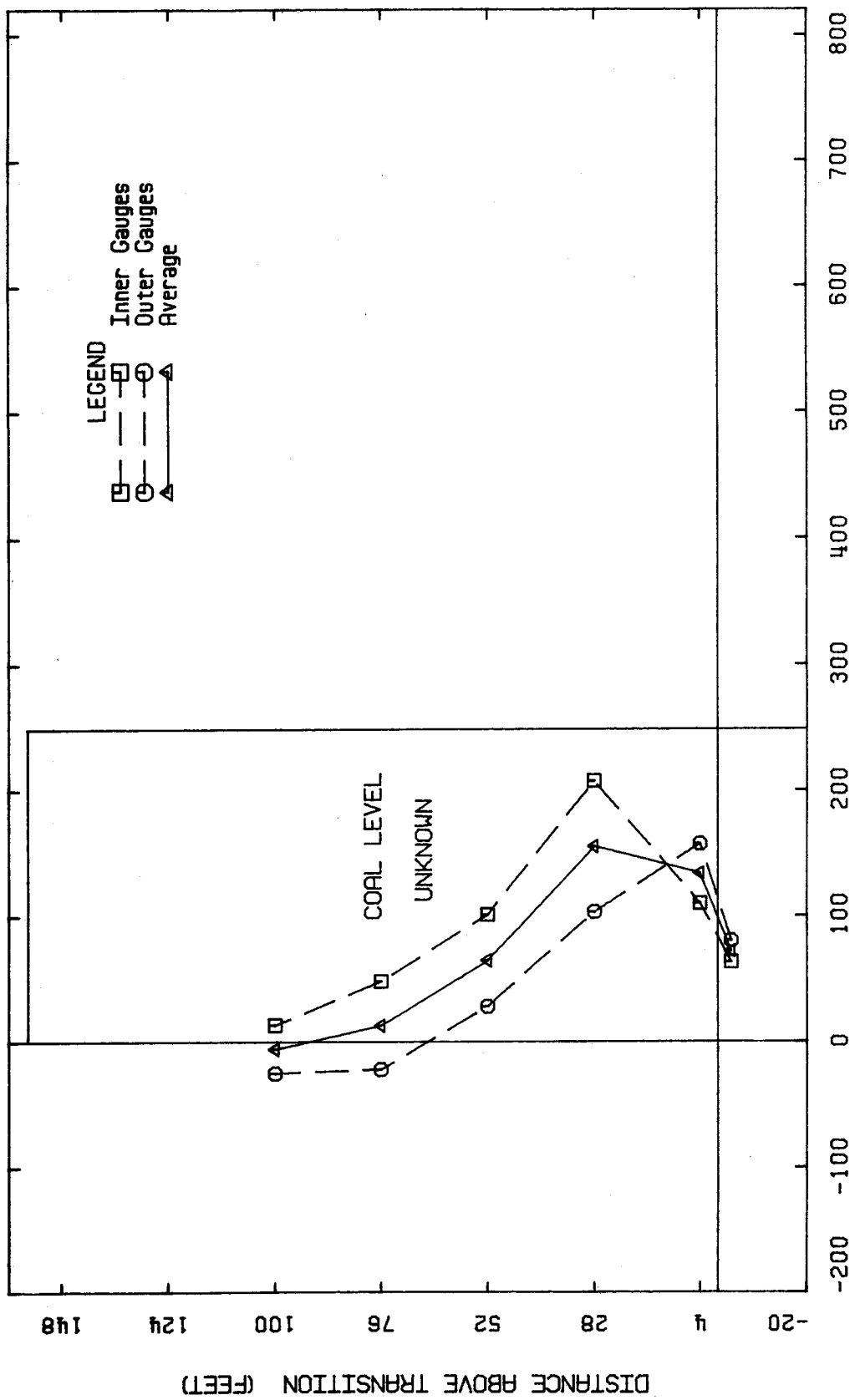

Figure J.B2 Vertical Variation in Hoop Strain - Prior to Run #3

8:00 AM Jan. 25

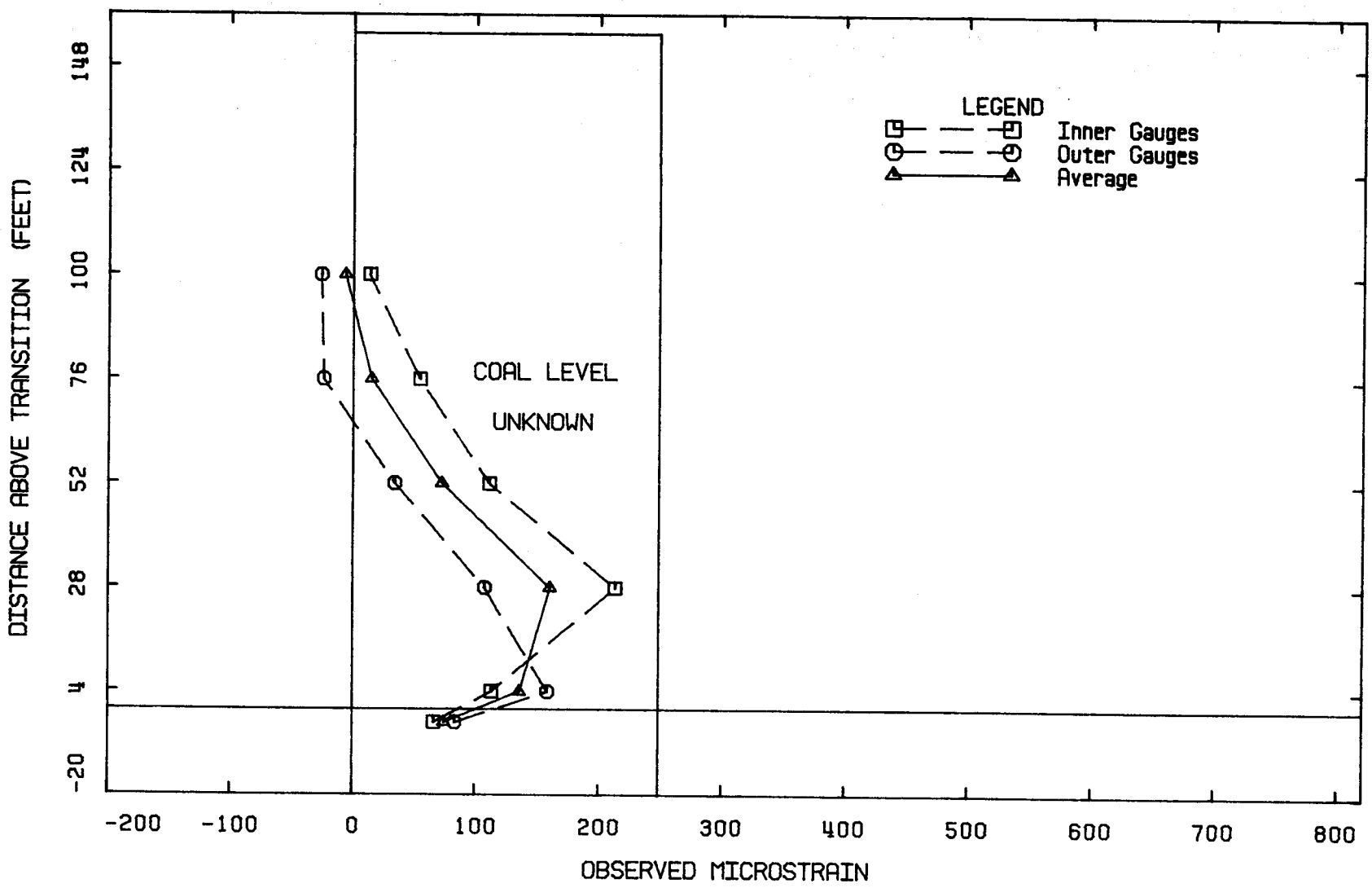

Figure J.B3 Vertical Variation in Hoop Strain - Prior to Run #3

9:00 AM Jan. 25

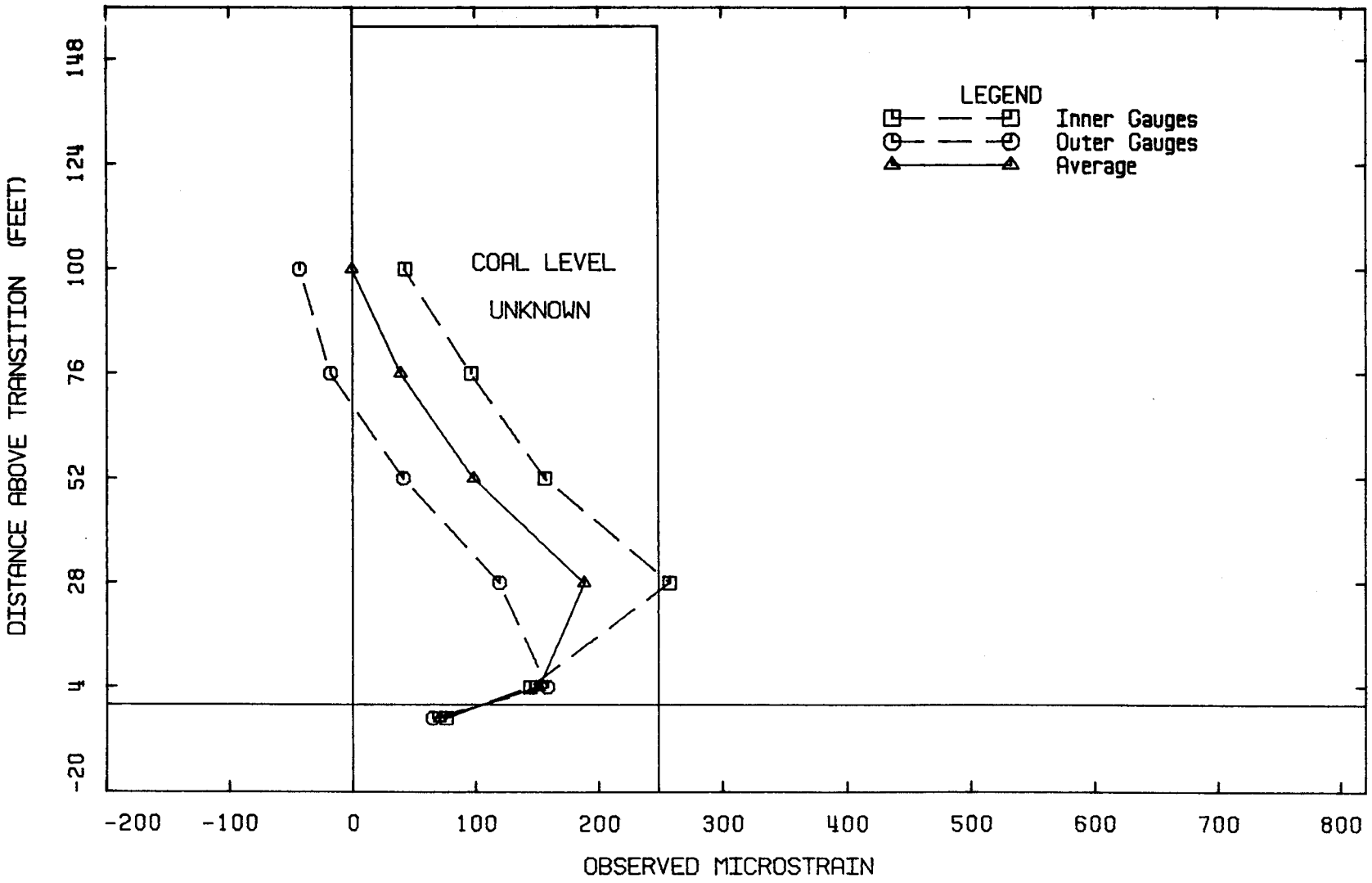

Figure J.B4 Vertical Variation in Hoop Strain - Prior to Run #3 1:00 PM Jan. 25

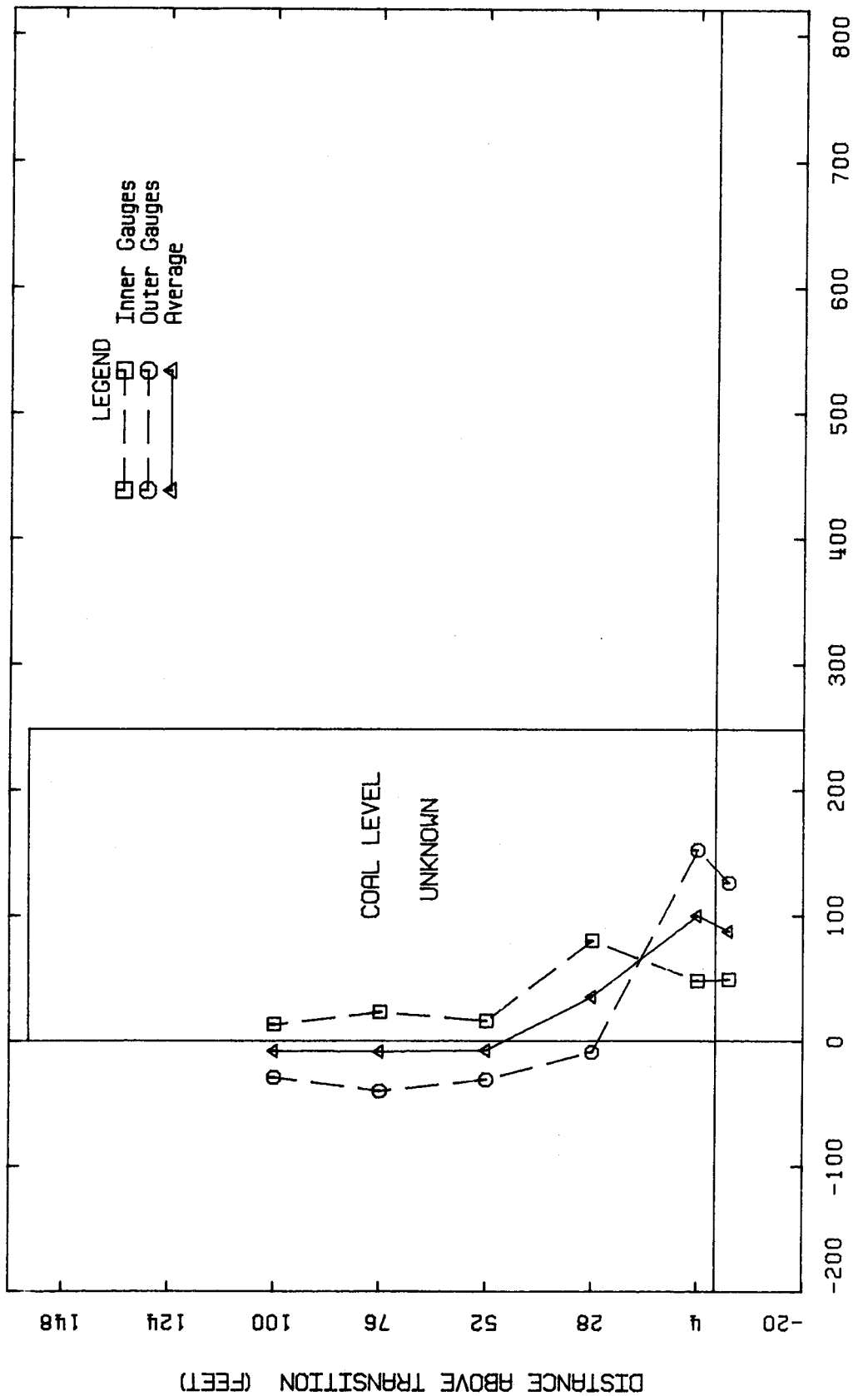

Figure J.B5 Vertical Variation in Hoop Strain - After Run #3

7:30 PM Jan. 25

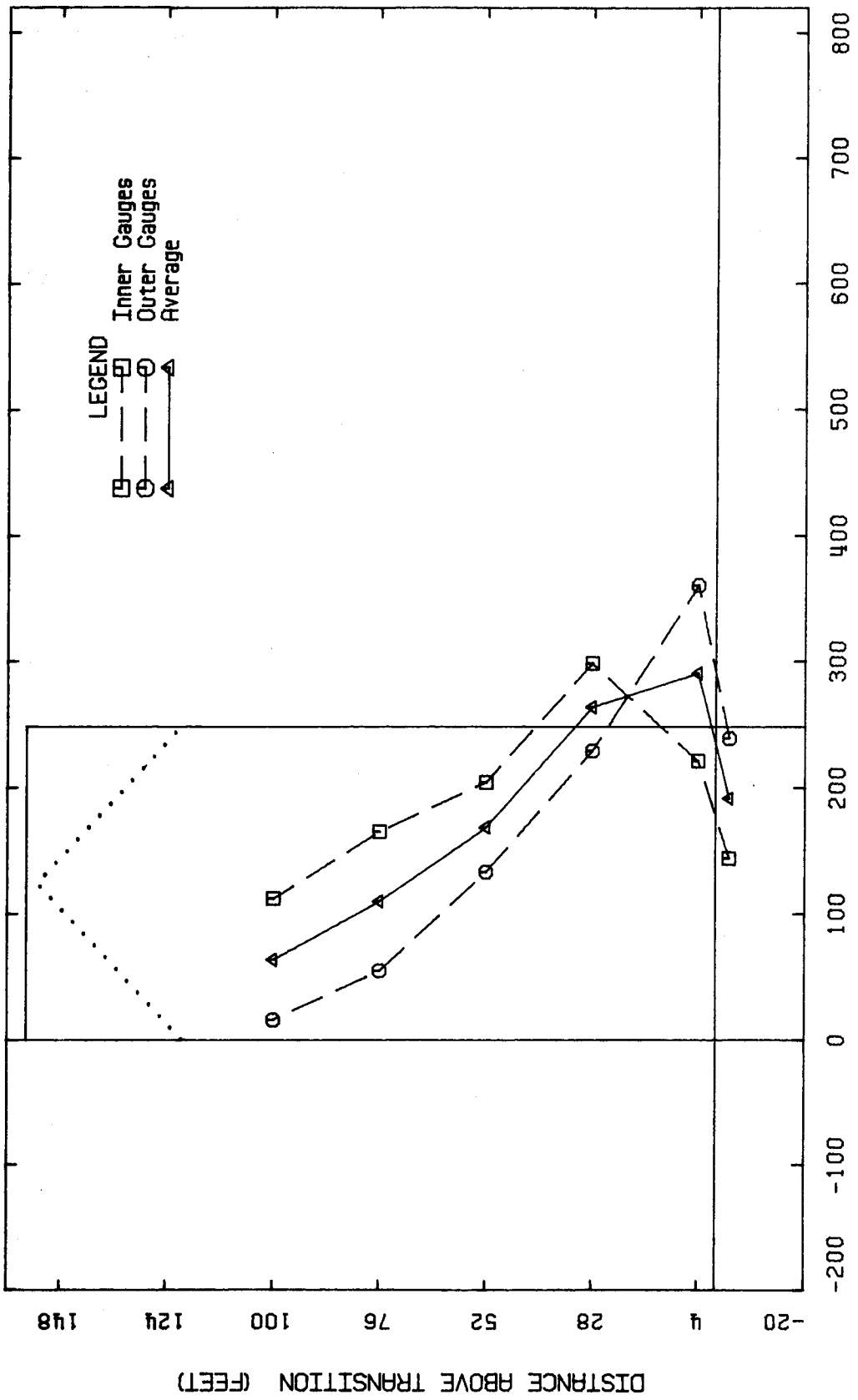

Figure J.B6 Vertical Variation in Hoop Strain - Full - Before Run #4 11:15 AM Jan. 26

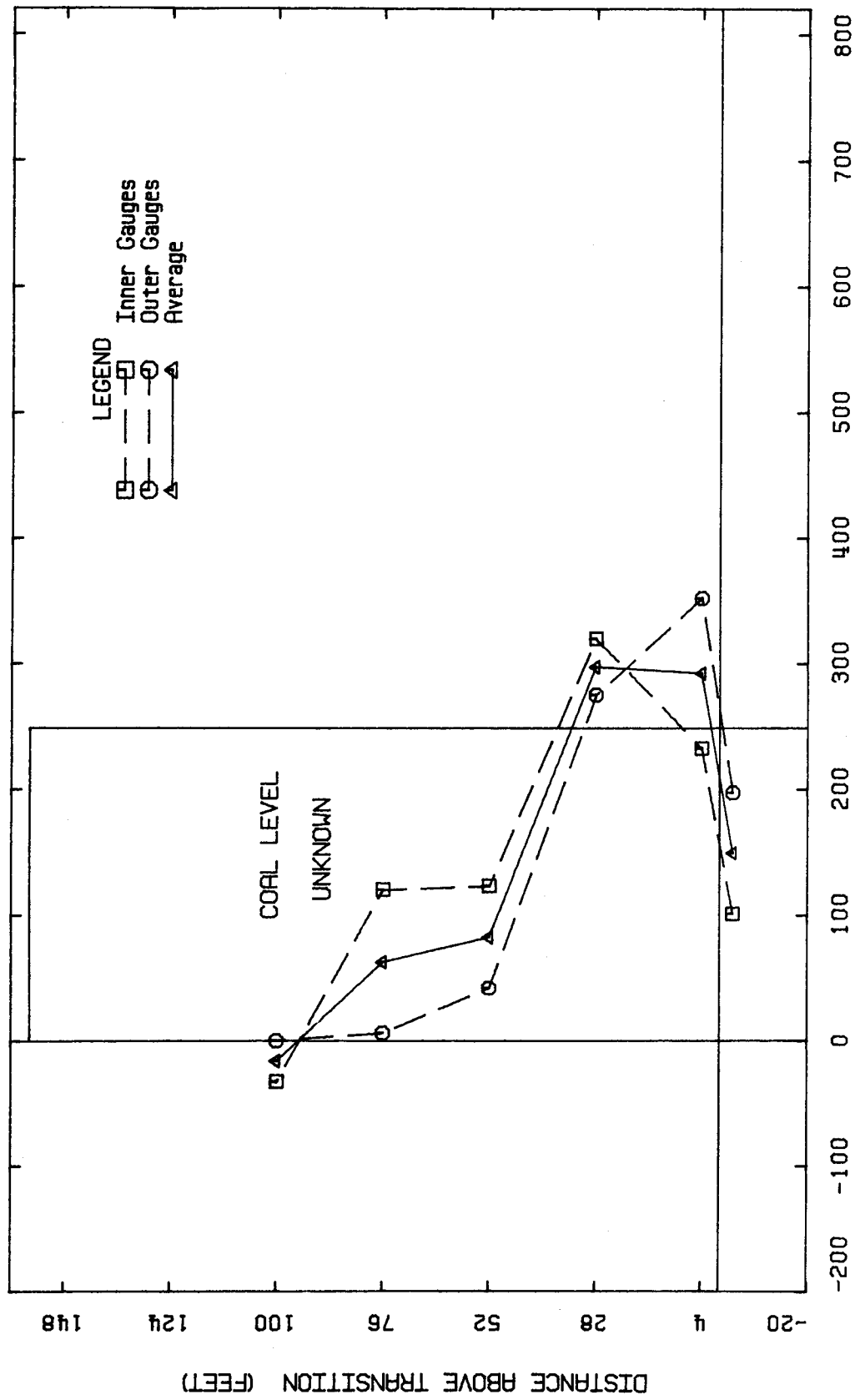

Figure J.B7 Vertical Variation in Hoop Strain - After Run #4

8:30 PM Jan. 27

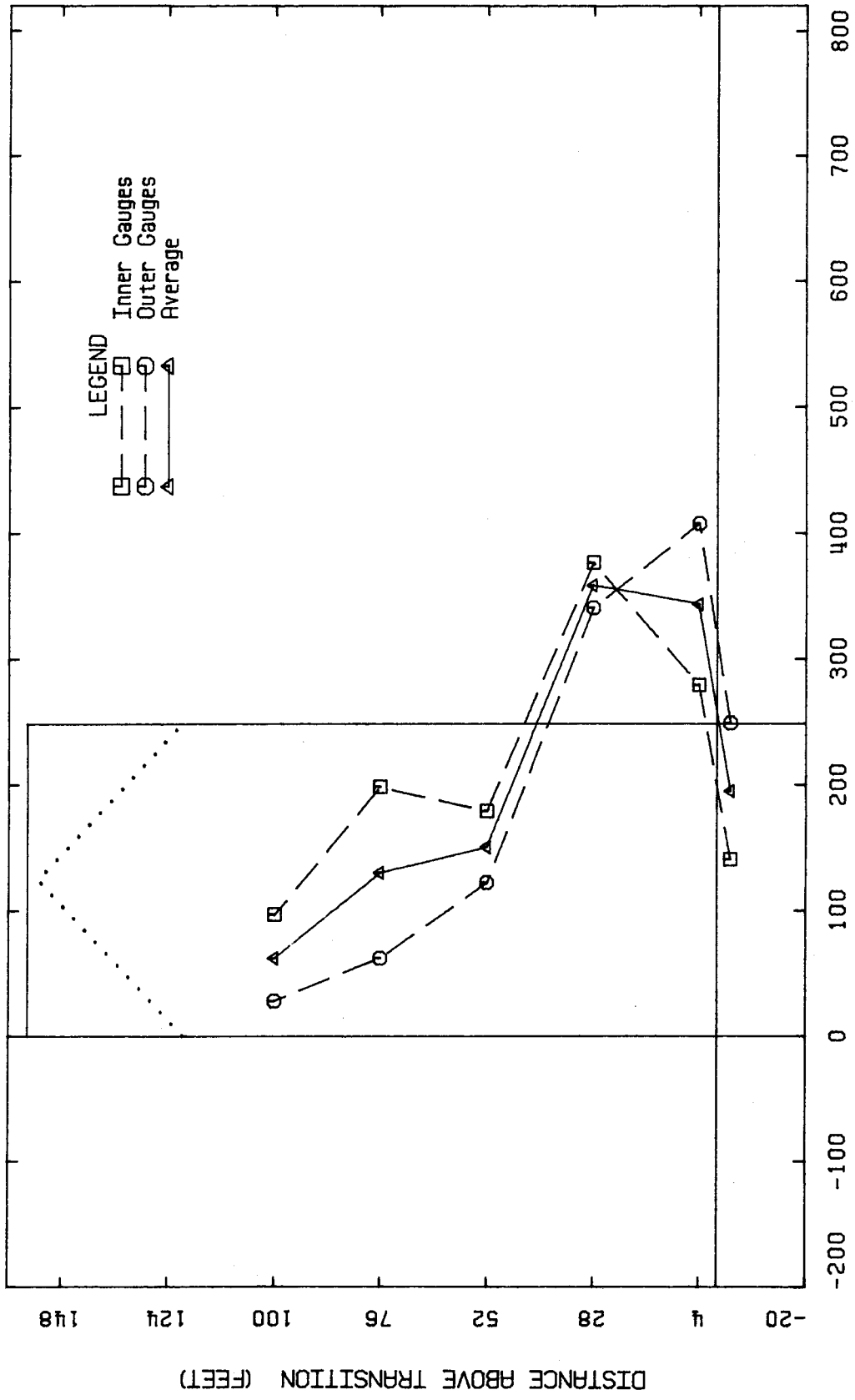

Figure J.B8 Vertical Variation in Hoop Strain - Start of Run #5 7:30 AM Jan. 27

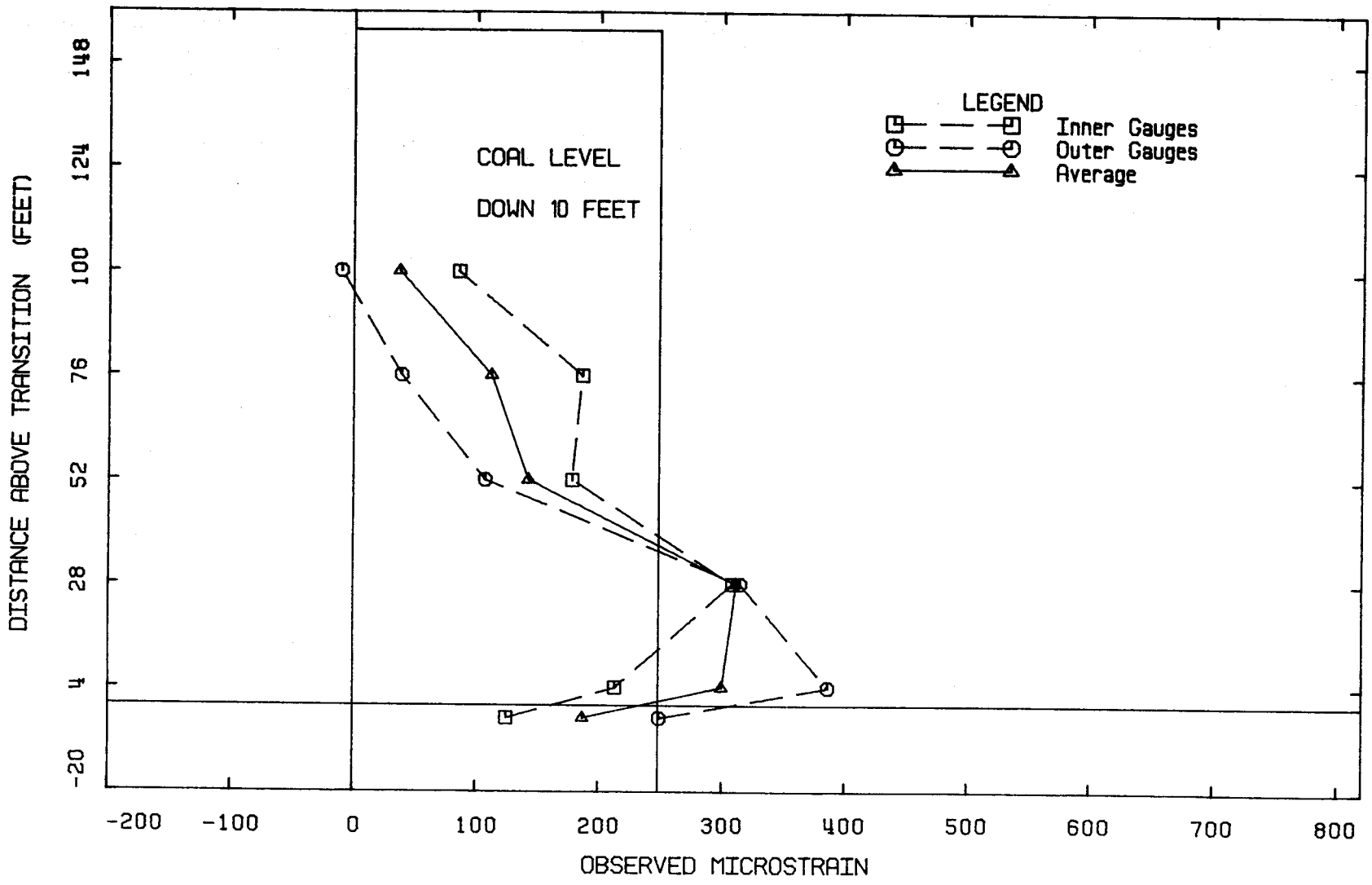

Figure J.B9 Vertical Variation in Hoop Strain - At 15th Car - Run #5

9:45 AM Jan. 27

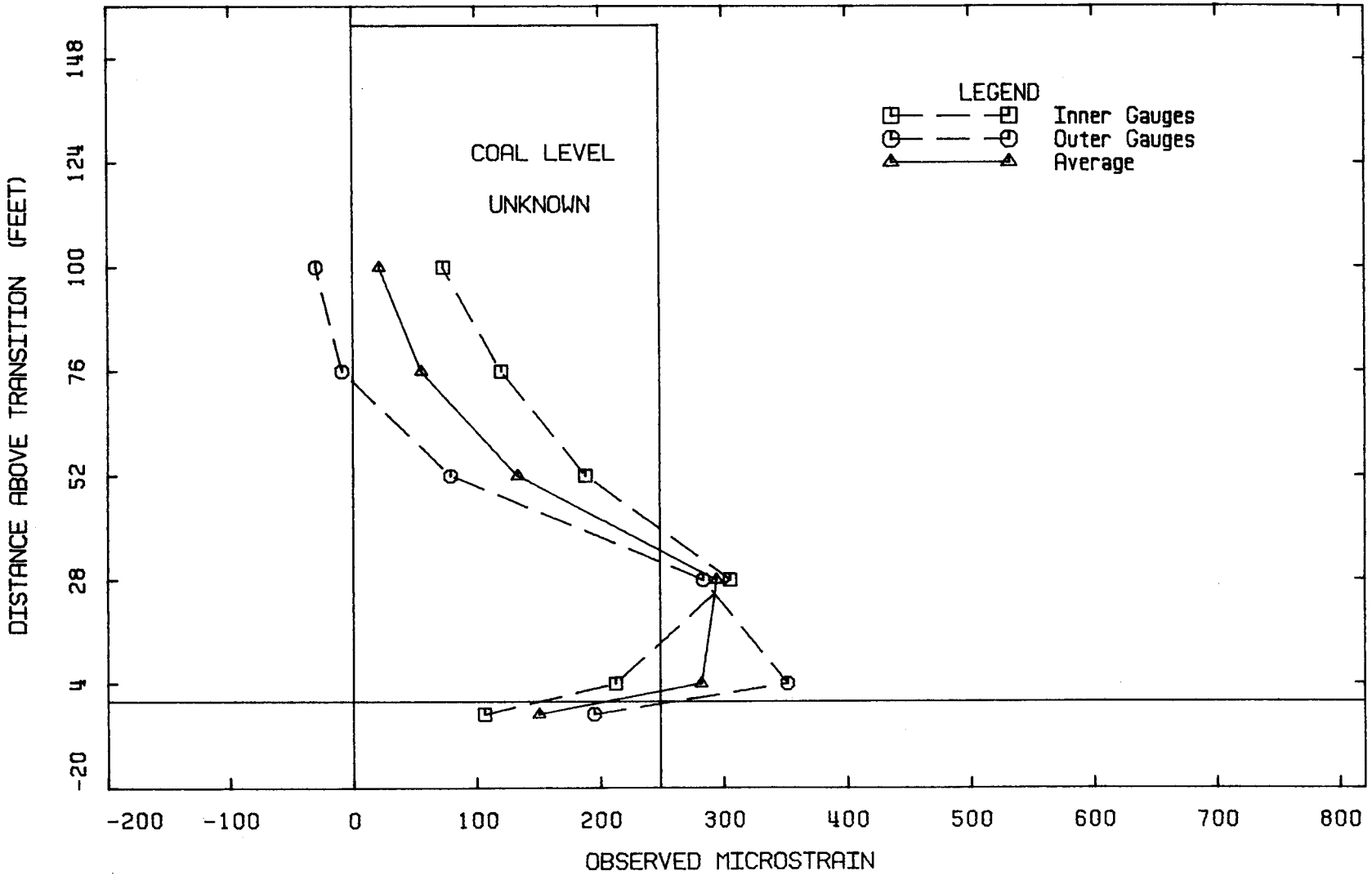

Figure J.B10 Vertical Variation in Hoop Strain - Robot Diesels - Run #5 12:00 AM Jan. 27

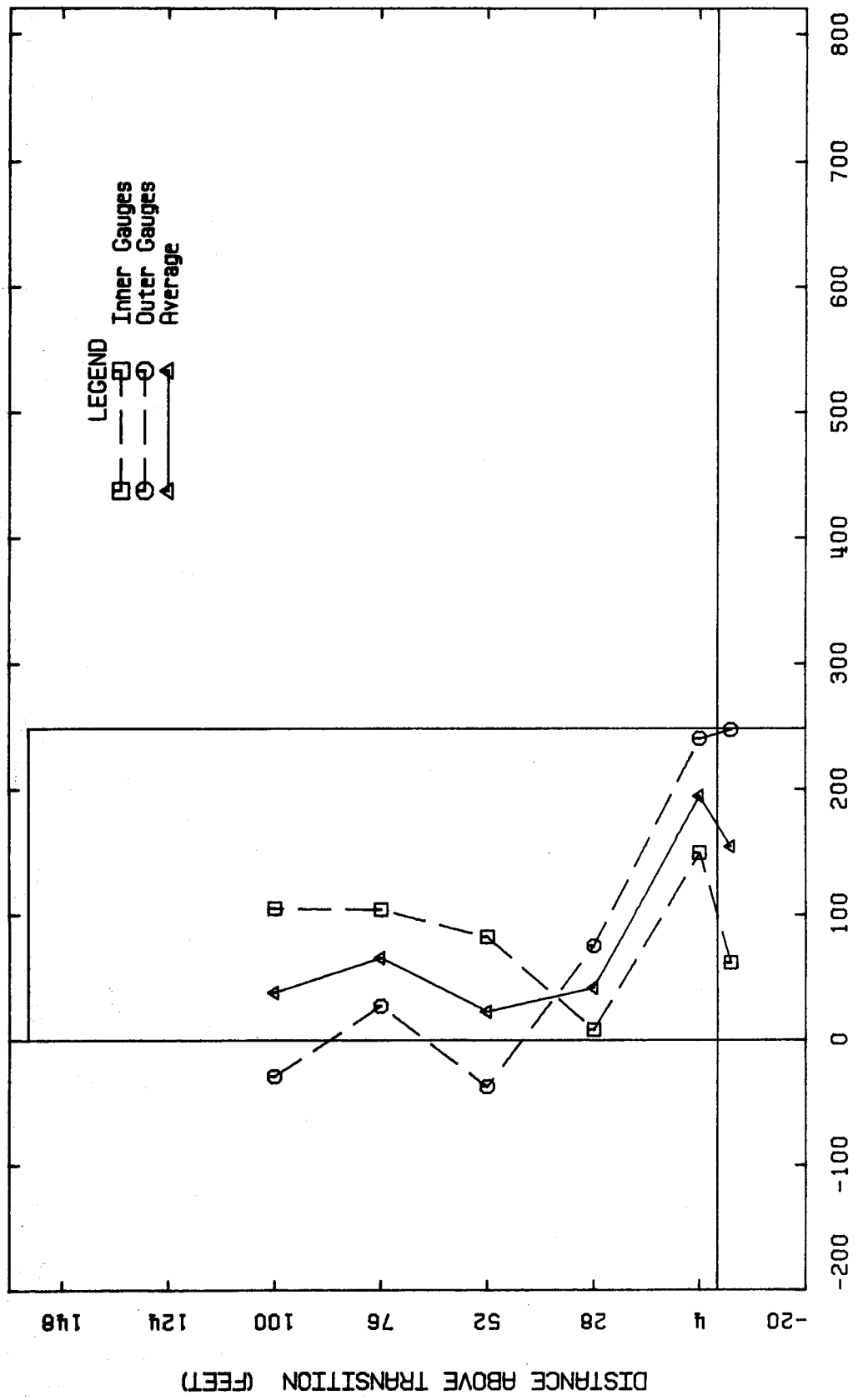

Figure J.B11 Vertical Variation in Hoop Strain - June-January References Compared

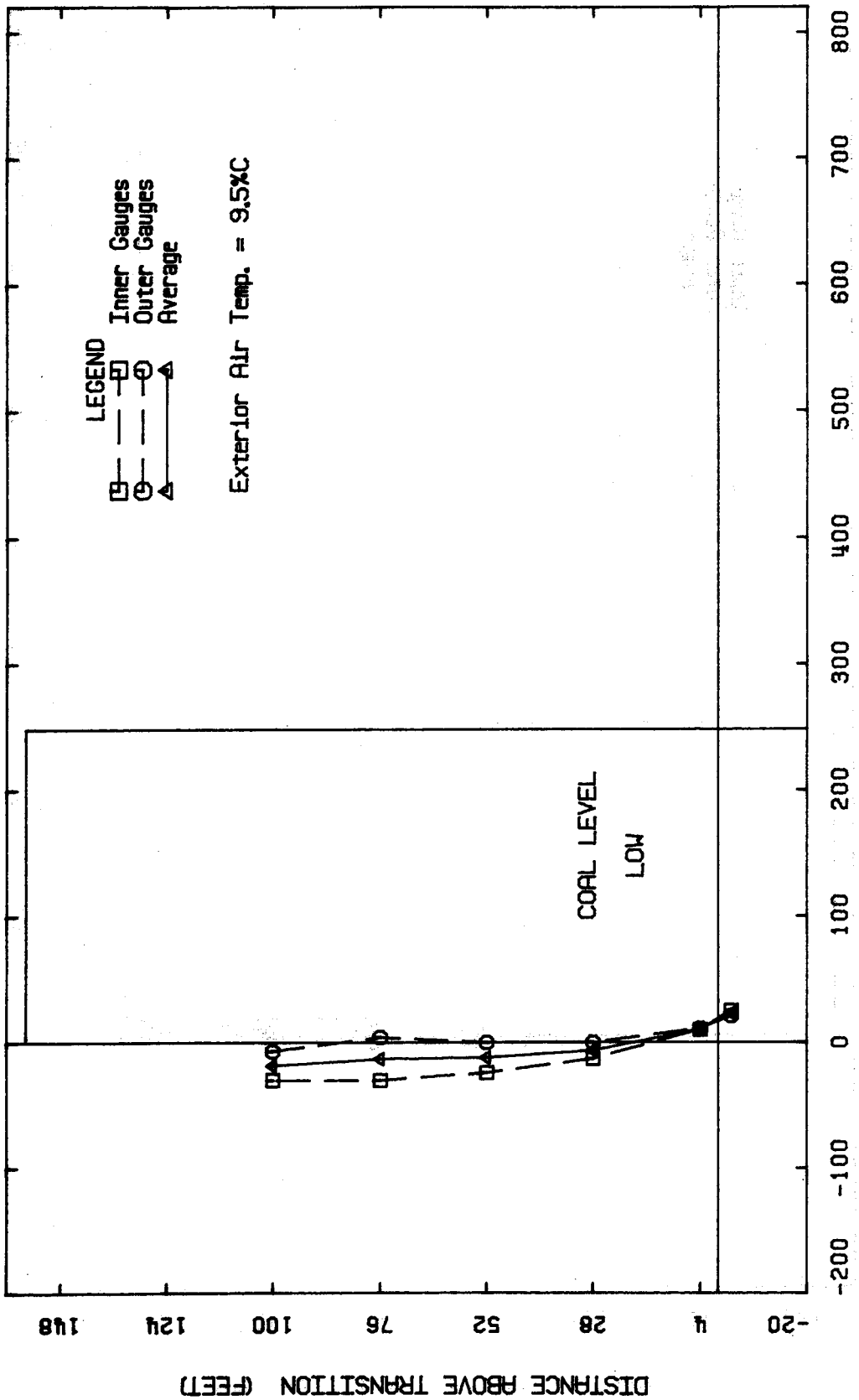

Figure J.C1 Vertical Variation in Hoop Strain - Silo < 1/3 Full 12:00 PM June 15

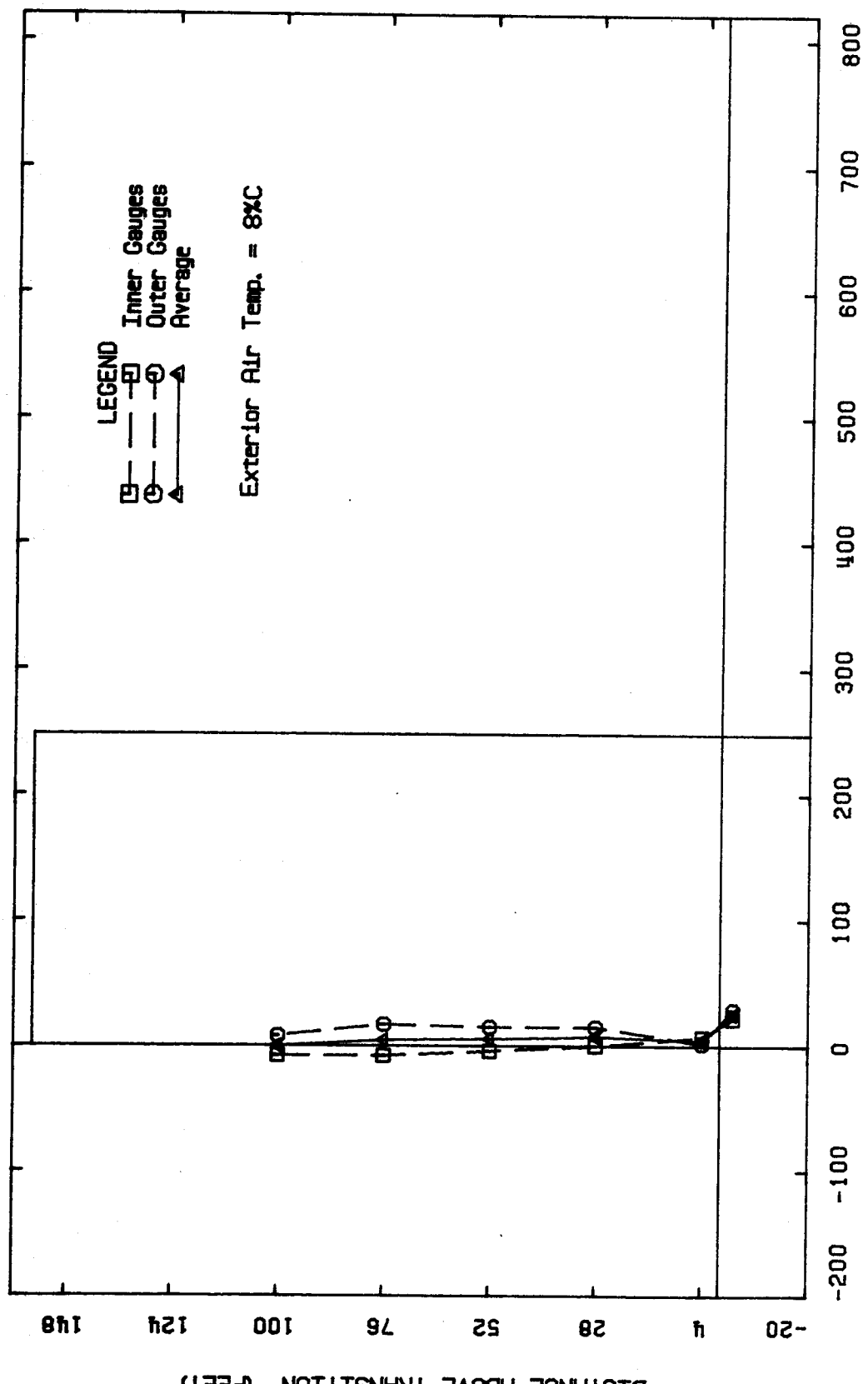

Figure J.C2 Vertical Variation in Hoop Strain - Silo Empty

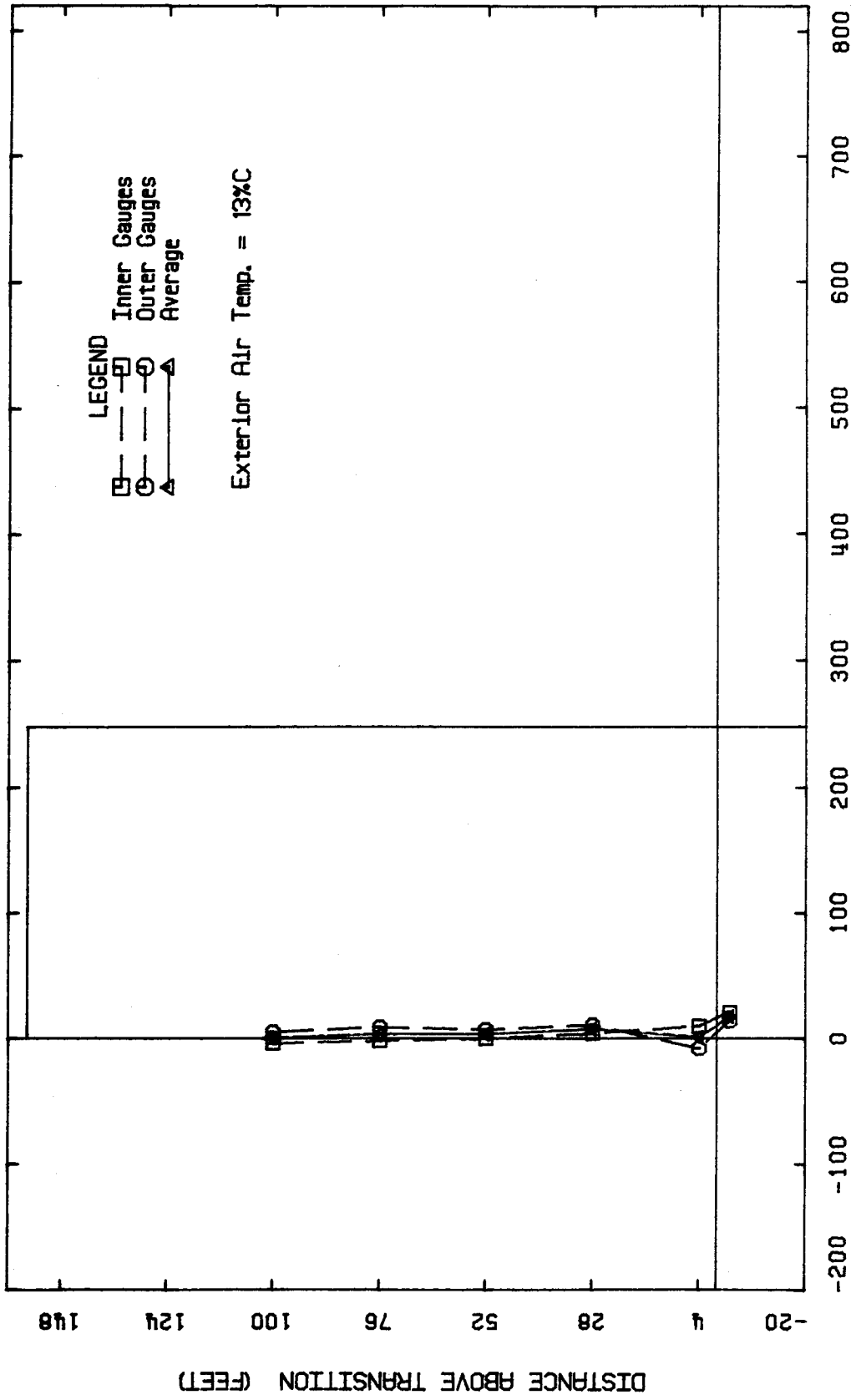

Figure J.C3 Vertical Variation in Hoop Strain - Silo Empty

1:00 PM June 16

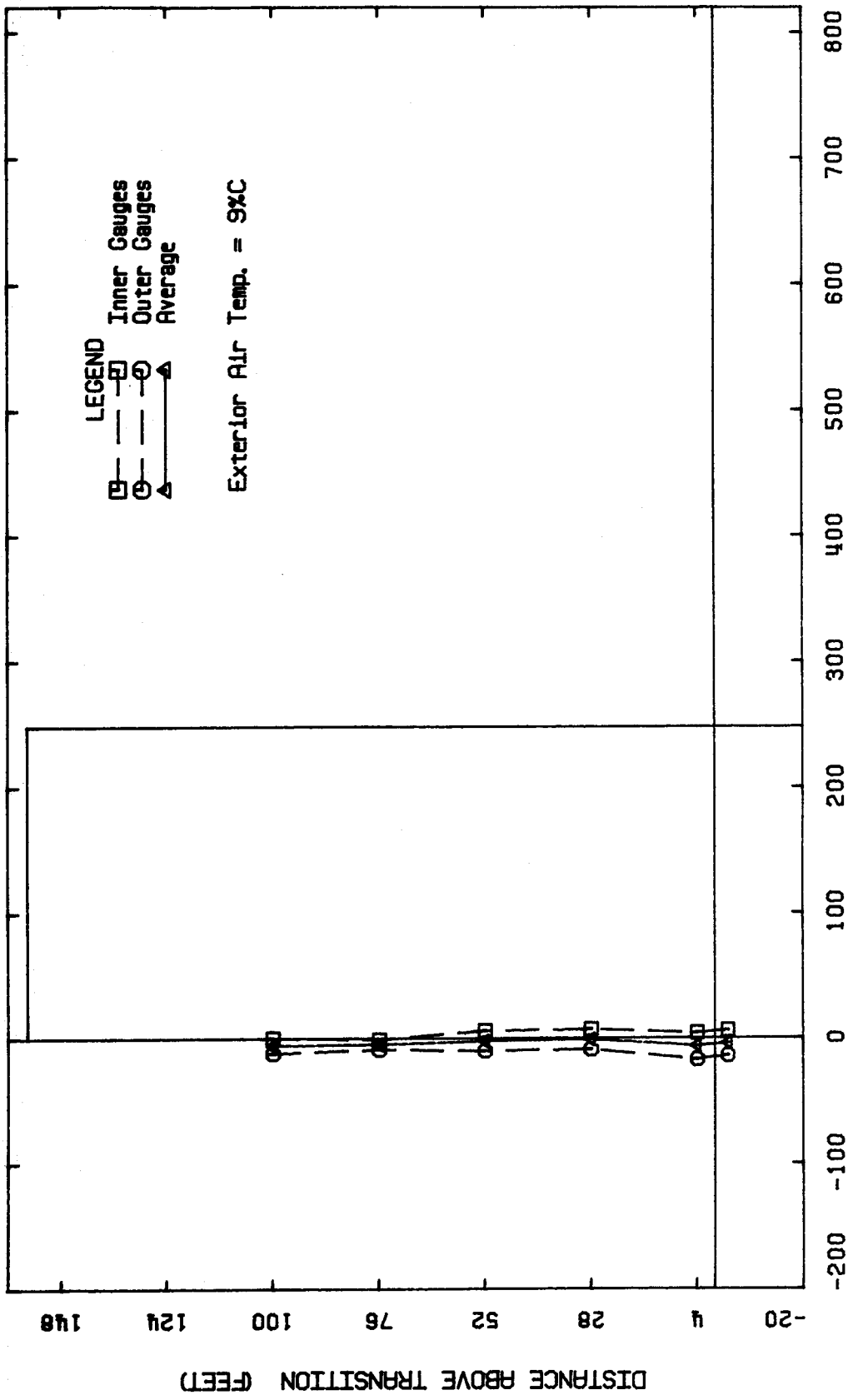

Figure J.C4 Vertical Variation in Hoop Strain - Silo Empty

10:15 PM June 16

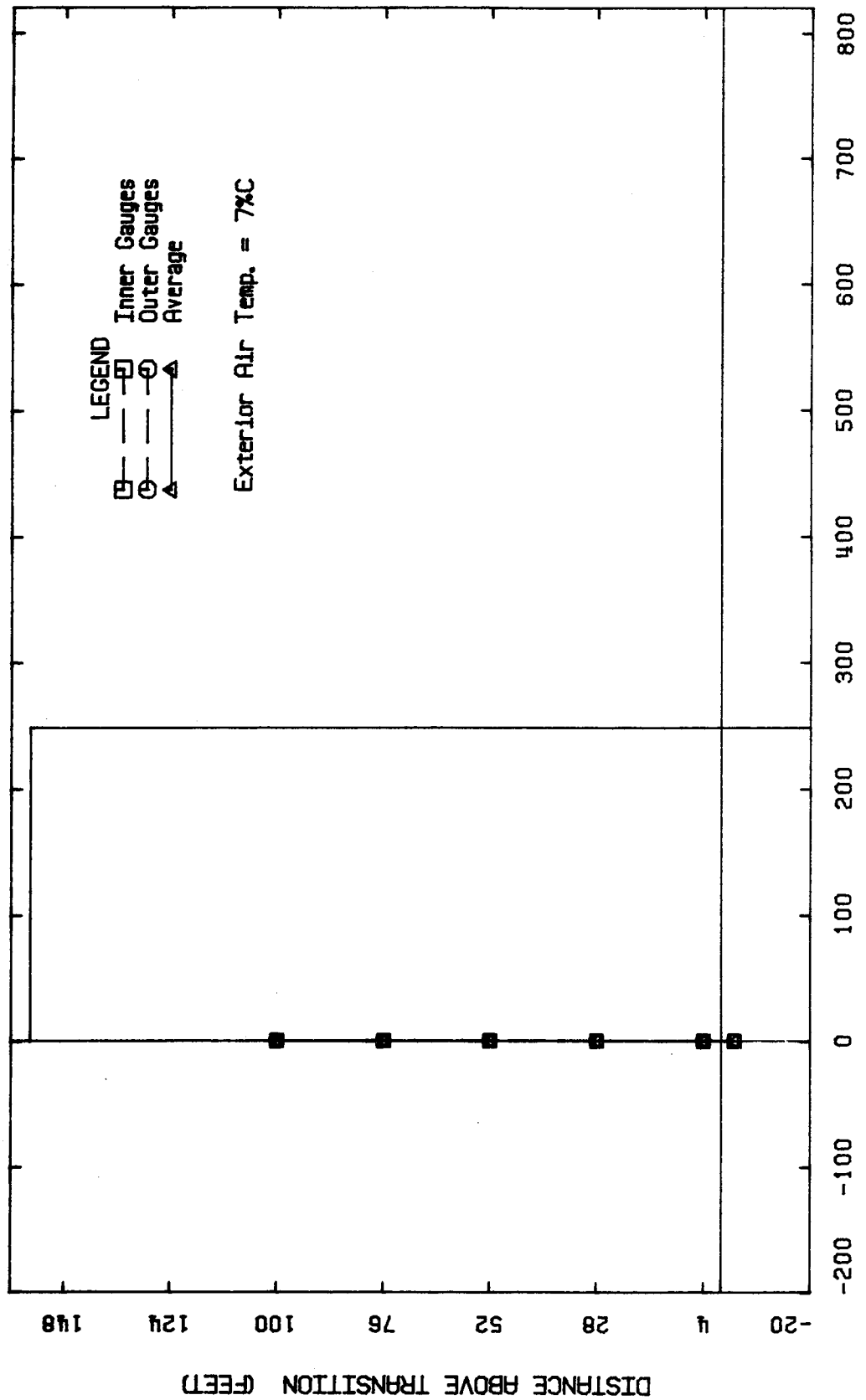

Figure J.C5 Vertical Variation in Hoop Strain - Reference Reading (zero strains) 2:00 PM June 16

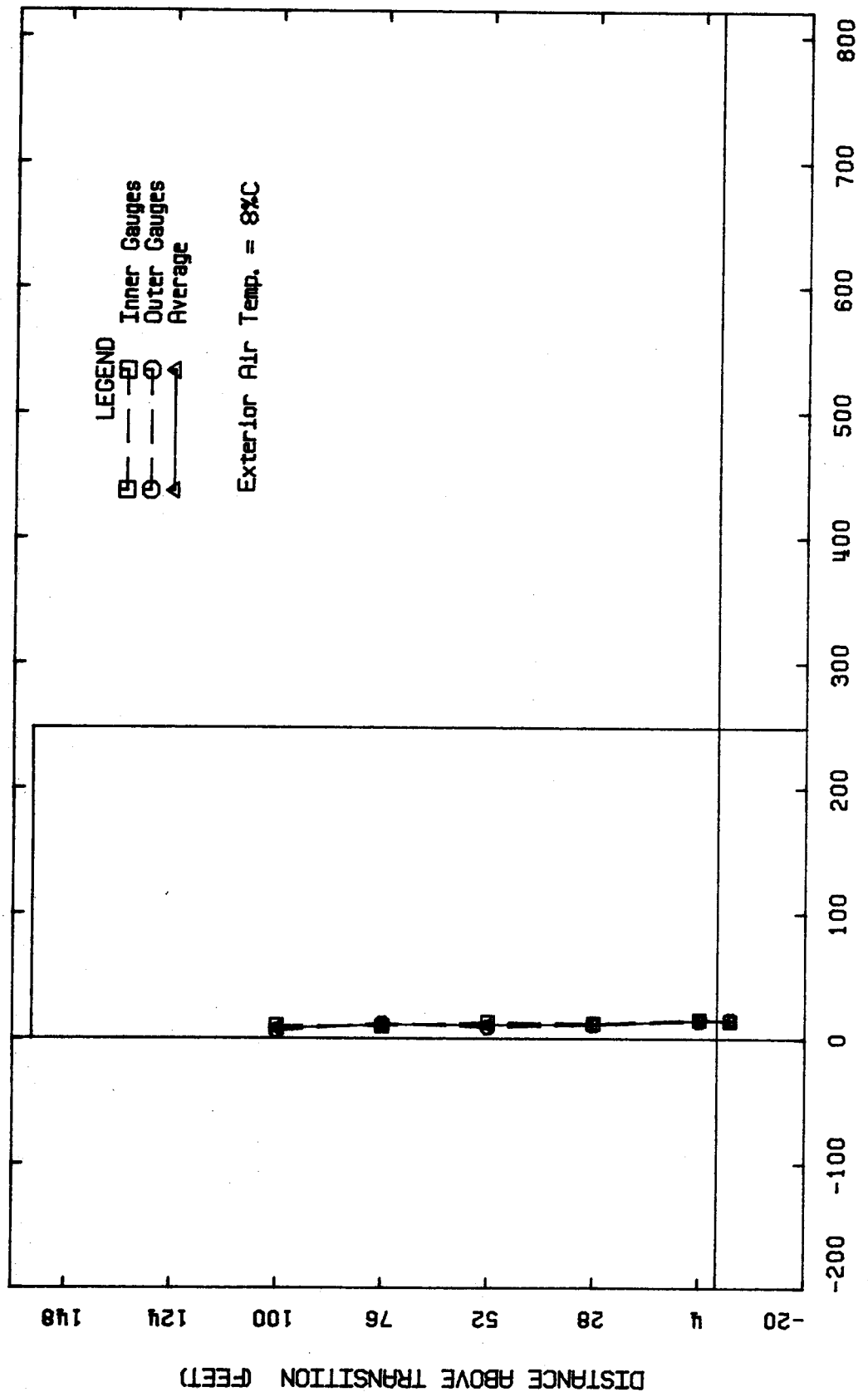

Figure J.C6 Vertical Variation in Hoop Strain - Silo Empty

1:15 PM June 17

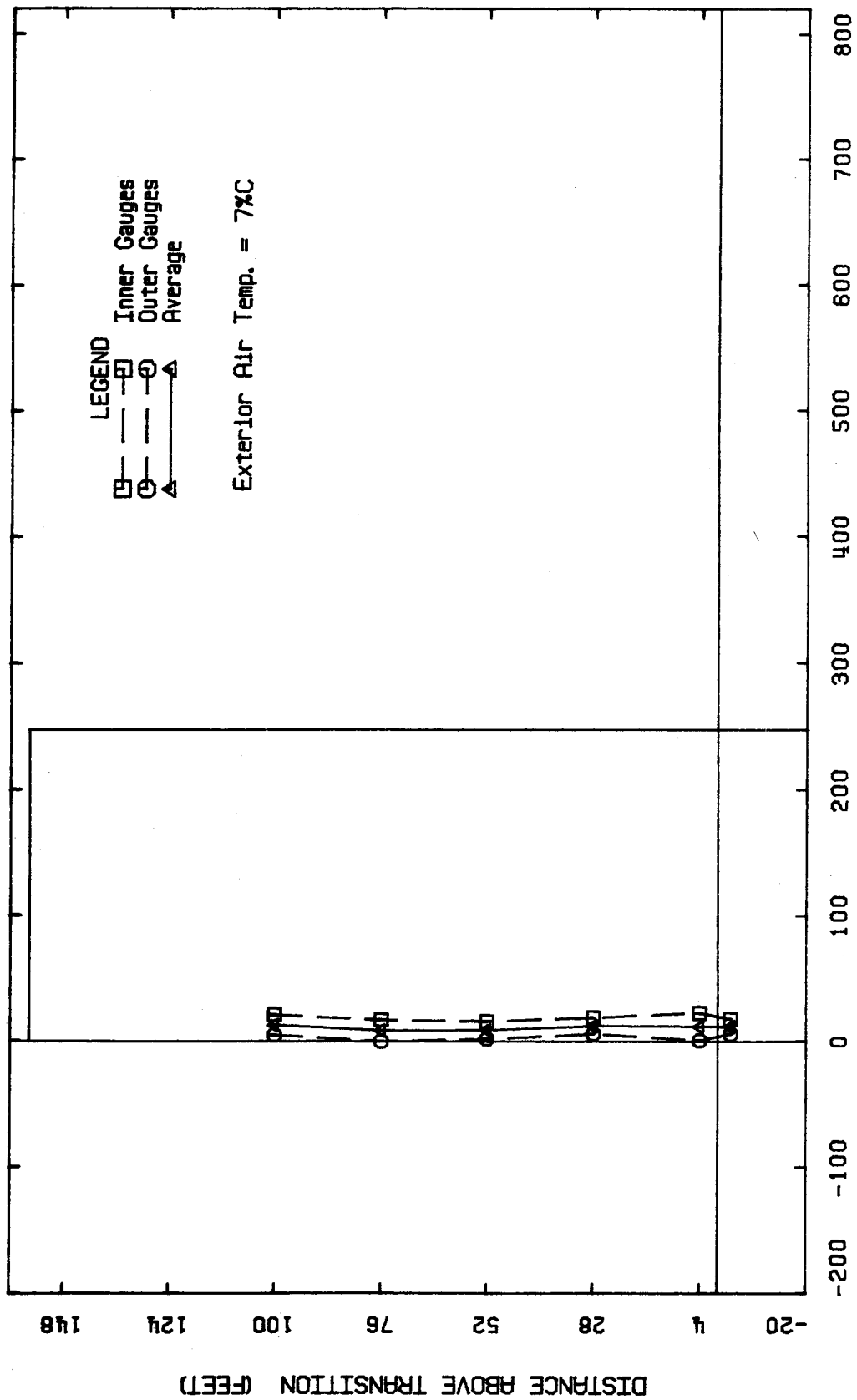

Figure J.C7 Vertical Variation in Hoop Strain - Silo Empty 4:00 PM June 17

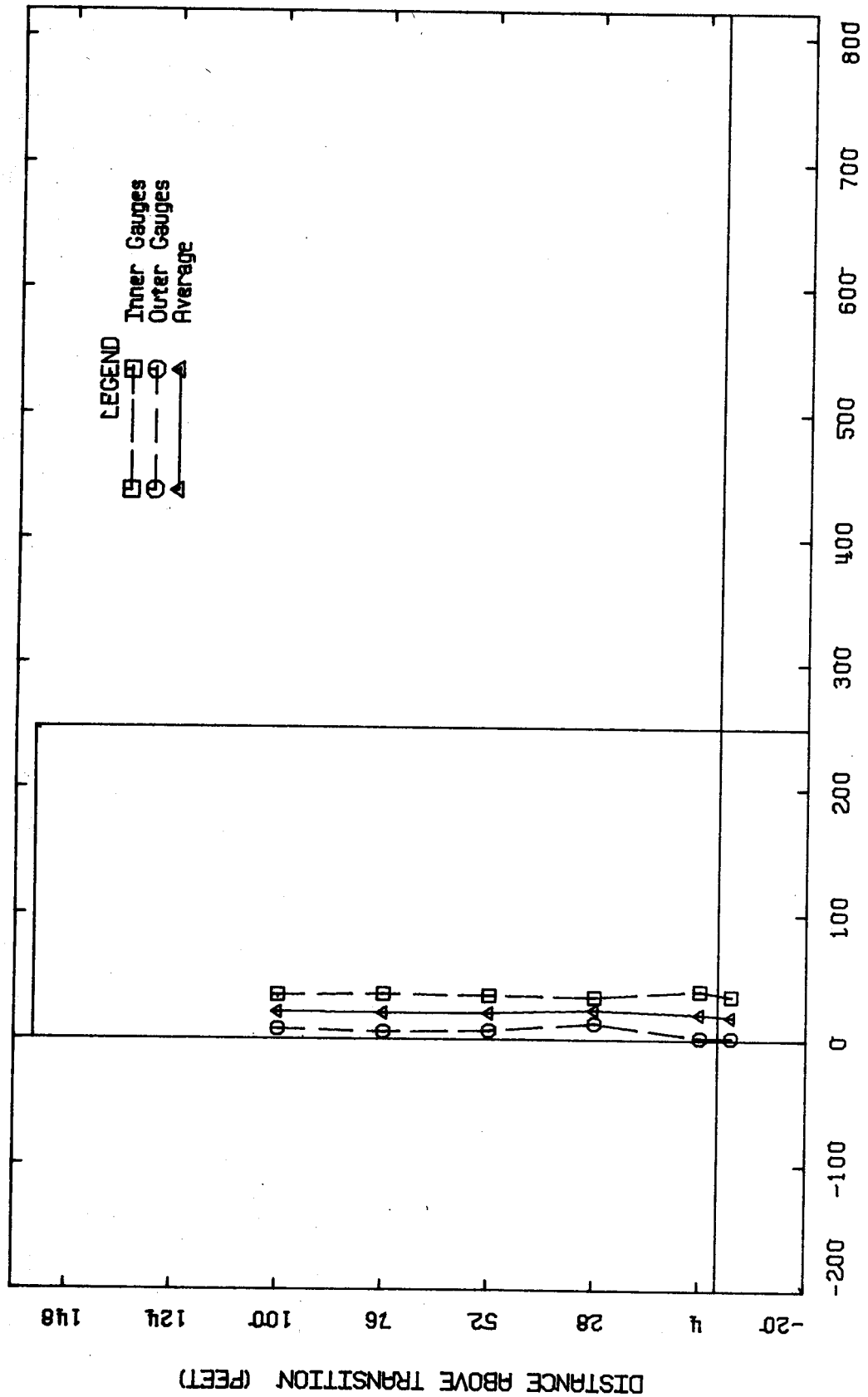

Figure J.C8 Vertical Variation in Hoop Strain - Empty - Start of Filling 7:00 PM June 17

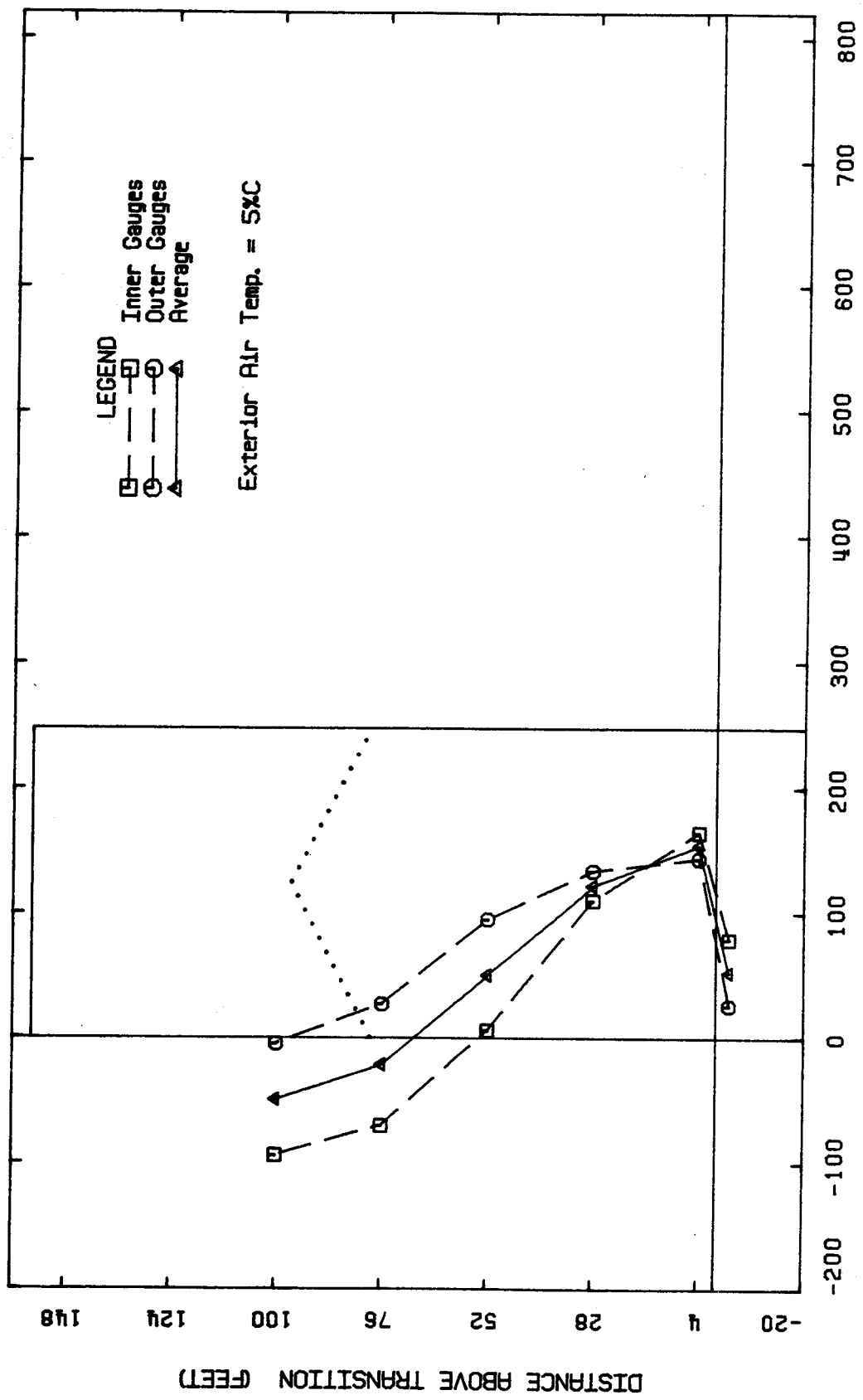

Figure J.C9 Vertical Variation in Hoop Strain - Start of Run #6A 8:00 PM June 18

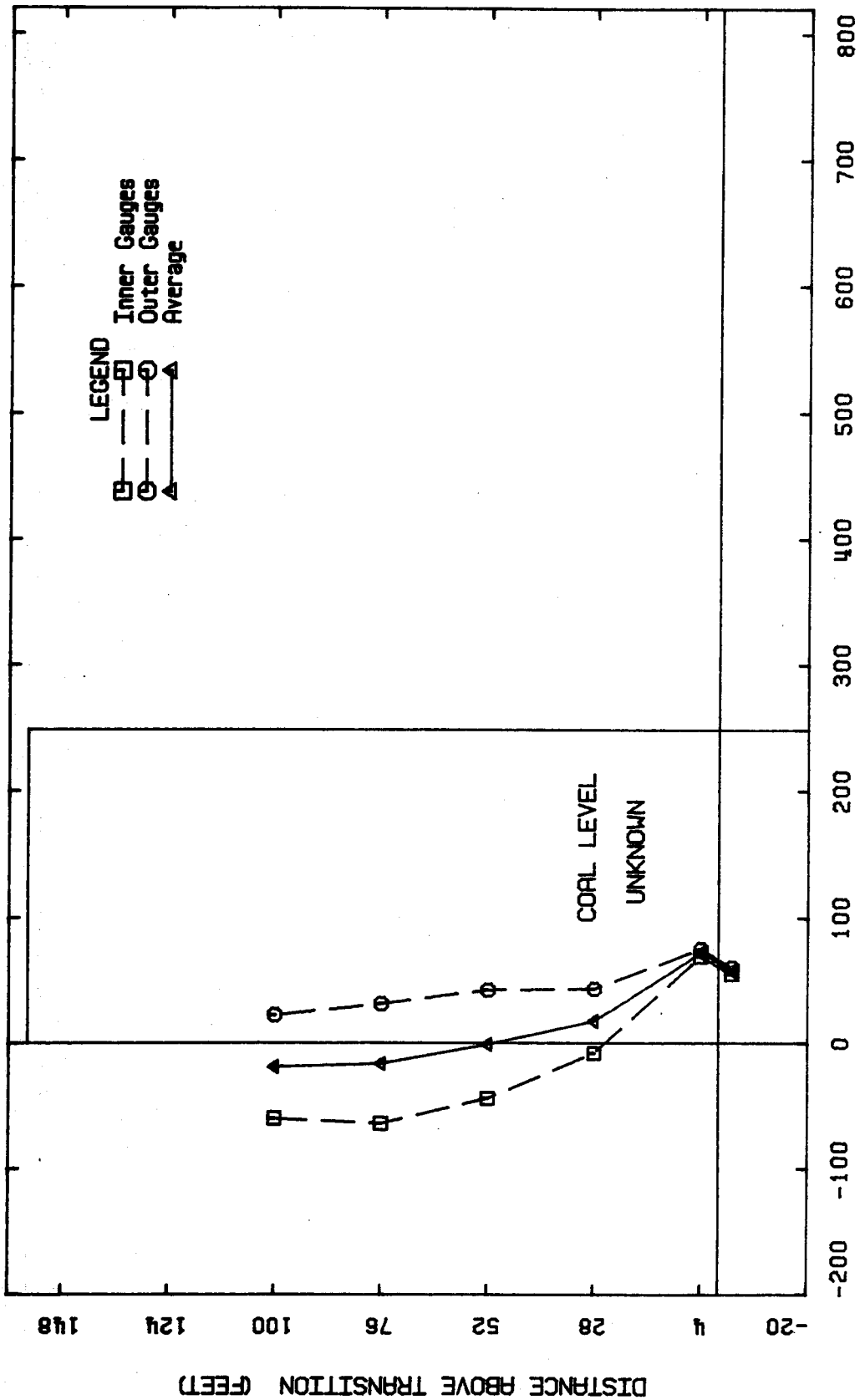

Figure J.C10 Vertical Variation in Hoop Strain - End of Run #6A

11:15 PM June 18

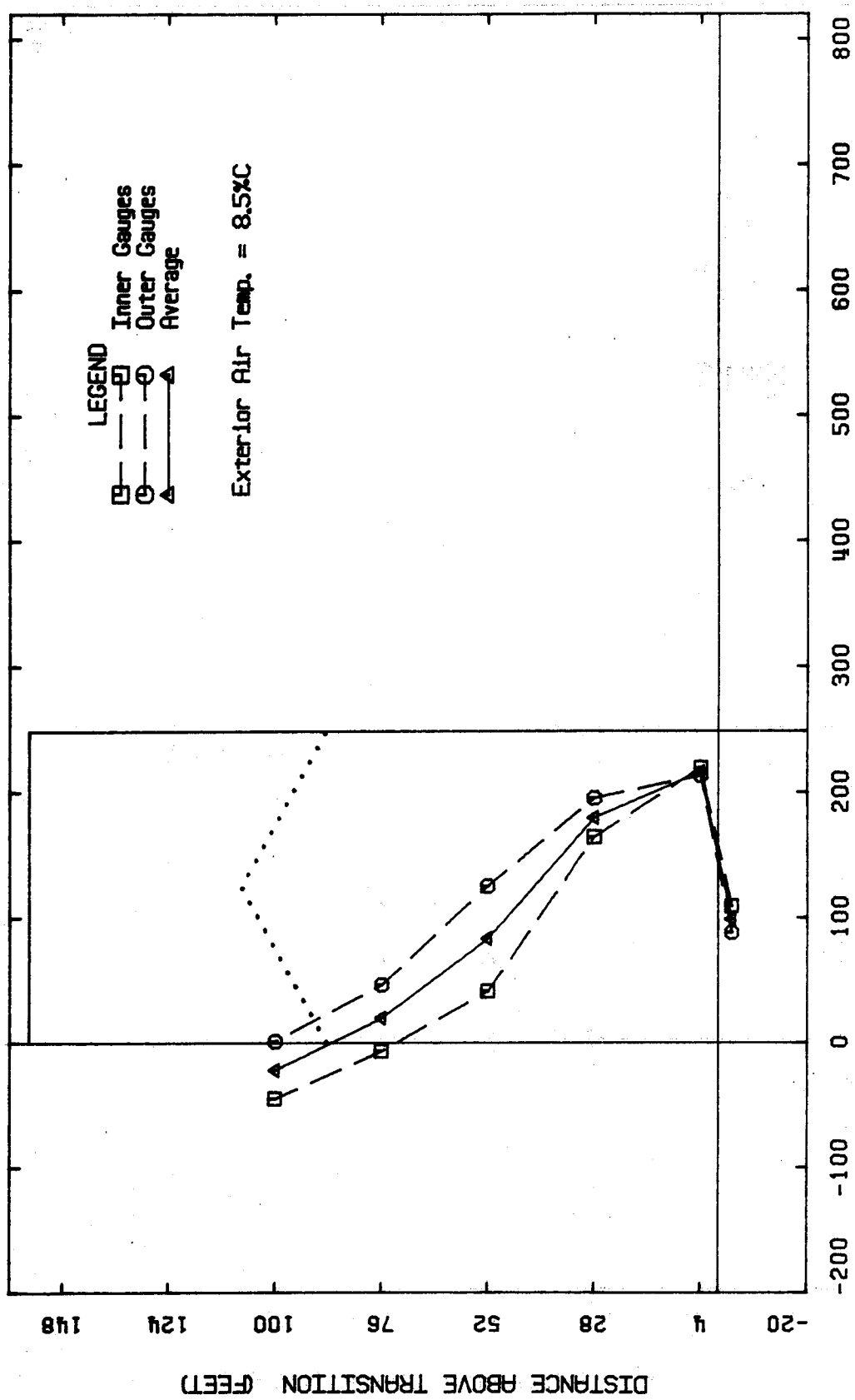

Figure J.C13 Vertical Variation in Hoop Strain - > 2/3 Full - Charging 2:00 PM June 19

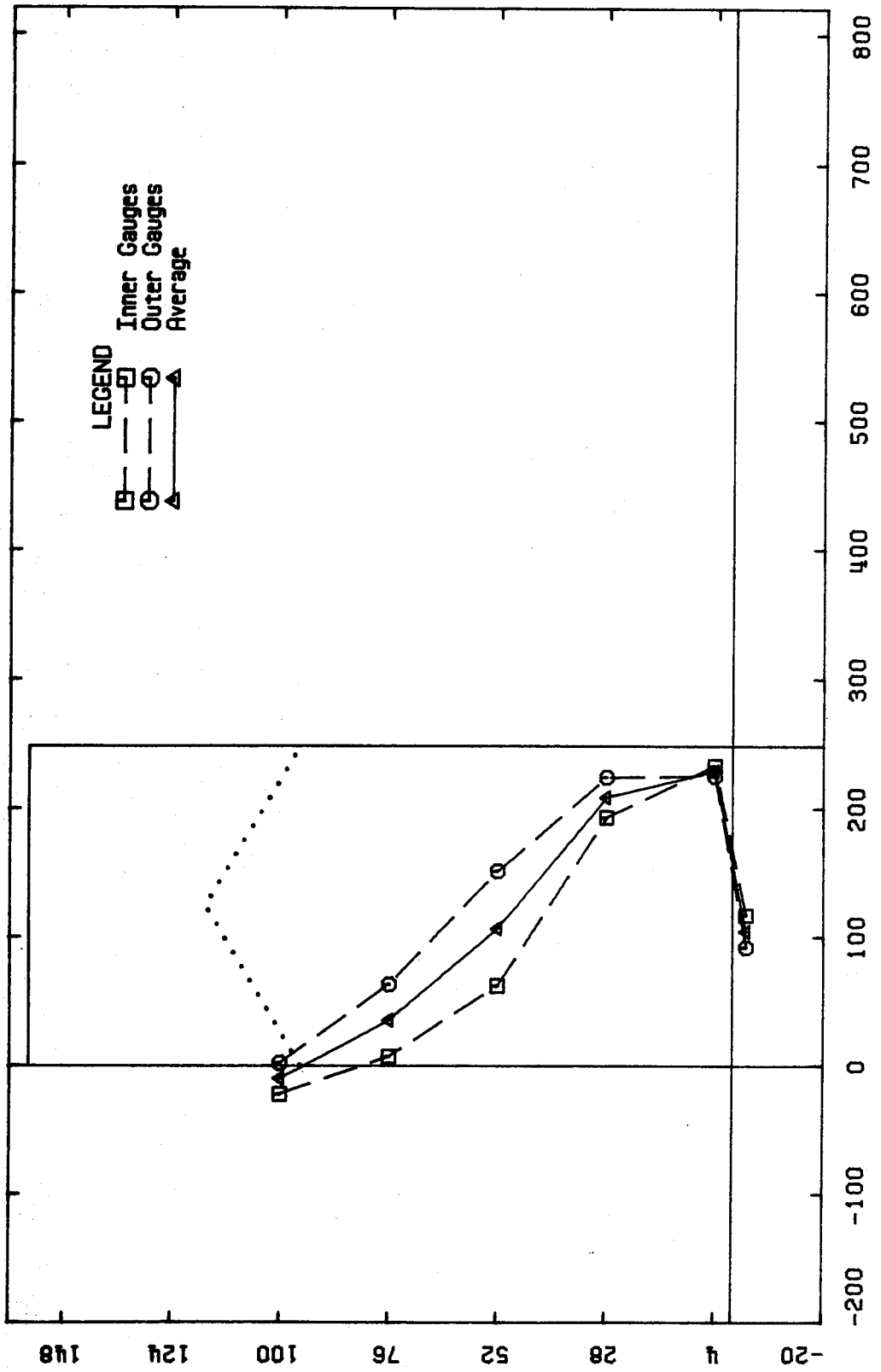

Figure J.C14 Vertical Variation in Hoop Strain - > 2/3 Full - Charging 3:00 PM June 19

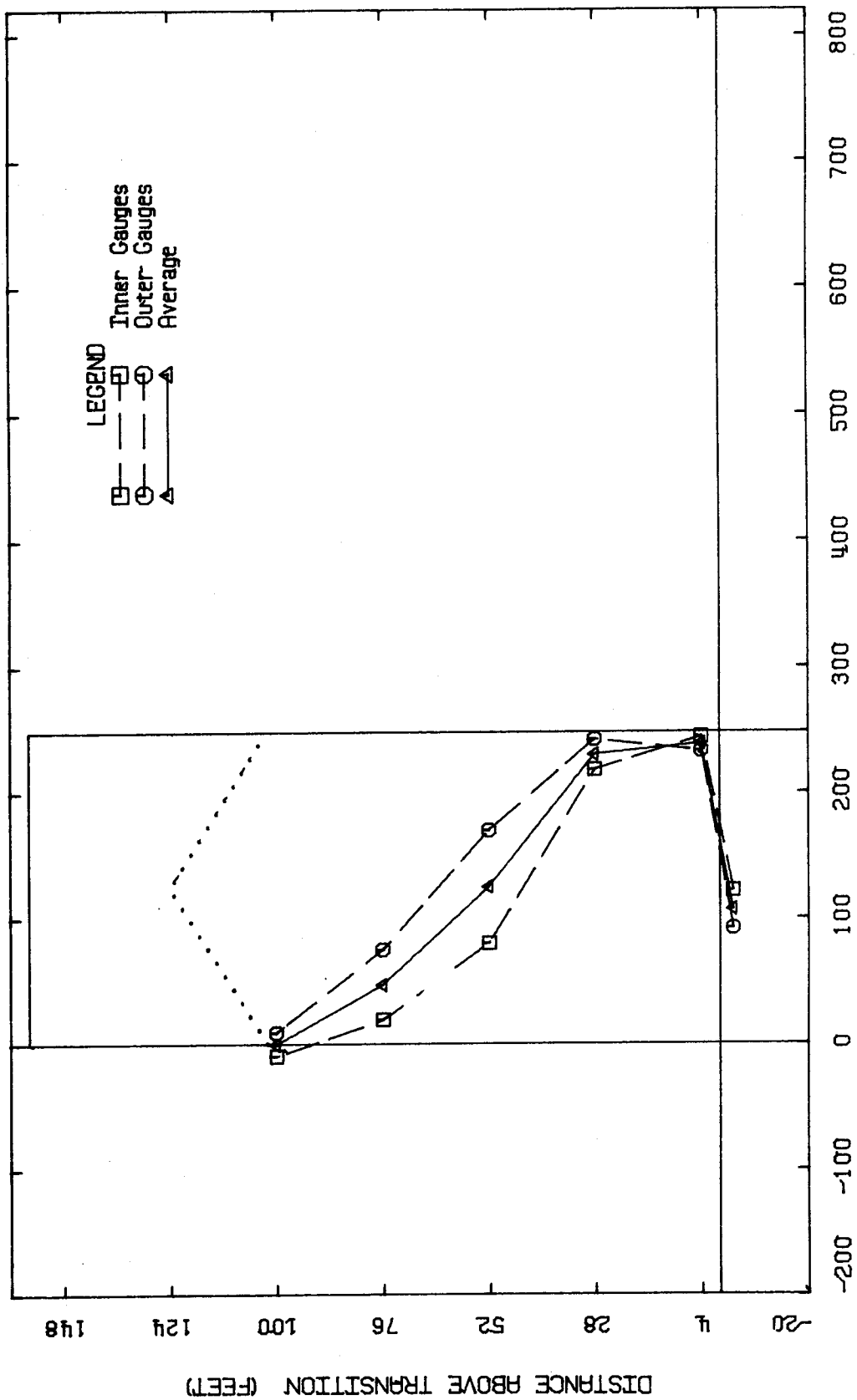

Figure J.C15 Vertical Variation in Hoop Strain - Prior to M Car Drawdown (Run #6B) 4:00 PM June 19

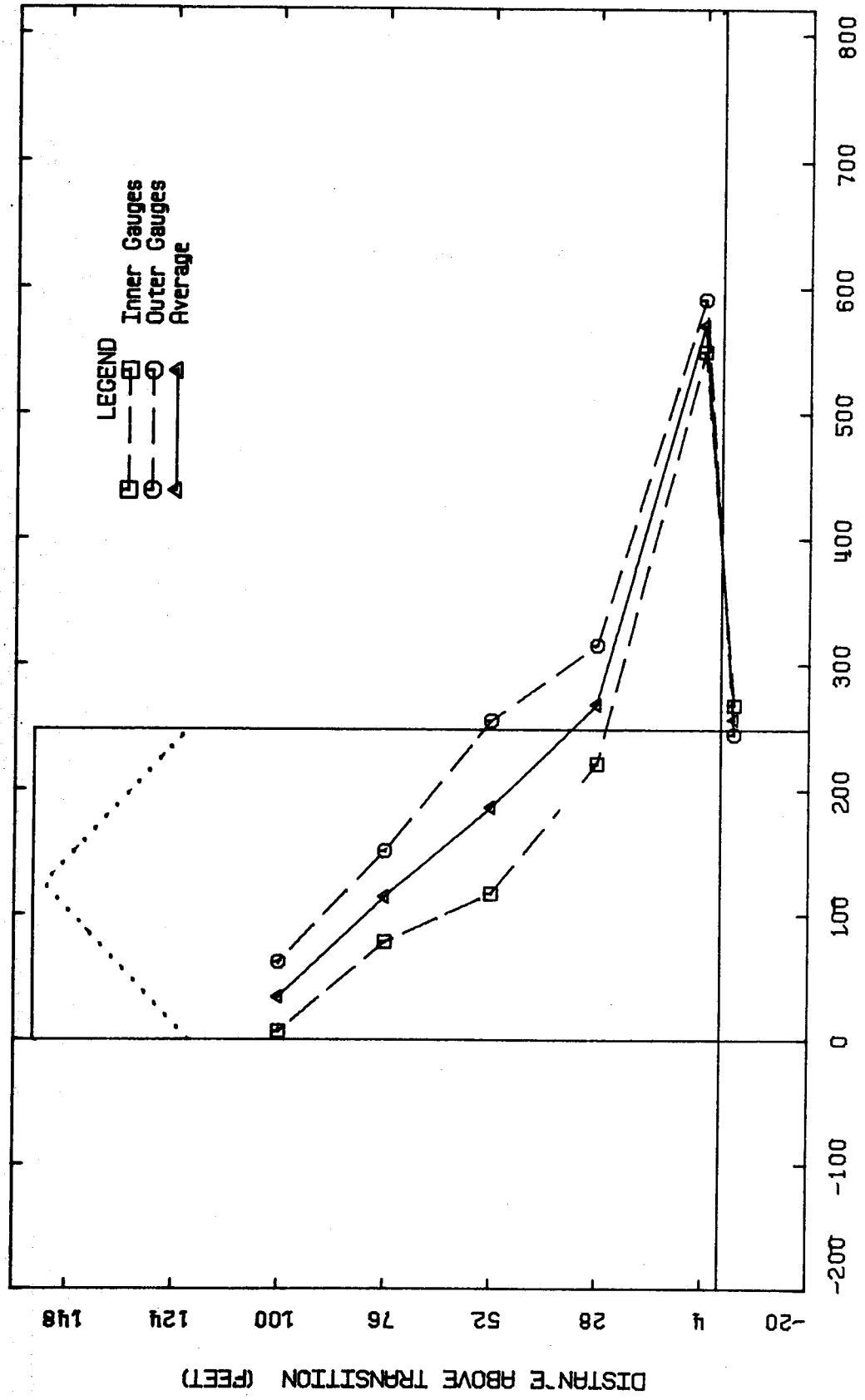

Figure J.C16 Vertical Variation in Hoop Strain - Silo Full After 11 Car Drawdown 11:30 PM June 19

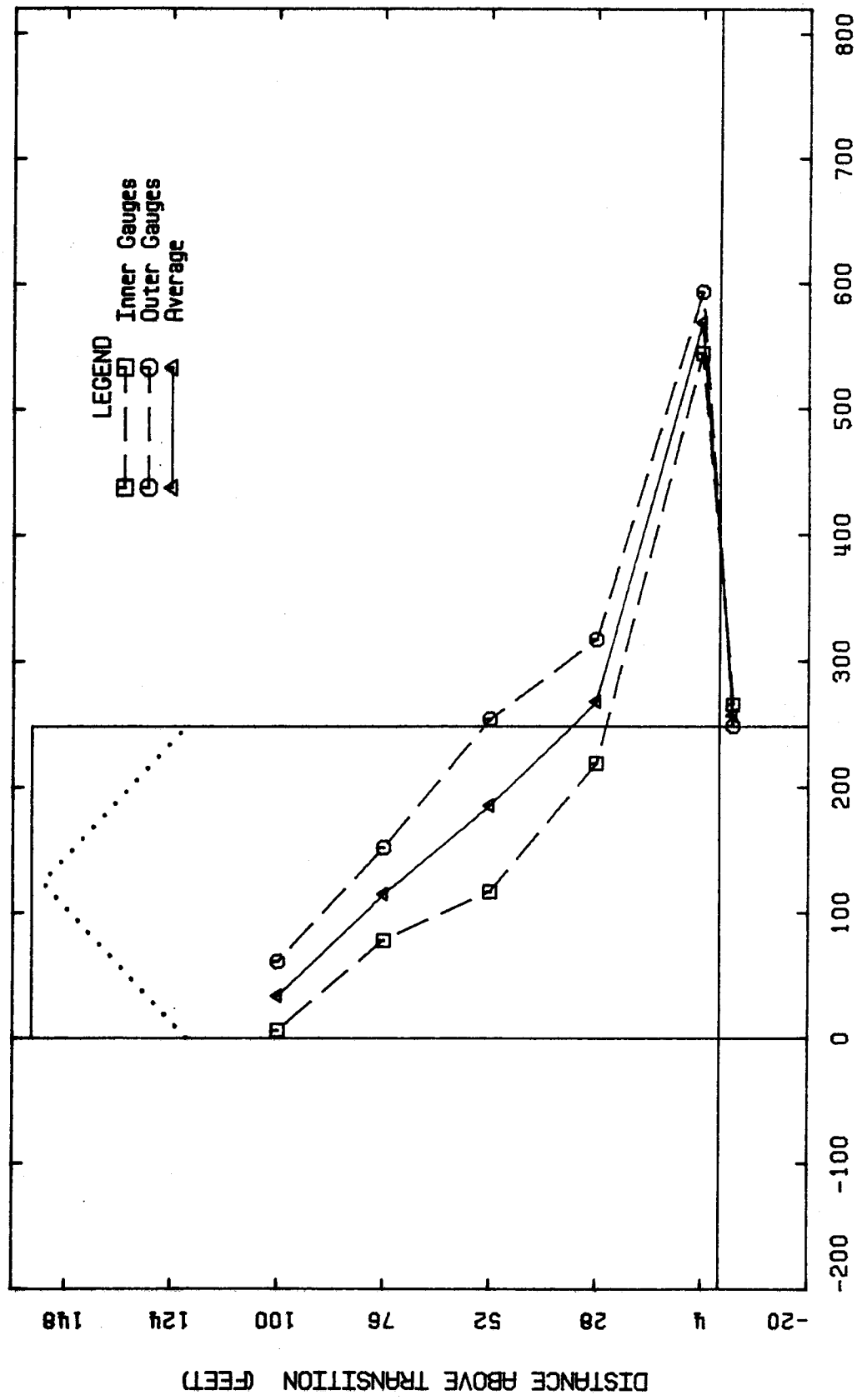

Figure J.C17 Vertical Variation in Hoop Strain - Silo Full

1:30 AM June 20

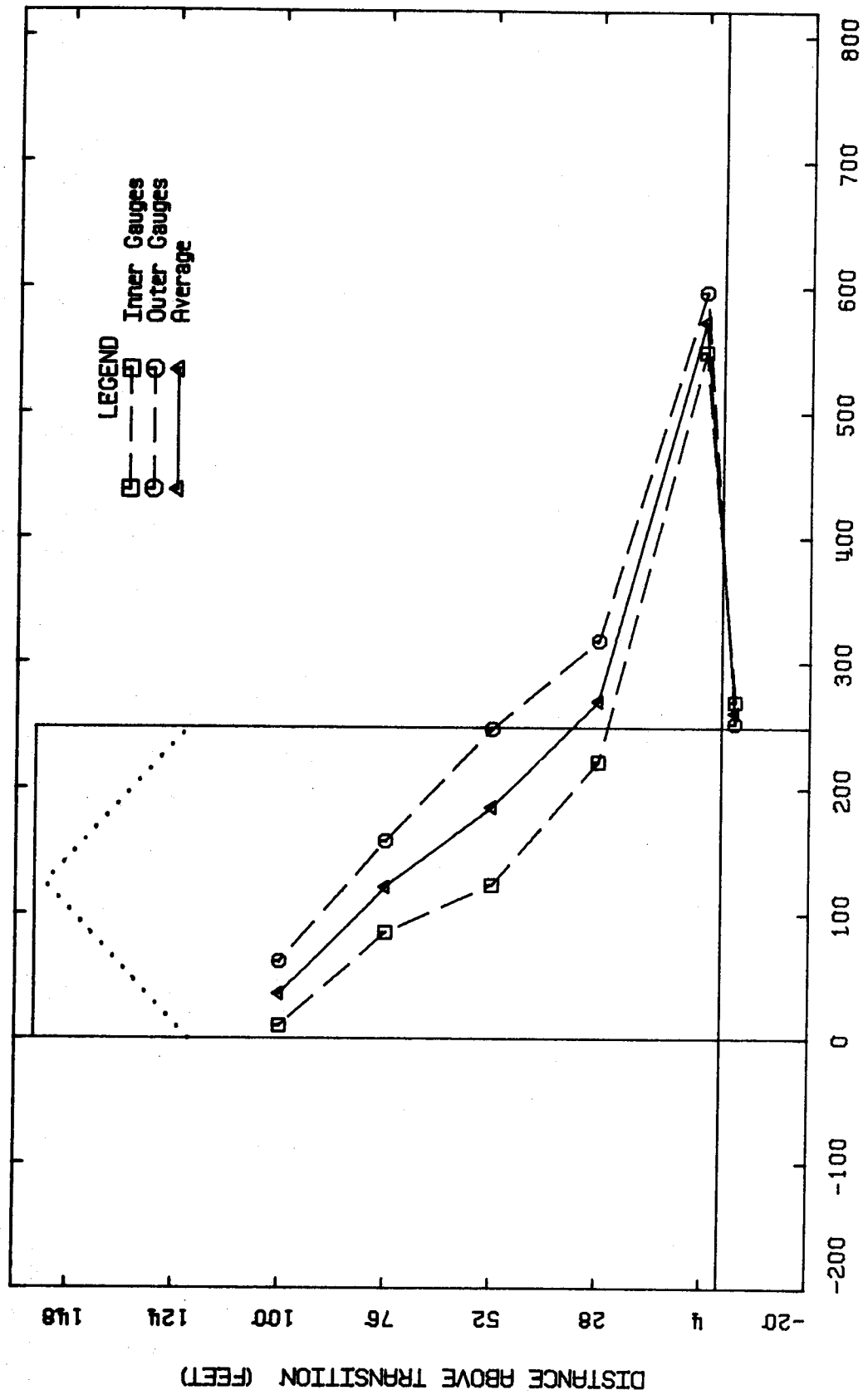

Figure J.C18 Vertical Variation in Hoop Strain - 3.5 Hours to Run #7 (Silo Full) 9:15 AM June 20

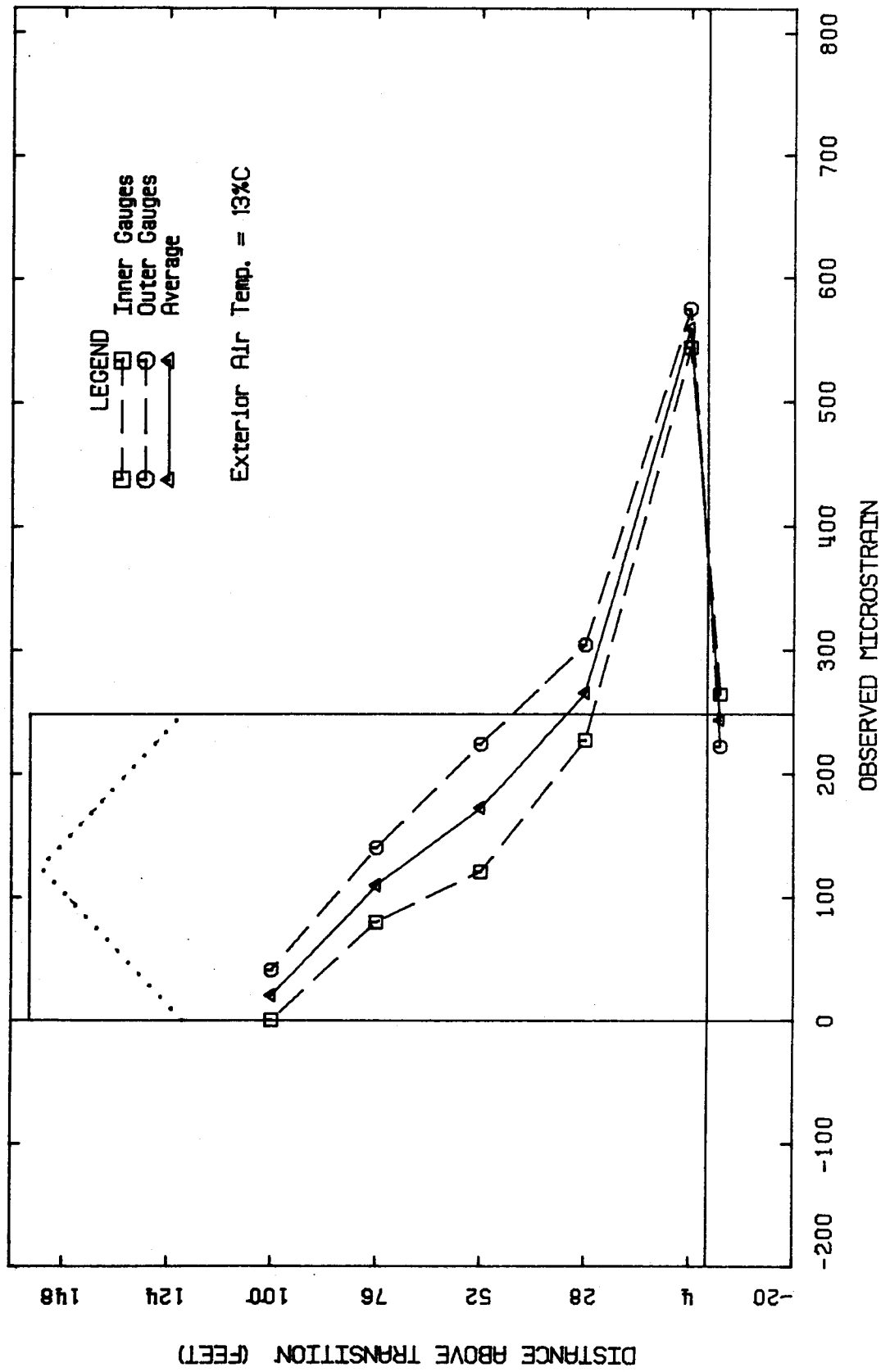

Figure J.C19 Vertical Variation in Hoop Strain - Start of Run #7 (Silo Full) 12:45 PM June 20

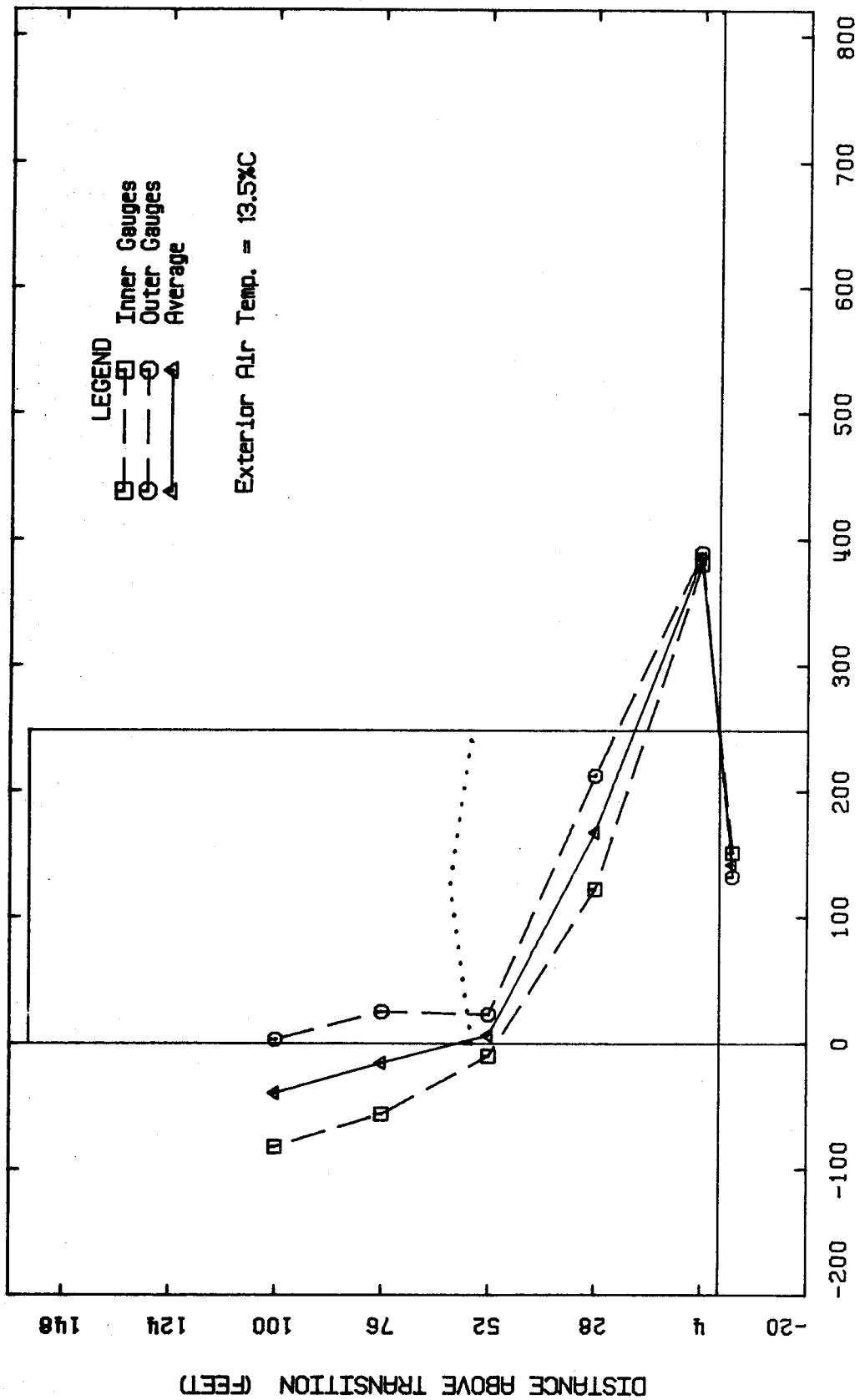

Figure J.C20 Vertical Variation in Hoop Strain - End of Run #7

4:45 PM June 20

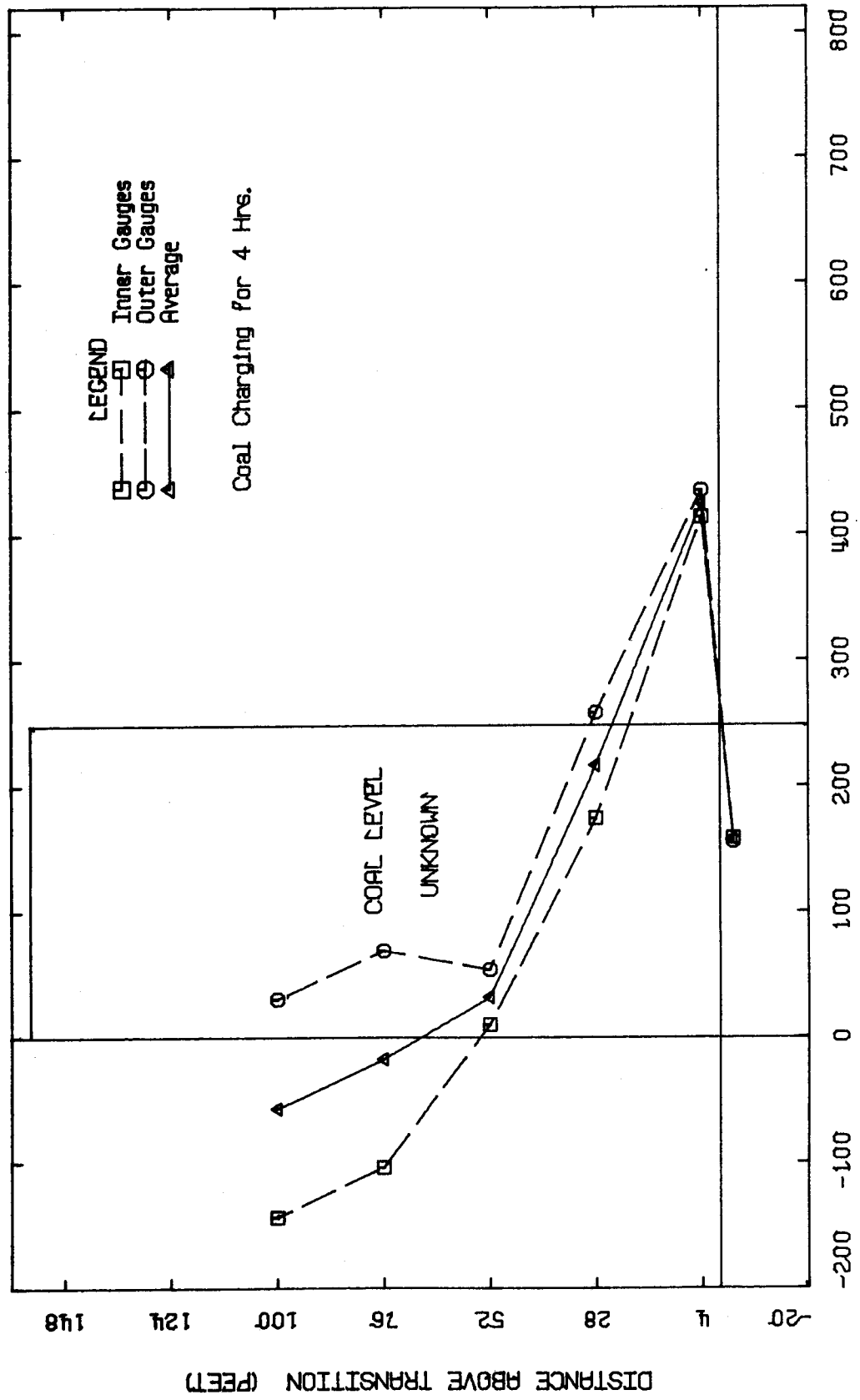

Figure J.C21 Vertical Variation in Hoop Strain - 3.25 Hours After Run #7 8:00 PM June 20

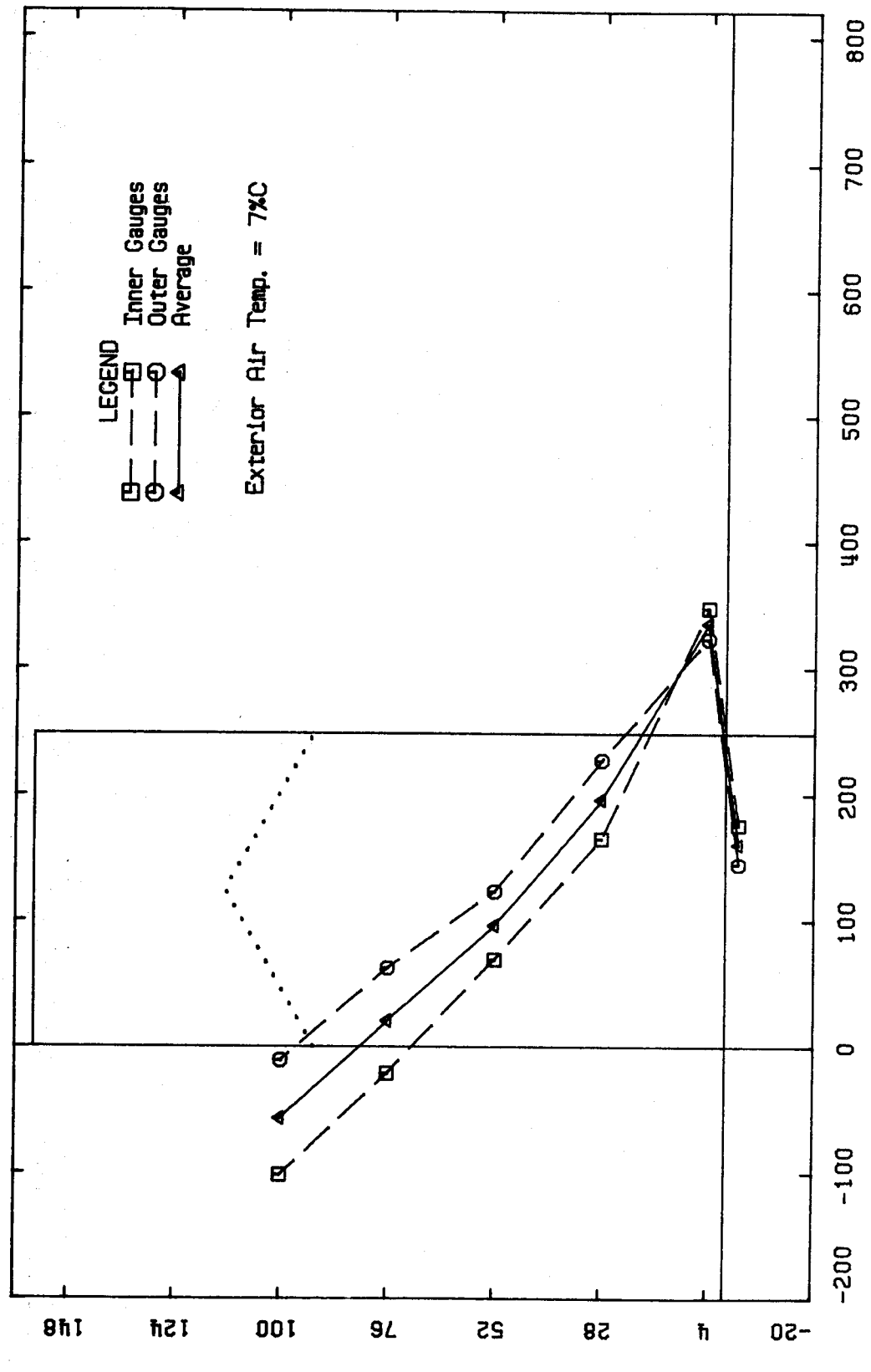

Figure J.C22 Vertical Variation in Hoop Strain - Start of Run #8

5:15 PM June 21

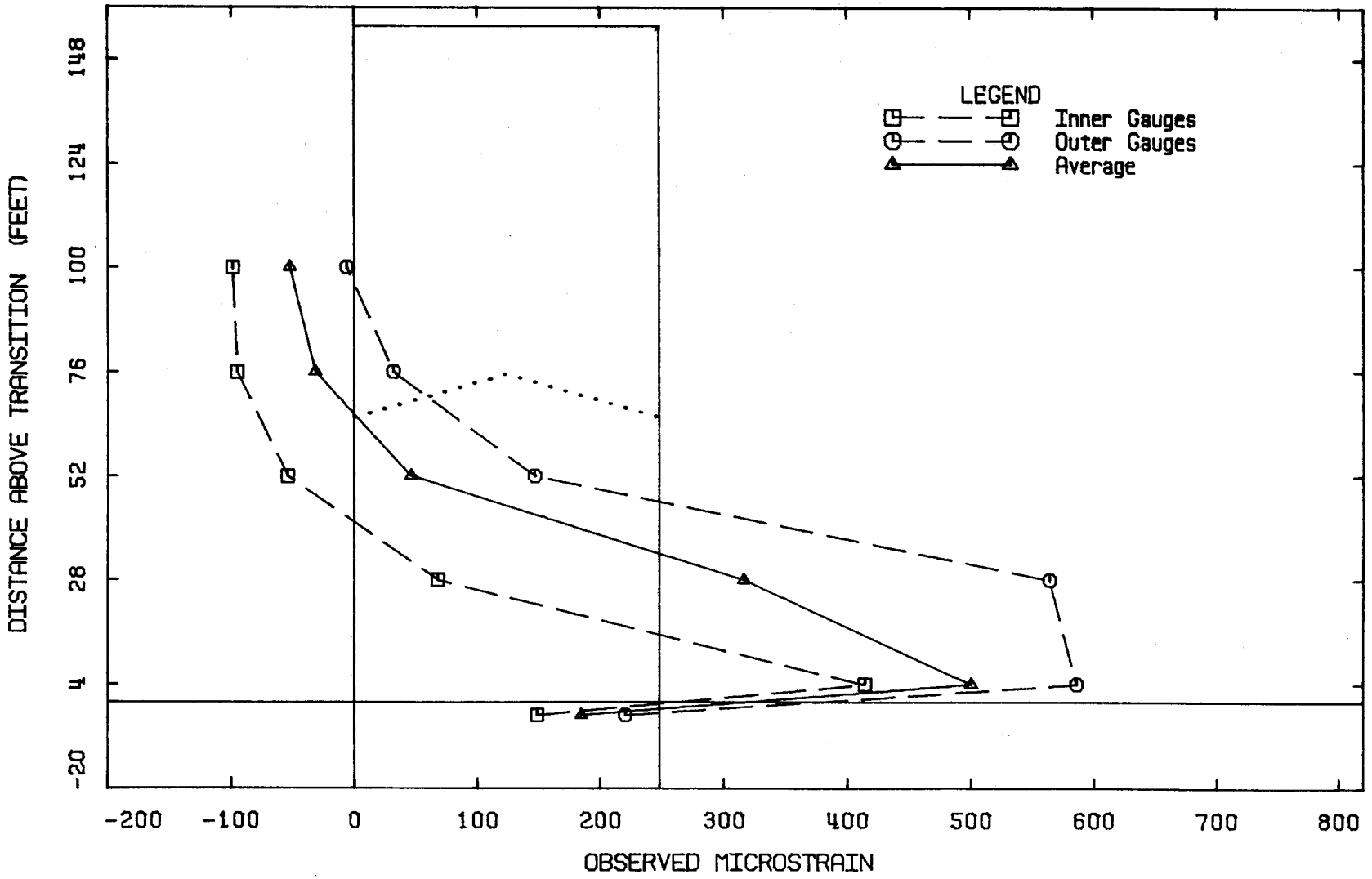

Figure J.C23 Vertical Variation in Hoop Strain - Robot Diesels Run #8 6:15 PM June 21

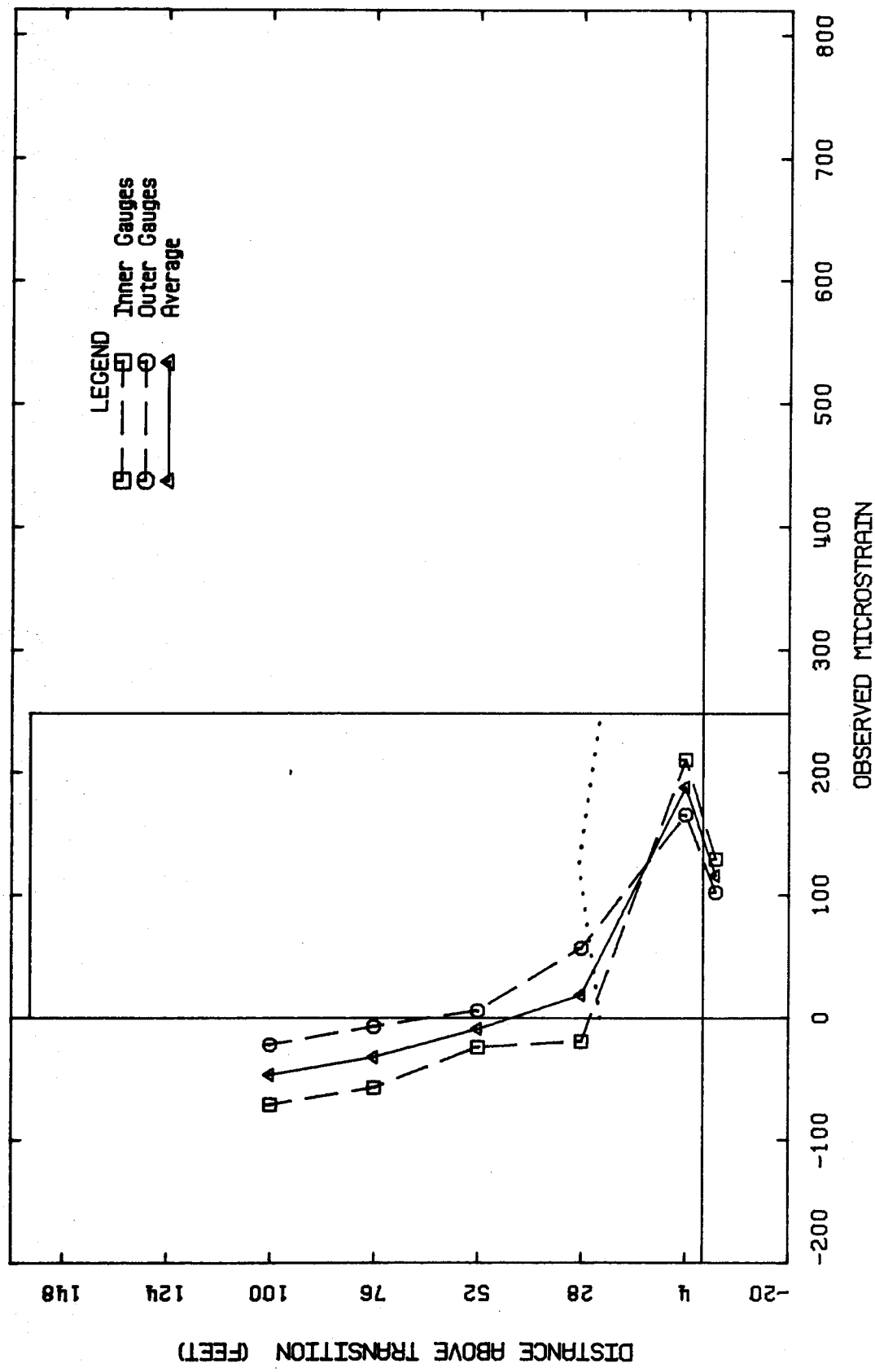

Figure J.C24 Vertical Variation in Hoop Strain - End of Run #8

7:15 PM June 21

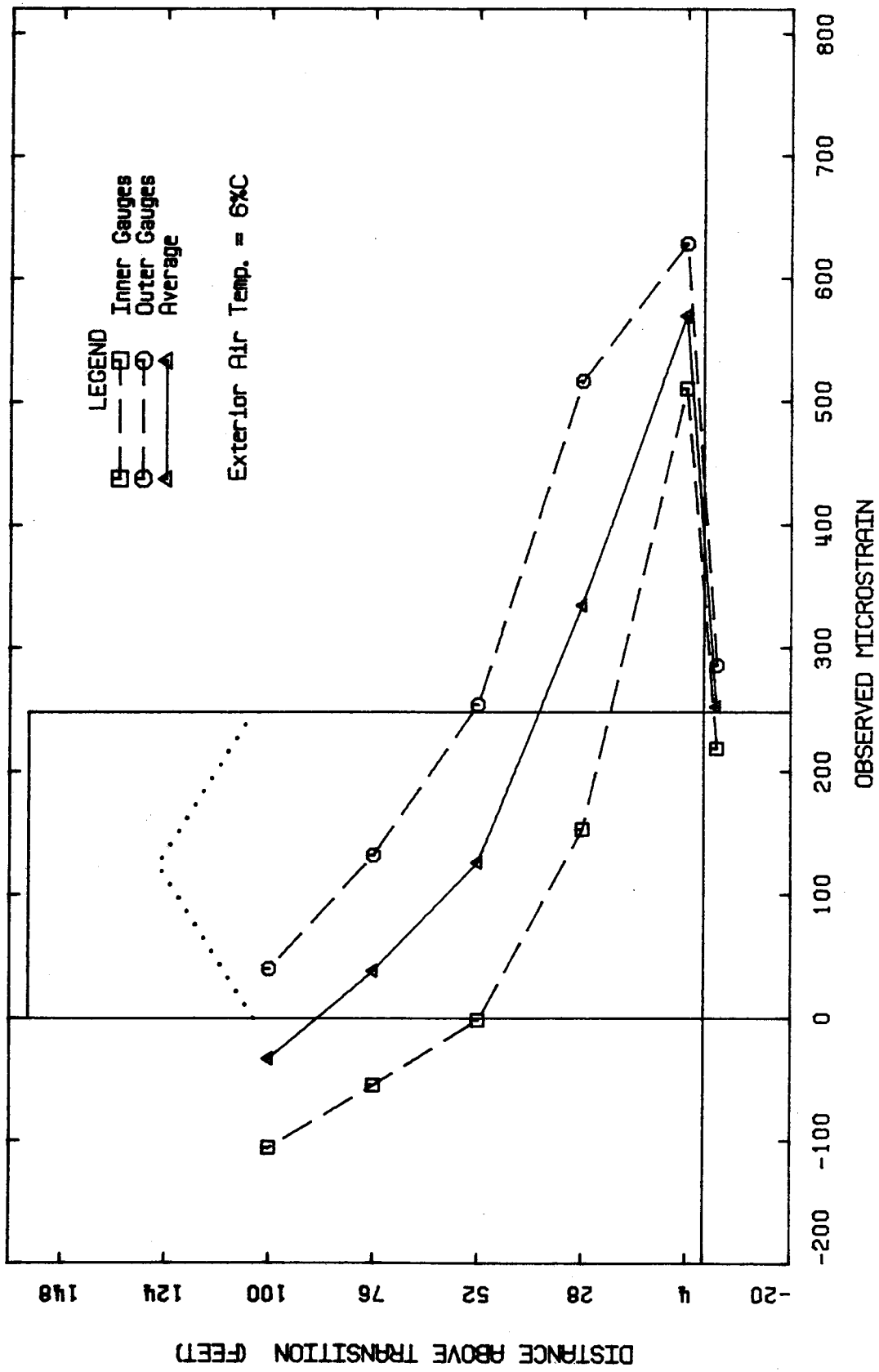

Figure J.C25 Vertical Variation in Hoop Strain - Evening Prior to Run #9 11:30 PM June 22

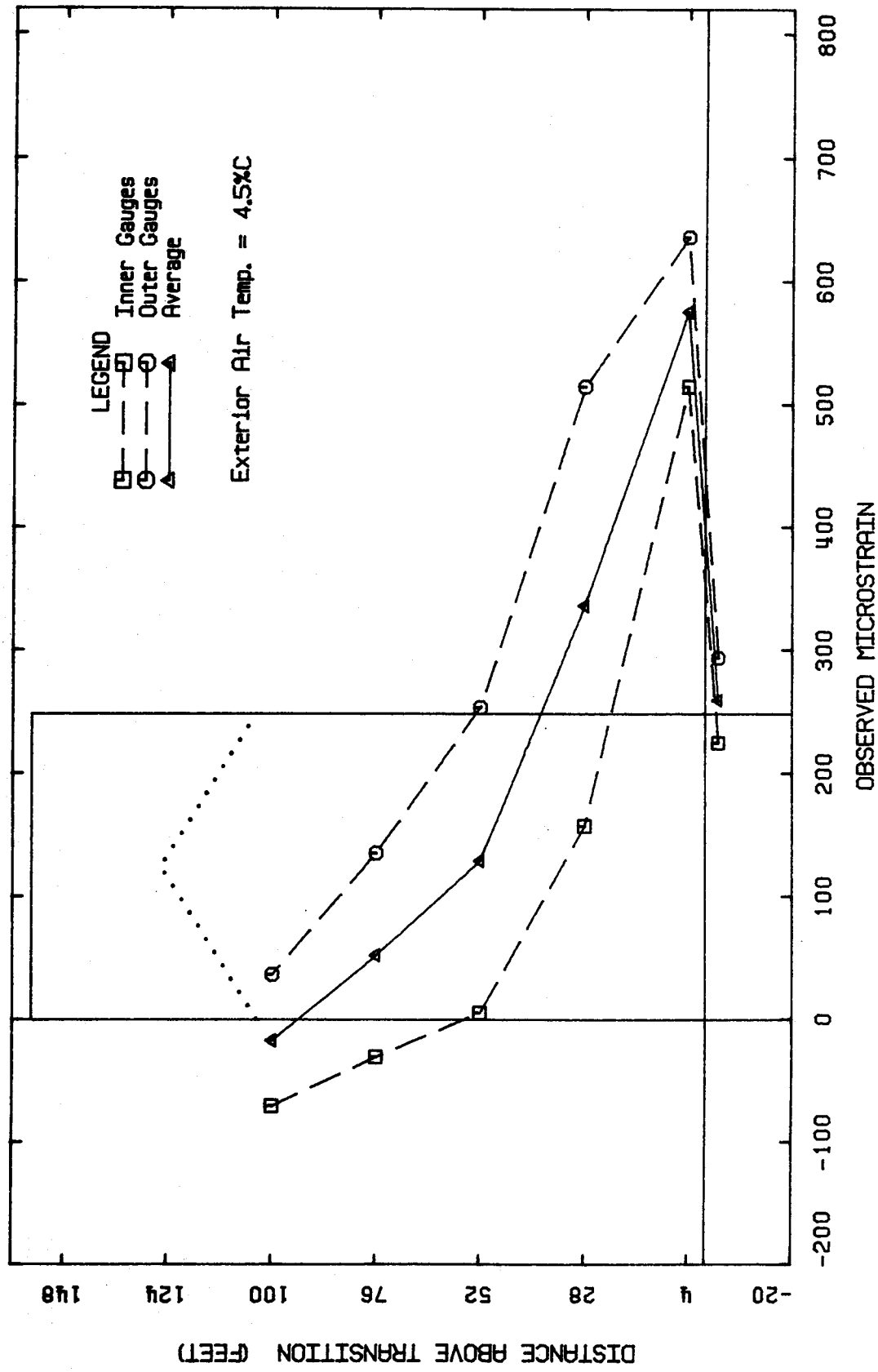

Figure J.C26 Vertical Variation in Hoop Strain - 1.25 Hours Prior to Run #9 7:00 AM June 23

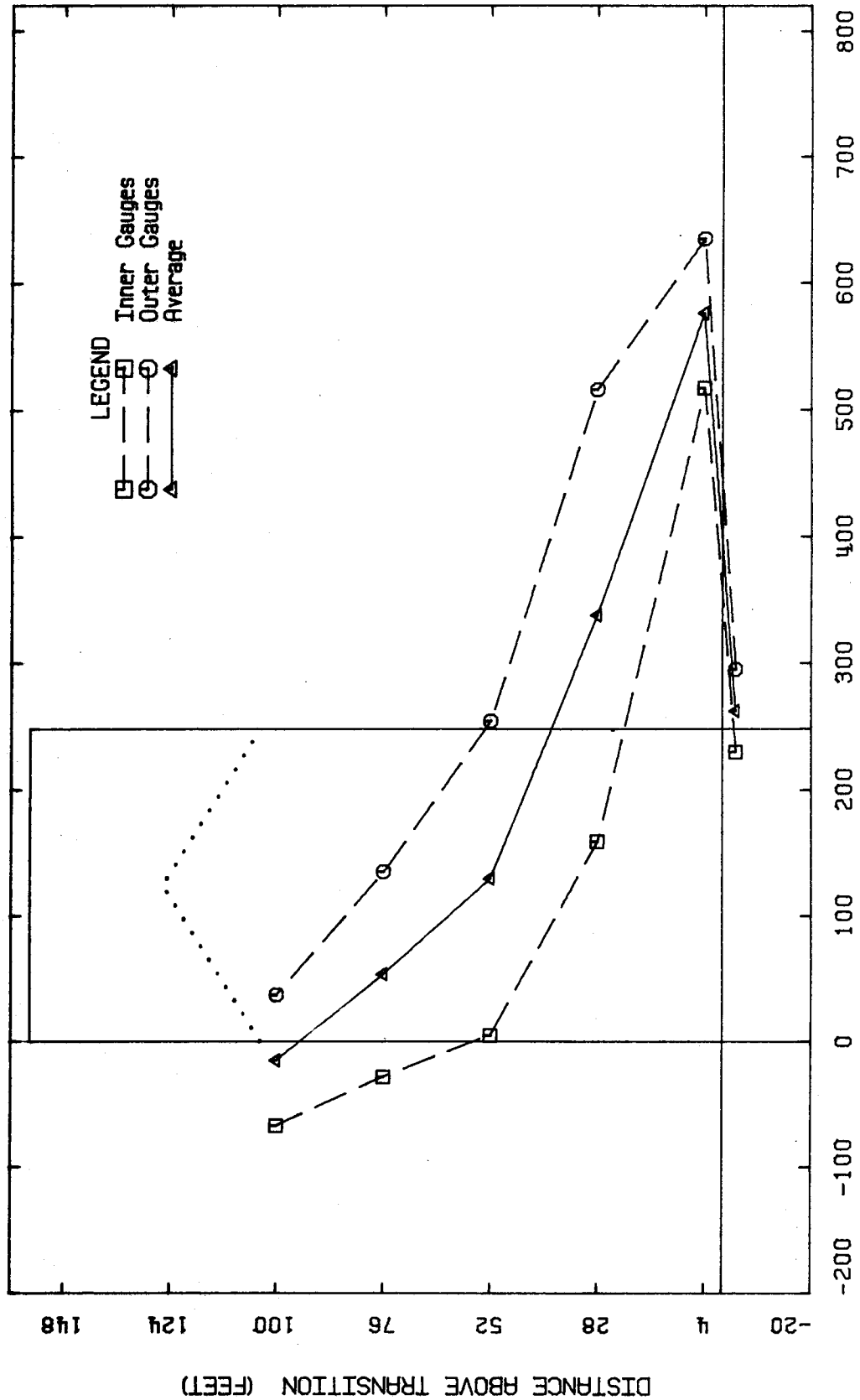

Figure J.C27 Vertical Variation in Hoop Strain - Start of Run #9

8:15 AM June 23

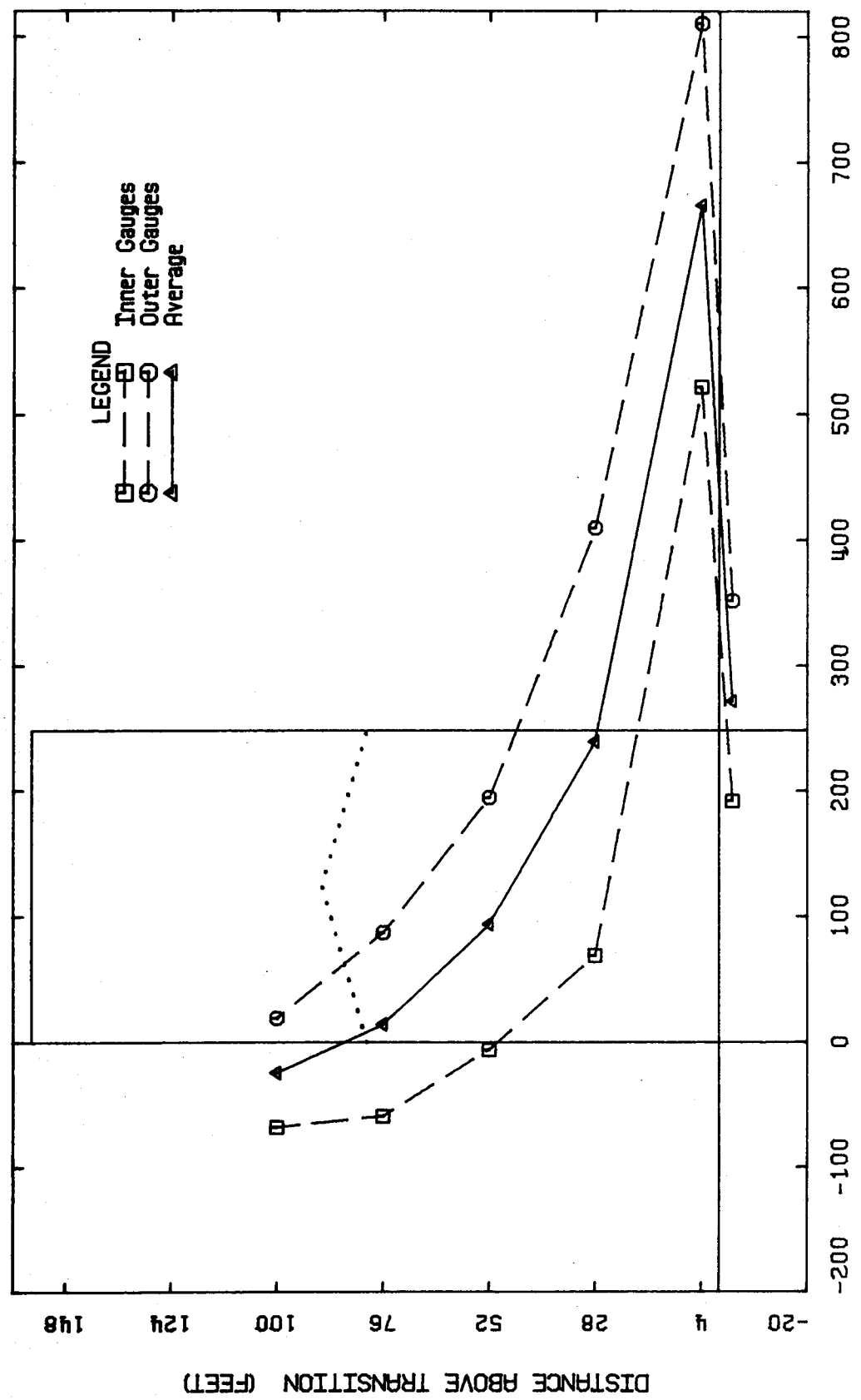

Figure J.C28 Vertical Variation in Hoop Strain - Robot Diesels Run #9 10:15 AM June 23

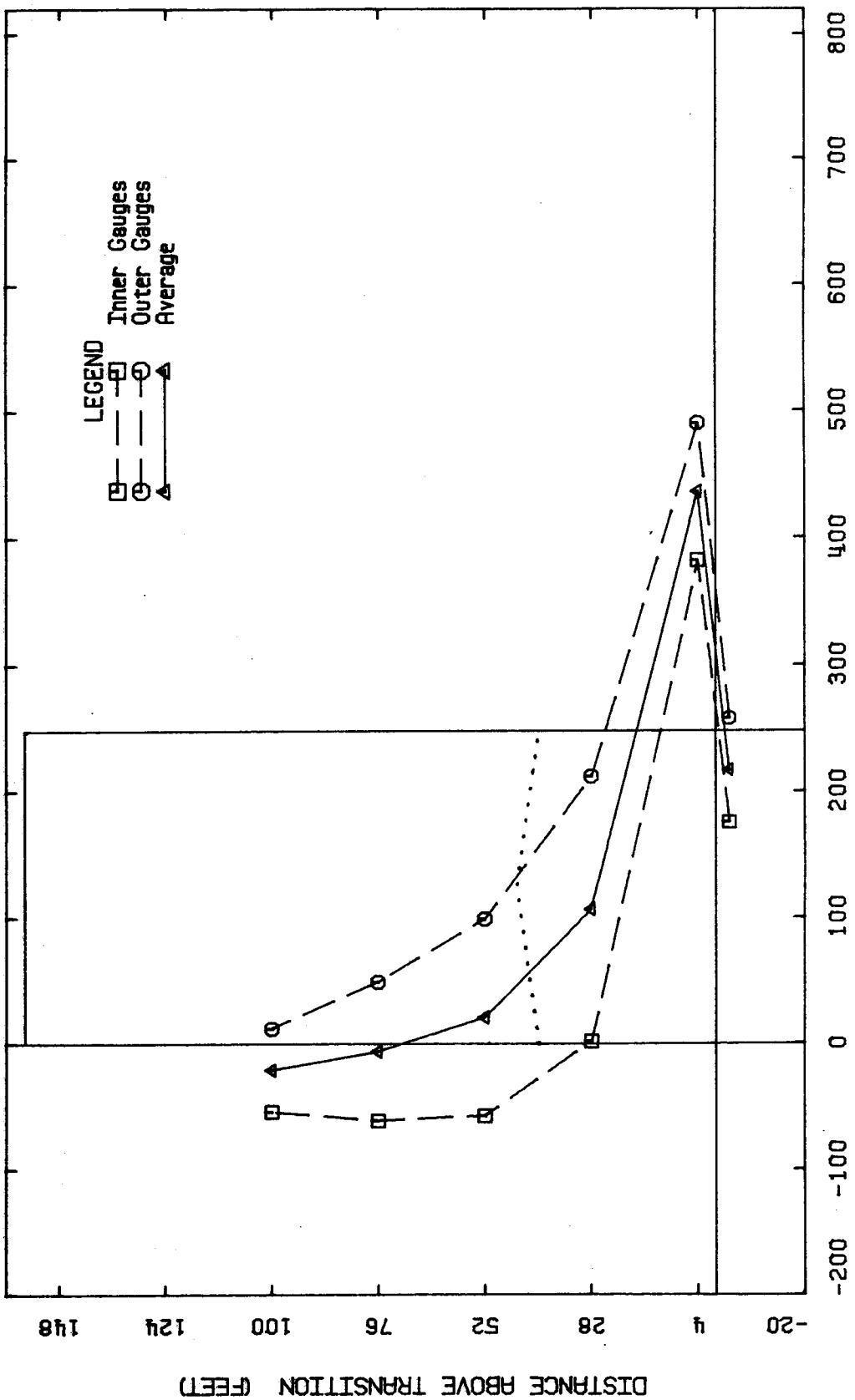

Figure J.C29 Vertical Variation in Hoop Strain - End of Run #9

11:00 AM June 23

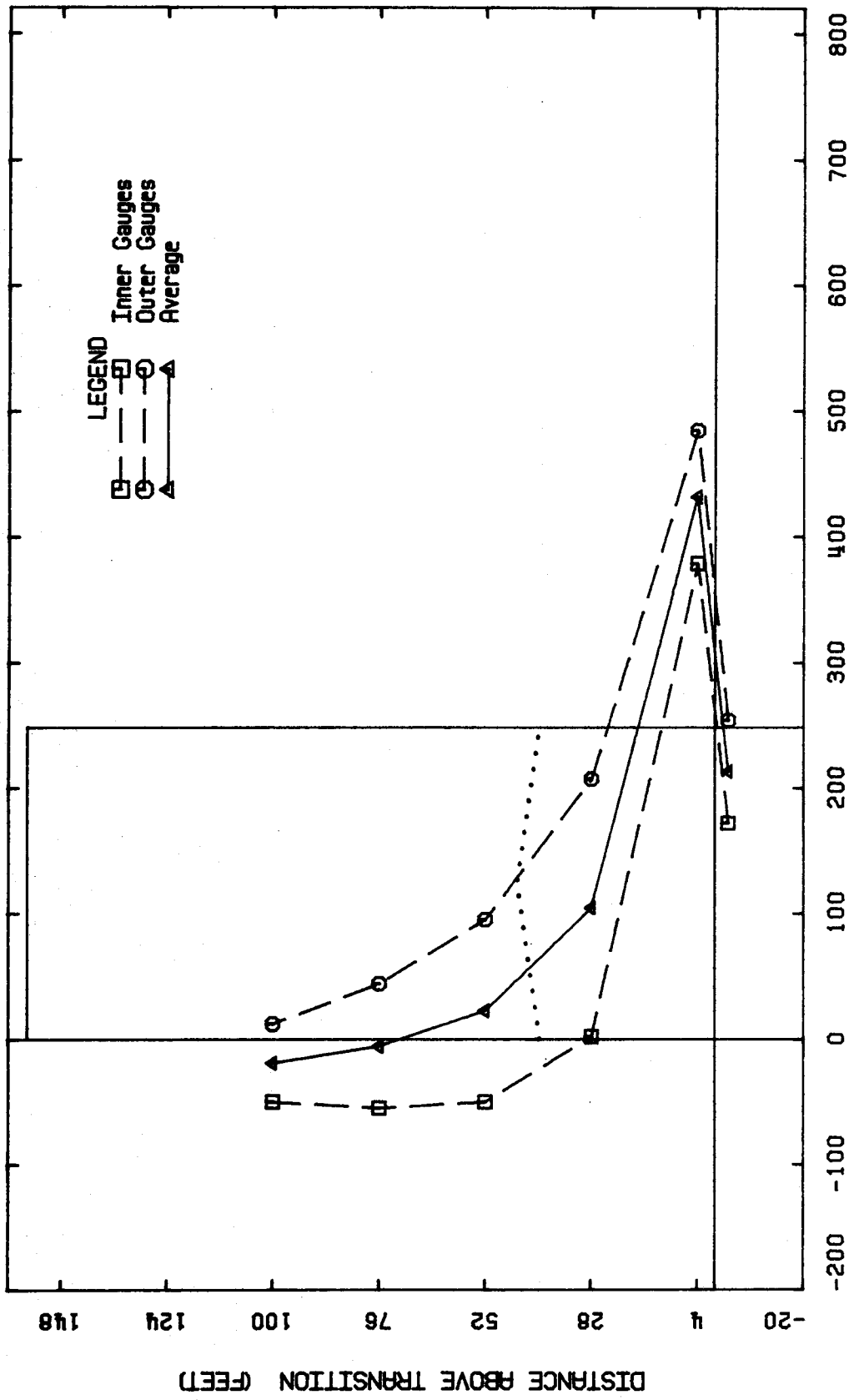

Figure J.C30 Vertical Variation in Hoop Strain - 1 Hour After Run #9 12:00 AM June 23

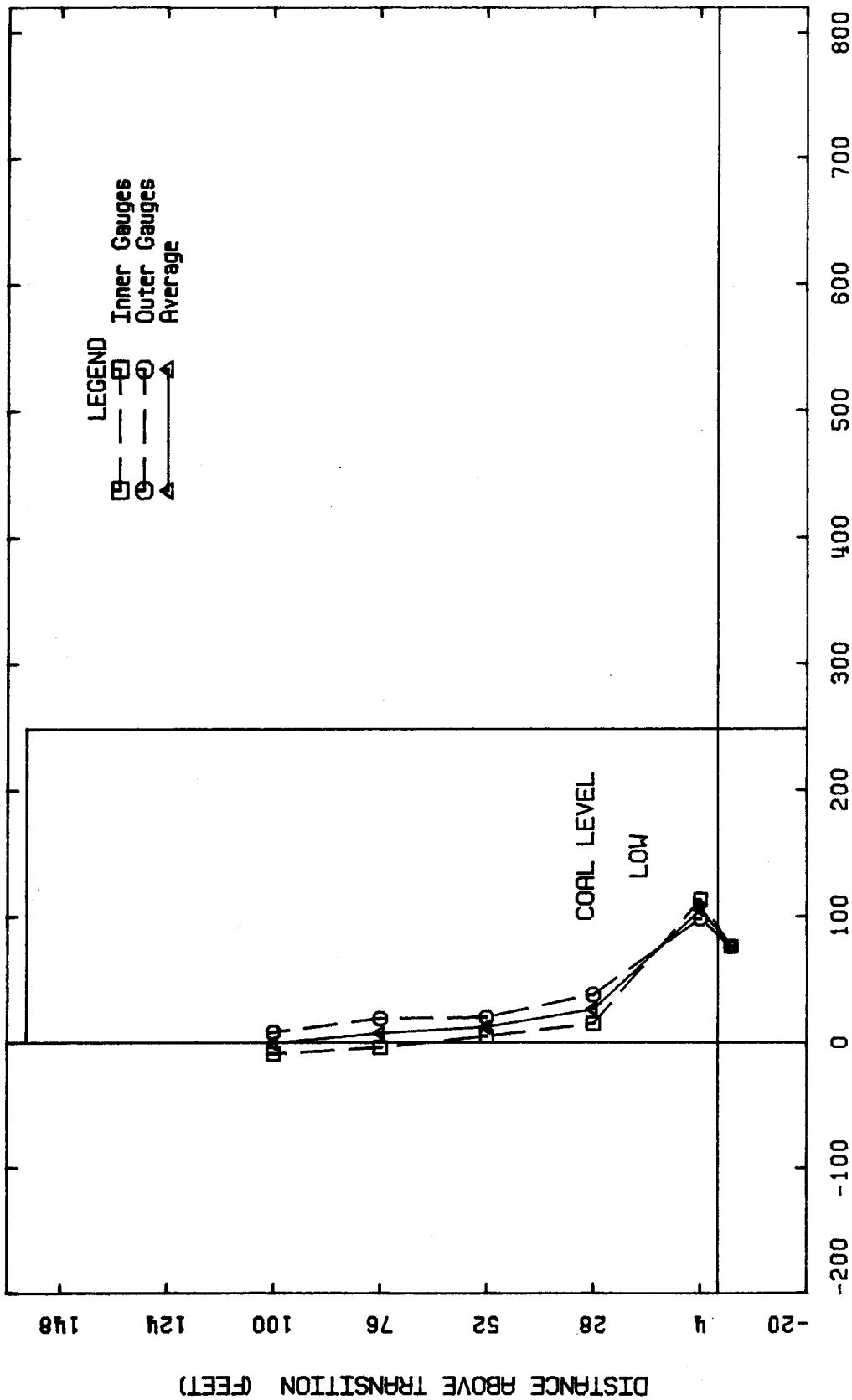

Figure J.C31 Vertical Variation in Hoop Strain - Silo Near Empty

1:30 PM June 24

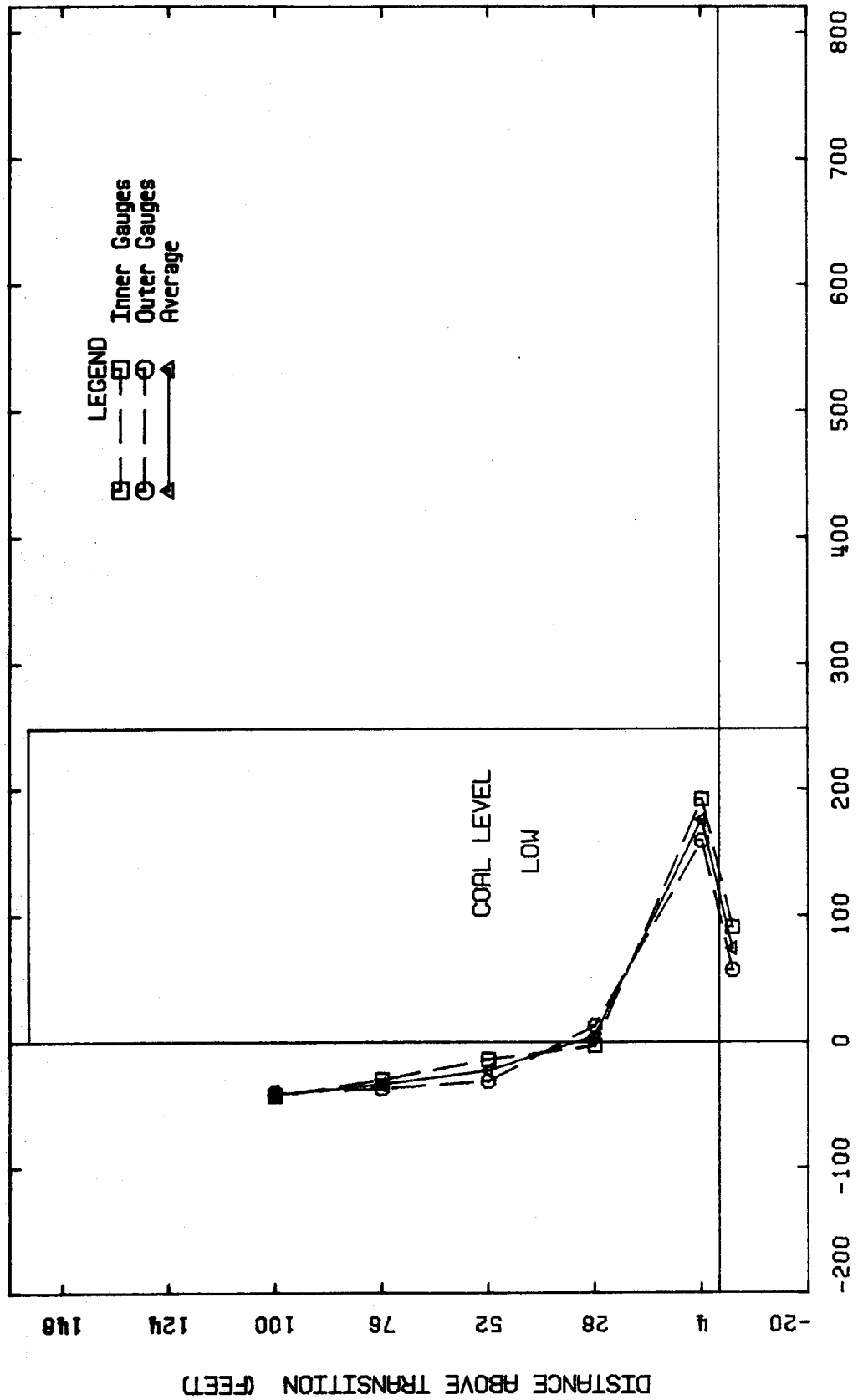

Figure J.C32 Vertical Variation in Hoop Strain - After Run #10

3:15 PM June 25

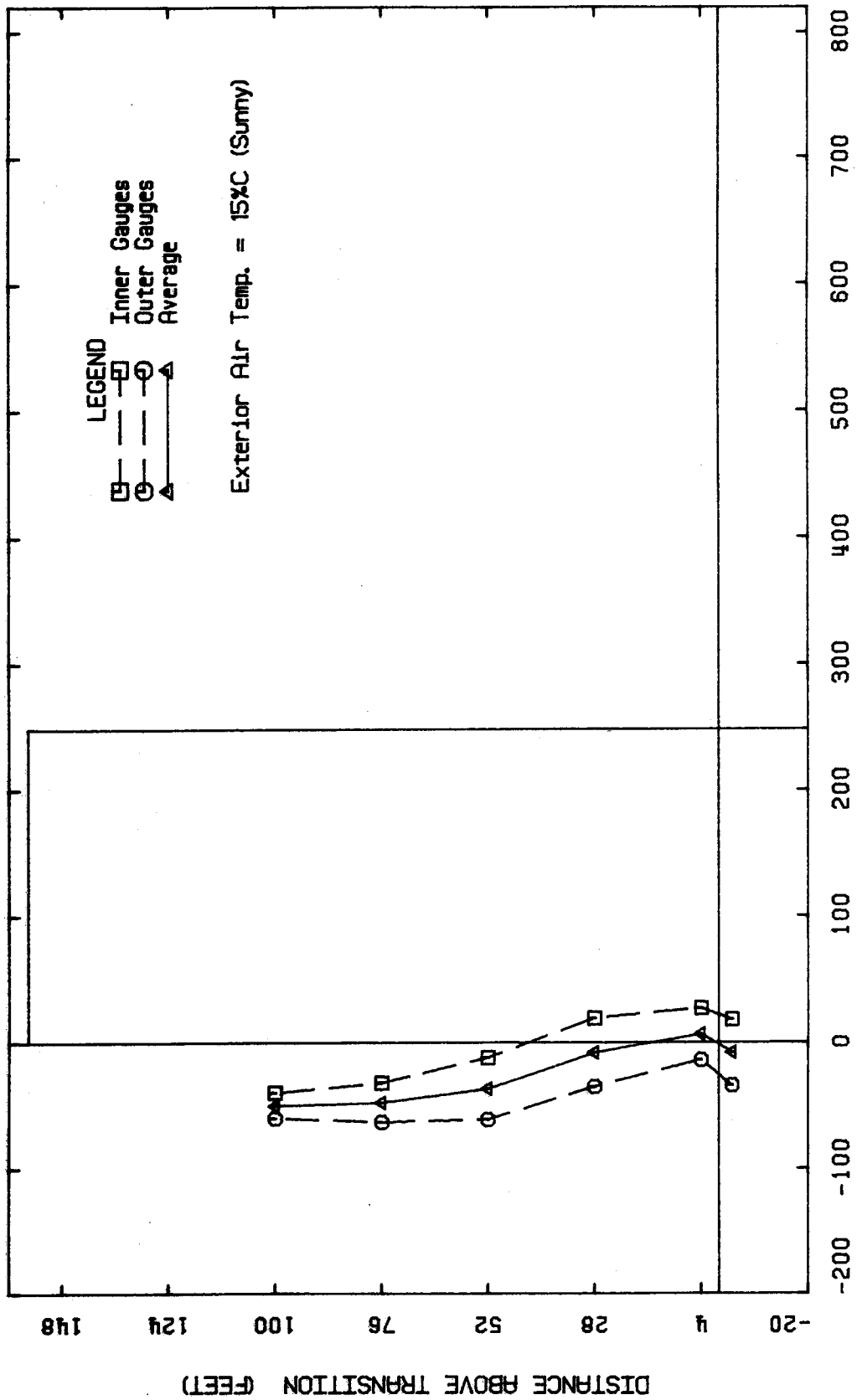

Figure J.C33 Vertical Variation in Hoop Strain - Silo Empty

10:00 PM June 26

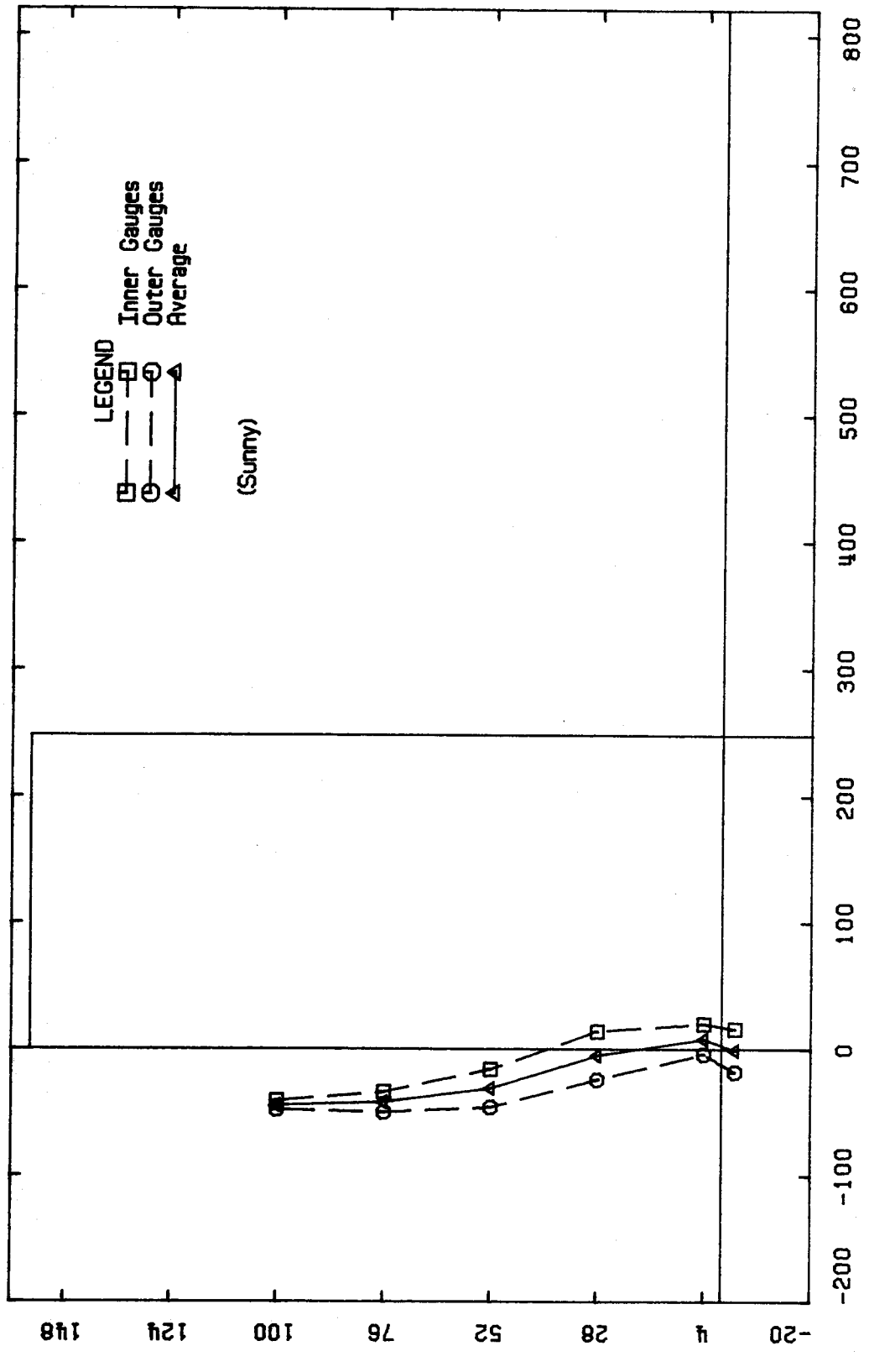

Figure J.C34 Vertical Variation in Hoop Strain - Silo Empty

11:00 PM June 26

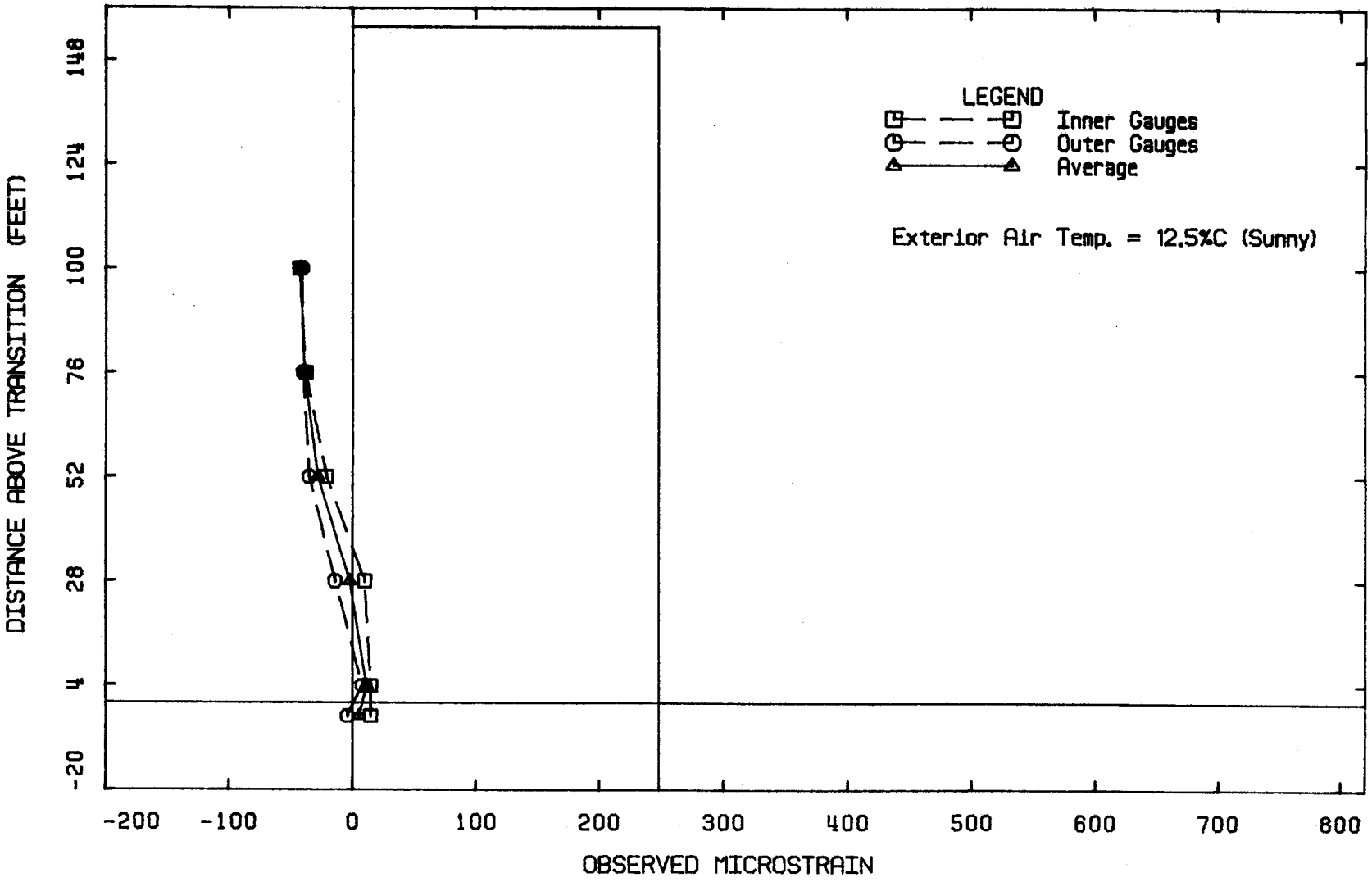

Figure J.C35 Vertical Variation in Hoop Strain - Silo Empty

11:45 PM June 26

RECENT STRUCTURAL ENGINEERING REPORTS

Department of Civil Engineering

University of Alberta

82. *Cracking of Reinforced and Prestressed Concrete Wall Segments* by J.G. MacGregor, S.K. Rizkalla and S.H. Simmonds, October 1979.

83. *Inelastic Behavior of Multistory Steel Frames* by M. El Zanaty, D.W. Murray and R. Bjorhovde, April 1980.

84. *Finite Element Programs for Frame Analysis* by M. El Zanaty and D.W. Murray, April 1980.

85. *Test of a Prestressed Concrete Secondary Containment Structure* by J.G. MacGregor, S.H. Simmonds and S.H. Rizkalla, April 1980.

86. *An Inelastic Analysis of the Gentilly-2 Secondary Containment Structure* by D.W. Murray, C. Wong, S.H. Simmonds and J.G. MacGregor, April 1980.

87. *Nonlinear Analysis of Axisymmetric Reinforced Concrete Structures* by A.A. Elwi and D.W. Murray, May 1980.

88. *Behavior of Prestressed Concrete Containment Structures - A Summary of Findings* by J.G. MacGregor, D.W. Murray, S.H. Simmonds, April 1980.

89. *Deflection of Composite Beams at Service Load* by L. Samantaraya and J. Longworth, June 1980.

90. *Analysis and Design of Stub-Girders* by T.J.E. Zimmerman and R. Bjorhovde, August 1980.

91. *An Investigation of Reinforced Concrete Block Masonry Columns* by G.R. Sturgeon, J. Longworth and J. Warwaruk, September 1980.

92. *An Investigation of Concrete Masonry Wall and Concrete Slab Interaction* by R.M. Pacholok, J. Warwaruk and J. Longworth, October 1980.

93. *FEPARCS5 - A Finite Element Program for the Analysis of Axisymmetric Reinforced Concrete Structures - Users Manual* by A. Elwi and D.W. Murray, November 1980.

94. *Plastic Design of Reinforced Concrete Slabs* by D.M. Rogowsky and S.H. Simmonds, November 1980.

95. *Local Buckling of W Shapes Used as Columns, Beams, and Beam-Columns* by J.L. Dawe and G.L. Kulak, March 1981.

96. *Dynamic Response of Bridge Piers to Ice Forces* by E.W. Gordon and C.J. Montgomery, May 1981.

97. *Full-Scale Test of a Composite Truss* by R. Bjorhovde, June 1981.

98. *Design Methods for Steel Box-Girder Support Diaphragms* by R.J. Ramsay and R. Bjorhovde, July 1981.

99. *Behavior of Restrained Masonry Beams* by R. Lee, J. Longworth and J. Warwaruk, October 1981.

100. *Stiffened Plate Analysis by the Hybrid Stress Finite Element Method* by M.M. Hrabok and T.M. Hrudey, October 1981.

101. *Hybslab - A Finite Element Program for Stiffened Plate Analysis* by M.M. Hrabok and T.M. Hrudey, November 1981.

102. *Fatigue Strength of Trusses Made From Rectangular Hollow Sections* by R.B. Ogle and G.L. Kulak, November 1981.

103. *Local Buckling of Thin-Walled Tubular Steel Members* by M.J. Stephens, G.L. Kulak and C.J. Montgomery, February 1982.

104. *Test Methods for Evaluating Mechanical Properties of Waferboard: A Preliminary Study* by M. MacIntosh and J. Longworth, May 1982.

105. *Fatique Strength of Two Steel Details* by K.A. Baker and G.L. Kulak, October 1982.

106. *Designing Floor Systems for Dynamic Response* by C.M. Matthews, C.J. Montgomery and D.W. Murray, October 1982.

107. *Analysis of Steel Plate Shear Walls* by L. Jane Thorburn, G.L. Kulak, and C.J. Montgomery, May 1983.

108. *Analysis of Shells of Revolution* by N. Hernandez and S.H. Simmonds, August 1983.

109. *Tests of Reinforced Concrete Deep Beams* by D.M. Rogowsky, J.G. MacGregor and S.Y. Ong, September 1983.

110. *Shear Strength of Deep Reinforced Concrete Continuous Beams* by D.M. Rogowsky and J.G. MacGregor, September 1983.

111. *Drilled-In Inserts in Masonry Construction* by M.A. Hatzinikolas, R. Lee, J. Longworth and J. Warwaruk, October 1983.

112. *Ultimate Strength of Timber Beam Columns* by T.M. Olatunji and J. Longworth, November 1983.

113. *Lateral Coal Pressures in a Mass Flow Silo* by A.B.B. Smith and S.H. Simmonds, November 1983.